Improving the sea defense of Central Termoeléctrica Antonio Guiteras

Multi-Disciplinary Project, 2020

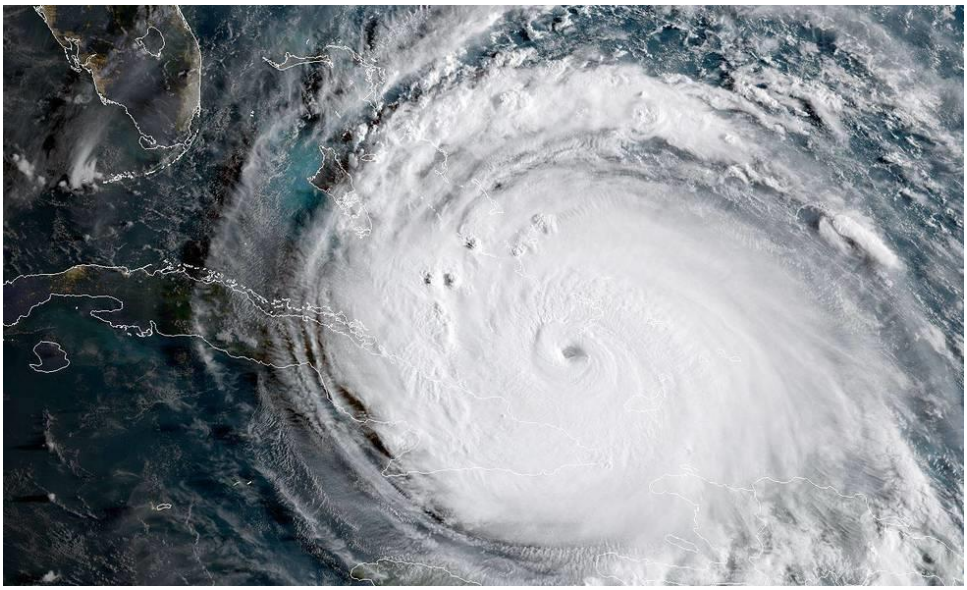

Document : Improving the sea defense of Central Thermo Electrico Antonio Guiteras
Place and date : Havana, January 2020

Authors : Robin van den Berg
: Matthijs Buijs
: Tjerk Krijger
: Alexandra Rijnink
: Wessel Vrijmoeth

University : Delft University of Technology
Faculty : Faculty of Civil Engineering & Geosciences
Department : Hydraulic Engineering

Supervisors
TU Delft : Dr. Robert Lanzafame, Dr. Olivier Hoes
CUJAE : Prof. dr. ir. Luis Fermín Córdova López

Cover photo:
Satellite image of hurricane Irma on September 8, 2017 at 8:00 a.m. (UTC -6:00)
(NOAA, 2017)

Sponsors

Delft Deltas, Infrastructures & Mobility Initiative (DIMI)

Universiteitsfonds Delft

Waterbouwfonds Delft
(not a logo available)

Universities

Delft University of Technology

Polytechnic José Antonio Echeverria
(Ciudad Universitaria José Antonio Echeverría)

Preface

This report is the result of a throughout study executed by five Civil Engineering students from the Technical University of Delft. A part of the master program is doing a project with students from different master disciplines. This project is performed by students from the Hydraulic Engineering and Water management disciplines. The goal of the project was to improve the sea defense in front of the Central Thermo Electrico Antonio Guiteras. This powerplant is situated in the province Matanzas, close to the capital of Cuba. To experience civil engineering in Cuba and obtain information directly from the source, the project team was situated in Havana.

For a little more than two months the project was executed at Universidad Tecnológica de la Habana José Antonio Echeverría (CUJAE). Here prof. dr. ir. L. F. Córdova López was to our everyday availability to answer all our questions. We want to thank him for his excellent guidance throughout the whole project.

Furthermore, we want to thank the people who helped us back in The Netherlands; our supervisors Dr. Robert Lanzafame, and Dr. Olivier Hoes. A special thanks to Chris Lashley who was of great help with our XBeach model. We would also like to thank Deltares for supplying us with the Delft3D license.

We have learned a lot from this project. A running Delft3D and XBeach model was created and a final solution which meets our requirements was designed. Next to this, we had a great experience in Cuba.

Robin van den Berg, Matthijs Buijs, Tjerk Krijger, Alexandra Rijnink, Wessel Vrijmoeth

Havana, January 2020

Abstract

The central Thermo Electrico Antonio Guiteras (CTE Antonio Guiteras) is a thermoelectric power plant located in the bay of Matanzas. In 2017, hurricane Irma passed the north coast of Cuba and destroyed the primary sea defense in front of the CTE, causing major damage to the plant. The power plant is renovated, and a new and improved sea defense is currently being constructed.

Before Irma, the coastal defense consisted of a wall parallel to the coastline. The wall was made of multiple impermeable rectangular concrete blocks, placed on a seal. The blocks were not anchored to the seal. During Irma the blocks were displaced and severally damaged. The new sea defense is designed by the Cuban engineering and architecture company EMPAI. The design consists of a concrete wall with a steep slope and a bullnose on top. It has a tooth-shaped anchorage to prevent the wall from sliding. Instead of reinforcement steel the wall is strengthened by carbon fiber strings. The wall can be divided in four sections: sections A-1, A-2, B and C. The sections differ in orientation and height. Section B and C are situated further away from the coastline and section C has a berm in front of the wall.

The goal of this report is to answer the following question: to what extend is the power plant protected during extreme weather conditions and what improvements are needed to ensure that the power plant can remain operational during these extreme weather conditions?

First it needs to be determined which extreme weather events are of importance in the scope of this project. Two extreme weather events occur in Cuba; cold fronts and tropical cyclones. Cold fronts generate maximum wind speeds corresponding to a category 3 tropical cyclone, meaning that a category 5 cyclone like Irma can generate wind speeds that are much higher than those of a cold front. Cold fronts have a higher probability of occurrence, but since the coastline of the CTE is located perpendicular to the North-East, waves generated by cold fronts have little influence on the project site. Hence, only tropical cyclones are assessed in this report.

To determine what the hydrodynamic and meteorological effects are of this extreme weather event, a synthetic tropical cyclone is created. This synthetic hurricane must generate large significant waves in combination with a big storm surge, to have severe impact on the CTE. It must also have a significant probability of occurrence. To determine this normative synthetic hurricane, multiple synthetic hurricanes are simulated in Delft3D and XBeach and their corresponding return period is determined. As Irma significantly damaged the CTE, this hurricane is taken as the basis for all synthetic hurricane combinations. The hurricanes each vary from Irma in maximum wind velocities, forward speeds and their tracks.

To set up a reliable Delft3D model, first hurricane Irma is simulated and iteratively validated with actual recorded data. To simulate the physics of hurricane Irma, a spiderweb grid is created at the locations of the hourly best track of Irma. The grid has a radius of 600 kilometers around the eye of the hurricane. This spiderweb grid is loaded into a Matlab script, which gives as output a spiderweb grid with for each grid point a pressure value, a wind speed value and a wind direction, all calculated according to the Holland formula. This is then used in the Delft3D model as input for the pressure and wind fields of the hurricane. The hurricanes follow one of the following two tracks; Irma's hourly best track or Irma's hourly best track shifted 1.5 degrees latitude to the North. During the period of 31st of August 2017 06:00 till the 11th of September 2017 12:00 Irma was classified as a TC. This period of six days is simulated with time steps of 10 minutes. Prior to this period of six days, the hurricane is pinned at the border of the Delft3D grid for two days together with a uniform wind over the entire grid, to simulate a fully developed sea state. The output of the Delft3D model is validated with recorded data of observations stations in the Gulf of Mexico. Recorded water levels and wind speeds of buoys near Key West are used for validation. Additionally, wave heights of buoys in the middle of the sea, quite far away from the CTE, are used.

XBeach is used to simulate the nearshore physical processes. XBeach can more accurately predict wave propagation and includes higher order processes in its simulation. As input for the XBeach model, the output of the Delft3D model is used.

After running all the synthetic hurricanes in Delft3D, the five resulting normative hurricanes are run in XBeach. The synthetic hurricane that creates the largest significant wave heights at the project area is taken as a basis for the final design. It has a return period of 1580 years. This combination has very high wind speeds with peak gusts of 80 m/s, a low forward speed of 3 m/s and follows Irma's track on the north side of Cuba, close to the shore of the CTE. This hurricane gives a maximum significant wave height of 8.8 m with a corresponding storm surge of 1.61 m at the location of the CTE. The mean significant wave height is 6.49 m with a standard deviation of 0.92 m during a period of 3.5 hours.

With these values a research on the current defense wall is done. This study shows that sections A-1, A-2 and B all have an unacceptable failure probability due to overtopping if the modeled normative synthetic hurricane would occur. Section C also shows an unacceptable failure probability but is less under-designed than the other sections. For all sections, adjustments to the current design need to be made. Section A-2 also contains an inlet channel for cooling water, this proves to be a difficult element in the design. In normal conditions an open channel to sea does not provide a problem, during a storm however large amounts of water can flood in and the defense wall can be damaged at this location.

To improve the existing design, several alternatives are possible for each function of the sea defense. Four functionalities can be distinguished and will be discussed separately. These are; wave reduction, barrier, gap protection and drainage capacity.

The first is wave reduction, which will cause waves to lose part of their height and consequently create less impact. The best way to improve this is by placing a pile screen on the foreshore. The second function is the barrier directly in front of the CTE. This is meant to stop the waves and limit overtopping. In this situation a seawall is the most suitable option. The slope can be adjusted, and design of the wall can be optimized to influence the overtopping.

To improve the existing sea defense, a solution needs to be sought for the inlet channel. The solution must allow the continuous flow of water but must provide more safety against flooding during an extreme storm condition. The option examined to protect the gap is to construct higher walls around the channel and basin.

Improving the drainage of the area of the power plant gives the advantage that water that enters as either precipitation, overtopping or overflow can be discharged and hence make sure that vital parts of the power plant are not flooded. There are several options to improve the drainage capacity of the area. It can be done by diverting the water, by pumping away the water using one or several pumping stations and by improving the capacity of the existing drainage channel.

The combinations of these alternatives per functionality result in variants and by means of a Multi Criteria Analysis for each section the optimal variant is determined. For sections A-1, A-2 and B an adjustment on the existing defense wall is proposed. A second but lower vertical wall with a bigger bullnose is placed in front of the existing one. This creates a triangular shaped stilling basin, from which the water can flow out at the seaside of the wall. No vital parts of the powerplant are located behind section C. Therefore, no adjustments on the wall are proposed but an improvement of the existing drainage capacity is proposed. The existing drainage channel, which lies behind this section, is widened and deepened. Additionally, a drainage wall is built around the powerplant, which diverts the overland flow caused by intense rainfall into the drainage channel. The inlet channel is improved by heightening the walls around the channel and basin with 1 meter. The wall is extended over the gap so that the water can flow underneath the wall like a pipeline.

Contents

List of Figures

Chapter 1

Introduction

1.1 General information about Cuba

1.1.1 Geography

Cuba is the largest island situated in the Caribbean Sea, located South of the United States of America and East of the Gulf of Mexico. It consists of multiple islands of which Cuba and Isla de la Juventud are the largest constituents with a total surface area of 110,860 km^2.

Figure 1 – Map of Cuba

Between Cuba and Jamaica, the North American and Caribbean tectonic plate meet. The tectonic movement of the plates causes the island to tilt which results on a large timescale in the rise of the northern side of the island, and a lowering of the south side. This creates a cliff shaped coastline and it also causes most rivers to flow towards the Caribbean Sea (and not the Atlantic Ocean).

Cuba has a large biodiversity and many different ecosystems and a very diverse landscape. It ranges from semi-deserts to tropical rainforests and has many beaches. The total beach length of Cuba is 5,746 km, of which most of the beaches are located at the North side of Cuba. The land is mainly flat, apart from a few mountain areas and the highest peak is the Pico Turquino on the South-East side of the island. Because it is a small and long island, not many big rivers flow through Cuba. Cuba's longest river is the Río Cauto, which is 343 km long and is only navigable by small boats. To compensate, 500 km^2 of reservoirs and dams have been created for irrigation and water supply (Sainsbury & McCarthy, 2017)

1.1.2 Climate

Cuba has a subtropical climate, which means it is warm and humid. The average annual temperature is around 25 °C. The coldest month is January with an average of 23 °C. The warmest month is August when it is on average 28 °C. On average annually 1,400 mm of rain falls in Cuba. The year can be divided in three seasons:

- Dry season: 32 - 99 mm of rainfall per month — December - April
- Wet season: 200 - 260 mm of rainfall per month — May - November
- Hurricane season: up to 300 mm of rainfall per day — July - November

During September and October, the Hurricane season is at its peak. Cuba has suffered from several hurricanes in the past. Notable are 2012's Sandy, which wrought more than 2 billion US$ in damage, and Hurricane Matthew, which touched down in Baracoa in 2016. The probability of occurrence of new hurricanes is high and the North-Eastern part of Cuba suffers the most from these hurricanes. Occasionally cold fronts appear from October till April, coming from the Gulf of Mexico, these fronts can also cause severe wave conditions. (Federal Research Division, 2002)

1.1.3 History, culture and economy

Cuba has a turbulent history, the country's history can be divided into three main periods; pre-colonial, colonial and post-colonial. The pre-colonial period was before 1500, after this, the colonial period started. A period of slavery and two Wars of Independence (the Ten Years' War and the Spanish Cuban American War) took place. After that the post-colonial period started with (in)famous men like Batista, Fidel and Raúl Castro, Camilo Cienfuegos and Che Guevara. This complex history results in the Cuba we know today (Sainsbury & McCarthy, 2017).

With the latest reforms of Raúl the economic growth is increasing, but it is still greatly affected by its history. Nowadays many companies are state-run and private enterprises are rare. The government plays a big role in the daily life, which has a significant effect on the development of the hydraulic structures, which also affects the design within this project. Not much money for (infra)structural initiatives is available and the investments are mainly made using public funds.

Total population	11.5 million
Population density	107.9 people per km^2
Life expectancy Male/Female	81.3 / 77 years
Infant mortality	5.5 per 1000

Table 1 A few facts (United Nations, 2018)

1.2 General information about CTE Antonio Guiteras

1.2.1 Geography

Matanzas is the second biggest province of Cuba; the province of Matanzas is one of the provinces with the greatest economic and productive potential in Cuba. In the industrial activity, the extraction of oil and gas, the electrical industry, the chemical industry and the light industry stand out for their importance. The equally named city Matanzas is the capital of this province and is located near the shore. Our project area is in the bay of Matanzas.

Figure 2 – Location of CTE Antonio Guiteras (Rubio Sauvalle, et al., 2018)

1.2.2 The powerplant

The central Thermo Electrico Antonio Guiteras (CTE Antonio Guiteras) is a thermoelectric power plant with a total surface area of 9000 m^2. It opened its doors in 1988 and had an initial capacity of 317 MW, nowadays its capacity is 250 MW.

On the site of the powerplant two heavy fuel tanks of 10,000 m^3 each are present, both with a diameter of 34.2 m. An extra wall is built around the two tanks for extra safety and to make sure nothing leaks into the environment.

The two big green tanks in Figure 3 are raw water tanks made of steel, they have a diameter of 22.79 m and can house 5,000 m^3 of water each. The two small green tanks contain demineralized water, their capacity is 1000 m^3 each and they have a diameter of 12 m.

To cool the generators of the powerplant, cooling water needs to be provided. Therefore, an inlet channel of about 15 meters wide is made from the sea to the powerplant, which is situated in front of the powerplant. To lead away the cooling water, a drainage channel is present on the backside of the powerplant which leads the disposed water to the sea.

Further on the project site a mechanic workshop, warehouses and an administration building can be found.

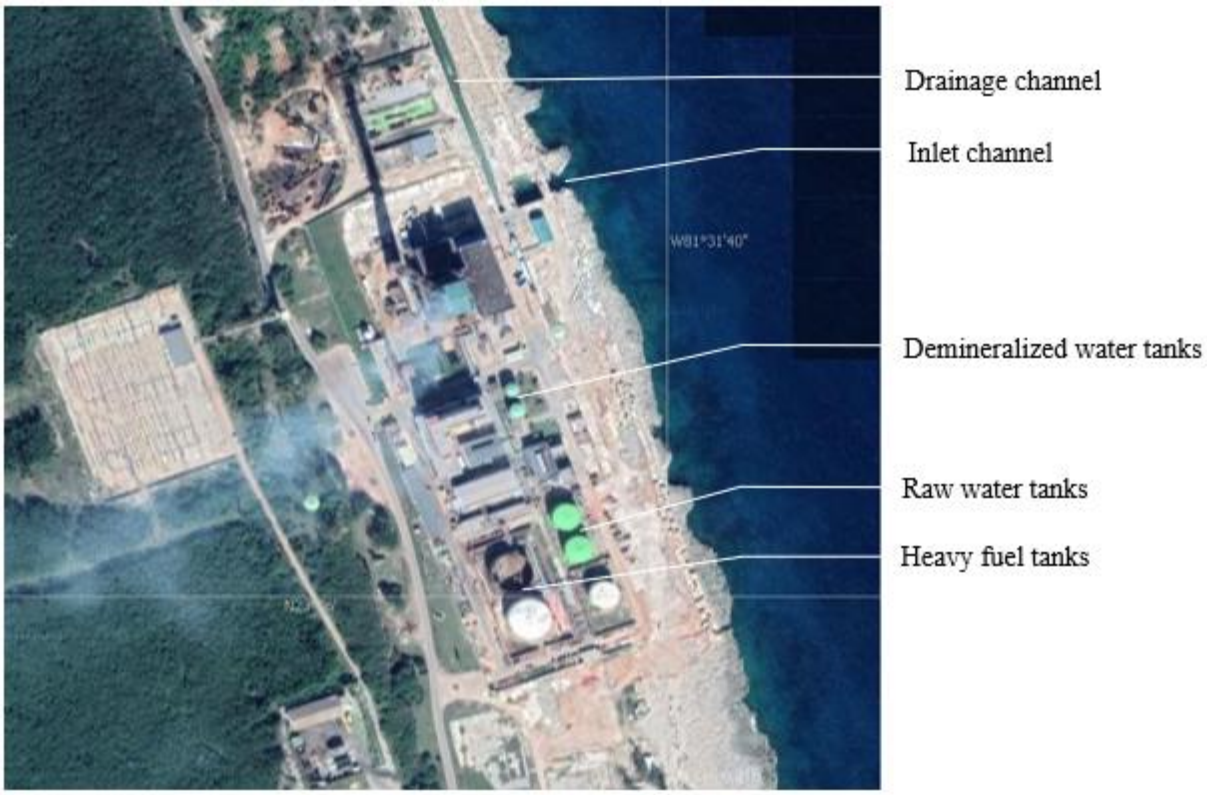

Figure 3 – Top view of CTE Antonio Guiteras (Rubio Sauvalle, et al., 2018)

Chapter 2

Problem description

2.1 Situation

In 2017 hurricane Irma passed the north coast of Cuba, turned around the coast of Matanzas and went north in the direction of Florida. Wind velocities of 255 km/h were measured, and the hurricane caused waves in the bay of Matanzas with significant wave heights of 5 - 8 m (Not validated).

Irma had destroyed the primary sea defense in front of the thermoelectric power plant in Matanzas, causing major damage to the plant. This power plant is of great relevance for the electricity supply of the surrounding area including Cuba's capital Havana. The power plant is rebuilt, and a new and improved sea defense is being constructed at the moment.

Figure 4 - Damage of the thermoelectric power plant caused by hurricane Irma (Rubio Sauvalle, et al., 2018)

2.1.1 Old situation

Before Irma, the coastal defense consisted of a wall parallel to the coastline. The wall was made of multiple permeable rectangular concrete blocks. The blocks were placed in three groups with each two rows of four meters. The blocks individually weigh between 52.8 and 67.2 ton and were placed on a concrete seal with a variable width. The blocks were not anchored to the seal. During Irma the blocks were displaced and severally damaged.

Figure 5 - Old defense wall

2.1.2 Current situation

The new sea defense is designed by a Cuban engineering and architecture company EMPAI and is currently being constructed. The design consists of a concrete wall structure on the coast in front of the water treatment plant. The wall is divided in three parts, part A, B and C. An overview can be found in Appendix A. They differ in dimensions and slope. The wall makes no use of reinforcement steel, instead it is strengthened by carbon fiber strings (see Figure 6). The general layout of the wall design can also be seen in Figure 6. Here can be seen that the new sea wall is extended into the northern area where no important elements of the plant are located. The predominant waves will most likely also come from this direction; to prevent flooding from the side the wall is extended. At the southern edge of the plant the wall stops where the tanks stop.

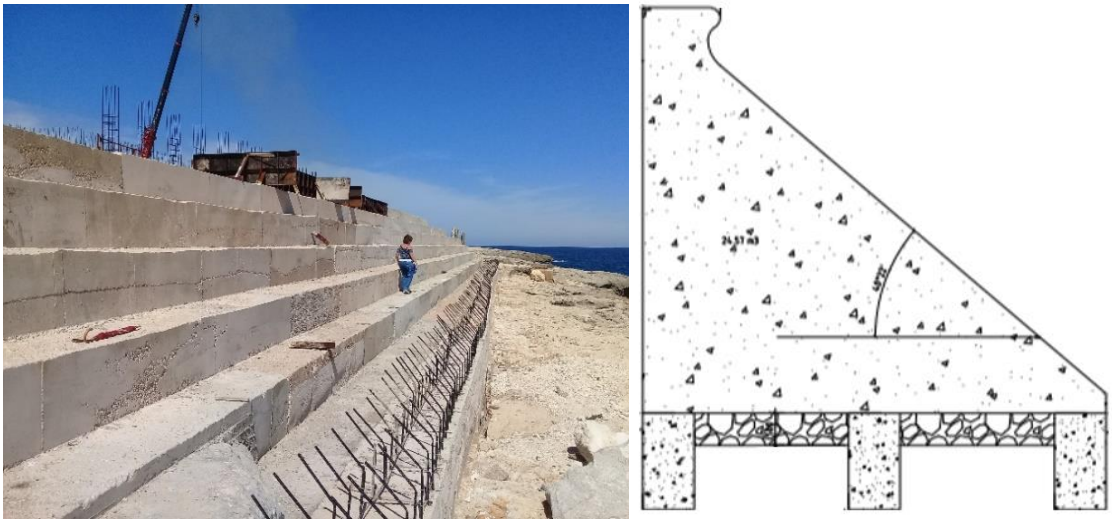

Figure 6 – Current defense wall under construction & Current defense wall design

However, the design of the new construction raised some questions, for instance about the slope of the defense wall, the length of the wall and the spare in the wall for the inlet channel for cooling water.

Slope

In the EurOtop (Allsop N. W., et al., 2018) a relation between the mean wave overtopping and type of structure is determined.

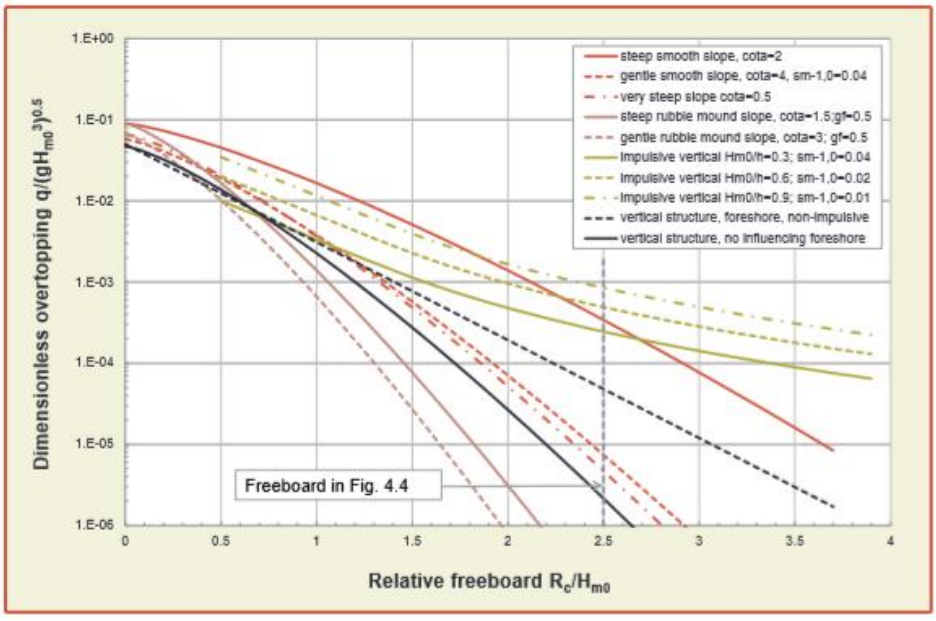

Figure 7 – Comparison of wave overtopping formulae for various kind of structures (Allsop N. W., et al., 2018)

The designed wall has a slope of 40 degrees, which gives a cota of 1.19. This cota is assumed to be steep. Taken into account that the structure is made of concrete, the solid orange line in Figure 7 will represent the current defense wall.

If an influencing foreshore is present, waves may become impulsive, break onto the structure and give overtopping for a very large relative freeboard. This will not be the case for non-impulsive waves, which give overtopping more in line with a structure without an influencing foreshore.

Figure 8 – Impression of the foreshore

The foreshore of the project area consists of a rocky cliff, which will affect the breaking of the waves before reaching the defense wall. Therefore, the assumption is made that the wall has an influencing foreshore and the waves therefore can be considered impulsive. The final design chapter contains an elaboration on this assumption.

In this case the defense wall is 4.6 (wall part B) to 6.3 (wall part A) meters high, which will give an approximate relative freeboard between 1.5 and 2. Looking at Figure 7, one can see that with a freeboard between 1.5 and 2, the overtopping with a steep smooth slope and with a vertical wall (the green lines) are more or less the same. In some cases, the designed defense wall might even give higher overtopping then a vertical wall. This suggests that a vertical wall could be as good as the designed defense wall. A vertical wall is more space efficient and easier to construct. It might be even possible to decrease the crest of the wall or the width of the wall which will save costs.

Length and dimensions

The wall consists of three parts, of which part C has a crest height of +11.30 m MSL. This seems rather over-designed as it mostly needs to protect the drainage channel. Furthermore, in the runup calculation the same approach as for wall part A has been used. The influence of the first berm of the wall is therefore neglected. However, this berm is of significant influence for the breaking of the waves, so it might be too big of an assumption to neglect it.

Inlet channel for cooling water

A weak point in the design is the inlet for cooling water, this 15-meter-wide channel is in direct connection to the sea and not protected. In Figure 9 it can be seen that the water flows under a concrete bridge, and at both sides of the inlet two walls are constructed to stop waves and spray. This causes there to be a gap in the wall and during an extreme weather event a lot of water can enter the plant through this channel. During hurricane Irma it was observed that major damage to the pumps and the wall were initiated at this gap.

Figure 9 - Inlet channel cooling water

2.2 Problem definition

The current sea defense is a big improvement on the protection of the powerplant. However, few studies on the effects of hurricanes have been done around the new sea defense. For example, it is unknown what will be the overtopping and precipitation if a new hurricane like Irma or a more destructive hurricane will occur. Knowing the importance of the power plant, a good sea defense is vital. This requires a thorough study on to what extend the power plant is protected during extreme weather conditions.

2.2.1 Research question

The general objective of this study is to protect the power plant from future hurricanes. To define the project scope the following main question will be answered: to what extend is the power plant protected during extreme weather conditions and what improvements are needed to ensure that the power plant can remain operational during these extreme weather conditions?

To answer this question, it is necessary to answer the following sub questions:

1. Which extreme weather events are of importance in the scope of this project?
2. What are the hydrodynamic and meteorological effects of these extreme weather events?
3. What are the possible failure mechanisms related to an extreme weather event and their respective consequences?
4. What are feasible protection solutions to minimize the impact and probability of occurrence of these failure mechanisms?

Chapter 3

Analysis

3.1 Stakeholder analysis

To execute the project properly, it is important to know which stakeholders are involved. To obtain clear insight into the actors and their goals, interests and power, a stakeholder analysis is done. Their relation and interaction will help to understand the position of different stakeholders in the project.

3.1.1 Actors

The actors of the project and their relations are shown in the figure below. They will be assessed individually in the paragraphs below.

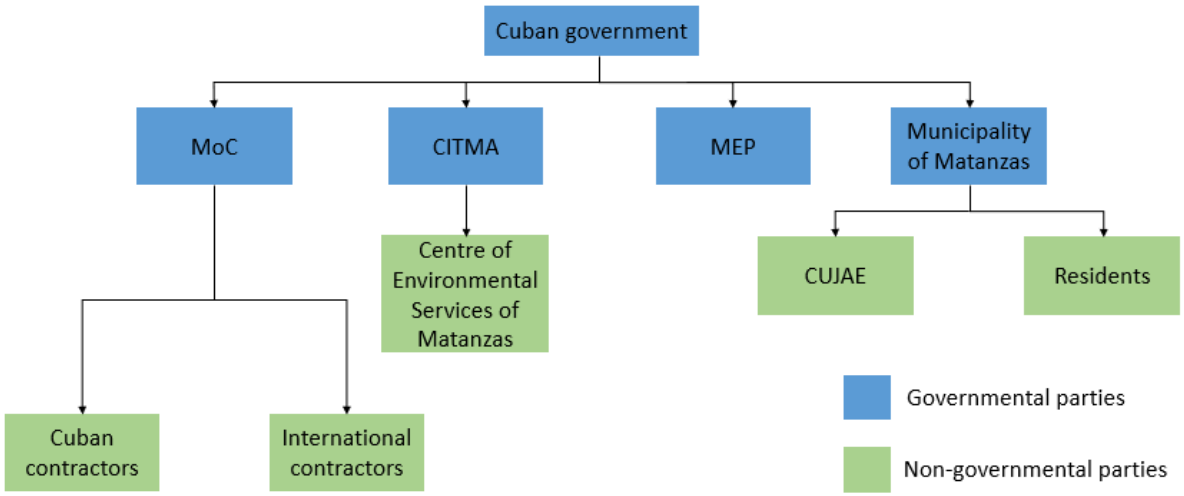

Figure 10 - Hierarchical overview of involved actors

Governmental parties

By most Cuban projects the government plays an important role in the development. This project involves mainly three Cuban ministries. These ministries and their connection to the project are listed below. Also, the municipality of Matanzas is one of the main actors in this project.

Ministry of science, technology and environment (CITMA)

The protection of the coast is done by the CITMA. They are responsible for the maintenance and development of the beaches and coastlines of Cuba. The CITMA also needs to protect the existing ecosystem. They have a long-term perspective on the projects that they are involved with.

Ministry of construction (MoC)

This ministry is responsible for the realization of all construction works in Cuba. The MoC also appoints the needed construction work to Cuban (or international) contractors. It is similar to the Rijkswaterstaat in the Netherlands. They receive technical input from the CITMA.

Ministry of Economics and Planning (MEP)

This ministry divides the available budget over all the ministries. There is no direct link to the project, but the MEP is indirectly responsible for the funding of the project.

Municipality of Matanzas

They represent the residents of Matanzas and need to provide them with electricity. They benefit of the project by improving the life quality of the municipality. They are investing some of their assets in the project and provide the project with construction permits.

Non-governmental parties

Cuban contractors

They will be provided with work so they can generate an income. They provide the knowledge for the construction of the new sea defense. By using Cuban contractors, the local economy will be supported. Therefore, the Cuban government strongly favors local contractors.

CUJAE and its Hydraulic Research Center (CIH)

This is the Universidad Polyténico José Antonio Echeverría de Havana. They provide knowledge of the hydraulic aspect of the sea defense. With this project they have the possibility to do research nearby Havana. CUJAE is regularly involved in projects and research for complex projects.

Residents

The residents of Matanzas and it surrounding area use the electricity of the powerplant. Their quality of life is connected to the project. They play no active role in the project.

Centre of Environmental Services of Matanzas

The improved sea defense and the construction of it, might interfere with the existing ecosystem. Therefore, there might be interest in the project from the Centre of Environmental Services of Matanzas. They enforce environmental regulations and laws and monitor the effects of these kind of projects on the environment.

International contractors

When local expertise is not sufficient, it might be necessary to contract international contractors. Their work will not be carried out by the MoC but will be private.

3.1.2 Goals, interests and power

In the paragraph above all actors are determined. Their goal, interest and power are expressed in the table below.

Stakeholder	Goal	Interest	Power
Ministry of science, technology and environment	Maintenance and protection of the coast	Safe coast protection, balanced ecosystem	High Political, money and expertise
Ministry of construction	Realization of the construction works	Construct the solution and contact the contractors	High Political, money, manpower, equipment and expertise
Ministry of Economics and Planning	Earn money on the project	Allocate the money to the reliable projects	Moderate Political and money
Municipality of Matanzas	Protect the interests of the residents	Protect the environment	Moderate Political

Cuban contractors	Earn money by building the solution	Construct the solution	Low Expertise and equipment
CUJAE and its Hydraulic Research Center	Funds and knowledge for research and education	Find a solution for the problem	Low Knowledge
Residents	Living in Matanzas	Improve the life quality	Low Political
Centre of Environmental Services of Matanzas	Protection of the environment	Protect the existing ecosystem	Moderate Regulations, expertise
International contractors	Earn money by building the solution and setting foot in Cuba	Construct the solution	Low Expertise and equipment

Table 2 – Goal, interest and power of each stakeholder

The table shows that not all the stakeholders share the same goal and their influence on the project differs a lot. Some stakeholders are strong affected by the project but have little power. To relate the power of the stakeholders to their interest a power-interest grid is made. From the figure it can be deducted which stakeholders are more important than others in the development of the project.

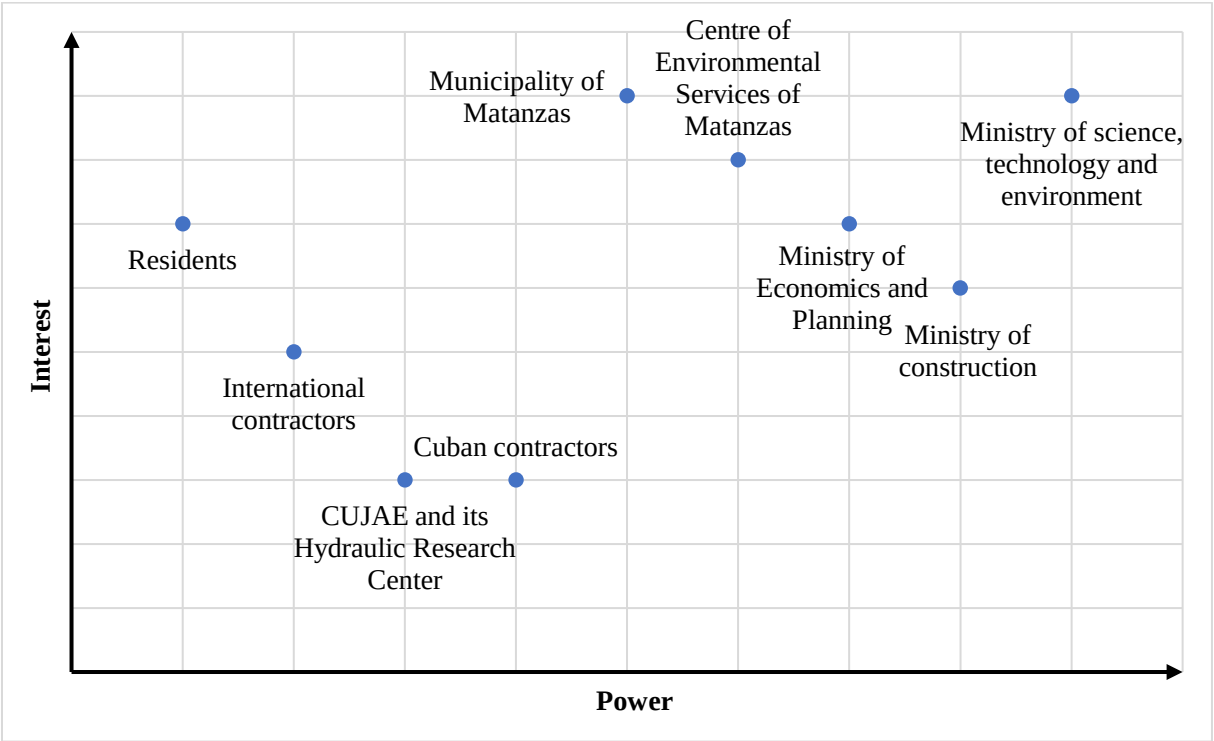

Figure 11 – Power vs interest grid

The figure shows that mainly the governmental parties have high interest and power in the project. The high power is mainly because the project is governmental funded. Their high interest is favorable for the execution of the project.

The parties with high interest and little power consist of mainly the residents and the municipality of Matanzas. The higher authorities must listen to their needs, so in this way they have indirectly more power than initially shows from the figure. The international contractors have more interest in the project than the local ones, because if they get in touch with the project, they also get in touch with Cuban authorities. On the long term they may be able to receive more work in the future. However, the local contractors have more power because the government will always prefer supplying the work to Cuban companies over internationals.

3.2 Program of Requirements

The program of requirements consists out of the functional-, geometrical-, technical- and executional requirements.

Functional requirements

- The CTE should remain operational during extreme weather events
- The design should allow cooling water to enter the CTE via an inlet channel
- The design should allow cooling water to exit the CTE via an outlet channel
- The design should be able to process overland flow due to rainwater
- The design should not create free passage for water during storm conditions through the inlet channel
- The design should create a wave reduction to minimize the impact on the current sea defence

Geometrical requirements

The geometrical requirements consist out of the geometrical boundary conditions that are present within the project area.

- The wall parts A, B and C have a height of respectively, 6.3, 4.6 and 6.3 m
- The inlet channel has a width of 15 m.
- The height of the coast near the CTE is located at MSL +5 m
- The difference in heights between the coast and the ground level is 9 m
- The HWL which includes storm surge is MSL +2 m
- The length of the berm for section A-1 is 17.2 m, B is 43.6 m and C is 38 m
- The distance between the current seawall and the coastline is 10 m for section A-1, 40 m for section B and 30 m for section C
- The foreshore has a slope of 11 degrees
- The outlet of the drainage channel is located at MSL + 5 m
- The coastline is orientated perpendicular to the North-East direction
- The main wave direction is 20 degrees from the coast, which corresponds to an angle of 70 degrees with the normal direction

Technical requirements

- The design should fulfil its functional requirements for a design lifetime of 50 years
- The design must be based on a normative hurricane that has a certain probability of occurrence
- The design must be considering the sea level rise
- The design must be considering the storm surge created by the normative hurricanes
- The design must be considering the significant wave heights created by the normative hurricanes
- The design must be tested on various failure mechanisms that are normative in the scope of the project
- The design should keep overtopping a to be specified minimum amount to prevent flooding due to this event
- The design should prevent flooding due to a combination of overtopping and heavy rainfall
- The design should be able to be built with the materials that are readily available to Cuban contractors
- The design should be able to withstand the impulsive forces created by large hurricane waves
- For the design structure, there should be slim to no settlement
- The failure probability for the different segments should be sufficient

Executional requirements

- The design should be constructible by the available contractors in combination with the approval of the stakeholders and governmental parties
- The design should be affordable

3.3 Fault tree and failure mechanisms

To make an inventory of events that can cause flooding of the CTE Antonio Guiteras a fault tree is constructed, with flooding as the top event. The fault tree is added in Appendix B.

Parallel systems are represented by the 'AND-gate', where all the events need to occur in order to pass the gate. Systems that are in series are represented by the 'OR-gate', where only one of the events must occur to pass the gate. This fault tree is meant as an inventory of failure mechanisms. Failure probabilities and dependencies are not added here. The assumption has been made that the sea defense has a reasonable design and thus is able to withstand a certain level of surge and high waves. Combinations that are very unlikely to occur have been omitted, e.g. tidal elevation alone cannot cause a significant water level rise. And for example, a water level rise alone cannot cause extreme overtopping of the sea defense.

Here the events will be elaborated. The power plant can be flooded either by failure of the sea defense or failure of the drainage system. First the failure of the sea defense will be elaborated.

Failure sea defense

Overtopping

In case of extreme overtopping this means that the sea defense does not fulfill its function and the CTE is flooded. In general, a heavy storm or hurricane will generate high waves which will overtop the sea defense. In combination with a significant water level rise this will lead to extreme overtopping. A significant water level rise can be due to tidal elevation in combination with surge. Surge is caused by three phenomena, wind set up, wave set up and atmospheric pressure. These can all be caused by hurricanes or heavy storms. Overtopping that exceeds a certain limit may cause flooding behind the sea wall leading to a situation where the power plant is not able to stay in operation.

Loss of structural integrity

The sea defense can also fail when strong waves slam into the sea defense and therefore undermine the structural integrity of the sea defense. These strong waves lead to a high peak dynamic load which the sea defense is not able to withstand. The defense can thus be significantly damaged making it unable to fulfill its water retaining function.

Construction and design errors

In case of construction and design errors the sea defense can also fail. This can be due to several factors, such as insufficient strength of the used construction materials, an underestimation of the loads or mistakes made in the execution of the design by the constructor. The consequences of such errors may vary from a little more overtopping due to a wrongly estimated crest height to the loss of structural integrity of the entire wall causing a massive increase in water entering the project area.

External and internal instability

Other events which need extra explanation are the external and internal instability. During hurricane Irma, the major failure of the old sea defense was due to the concrete blocks being displaced. The blocks were not anchored to the seal and could not withstand the external forces of the waves and therefore moved. The new design has a tooth-shaped anchorage to prevent this scenario.

The anchorage needs to suffice on external instability in two ways; the first one is that the teeth might slide together with the soil. Considering the soil is very hard and strong, this is highly unlikely. The second one is that the wall might tilt around the most land inwards tooth.

The anchorage needs to suffice on internal instability as well. The most plausible failure could be that the anchorage is not strong enough and the teeth break off.

As was observed during hurricane Irma, the pushing away of the sea wall elements can cause an opening in the sea wall. This may clear the way for water to flow freely onto the plant site.

Failure of drainage system

Failure pumping station

When heavy rainfall occurs due to a hurricane or heavy storm, this can result in a storm discharge which is more than the capacity of the pumping system, causing flooding of the CTE. The equipment can also malfunction due to other causes such as poor maintenance or equipment that is outdated. Malfunctioning of the equipment might not be a problem if no heavy rainfall occurs and vice versa.

Obstruction drainage channel

The drainage channel can be obstructed by debris that enters during the hurricane. Debris can be vegetation, equipment on the site, pieces of sea wall that have broken off and many other things. An obstruction can limit the draining function as it decreases the cross-sectional area of the channel. This limitation can therefore lead to flooding in the surrounding area.

Conclusion

Using the fault tree, the third sub question can be answered. The two main failure events are failure of the sea defense and failure of the drainage system. The final solution must comply with both failure mechanisms. Improving the existing sea defense is the main objective of this project, but during an intense hurricane the accompanied rainfall must also be considered. Improving the drainage capacity will also be a part of the ultimate design. Also, attention needs to be given to the anchorage of the sea defense, because this was the main failure of the old defense wall.

3.4 Extreme weather conditions

3.4.1 Definition and classification of Tropical cyclones

According to the Hurricane Research Division a tropical cyclone is defined as; 'the generic term for a non-frontal synoptic-scale low-pressure system over tropical or sub-tropical waters with organized convection and a definite cyclonic surface wind circulation (Holland, Belanger, & Fritz, 2010)'. Tropical cyclones (TCs) are further categorized by their maximum wind speed (U10), where U10 is defined as the maximum windspeed at an altitude of 10 m, averaged over 10 minutes (Emanuel). The different TC categories with their respective windspeeds are given in Table 3.

Category	Wind speed [m/s]
Tropical depression (formative stage)	< 17
Tropical storms	17 - 32
Tropical Hurricanes[1]	> 33

Table 3 - Tropical Cyclone Categories

Hurricanes can be classified by their intensity on a scale from 1 to 5 (Saffir-Simpson). This overview is given in Table 4.

Category	Wind speed [m/s]	Central pressure [mb]	Damage
1	33 - 42	> 980	Minimal
2	43 - 49	979 - 965	Moderate
3	50 - 58	964 - 945	Extensive
4	59 - 69	944 - 920	Extreme
5	> 70	< 920	Catastrophic

Table 4 - Saffir-Simpson hurricane damage scale

[1] This is the case in the western North Atlantic and the eastern North Pacific regions. They are called typhoons in the western North Pacific, and severe tropical cyclones elsewhere.

3.4.2 Tropical cyclone formation and development

The formation of Tropical Cyclones starts over ocean waters with a minimum surface temperature of 26 degrees Celsius (Emanuel). Another condition for the formation of TCs is that the earth's angular velocity vector, projected into the local vertical is non-zero. In practice this generally means that TCs originate between latitudes of 5 - 20 degrees NH.

Heat transfer occurs from warm water to air. The warm air rises into the atmosphere resulting in a low-pressure field. Consequently, large amounts of heat energy are release into the atmosphere, generating strong winds. In combination with the pre-existing atmospheric disturbances (on a scale of 1000 - 3000 km) this can result in the development of a TC. The moving air in the atmosphere is deflected by the Coriolis Effect, which leads to the observed counterclockwise rotation of TCs in the northern hemisphere.

In Figure 12 a cross-section of a TC is displayed; the figure is split in two halves which will be discussed separately.

Left half

The colors show the differences in temperature between a point in the hurricane and a point far away at the same altitude. It is seen that the center of the TC has a very high temperature compared to the distant environment at the same altitude. The contour lines displayed in red and white show the radial components of motion. The white lines are the inflow and the red lines are the outflow. Where the inflow reaches wind speeds of around 10 m/s and the outflow speeds of multiple tens of m/s. The most upper red line is not to be mistaken with outflow, but represents a weak inflow, flowing into the center of the TC (Emanuel).

Right half

The black contour lines are the absolute angular momentum. This is defined as:

$$M = rV + \frac{1}{2}fr^2$$

The radius from the storm center is given by r, the tangential velocity is given by V, the Coriolis parameter is given by f. Where the Coriolis parameter is twice the earth's angular velocity vector, placed on the local vertical plane. Figure 12 shows a decrease of M upward and inward, with a strong gradient in the center of the TC (Emanuel).

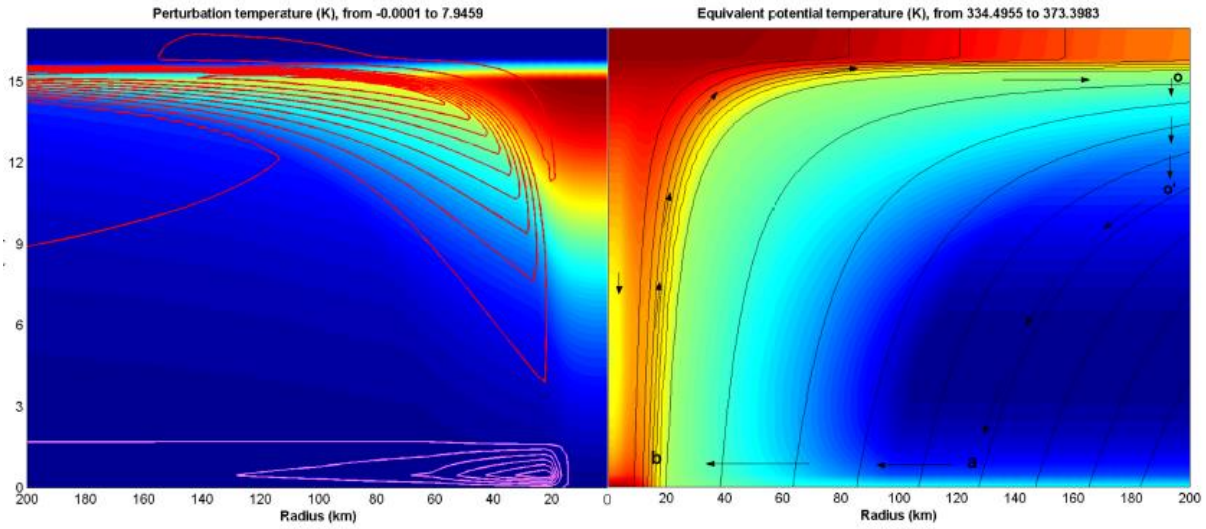

Figure 12 - Cross-section hurricane (Emanuel).

The initial condition for the development of a TC is defined by a low-level vortex of 10 m/s maximum winds. There is an incubation period present which denotes the time period in which the low-level vortex does not

generate maximum windspeeds associated with a TC. In Figure 13 (deep & shallow water), it is seen that after the incubation period has passed the maximum wind speeds drastically increases leading to a TC (Montgomery & Smith).

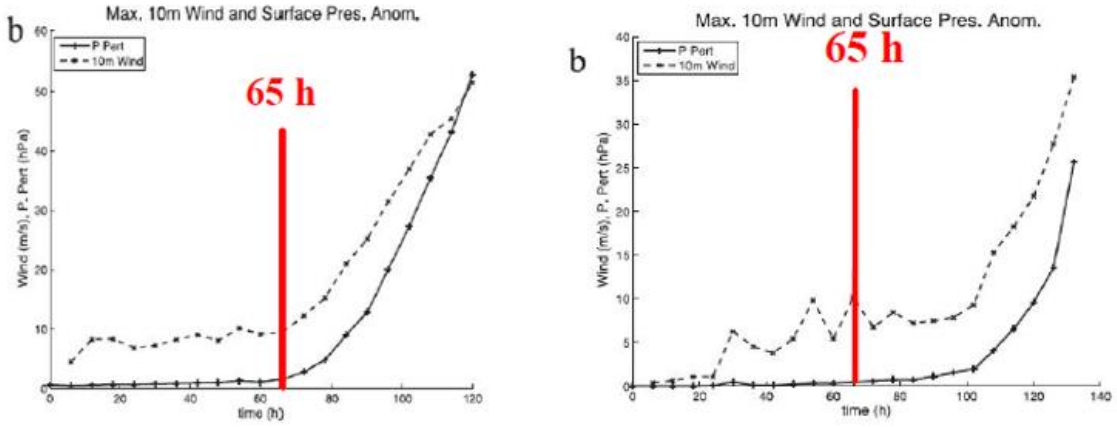

Figure 13 - Incubation period (Montgomery & Smith)

During this incubation period the relative humidity in the midlevel's increases in the presence of a midlevel vortex. The starting point of a TC is the position in which the inner-core air achieves near saturation. A much smaller-scale intense vortex then forms near the surface within this initial vortex and becomes the central core of the developing cyclone (Montgomery & Smith).

3.4.3 Tropical Cyclone Paths

When the TCs originate from the North Atlantic region they tend to move to the west with speeds of around 3 to 8 m/s. This tendency is caused by the trade winds over the tropical latitudes from east to west. The Coriolis effect makes the TCs usually deviate towards the northwest in the northern hemisphere. Since the TCs produce very high wind speeds and pressure difference the direction and speed of these TCs become erratic. Once the TCs hit land or cold water the TCs are not fed with energy anymore, the intensity of the TC decreases and as a result moisture is released which causes intense rainfall. If the TCs manage to survive long enough or are formed at a high altitude, they tend to recurve pole- and eastward. Since they are entrained into the west to east winds that occur in the middle and upper troposphere (2 - 10 km altitude).

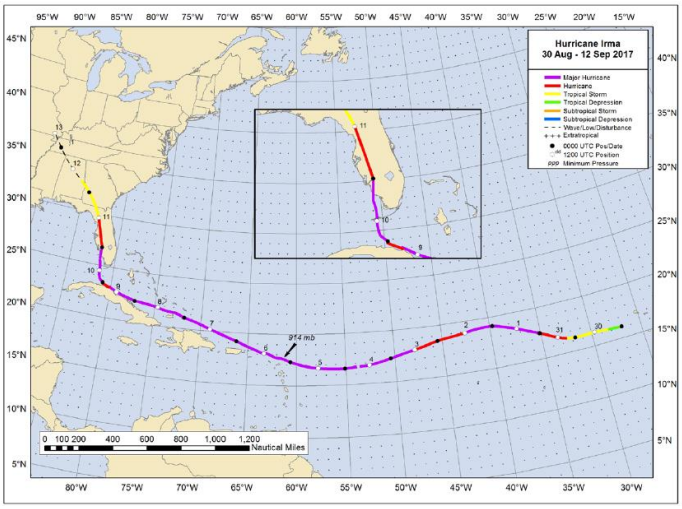

Figure 14 - Best track positions for hurricane Irma (P. & al., 2018).

Furthermore, a seasonality can also be observed in the TC's pathways. A direct link can be made between the path of a tropical cyclone and the global atmospheric pressure field. Since air always moves from high

pressure areas to low pressure areas, low pressure fields attract the TC while a high-pressure field causes the TC to deflect. In august low-pressure fields are common over Florida, causing the TC to travel towards Florida. In September there is a shift towards high pressure in the East coast of the United states causing TCs to deflect more towards the Atlantic. In October the high pressure is located over a large part of the eastern region of the US and TCs hardly go over land. In November the whole eastern region is covered by a high-pressure field and all TCs go to the Atlantic.

3.4.4 Influence of Climate Change on Tropical Cyclones

The year 2017 was denoted as a severe hurricane season in the North Atlantic region. Next to this due to the technological development, urbanization of the coastal areas and greater wealth the economic losses are greater from hurricanes than they were in the past few decades. It is claimed that due to global warming the hurricanes appear more frequently and are more intense. This is said to be true because of the physical cause of the hurricanes, where they feed on warm water and the warmer the water is the more intense the hurricane will be (Homewood, 2019).

From the NOAA's Hurricane Research Division however, it can be concluded that there has not been an increase in the frequency of hurricanes or major hurricanes (hurricanes of category 3 and over) in the North Atlantic region since 1851 when the first records started. These conclusions were drawn based on their HURDAT database, this database also shows that the recent occurrence of hurricanes is not unusual compared to the historical data. Atlantic hurricanes and most importantly the major hurricanes were recorded more frequently between the year of 1930 and 1960 than in the following 3 decades. Then after the year 1990 the frequency of hurricanes returned to the earlier levels of the period between 1930 and 1960. This periodic increase and decrease in the frequency of hurricanes is linked to the Atlantic Multidecadal Oscillation (AMO), which is a natural reoccurring cycle of temperature changes in the temperatures of the sea surface. The tropical storms and the weak hurricanes are not affected that much by the AMO.

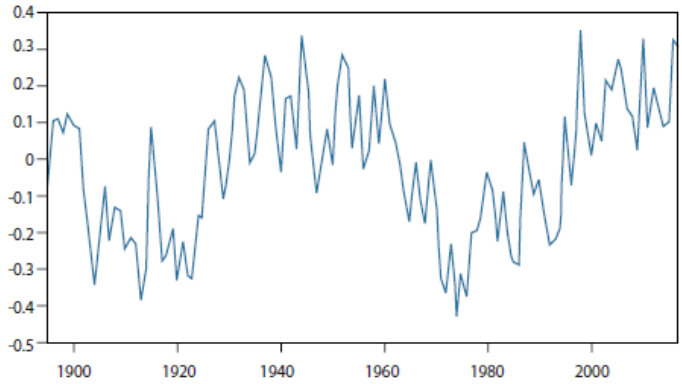

Figure 15 - Atlantic Multidecadal Oscillation 1895-2017

In short, from historical data no statements can be made as to the increase of hurricane frequency. Large hurricanes however have become more extreme.

3.4.5 Physical aspects tropical cyclone

Many physical processes are involved when describing tropical cyclones, which can become very complex. The main interests for the sea defense at CTE Antonio Guiterás are the waves and surge generated by the tropical cyclones. For this reason, that will be the focus in this report.

Wave Generation

Wave generation due to TCs is different from a regular storm; the energy source is moving and rapidly changing direction. The rate of change of the wind speed in a tropical cyclone is therefore much larger, and the duration of a certain wind speed in a TC is extremely short.

Several factors can be distinguished that influence the wave generation due to TCs:

- Conditions prior to hurricane
- Distance to the eye (fetch)
- Maximum wind speed
- Propagation speed of the hurricane
- Central pressure

These items and their interaction will be described in the remainder of this section.

Firstly, the conditions prior to the TC play a large role in the so-called sea severity during the TC. The sea severity is defined by the significant wave height, where a large significant wave height means a severe sea. According to (Ochi, 1993) there are two different situations that can be distinguished that show a clear relationship between wind speed and sea severity.

Situation 1: Calm seas prior to the TC
Situation 2: Continuous winds for larger periods prior to the TC

For the first situation an almost linear situation can be identified between significant wave height and wind speed, which is derived from Figure 16. In Figure 16 it can also be seen that the sea severity during the growing stage of the tropical cyclone is less than in a fully developed sea.

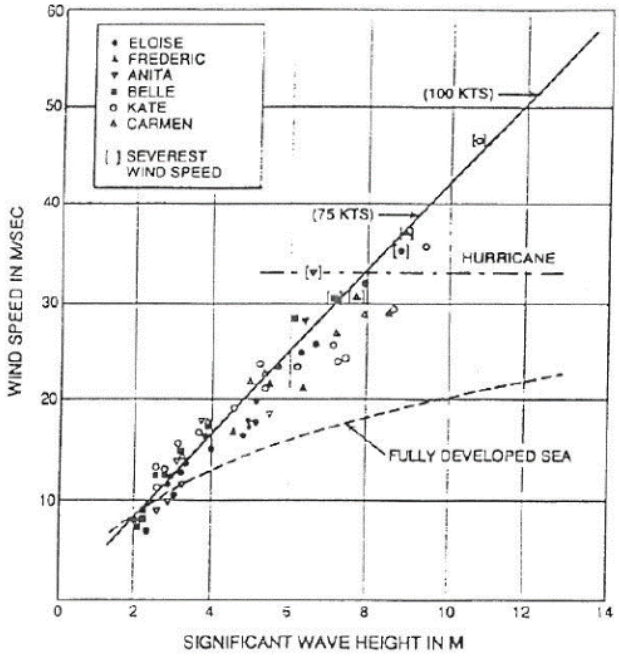

Figure 16 - Significant wave height vs wind speed moderate seas (Ochi, 1993).

For the second situation where moderate winds have continuously been blowing for approximately 10 days this leads to more severe seas even for a moderate TC. Since in this situation the seas more closely resemble a fully developed sea the wind energy can be fully transferred into wave augmentation and not in wave generation, causing higher significant wave heights and thus a more severe sea. This is illustrated in Figure 17 where the significant wave height is plotted against the wind speed for hurricane Gloria, a hurricane that matches with situation 2.

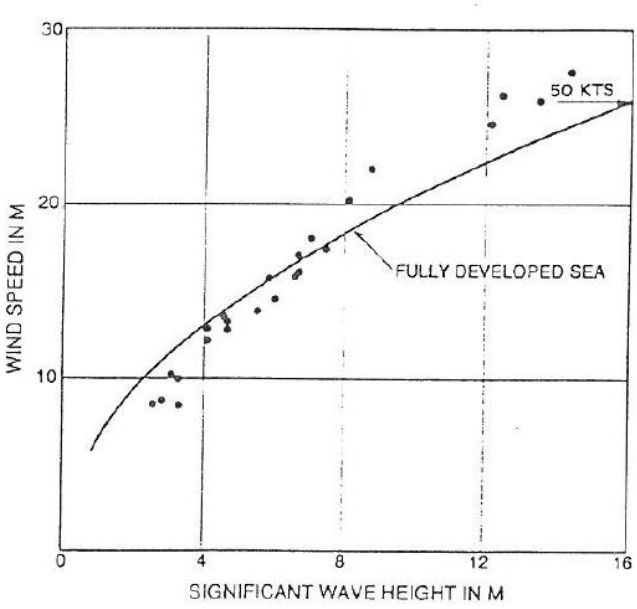

Figure 17 - Significant wave height vs wind speed hurricane Gloria (Ochi, 1993)

As can be seen in Figure 17 the wind wave relationship more closely matches the fully developed sea trend, and already for smaller wind speeds the sea is more severe than for TCs in Figure 16.

Distance to the eye

The winds within the TCs flow cyclonically (following the local vertical component of the earth's rotation). However, near the upper part of the TC the winds reverse and flow anticyclonically (apart from the TC's center). The wind speeds rapidly increase going outward from the TC's center. At a distance between 10 and 100 km from the center the wind speed is maximum, in this area the generated waves will also be largest. The exact wave height distribution in a TC will be discussed more in depth in the following section. Going further away from the TC's center the wind speed decreases more gradually, following an $\frac{1}{\sqrt{r}}$ decay close to the position of the maximum wind speeds. Further away from the center of the TC the wind speed starts to decrease more rapidly. At a radius of about 100 to 1000 km from the center the wind speeds are of a magnitude that is comparable to normal wind speeds observed in the atmosphere day in and day out. The maximum wind speeds generated by the TC occur near the sea surface. An approximation of the wind near the sea surface can be made by taking the vector sum of the wind and translation velocities generated by the storm (Emanuel).

Coupling the wind to the waves, a non-linear relationship exists between the maximum wind speed and wave height. The difference between the intensities of TC's result in a different distribution of wave heights with respect to the distance from the TC's center. For a higher maximum wind velocity there is a more gradual decline in the significant wave height with increasing distance from the TC's center.

Maximum wind speed and forward speed of the Tropical Cyclone

The forward movement of the hurricane plays an important role in the generation of the wave field in combination with the maximum wind speeds. In the northern hemisphere the TC rotates counterclockwise, thus the maximum wind speed occurs in the right quadrant where wind speed and TC speed are in the same direction. The maximum wind speed is observed 70 degrees from the direction of the forward movement; this is consistent with NOAA observations (Young, 1988). The right quadrant is also where the waves are largest, since these waves travel approximately in the same direction as the TC this maximizes the duration over which they experience strong winds.

The forward speed of the TC relative to the wind speed is also important for the wave pattern. If a TC is relatively slow, the dominant waves will have a group velocity larger than the velocity of the TC and will therefore travel ahead of the TC as swell. In the case of a relatively fast TC there is no swell travelling in front of the TC. The average forward velocity of a hurricane is 2.5 - 5 m/s.

The maximum wind speed also influences the amount of swell travelling in front of the TC. With increasing maximum wind velocity, the peak frequency in the wave spectrum decreases which consequently means the group velocity of the waves increases. A larger group velocity means that the waves also travel in front of the TC, dependent on the forward speed of the TC.

The relationship between the significant wave height and V_{fm} (forward speed of the TC) for different V_{max} (maximum wind speed) is given in Figure 18. A clear peak can be seen for different wind speeds where the different combinations of V_{max} and H_s result in a shift of the peak towards a higher V_{fm} for higher maximum wind speeds.

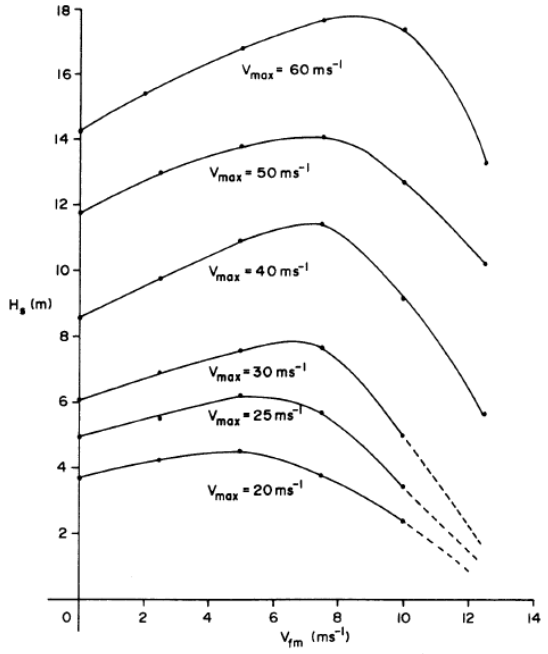

Figure 18 - Significant wave height vs Vfm for different Vmax (Young, 1988)

(Bretschneider, 1957) proposed that the maximum wave conditions occur when the forward speed of the TC equals the maximum group velocity. In this case waves move forward with the TC and therefore experience an extended fetch.

Surge & Central pressure

Surge is a phenomenon created by the combination of inverse barometric effects and air-sea interactions. The inverse barometric effects create a local atmospheric low-pressure field, which causes the water level to rise locally. This is seen most extreme in the eye of the cyclone, where the most extreme low-pressure field creates the biggest disturbance of the water level, resulting in an increase of the water level from about 0.5 to 1 m. These low-pressure fields also create winds which in turn amplify the surge due to the interaction of the air with the sea-surface which is denoted as shear stress.

More specifically, during the extreme conditions of a cyclone, the momentum transfer from the atmosphere into the ocean is the dominant process. This results in the generation of surge and waves that then interact with each other. The wave field that is generated results in radiation stress gradients which affect the water level and the currents (Vatvani, Zweers, & al., 2012).

The center of the TC is continuously moving, and thus the rise in water level associated with the low pressure in the center is also moving. At the new location a rise in water level is induced which interferes with the previous point, in this manner a forcing pattern is introduced causing infra gravity waves with a complex interference pattern. In combination with wind this also causes surge.

It is important to also consider the amplifications of the shallow area near the coast, including wave setup and in the case of a gentle slope also the wind setup.

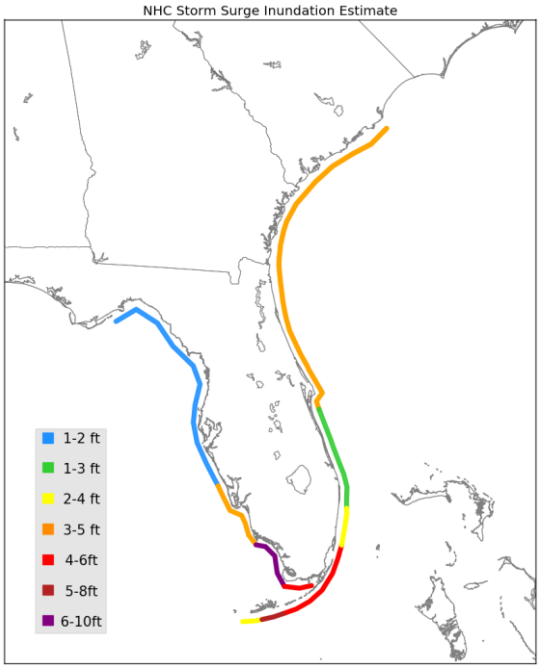

Figure 19 - Storm surge inundation (ft above ground level) from hurricane Irma (P. & al., 2018).

3.4.6 Cold fronts

Other meteorological events that may cause a water level rise, are cold fronts. A cold front is a surface which separates a mass of cold, dry air at a high altitude from a mass of warm, humid air at a lower altitude. The warm and cold masses are passing over each other, therefore the warm and humid air condensates and rain is formed. For this reason, cold fronts are characterized by a mass of dry air accompanied with very strong winds and heavy rainfall. The winds can be very strong, especially when they come from the North-West due to the big fetch.

Cold fronts can by categorized by their wind velocities (Table 5), but also on their origin based on the turning of the wind at the surface. The Cuban Meteorological Institute uses the following classification:

- **Classical fronts** move in the Gulf of Mexico or territories adjacent to the United States. This type of cold front at first produces southerly winds. When the low centre moves towards Cuba the direction of the wind changes to west/northwest. Along with the change of direction the wind velocity increases. Behind the cold front a high-pressure zone with low temperatures is located.
- **Revised fronts** produce a wind from eastern to northern direction when affecting Cuba. These are accompanied by a temperature drop and increasing rainfall.
- **Secondary fronts** strike Cuba one or two days after a classical cold front. These maintain the previous barometrical system but results in small discontinuities in the meteorological elements.

Classification	Maximum mean wind velocity (km/h)
Weak	< 35
Moderate	36 - 55
Strong	> 55

Table 5 – Classification of cold fronts by wind velocity

The occurrence of cold fronts in Cuba have been measured by the Instituto de Meteorologia, Cuba, over a period of 60 years. In the past 60 years the maximum number of cold fronts observed is 35 and the minimum is 11 in one year. On average some 21 cold fronts are observed in a year (Instituto de Meteorlogia Cuba, 2013).

Cold fronts are most likely to occur during the winter months December till March. The fronts originate in the North Pole and travel southbound through the Gulf of Mexico and from there they travel eastward through the Caribbean. They have a big impact on the coastal areas of Cuba, such as Havana and Varadero. However, the coast of Matanzas is less affected by these cold fronts. Analyzing this phenomenon in the past, a cold front never caused flooding in the project area. One of the consequences of a cold front is that the waves will arrive from the North-West. The coasts of Havana and Varadero are located perpendicular to the North-West, which is not the case for Matanzas, which is located perpendicular to the North-East. Therefore, waves generated by cold fronts have little impact on the project site. For this reason, the project focusses only on tropical cyclones.

3.5 Coastal analysis of the project area

3.5.1 Bathymetry around the project area

The bathymetry around the project site is displayed in two figures. Figure 20 shows a 2D top view of the bathymetry of the project location. The deepest part visible on this figure has a depth of MSL -570 meters and is visible with the dark blue color in Figure 20. The highest part of the figure is about MSL +133 meters and can be observed with the green colors. Figure 21 shows a 3D plot of the bathymetry around the project area. Also, in this plot, the deepest part is around MSL -570 meters and the highest part is located at MSL +133 meters.

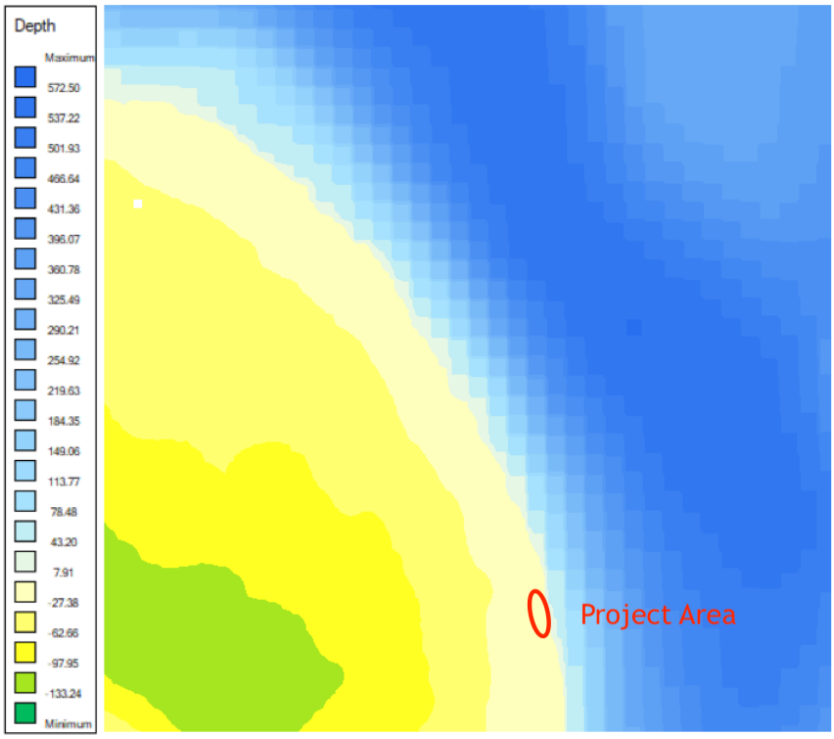

Figure 20 - Top view of the bathymetry of the project location (Deltares, 2019)

The area of interest is placed on a shelf close at the coast. The bathymetry and available videos of the project area show that the project area is situated on a horizontal section of land. This information comes in handy for the water management study later in this report. A horizontal area gives less opportunities for the overtopping of water and precipitation to be discharged under natural circumstances back to sea or other destinations.

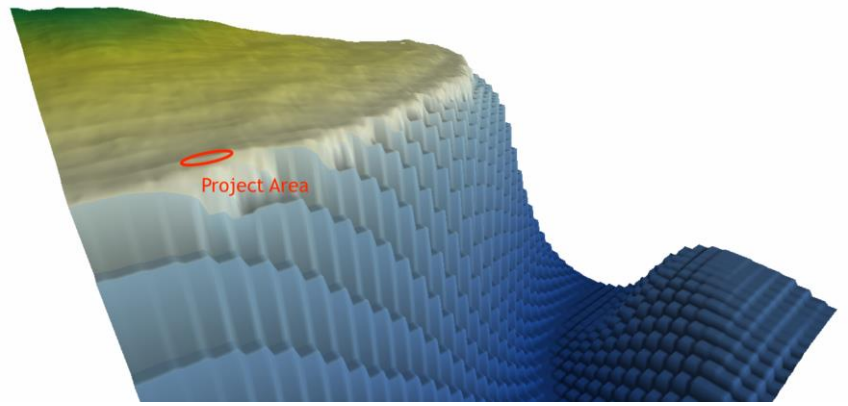

Figure 21 - 3D perspective of the bathymetry of the project area (Deltares, 2019)

Another observation of Figure 20 and Figure 21 is that the depth right in front of the project area is increasing rapidly. The expectation will be that this bathymetry will hardly lead to any nearshore hydrodynamic changes. Less nearshore hydrodynamic changes will lead to less increased surge and less increased wave heights, which may give opportunities to have a lower crest of the sea defense as compared to sea defenses in other regions. However, those near shore processes will be evaluated by XBeach more properly later in this research and the opposite may be stated.

3.5.2 Bathymetry of the project area

The height of the project area behind the sea defense and the height of the old sea defense is of much relevance in this study as well. The bathymetry of the project area relative to MSL may define whether the overtopped water and precipitation will be able to flow back to the sea under natural circumstances. Also, the level of the old sea defense defines the basis for the new sea defense. These levels can be estimated with help of the available videos, available bathymetry and the available reports. Unfortunately, the drawings of the new sea defense are very limited, and levels are not clearly specified.

Use of estimated high-water level

The videos show that the land behind the sea defense is higher than the storm surge of hurricane Irma together with maximum tides. This can be concluded since water is not directly flowing into the project area between the broken sea defense parts. Furthermore, the water in the entrance channel takes more or less the same water level of the high-water level, since it is directly connected through a gap with the sea. While the waves and surge, are attacking the sea defense, the videos show clearly that the water in the entrance channel is lower than the height of the project area. Figure 22 shows these descripted circumstances. It can be safely assumed that the water level in the entrance channel is about 1 meter higher than the high-water level at sea, due to wave set up pressures and overtopping that ends up in the channel. Also, visual observations from Figure 22 show that the project area is about 2 meters higher than the high-water level.

Figure 22 - Overview of entrance channel and overflow through broken sea defense (Video footage of Irma razing over the power plant, 2017)

The tide around Varadero take maximum values of about MSL +0.34 m (de Boer, Poelhekke, Schlepers, & Vrolijk, 2014). For this rough assessment, these values can be applied on the Matanzas coast as well. Furthermore, the National Hurricane Centre gives rough estimates of the storm surge around the coast of Cuba. The NHC describes that the storm surge in front of the northern coast of Cuba due to Irma was between two and three meters (National Hurricane Center, 2018). The high-water level could be estimated to be around MSL +3.5 m. By adding all the aspects of this rough analysis, the project area could be estimated to be 6.5 meters above mean sea level.

Use of wave heights

Another estimation technique consists of using the overtopping wave heights. The videos show that only a few waves result in overtopping over the sea defense that has still its integrity. This means that the waves that cause overtopping have heights of about $H_{over} \approx 1.5 \cdot H_s$. Observed wave heights in front of the coast of Cuba differ between 5 and to 8 meters (National Hurricane Center, 2018). The wave heights that result in overtopping have heights of about $H_{over} \approx 1.5 \cdot H_s \approx 10.5\,m$. The crest of the overtopping waves is in general higher than half of the wave height above the high-water level due to skewness. Therefore, the top of the structure will have a height of $3.5 + 0.6 \cdot 10.5 = MSL + 9.8\,m$. The top of the structure is about 3 meters higher than the height of the project area. The height of the project area can be estimated to be about MSL +6.8 meters.

Use of bathymetry

The last estimation technique used to determine the height of the project area above MSL, looks at the available bathymetry of the project area. Delft3D – QUICKIN reads out the provided bathymetry of the area. Some problems can come along with reading out this bathymetry. The values of the bathymetry might have an unknown offset. Also, the bathymetry points are not closely packed. In the interpolation in between these points, errors may arise as well. The best estimate of the height of the land of the project area based on the bathymetry would be MSL +10.3 meters.

Figure 23 - Entrance channel barrier under calm weather conditions

Use of photos

Photos have been made of the damage due to hurricane Irma. One of the photos was made of the entrance channel and can be observed in Figure 23. This channel connects with the sea and, hence, the water levels within the entrance channel correspond to the water level. The photo is made under calm sea and weather conditions. The assumption may be safely made that storm surge is not present in the photo. The tides vary between MSL -0.20 m and MSL +0.34 m. These are rather small tides and the water level on the photo is assumed to be more or less equal to MSL +0.0 m. It is assumed that the man in the photo has an average length of a Cuban man of 1.70 m. With help of the ratio of the size of the man compared to the height of the

sill, the height of the entrance barrier can be calculated. This estimation method offers a height of the entrance barrier of more or less MSL +6.0 m.

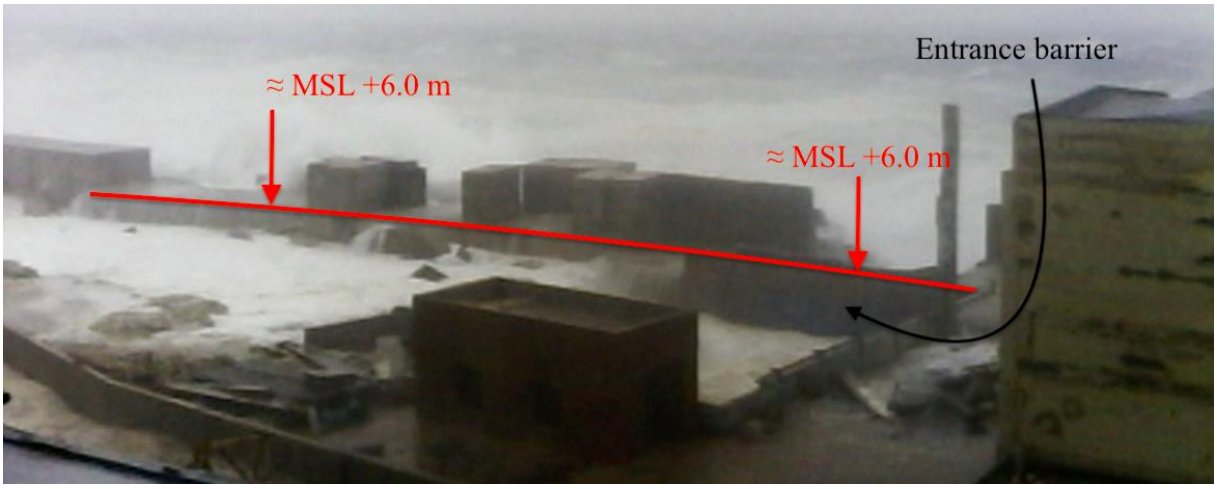

Figure 24 - height of the sill of the original barrier foundation

Figure 24 shows how the height of the entrance barrier compares to the height of the sill of the original barrier foundation. The photo is taken from one of the videos that was made of the hurricane that was rushing over the project site. This photo shows how the sill of the original barrier foundation is situated at the same level as the entrance barrier at MSL +6.0 m.

Figure 24 also gives information about the surface level of the project site. The figure shows how the project site is situated one meter below the level of the sill. The project site is situated at about MSL +5.0 m. The surface level of the project site is not perfectly horizontally. The videos made of the event show how overtopped water is flowing over the project site parallel to the coastline. This current showed unevenness in surface level and deviations of ±1 meter may occur.

Conclusion – height of the sill of the old foundation

By taking the different methods of determining the height of the project area into account, an estimate can be made of the height of the sill of the foundation and the height of the ground of the project site. An overview of the estimated heights can be found in Table 6. The bathymetry method is not reliable at all, also since the estimated height of the bathymetry differs much from the other estimation methods. Therefore, it is chosen to leave this result out in combining the different methods to one result. The photo method is a very reliable method and the other two estimation methods are reliable enough to confirm the order of magnitude of the photo method. The height of the sill of the old barrier can be estimated to be at ±MSL +6.0 meters. The height of the project area could be estimated to be ±MSL +5.0 meters.

Type of Method	**Height compared to MSL**
High-water level method	+6.5 m
Wave height method	+6.8 m
Bathymetry method	+10.3 m
Photo method	+6.0 m

Table 6 - Estimated heights of the sill of the old barrier

A report presented by prof. Cordova displays a certain cross section of a piece of coastline in front of the CTE of Matanzas (Unknown Author, 2017). This cross section can be observed in Figure 25. The figure shows a submerged shelf just below the water line. Bathymetry data shows how the depth is increasing rapidly after this submerged shelf has finished. This rapidly increasing depth happens just outside the figure on the right side. The figure also shows how there is a small coastal cliff above the water line. The top of this

cliff is at MSL +5.0 m. From there on the land gradually rises. All the ground materials consist of stone with macro pores (Cordova, 2019).

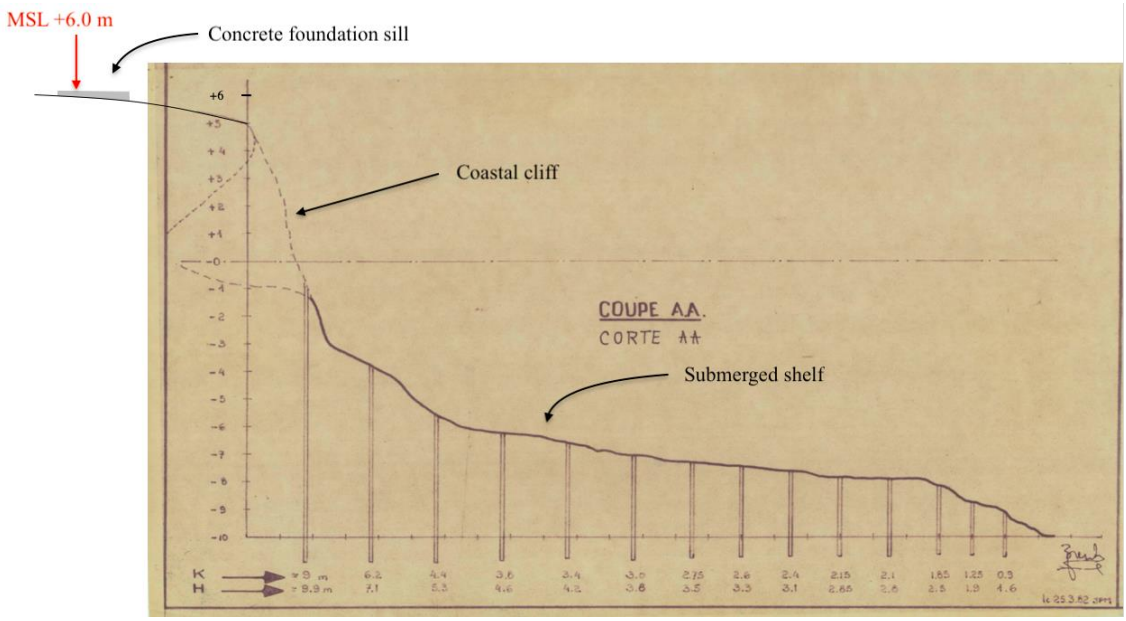

Figure 25 – Certain cross section of coastline in front of the CTE of Matanzas

The sill of the old coastal defense is poured right on the existing ground material of stone with macro pores. This sill is poured about 10 to 25 meters more land inward, measured from the corner of the coastal cliff. Figure 26 shows how the old foundation sill is destroyed by the hurricane as well (Video footage of Irma razing over the power plant, 2017). A few conclusions can be drawn from visual observations of the photo made after the destructive hurricane Irma passed by. It can be concluded that:

1. the concrete sill is not reinforced with steel;
2. the sill is not anchored to the ground stone material;
3. the concrete blocks are not anchored to the sill.

The damage might not have been of the same scale if reinforcement in the sill would have been applied and anchors between the blocks, sill and ground would have been used.

Figure 26 - Concrete sill as foundation for the old sea defense (Video footage of Hurricane Irma, 2017)

Conclusion – height of the sill of the new foundation

For the new design, a height of MSL +5 is used. This is based on the heights that the Cuban contractors use for the new sea wall.

3.5.3 Sea level rise

With designing a coastal defense, the sea level rise (SLR) due to the changing climate should be considered. The changing climate is driving different mechanisms that influence the SLR up or down. The SLR is different for each location due to those different mechanisms that are different for each location. Studies that estimate the SLR differ much in their prediction due to different interpretation of those driving mechanisms. The SLR is accelerating and will further accelerate due to the anthropogenic influences. There are also positive feedback systems built in the SLR, which may lead to even more acceleration in the SLR later on (Scott, Simpson, & Sim, 2012).

A study of Scott, Simpson and Sim combines results of different studies to SLR in one paper (Scott, Simpson, & Sim, 2012). Scott, Simpson and Sim report that the average SLR has been 3.4 mm/year between 1995 and 2010 (Rahmstorf, 2010). This SLR has been greater for these years than earlier has been predicted. If this value is adapted in the design life of the coastal defense at the CTE, then the SLR to consider would be 17.0 cm. However, this value would be an extrapolation that does not take the positive feedback factors in account that accelerate the SLR. Therefore, a different approach should be considered.

Another approach could be to look at different studies that make a prediction and take positive feedback and other acceleration factors into account. Scott, Simpson and Sim have investigated five different studies of which four of those studies predict that the SLR will be at least 1 meter in 2100. 2010 is chosen as the base year where SLR was set equal to 0 m. Figure 27 shows a schematic graphical representation of the SLR up to 2100. The year 2010 is chosen as the base year and the years in which the sea defense should be functioning is marked as well. By interpolating within the graph, an estimated SLR of ± 46.0 cm can be found.

Some deviation in this value should be considered. An estimate of the standard deviation would be 10% of the nominal value, $\sigma = 4.6\ cm$. This standard deviation can be adopted based on the following reasons. The predictions of 1.0-meter SLR might differ from the actual value. Also, the course of the graph is not based on any formula with scientific proof. The course of the graph is based on visual observations of similar graphs of SLR that were polluted with many other unnecessary curves. However, the fact that the course could be a bit off, means that the predicted SLR would not necessarily lead to much difference in value.

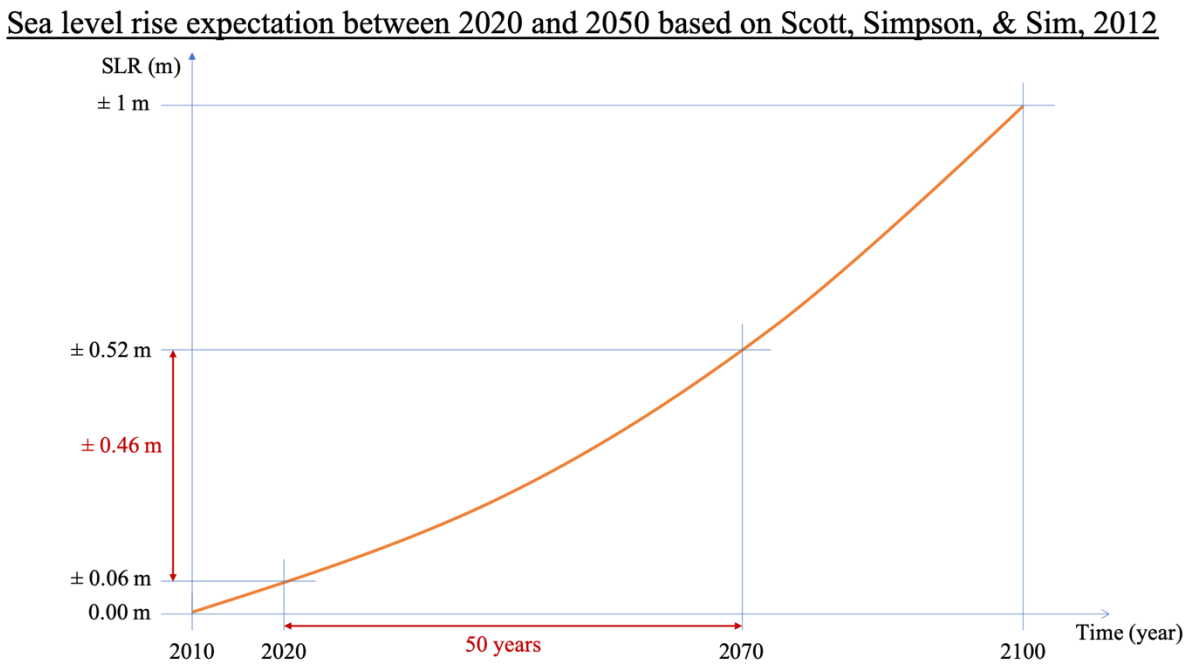

Figure 27 - Sea level rise between 2020 and 2050 based (Scott, Simpson, & Sim, 2012)

3.5.4 Rainfall

Along with the extreme hydrodynamic events of hurricanes, extreme rainfall events come along with hurricanes as well. This extreme precipitation might be the cause for water problems at the project area as well. At first, the catchment area that will be responsible for potential water management problems will be defined. Secondly, a lumped model will be used to make a grounded estimate for the water problems. Finally, the different parameters of the lumped model are defined.

Precipitation catchment area

The project site is situated at the coastline at the toe of a slope. The catchment area will define the domain in which all precipitation will fall and consequently run off to the project site. Fallen rain find its way by running off over parts with the steepest slopes. The water catchment area can be shaped. Due to the lack of much data about the project area, a simple model will be constructed.

Figure 28 shows the basis for the run-off model that will be used in this study for the precipitation. The figure shows the bathymetry uphill of the project area. The figure shows the depth contours of the area. All visualized areas have values above sea level. Based on this bathymetry, a prediction can be made which water particles will run off into the project area. Run off routes of water particles will follow lines perpendicular to the contour lines of the bathymetry map. A catchment area can be constructed by following those lines perpendicular to the contour lines starting with the size of the project area. The catchment area is defined by the two outer two lines that run perpendicular to the contour lines. In Figure 28 these are represented by the outer dark blue lines.

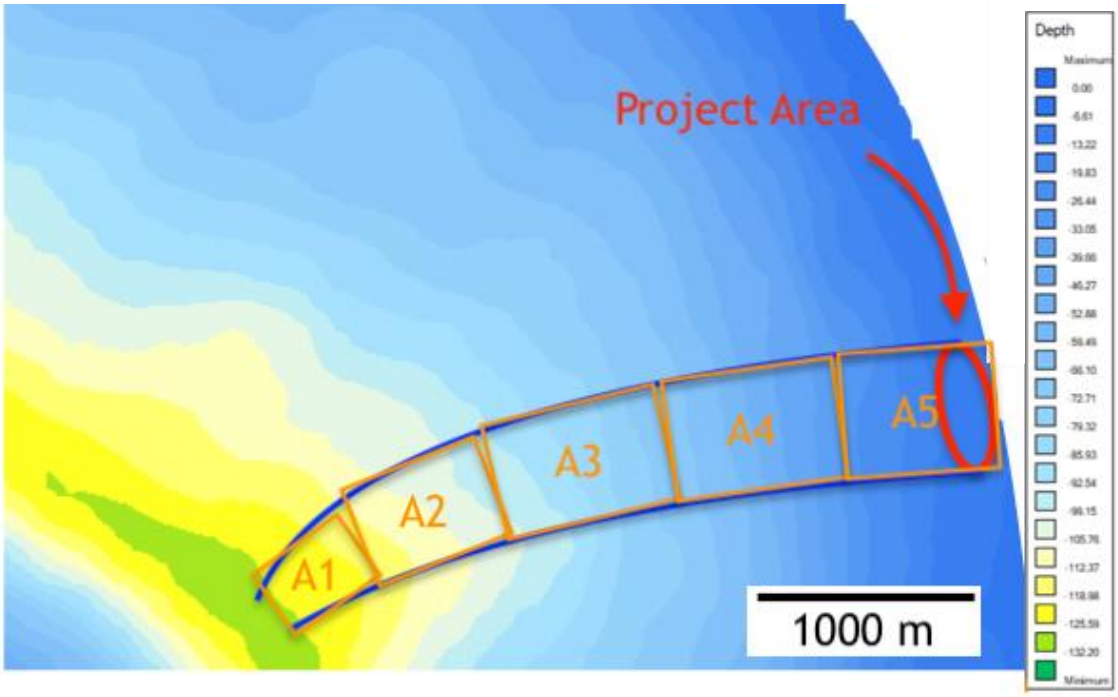

Figure 28 – Basic lay-out of run-off model (Deltares, 2019)

The catchment area is divided in five sub-areas. These sub-areas are drawn in Figure 28 as well. The sub-areas are chosen such that their shapes fall nicely within the boundaries of the total catchment area. These smaller squared sub-areas within the total catchment area make it possible to calculate with a randomly shaped catchment area, since squares are easy to calculate with. Also, for a few sub-areas the outer catchment area lines can be followed more naturally. The size and steepness of those sub-areas will be considered in the study below.

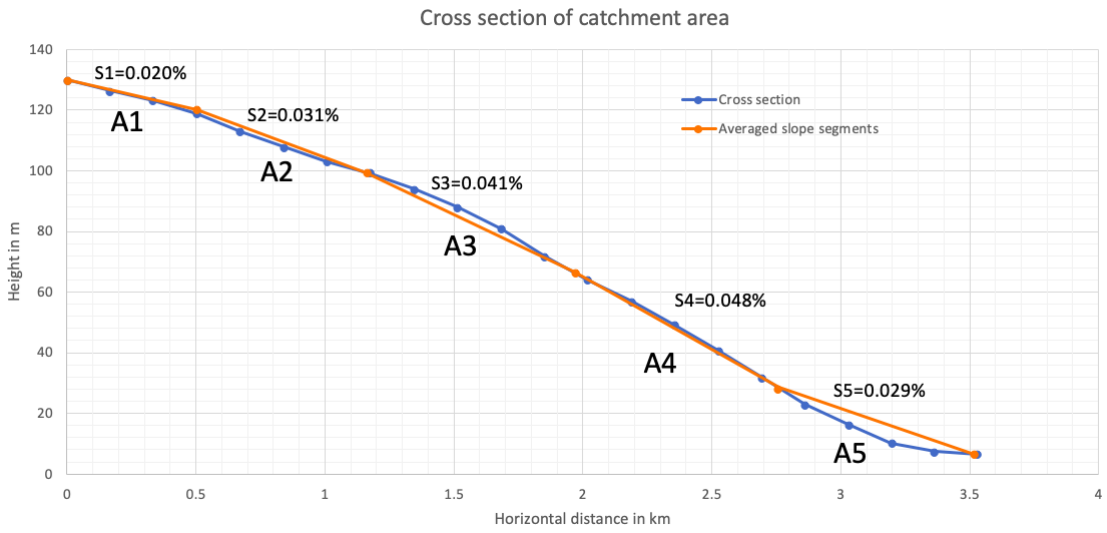

Figure 29 - Cross section of catchment area

The area is estimated by measuring the sizes of the sub-areas and by scaling these measurements to the right units. Furthermore, a line is drawn through the middle of the catchment area that runs from the highest point to the lowest point at the project site. Along this line, the bathymetry is evaluated and plotted in Figure 29. The steepness of the different sub-areas is evaluated using this plot. The area and the steepness of the sub-areas are orderly displayed in Table 7. Furthermore, information about the steepness is also found graphically in Figure 29.

Section	**Area (km^2)**	**Length (km)**	**Height (m)**	**Steepness (m/km)**
A1	0.156	0.50	10	20
A2	0.304	0.66	20,5	31
A3	0.444	0.81	33	341
A4	0.397	0.79	38	48
A5	0.415	0.76	22	29
Total	1.716	3.52	123.5	33.8 (avg)

Table 7 - Areas and steepness of the sub-areas in the catchment area

Lumped model

The lumped model will be used to make an estimate for the precipitation that will run off into the project area. The lumped model as used in this report can be graphically observed in Figure 30. The lumped model of this project considers that sub-areas have a precipitation input, storage capacity, infiltration flux and a transportation flux. The lumped model could also be observed as different buckets that have fluxes into and out of this bucket. The modelled catchment area has five sub-areas. Hence, the lumped model of this project has five of those buckets. The different fluxes will be discussed in the underlying summation before quantifying the different fluxes:

- **Precipitation**: Rain will fall into the sub-area. The magnitude of this flux is depending on the precipitation rate and the size of the simulated area. The precipitation flux in the lumped model is a discharge. This flux can be observed in Figure 30 with the dark blue arrows as Qt. In reality, it might happen that the precipitation rate may be different for the different sub-areas. This refinement will be left out of the model to the lack of enough information.
- **Storage**: Every sub-area has some potential to hold some volume of water. The fallen water may be held in forms of saturated soil, pools, puddles, and water that hangs on or lays on top of vegetation. The storage capacity of the sub-areas depends on the steepness of the slope of the sub-areas. Puddles, pools and other small basins have less potential to be created on steeper grounds. This storage factor

in the lumped model will therefore be compensated with a factor depending on the steepness of the hill. The storage is expressed as a volume and can be observed in Figure 30 (S).

- **Infiltration**: Another flux in the lumped model consist of the infiltration. A part of the fallen rain will infiltrate into the soil such that less water will run off into the project area. This infiltration is different from saturation. Saturated soil contributes to the storage capacity and a saturated soil will not allow for further saturation. However, infiltrated soil will still allow for more water to be infiltrated. In this lumped model, the infiltration of the water in the soil is dependent on the storage of the area. This assumption is based on the fact that more storage will lead to more potential to find new ways to infiltrate in the soil. The quantity for this infiltration is a discharge flux. This flux is observed in Figure 30 with the red arrows as Qi.
- **Transportation**: All water that comes into the model and that does not find a way to be stored or infiltrated in the soil, will be passed on to the next sub-area. The quantity for transportation is a discharge flux. This flux is to be observed in Figure 30 with the brownish arrows as Qt.

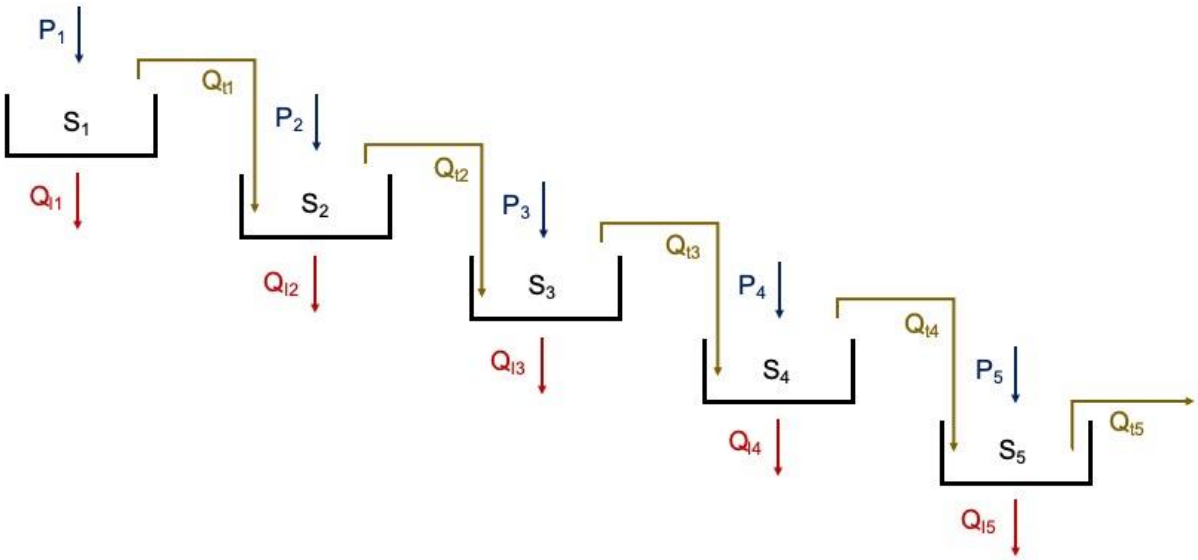

Figure 30 - Lumped model.

The last transportation flux, Q_{t5}, will run off into the project area of interest. This flux is of relevance for the project as the drainage systems will be designed around the area of interest to prevent for flooding.

Evaporation is kept out of this lumped model for simplicity and due to fact that the evaporation is insignificant. Evaporation becomes interesting as longer time scales will be modelled. This model will be used to simulate a maximum amount of about five days. For those short periods of time, the evaporation fluxes will be insignificant and the other fluxes in the model are of much more relevance. Furthermore, hurricane events go together with cloudy circumstances. Less evaporation will happen due to the lack of decent radiation that can contribute to evaporation under cloudy circumstances.

Quantifying parameters of the lumped model

Short descriptions of the chosen quantified parameters for the lumped model will be given. These quantified parameters are dependent on the catchment area characteristics and the sensitivity to receive much precipitation with hurricanes.

Precipitation

A good estimate for the amount of precipitation is the basis for the water management model in this study. However, the total amount of rainfall and the intensity of the rainfall events due to hurricanes may differ greatly per hurricane. The short summation below gives more insight in the different phenomena that lead to the large differences in rainfall events between different hurricanes. Schauer tries to explain these phenomena

of rainfall events due to hurricanes in her study and concludes that the precipitation due to tropical cyclones may depend on (Schauer):

- Movement: Slower moving hurricanes have more potential to lead to more precipitation.
- Storm size: Larger storms cover larger areas and have more potential to result in more precipitation at a specified location.
- Storm track: The hurricane track determines where precipitation will occur. In general, the most precipitation will fall closer to the hurricane eye.
- Topography: Upslope areas relative to the hurricane track movement are prone to receive more precipitation.
- Moisture: Entrainment of moisture results generally in more precipitation.
- Interaction with other meteorological features: The rainfall distribution may be greatly affected by interactions with different meteorological phenomena.

The summation above shows the complexity of making good estimates for the amount and the intensity of precipitation in the catchment area upstream of the Matanzas CTE. To be able to find precipitation data that can be used for this water management study, data of past hurricanes will be used. Hurricanes that have had severe impacts on the Matanzas area have been selected. These results have been plotted in a scatter plot and a fit is made through the scarce amount of data. The results of this plot are found in Figure 31.

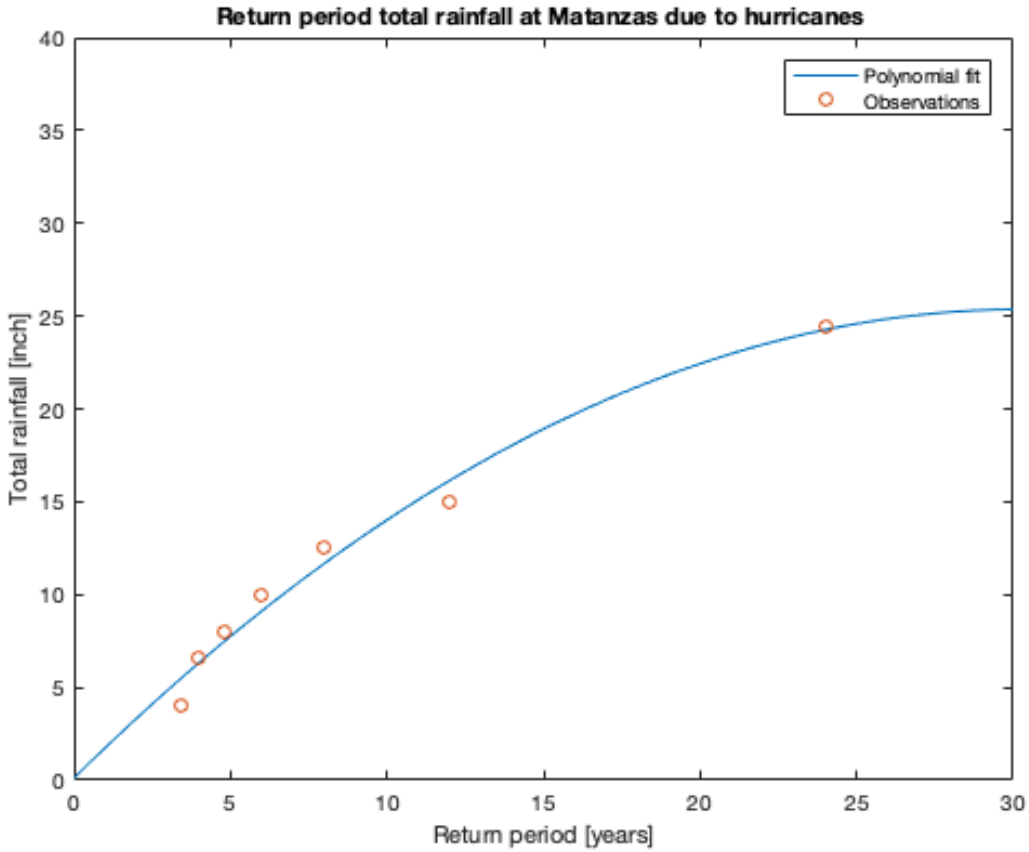

Figure 31 - Return period total rainfall at Matanzas due to hurricanes found in several 10 different hurricane reports of the national hurricane center (National Hurricane Center, 2018)

The result that is present around a return period of 24 years seems a bit off compared with the other results. Hurricane data shows that such heavy rainfall is possible. For the other data points, it could be the case that factors, described in the paragraph above, were not in favor of much rainfall at Matanzas. It can be safely assumed that a total rainfall of at least 25 inches (635 mm) is a possibility for the area of the CTE at Matanzas with a return period of 30 years. The lifetime scope of the project consists of 50 years. The expected total rainfall will therefore take higher values than the value that has a return period of 30 years. Unfortunately,

the fitted curve and the available data does not suit well for drawing conclusions about rainfall expectations larger than 25 inches. The value of 25 inches as total rainfall will be used in this study with the side note that larger values might be realistic.

Figure 31 describes the total rainfall in the total period that the hurricane is passing the project site. Besides the total amount of fallen rain, the precipitation rate is of interest for this water management study as well. The maximum precipitation rate will give information about the intensity of the precipitation, how much precipitation will fall in a short period of time. The intensity of the precipitation is more related to the maximum discharges of the runoff levels and the challenges that come along with high discharges. Large total rainfall amounts that are spread out over large periods of time give less challenges due the smaller discharges that come with larger time spans.

The data available for this study tells unfortunately not much about precipitation rates in tropical cyclones and hurricanes. One study of the precipitation about hurricane Harvey can provide new information for this water management study (van Oldenborgh, et al., 2017). Van Oldenborgh et al. investigates the precipitation rates of Hurricane Harvey. Figure 32 shows the precipitation rates and the cumulative precipitation fallen in Houston, TX due to hurricane Harvey. The study was executed as a result of the extreme rainfall that came along with hurricane Harvey.

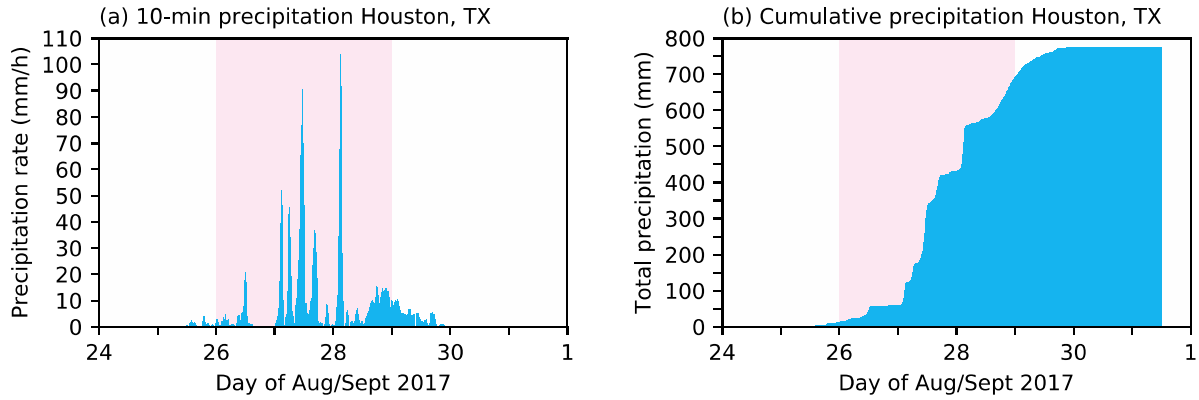

Figure 32 – 10-min precipitation rates and cumulative precipitation fallen in Houston, TX due to hurricane Harvey (van Oldenborgh, et al., 2017)

The study shows the maximum observed precipitation rates in time spans of at least 10 minutes. For hurricane Harvey this intensity had a maximum of 100 mm/hour. The cumulative precipitation for the hurricane analyzed was about 800 mm and was fallen in a period of five days. The cumulative precipitation of 800 mm is of the same order of the maximum precipitation of 635 mm that was found to have happened at Matanzas as well. This maximum precipitation rate of 100 mm/hour has happened in a hurricane that showed extreme rainfall events. This rate may be a realistic rate to consider in this water management study for the CTE at Matanzas as past extreme events may form a good basis for this study. It is important to take note of the theory discussed before about precipitation due to hurricanes. The precipitation is strongly depended on many factors. Also, this maximum precipitation rate should be used with care and with the information that it can change much locally, per hurricane, and for the metrological conditions at time.

Storage

The next parameter that needs to be defined is the storage parameter. In the used model, this parameter is defined by a length. This length defines the depth of the volume of water that is equally distributed over the catchment area. The ground material consists of stone with macro pores (Cordova, 2019). This ground material only allows storage capacity on top of the major ground material in forms of puddles, pools, other small basins and natural trenches. Furthermore, the catchment area is vegetated with bushes and grasses. Fallen rain will be trapped between the vegetation as well and the rain will find storage in the soil where the roots of the vegetation find its way. A rough estimate for this average storage capacity would be about 100 mm.

Infiltration

Stone material with macro pores can allow for some infiltration within the natural pores and trenches. This infiltration is limited to the number of gaps and the amount of vegetation that is limiting the access to those gaps. Like explained before, the infiltration depends on the storage magnitude of the specific sub-area. The different slopes will have different infiltration values depending on the storage of the sub-areas. These different infiltration values will be weighted with the magnitude of the land area of each sub-area. The average infiltration can consequently be calculated. The average infiltration is estimated to be around 10 mm per hour and this value is consequently used in this model.

Transportation

All fallen precipitation which does not get stored or infiltrated, will run down to the next sub-area. The water that is transported out of the last sub-area will find its way onto the project area. This is symbolized by the arrow Q_{t5} in Figure 30. This discharge can be expressed in m^3/s. With the parameters explained above, the transportation flux due to precipitation that runs into the project area has a maximum value of 43 m^3/s. The drainage system in the project area needs to be engineered such that at least this quantity can be discharged. The peak runoff of 43 m^3/s will last for a maximum of about five hours. However, it will be unlikely that this peak runoff will last for five connected hours. Figure 32 shows a realistic representation of the maximum precipitation rate how it is found by van Oldenborgh et al. The maximum precipitation rate comes in short peaks. The runoff response that is experienced downhill will not be like those sharp peaks. The runoff response will be more of a gradual flux. The next paragraph will dig deeper into this subject.

Runoff response

The maximum precipitation rate that is considered will last for at least 10 minutes (van Oldenborgh, et al., 2017). It will become less probable that this maximum precipitation rate will last for much longer than 10 minutes. Hence, the maximum precipitation rate is more or less a peak value and the precipitation rates around this peak value take lower magnitudes. The calculations following the lumped model do not consider that the runoff response may differ from instantaneous results as run off times are not considered. The peak precipitation rate will fall in the catchment area following the presented studies. However, the runoff process gets lagged randomly for different water particles by friction due to vegetation and unevenness in the soil. Therefore, the peak as fallen in the catchment area gets spread out over a larger period. Unfortunately, there is no data available about this run off lag and quantifying this runoff lag can only be done by executing practical measurements.

Discussion

Many unknown parameters had to be estimated while setting up this water management mode. These unknown parameters could not be answered by readily available literature or other sources. Some more background information about precipitation in hurricanes and tropical storms would have come in handy. More detailed information about the project site like more precise bathymetry and more profound information of the soil composition where missing as well. This lack of data has given much uncertainty in the result.

Furthermore, the estimation of the runoff could potentially be modelled better with a computer model instead of a lumped model set up by hand. A computer model can consider the bathymetry more precise and the runoff response of the specific area as well. It will be hard to validate and calibrate the model since no readily available data is present, which could be a positive argument that speaks for the model made by hand.

Chapter 4

Probabilistic approach for synthetic hurricanes

4.1 Probabilistic approach

The first way to assess the risk associated with tropical cyclones is to set up a probabilistic method where previous storms are analysed. The different characteristics of these storms are combined to create occurrence probabilities of normative tropical cyclones. From the National Oceanic and Atmospheric Administration (NOAA) tracks of tropical cyclones in the Western Atlantic from 1851 - 2018 are obtained (National Oceanic and Atmospheric Administration, 2019). In the data that was gathered, the 6-hourly locations, maximum velocities (v_{max}) and central pressures (p_c) can be found. In this period a total of 1873 tropical cyclones were observed. However, technology to measure the central pressure of these storms was not there until the 1980's.

4.1.1 Extreme value distributions

The first step of the probabilistic approach is to find the return periods or probability of occurrence of certain values of P_c and v_{max} by creating a series of yearly maxima and fitting a Generalized Extreme Value (GEV) distribution using Maximum Likelihood parameter optimization (Embrechts, Klüppelberg, & Mikosch, 1997). The maximum velocity is converted into m/s and the central pressure is converted into a pressure difference compared to atmospheric pressure (*1 atm*). The GEV distribution consists of three parameters: the shape, scale and location parameter. The shape parameter defines whether the GEV distribution behaves as a Type I, II or III distribution. Here Type I is a Gumbel distribution, Type II a Frèchet (fat tail) and Type III a reverse Weibull distribution (short tail). This means that for a Type II distribution the variable values increase relatively more for larger return periods than the standard Type I distribution and for a Type III distribution the curve flattens out leading to a relatively smaller values of the described variable compared to a Type I distribution (Kotz & Nadarajah, 2000). In Figure 33 the different types of extreme value distributions are visualised on semi-log axes.

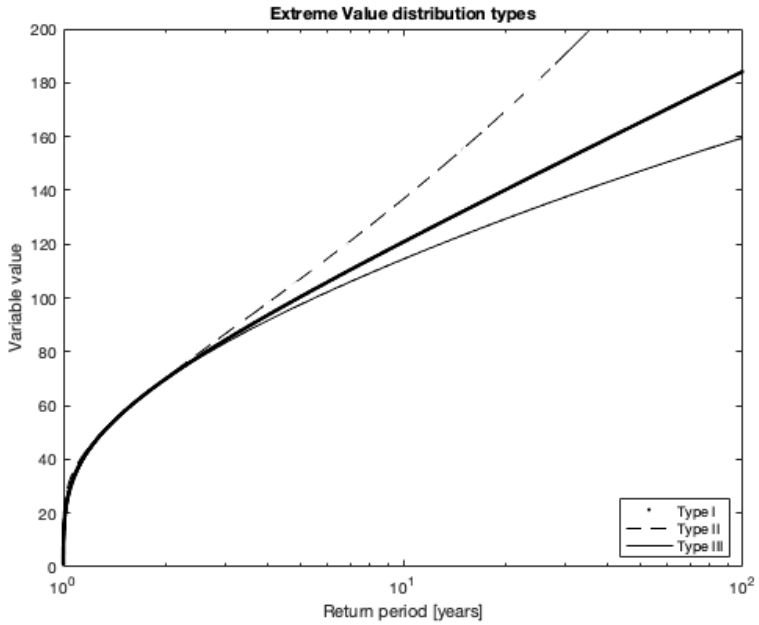

Figure 33 – Extreme Value types

For the data obtained from NOAA a similar figure is generated. The values for the maximum velocity and the central pressure are extrapolated for a return period of 100 years, this can be done for a longer time span. Additionally, a 95% confidence interval of the GEV fit is given. This interval is dependent on the length of the data set but does not include the inaccuracy of the measurement data. This cannot be forgotten when using such extreme value extrapolations.

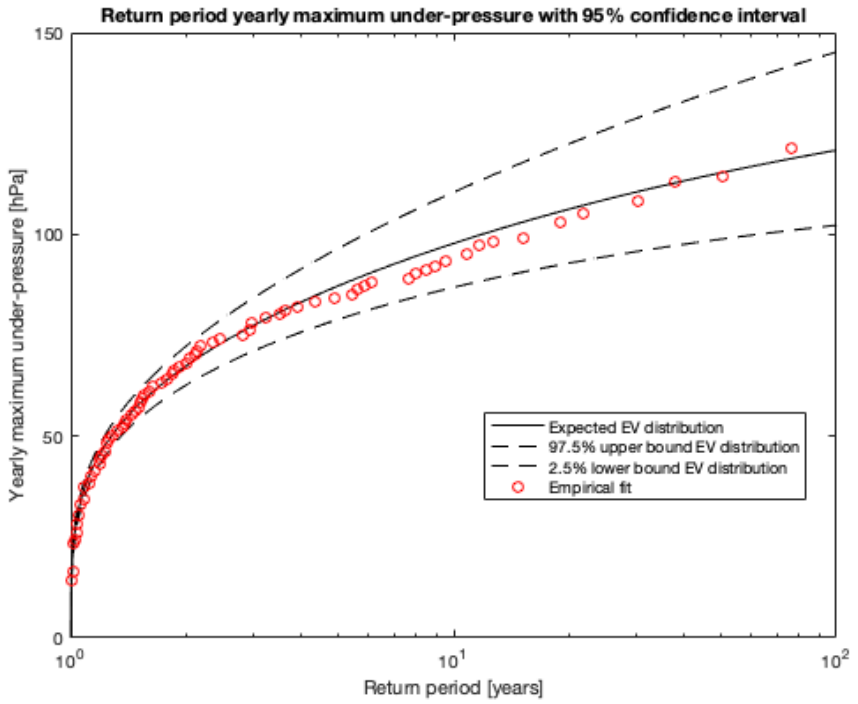

Figure 34 – GEV fit under-pressures

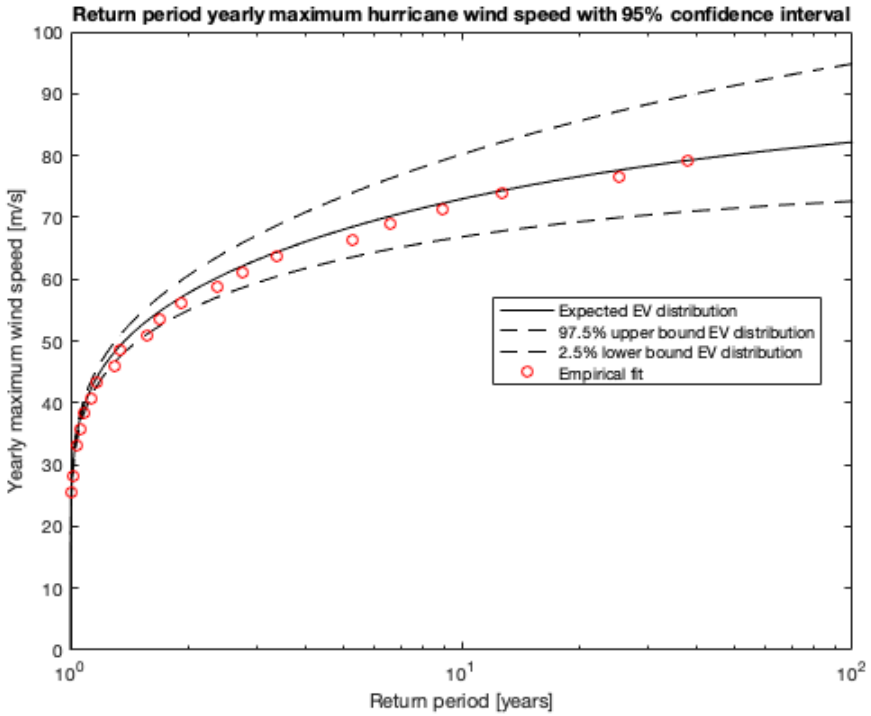

Figure 35 – GEV fit wind speeds

In Figure 34 and Figure 35 one may see the expected GEV distribution, the upper and lower bounds and the empirical data with the associated return periods. One can see that the GEV fit shows a slight under-estimation for return periods in the order of 1 year but starts to over-estimate for return periods larger than 2 or 3 years. This is however a very small deviation and therefore the GEV Maximum Likelihood parameter optimization seems to be good enough.

4.1.2 Correlations between variables

To perform a proper probabilistic analysis, the correlations between the different variables need to be determined. To do so, the values of two variables are compared. In the scatter plot in Figure 36 one can see the under-pressure and the wind speed plotted against each other.

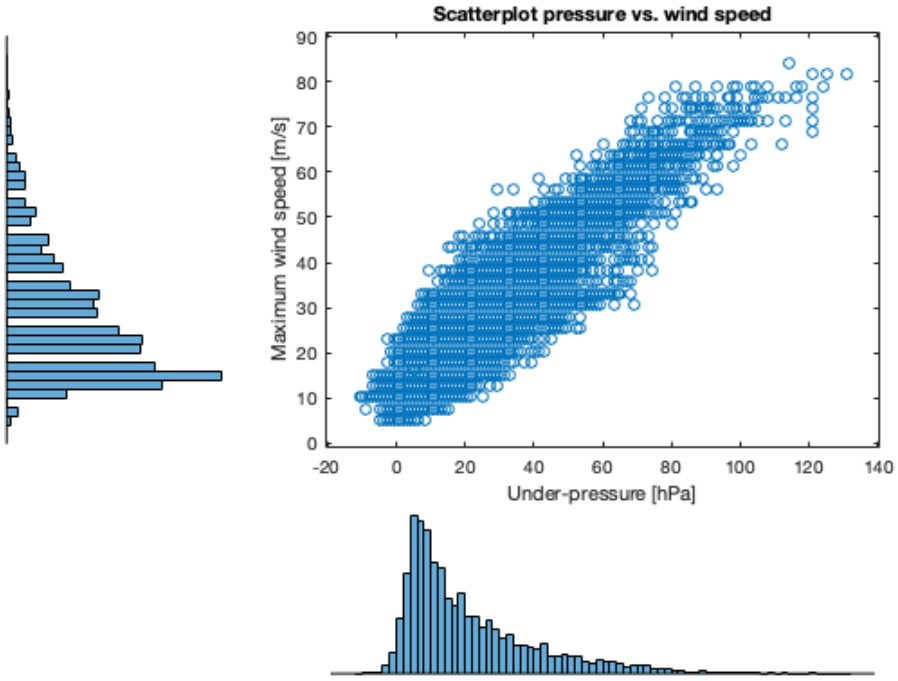

Figure 36 – Scatterplot under-pressure vs. wind speed

Here one can already visually observe the positive correlation between the two variables. However, to obtain a more meaningful insight in the covariance of the two datasets, the ranked correlation is used. Ranking a dataset means that each data point in a one-dimensional set is given a number from 1 to N, where N is the total number of data points. By dividing the ranked dataset by $N+1$ an array with values from 0 to 1 is created. By taking the correlation of the ranked datasets, the marginal behavior of the datasets is neglected. This means that the copula or joint behavior of the two datasets is not influenced by monotone increasing or decreasing transformations of the marginal distributions (Genest & Favre, 2007). Another benefit to using ranked datasets is that the Pearson correlation coefficient (r) can be used to describe the correlation just as well as the Spearman correlation coefficient (ρ), since all non-linear effects in the joint distributions are disregarded (Borkowf, 2002). All in all, it can be concluded that to more accurately describe the correlation between for example the maximum wind speed and the maximum under-pressure, both the datasets should be ranked as described. In Figure 37 a scatter plot of such ranked datasets can be found.

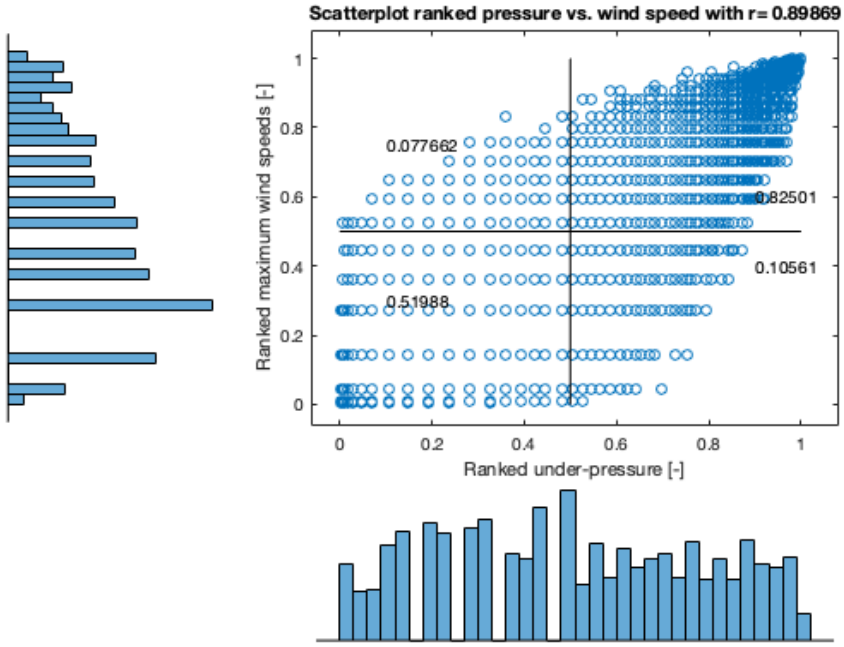

Figure 37 – Scatterplot ranked under-pressure vs. wind speed

As one can see, the scatter plot of the ranked datasets looks largely different from the scatter plot of the original marginal distributions. Visually one can observe that for large values of under-pressures and wind speeds the correlation is much larger than for small values where lots of scattering is observed. When combing marginal extreme value distributions, one is often only interested in the correlation among relatively large values for each of the marginal distributions. Therefore, it is best to find the correlation for the upper regions of the joint distribution additionally to the total correlation. However, one should consider that the working point, i.e. all the values of the different marginal distribution for which the structure is designed, is not necessarily a combination of only extreme values. This should always be checked.

In the table below the correlations between all different variables are given. The corresponding figures can be found in Appendix C.

r [-]	$\mathbf{V_{max}}$	$\mathbf{P_c}$	$\mathbf{V_{tras}}$
$\mathbf{V_{max}}$	1	0.90	0.03
$\mathbf{P_c}$	0.90	1	0.00
$\mathbf{V_{tras}}$	0.03	0.00	1

Table 8 – Correlation matrix all variables

In the table below the correlations for large values are given.

r [-]	$\mathbf{V_{max}}$	$\mathbf{P_c}$	$\mathbf{V_{tras}}$
$\mathbf{V_{max}}$	1	0.96	0.00
$\mathbf{P_c}$	0.96	1	-0.07
$\mathbf{V_{tras}}$	0.00	-0.07	1

Table 9 – Correlation matrix large values all variables

4.2 Synthetic Hurricane

The design lifetime of the sea defense is 50 years. Failure of the structure would lead to severe damage to the power plant. When the power plant is damaged this leaves a large portion of Cuba without electricity, which has severe consequences for human life and economic activity. For this reason, a very low probability of failure is desired for the structure. According to NEN-1990-1 the CTE can be classified as a CC3 type building, the corresponding reliability index is RC3 (The Netherlands Standardization Institute, 2011). For this reason, the failure probability over the lifetime of 50 years is set to be 0.01 at maximum. Hence the β index for the ULS is set at 2. The ULS is defined as a situation where too much water enters the site of the CTE, and operation must be stalled.

For the synthetic hurricane several factors are important in creating high waves and a high-water level rise at the location of interest. The variables which will have the most influence are the maximum wind speeds, central pressure, the translational velocity of the hurricane itself, the track and the initial sea conditions prior to the hurricane (calm sea or fully developed sea state). It is interesting to investigate correlations of these phenomena and establish the return period of certain combinations. To see what the normative synthetic hurricane should be for this design.

It is important to consider how these variables interact in creating waves and surge. Looking at an isolated variable while keeping the others constant, does not give a representative result of influence of this variable on wave and surge generation. For example, a hurricane far away with high wind speeds can generate as much waves as a hurricane close to the coast with a lower wind speed.

The normative hurricane will be the one that generates the highest waves and surge for the return period that is determined based on the lifetime and consequence class of the structure. For example, a strong hurricane (high wind speed) has a lower probability of occurrence but can follow a very likely track with a likely translational speed.

For this reason, multiple combinations with varying variables are made, which are tested in Delft3D. This gives the optimal combination for the most damaging hurricane. To determine these combinations, first past hurricanes are evaluated to obtain more insight.

4.2.1 Evaluation hurricanes from the past

Past hurricanes that have caused significant damage to the province of Matanzas are Inez (1996), Lili (1996), Georges (1998), Irene (1999), Michelle (2001), Dennis (2005), Rita (2005), TC Fay (2008), Gustav (2008) and Ike (2008) (Instituto de meteorología, 2018). Therefore, these hurricanes are chosen for further analysis.

The hurricanes are analysed and after that categorized based on four characteristics: windspeed, forward speed, distance to shore and the initial sea-state. The distance to shore and their initial sea-state will be described for each hurricane.

Windspeeds between 33 and 49 m/s will be qualified as low, this corresponds to a category 1 or 2 hurricane on the Saffir-Simpson scale. Windspeeds between 50 and 58 m/s will be qualified as medium, which is equivalent to a hurricane of category 3. From 59 m/s and above windspeeds qualify as high, corresponding to a category 4 or 5 hurricane.

The forward speed of a hurricane is assumed to be low if it is below 7 m/s. Forward speeds of 7 m/s or higher are categorized as high forward speed.

Further aspects of the hurricanes are stated, such as the dates during which the tropical cyclones were classified as ‘hurricane’. The category of the hurricane is stated according the Saffir-Simpson scale and the total rainfall caused by the hurricane is also described.

The evaluated hurricanes that can be found in Appendix D and are summarized in Table 10.

Hurricane	Category	Windspeeds	Forward speed	Track	Initial sea-state
Inez (1966)	4	High	High	Over land, close to shore	Unknown
Lili (1996)	3	Medium	High	Over land, close to shore	Unknown
Georges (1998)	4	High	Low	Close to shore	Unknown
Irene (1999)	2	Low	High	Over land, close to shore	Rough
Michelle (2001)	4	High	Low	Over land, close to shore	Rough
Dennis (2005)	4	High	High	Over land, close to shore	Unknown
Rita (2005)	5	High	Low	Medium distance to shore	Rough
Fay (2008)	N.A.	Very low	Low	Over land, close to shore	Unknown
Gustav (2008)	3	High	High	Over land, close to shore	Rough
Ike (2008)	3-4	Medium	High	Over land, along southern shore	Rough

Table 10 – Summary of the past hurricanes

4.2.2 Determination of possible combinations

Windspeeds

Windspeeds are uncorrelated with the impact of the hurricane. Low windspeeds in combination with other variables can still be very damaging, and vice versa. Therefore, all three types of windspeeds will be combined with the variables and simulated.

The existing Delft3D model makes use of a spiderweb file with the wind speeds of Irma. Irma had windspeeds of 80 m/s (155 kt), which is high compared to the evaluated past hurricanes and according to the Saffir-Simpson scale. Therefore, to simulate hurricanes with high windspeeds, the windspeeds of Irma are used. To simulate windspeeds classified as 'medium' and 'low', the windspeeds of Irma will respectively be speeded down 1.5 and 2 times. The synthetic hurricanes with medium windspeeds will have peak windspeeds of $\frac{80}{1.5} = 53$ m/s. The hurricanes with low windspeeds will have peak windspeeds of $\frac{80}{2} = 40$ m/s. This corresponds to the classification that was determined earlier, which was based on the Saffir-Simpson scale.

Forward speed hurricane

As mentioned in the previous chapter, there is a relationship between the forward speed of the hurricane and the height of the generated wave. It was suggested that when the group velocity of the waves equals the forward velocity of the hurricane this will generate the largest fetch and thus the largest waves. According to linear wave theory, the group velocity in deep water can be calculated with equation Equation 1.

Equation 1 - Group velocity

$$c_g = \frac{g\,T}{4\,\pi}$$

In general, the wave period varies with hurricane intensity. This also means that the forward velocity which is the most damaging would differ for different hurricane intensities. The correlation between hurricane intensity and the wave period is shown in Table 11.

Category	Wind Speed [m/s]	Wave height range [m]	Wave period [sec]
1	33 – 42.5	4-8	7-11
2	42.5 – 49.15	6-10	9-12
3	49.15 – 58.05	10-14	12-15
4	58.05 – 69.15	10-14	12-15
5	> 69.15	12 - 17	13 - 17

Table 11 – Hurricane category in correlation with windspeed, wave height range and wave period

Important to note is that the group velocity of the waves generated by the hurricane does not have one value but is highly variable and dependent on the wind they're generated by. In the previous paragraph it is stated that three types of wind speeds are modeled. First a high windspeed of 80 m/s is assumed, which is a category 5 hurricane. This corresponds to a very high wave period, so here a wave period of 17 seconds is assumed. The medium windspeeds of 53 m/s, correspond to approximately a wave period of 13 seconds. The hurricane with low windspeeds of 40 m/s, would approximately have a wave period of 10 seconds.

To test this theorem a synthetic hurricane will be generated which has a forward velocity equal to the group velocity of the waves observed in the hurricane.

Windspeeds		Forward speed [m/s] based on group velocity
High	80 m/s	13.3
Medium	53 m/s	10.2
Low	40 m/s	7.8

Table 12 – Forward speeds of synthetic hurricanes

On the other hand, one can reason that a low forward velocity of the hurricane means that the hurricane has more time to generate waves on a certain location and that this will create larger waves. In general (as can be seen in Table 12) the group velocity and consequently the forward speed of the hurricane will be quite high. To test both theories, the hurricanes will also be modelled with a very low forward speed. In Chapter 3.4 it is stated that TCs originated from the North Atlantic region tend to move to the west with speeds of around 3 to 8 m/s. Taking this into account and also looking at the evaluated hurricanes, the 'low' forward speed is set to 3 m/s.

Track

A clear correlation between the hurricane's path and high waves at the site of interest is not yet known. Looking at past hurricanes three damaging paths can be distinguished.

- Track 1: A path on the north side of Cuba, close to the shore of the CTE
- Track 2: A path on the north side of Cuba, far from the shore of the CTE
- Track 3: A path which crosses Cuba vertically, very close to the CTE

As a starting point for the two tracks on the north side of Cuba, the track of hurricane Irma will be used, since this hurricane caused a lot of damage to the CTE. A new path will be programmed over Cuba for the third track. To keep the programming simple, the start of this track will look like Irma's track. The first part of the tracks, when the hurricane is approaching Cuba, is of less importance for the analysis. The most important part of the track is when the track is approaching the CTE. Here the highest waves and surge at our location of interest are generated.

Paths on the southside of Cuba occur, but will not cause significant damage to the CTE, therefore these tracks are not of interest in this case. The same goes for hurricanes on the northside of Cuba, which pass the CTE at more than 100 km distance from the shore.

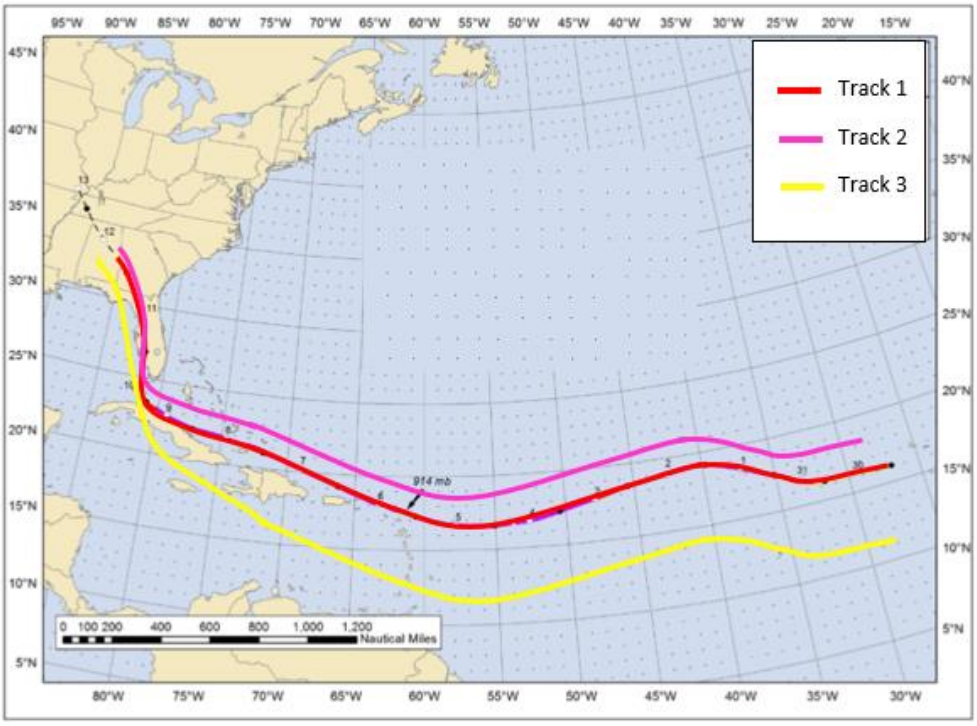

Figure 38 – Three types of tracks

By looking at the same database of past hurricanes as in chapter 4.1 Probabilistic Approach the number of hurricanes which comply with the three tracks are established. For each track two or three lines (blue in the graphs) are placed. The hurricanes passing these lines are counted and showed in the graphs. In Appendix C one can find the Matlab sheet that is written to find the hurricanes with these tracks.

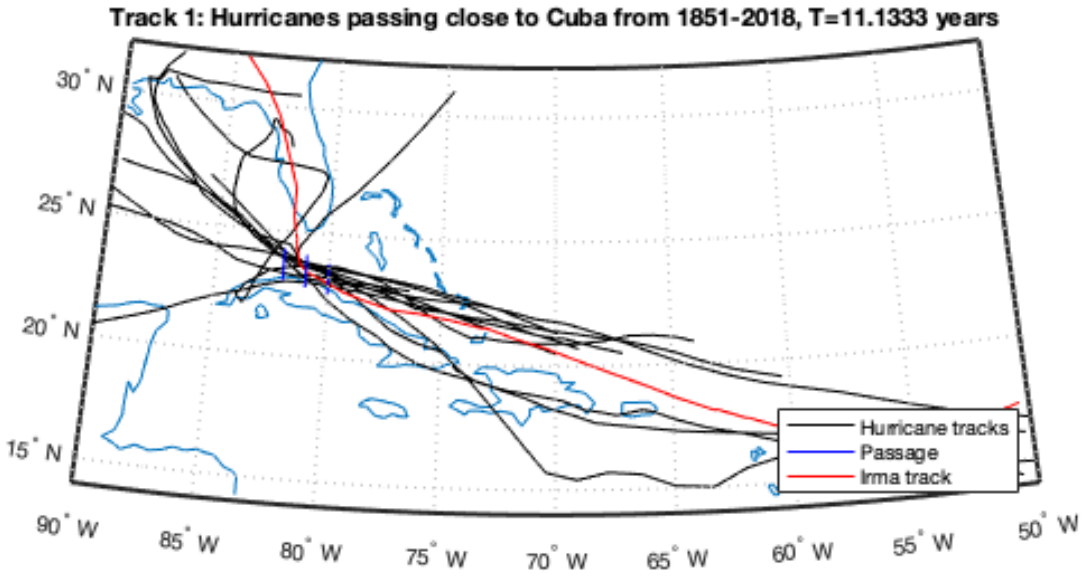

Figure 39 – Past hurricanes which comply with track 1

Track 1 has three passage lines. To be qualified as a track 1 hurricane, the hurricane needs to pass the middle line and either the line on the right or the line on the left. The lines are overlapping with a small part of the coast and are about 120 km long, so all hurricanes briefly touching the coast and in between the coast and 100 km from the coast are showed in this graph. The number of hurricanes which have followed a path like track 1 in the past 167 years is 15.

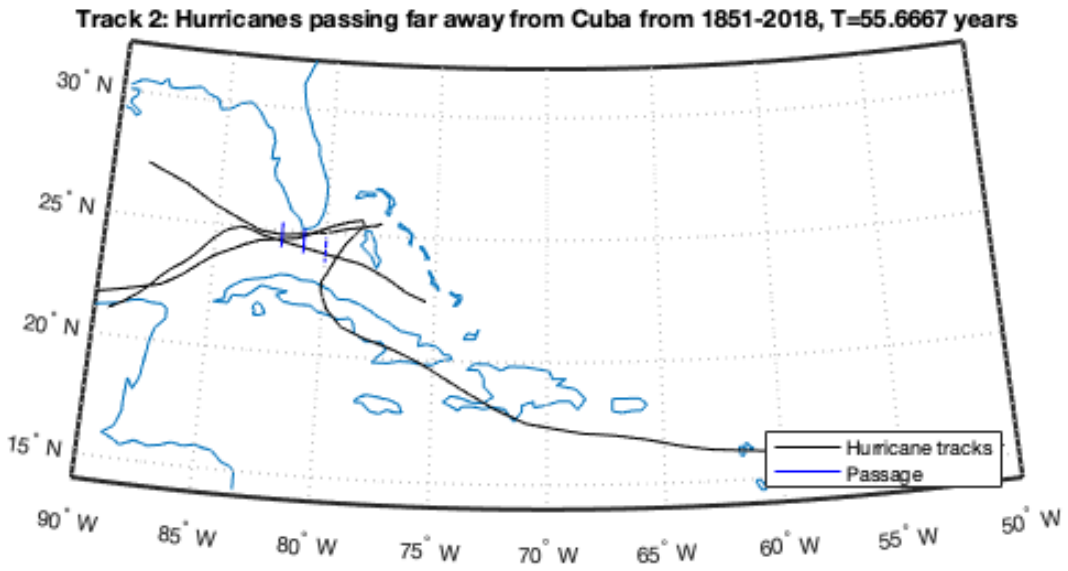

Figure 40 – Past hurricanes which comply with track 2

Track 2 has three passage lines. To be qualified as a track 2 hurricane, the hurricane needs to pass the middle line and either the line on the right or the line on the left. The lines start where the passage lines of track 1 stop. The lines are again 120 km long, so all hurricanes in between 100 and 120 km from the coast are showed in this graph. The number of hurricanes which have followed a path like track 2 in the past 167 years is 3.

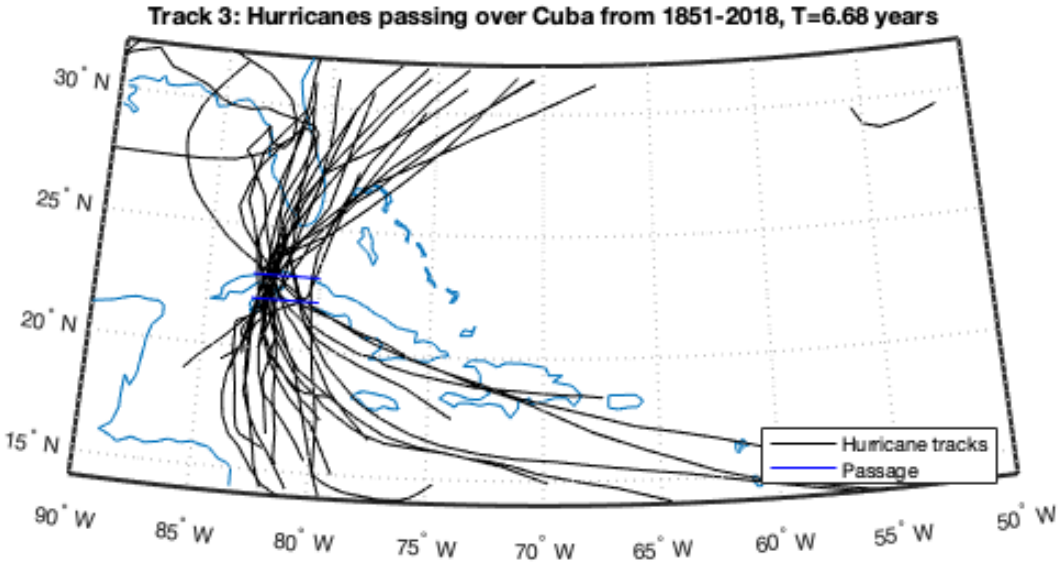

Figure 41 – Past hurricanes which comply with track 3

Track 3 is easier to identify and only has two passage lines which the hurricanes need to pass both. The lines are placed at the location of the CTE and on the other side of Cuba. The lines cover a length of 300 km. All hurricanes making landfall within a distance of 150 km East or North of the CTE, are showed in the graph. The number of hurricanes which have followed a path like track 3 in the past 167 years is 25.

Looking at Figure 40 only three hurricanes in the past have followed a path similar to track 2, which is very few. Taken this into account and considering the simulation time, it is chosen to not simulate combinations with track 2 hurricanes.

Initial sea conditions

Looking at the past hurricanes, not much information can be obtained about the initial sea state because not enough data is available. It shows that intense and less intense hurricanes (categories 2 and 5) can both occur with rough initial sea states, but no exact initial sea states can be determined.

Because no exact measurements are available, it is hard to determine the initial sea state statistically. Assumptions are made in this case. The chance of a hurricane occurring in combination with a smooth initial sea state will be lower than a hurricane combined with rough initial conditions. For example, the rough initial sea state shows a better fit for hurricane Gloria as shown in Figure 17. A rough initial sea state is also more normative for determining the final design. For this reason, considering the modeling time and the fact that not much data is available, the model will always be run with a rough initial sea state.

Specifically looking at Irma and the Delft3D model, the initial sea state is simulated by running uniform wind for two days prior to the hurricane. The wind speeds are obtained from real time wind data measured at that time. To simulate an initial sea state for the synthetic hurricanes, the same approach will be used. The wind speeds prior to hurricane Irma will be used. No adjustments are made because the exact values are not important for the effect on the model, just the fact that the sea is not completely smooth. Running the model with two days of windspeeds prior to the hurricane, will be considered as a 'rough' initial sea state.

Combinations

Based on the analysis on the wind speeds, the forward speed, the tracks and the initial sea conditions 18 combinations are made, shown in Appendix C. However, as mentioned before track 2 hurricanes are not simulated creating Table 13 with 12 combinations. These are all the combinations that are simulated in Delft3D and XBeach.

Combination	Wind speed	Forward speed [m/s]	Track	Initial sea conditions
1	High	13.3	1	Rough
2	High	3	1	Rough
5	High	13.3	3	Rough
6	High	3	3	Rough
7	Medium	10.2	1	Rough
8	Medium	3	1	Rough
11	Medium	10.2	3	Rough
12	Medium	3	3	Rough
13	Low	7.8	1	Rough
14	Low	3	1	Rough
17	Low	7.8	3	Rough
18	Low	3	3	Rough

Table 13 – Adjusted combinations of variables of the synthetic hurricanes

4.2.3 Probability of occurrence of the combinations

There are three variables on which the hurricanes are characterized. The maximum wind speeds, the time-averaged translational speed and the track of the hurricane. In order to calculate the probability of occurrence of each combination first the marginal distributions and the correlations need to be considered to come to a correct probabilistic calculation.

In Appendix C one can find that the correlation between the maximum wind speed and the translational speed is close to zero and hence approximated to be so to make calculations more convenient. Additionally, no correlation is found between the track of the hurricane and the maximum wind speed and hence this correlation is also taken to be zero. This reduces the probabilistic calculation to Equation 2. It should be noted

that setting the translational speed equal to some value means that in reality an interval of 0.5 *m/s* is taken to be equal to this speed.

Equation 2 - Probability of occurrence of combination

$$P(V > v_m \cap V_{tras} = v_{tras} \cap T = t_i) = P(V > v_m \cap V_{tras} = v_t) * P(T = t_i \mid V > v_m \cap V_{tras} = v_t)$$

In Equation 2 the variables *V*, V_{tras} and *T* are the maximum velocity, the translational speed and the track of the hurricane respectively. In lower case letters, the values of these variables are defined, namely v_m, v_{tras} and t_i.

The first part of Equation 2 is not known and can be derived as done in Equation 3. It uses the assumption of no correlation between the maximum velocity and the translational speed of the hurricane. This means that the probability of a certain wind speed is multiplied with the conditional probability of a certain translational speed given the beforementioned wind speed.

Equation 3 - Joined probability maximum velocity and translational speed

$$P(V > v_m \cap V_{tras} = v_{tras}) = P(V > v_m) * P(V_{tras} = v_{tras} \mid V > v_m)$$

To implement these equations a Matlab script is written, which can be found in Appendix C.

Maximum wind velocities

Firstly, the probability of exceedance of the maximum wind velocities is determined. From Figure 35 the annual probability of occurrence for the maximum wind speed can be found. In order to capture the uncertainty of the extreme value distribution, the 95% confidence interval is considered.

	Lower bound (year^{-1})	**Expected value (year^{-1})**	**Upper bound (year^{-1})**
V_{high}	0	0.021	0.1021
V_{med}	0.5718	0.6735	0.6983
V_{low}	0.9014	0.9174	0.9297

Table 14 – Annual probabilities of occurrence of maximum wind speeds

Translational speeds

Next, the conditional probabilities of the translational speeds given certain maximum wind velocities are considered. This is done by dividing the number of hurricanes that have both the characteristic of the maximum wind velocity and the translational speed by the total amount of hurricanes that have the characteristic of the maximum wind velocity. In mathematical terms this can be represented as in Equation 4.

Equation 4: Conditional probability translational speed given maximum wind velocities

$$P(V_{tras} = v_{tras} \mid V > v_t) = \frac{\sum hurricanes[V > v_t \,\&\, V_{tras} = v_{tras}]}{\sum hurricanes[V > v_t]}$$

For the 12 different combinations, all the conditional probabilities can hence be found. In Table 15 the different empirical conditional probabilities can be found.

	$V_{max,low}$	**$V_{max,med}$**	**$V_{max,high}$**
Low = 3 m/s	0.0505	0.0204	0
High = 13.3 m/s	0	0	0.0023
Medium = 7.8 m/s	0.5	0.1429	0.1376
Medium = 10.2 m/s	0	0.0255	0.0275

Table 15 – Conditional probabilities translational speeds given maximum wind velocities

Tracks

Lastly, the conditional probabilities of the tracks given a certain translational speed and maximum wind velocity are determined. This is done by dividing the number of hurricanes that the characteristic of the

maximum wind velocity, the translational speed and a specific track by the total number of hurricanes that have the characteristic of both a certain maximum wind velocity and a translational speed. In mathematical terms this can be represented as in Equation 5.

Equation 5 - Conditional probability track given maximum wind velocity and translational speed

$$P(T = t_i \mid V > v_t \cap V_{tras} = v_{tras}) = \frac{\sum hurricanes[V > v_t \,\&\, V_{tras} = v_{tras} \,\&\, T = t_i]}{\sum hurricanes[V > v_t \,\&\, V_{tras} = v_{tras}]}$$

For the 12 different combinations all the conditional probabilities can be found. In Table 16 one can find all the conditional probabilities of the tracks. It can be quickly observed that for track 3 the conditional probabilities are all equal to zero. This means that in the period from 1851 to 2018 no hurricanes have been observed that comply with the set maximum wind velocities and translational speeds.

	V_{max}	V_{tras} [m/s]	Track	Cond. Prob.
1	High	13.3	1	0
2	High	3	1	0
5	High	13.3	3	0
6	High	3	3	0
7	Medium	10.2	1	0
8	Medium	3	1	0.25
11	Medium	10.2	3	0
12	Medium	3	3	0
13	Low	7.8	1	0.0167
14	Low	3	1	0.0909
17	Low	7.8	3	0
18	Low	3	3	0

Table 16 – Conditional probabilities tracks given maximum wind velocity and translational speed

Probability of occurrence

Probabilities

Now the total probability of occurrence or return period can be determined for each of the combinations. This is done by combining Equation 2 and Equation 3 and using the computed conditional probabilities.

	V_{max}	V_{tras} [m/s]	Track	Probability 2.5%[year^{-1}]	Probability expected [year^{-1}]	Probability 97.5% [year^{-1}]
1	High	13.3	1	0	0	0
2	High	3	1	0	0	0
5	High	13.3	3	0	0	0
6	High	3	3	0	0	0
7	Medium	10.2	1	0	0	0
8	Medium	3	1	0.0029	0.0034	0.0036
11	Medium	10.2	3	0	0	0
12	Medium	3	3	0	0	0
13	Low	7.8	1	0.0075	0.0077	0.0078
14	Low	3	1	0.0017	0.0017	0.0017
17	Low	7.8	3	0	0	0
18	Low	3	3	0	0	0

Table 17 – Probability of occurrence of each combination

From Table 17 one can conclude that the probabilities of occurrence of the different combinations are mostly equal to zero. Only combinations 6, 9 and 10 show a probability of occurrence larger than zero. The return periods of these combinations are calculated to be about 294, 130 and 588 years respectively.

Discussion

One should however consider that these calculated probabilities are based on empirical data and the fact that certain combinations of wind velocities, translational speeds and tracks have not occurred yet, does not mean that the probability of occurrence is actually zero. The 95% confidence interval of the probability is therefore only a range induced by the uncertainty of the marginal extreme value distribution of the maximum wind velocity and not of the total probability calculation.

Additional probabilistic calculation for combination 2

In order to capture the probability of occurrence of all the different combinations, another method is suggested. Now the marginal extreme value distribution of the maximum wind speed is adjusted to become a conditional extreme value distribution. This analysis is done for combination 2. It is done by reducing the dataset to hurricanes with track 1. In Figure 42 one can see this conditional extreme value distribution. Since combination 2 is for high wind speeds, the return period of a maximum wind speed of 80 m/s needs to be taken. This expected return period is equal to 51.9 years. Additionally, the return period of track 1 is found to be 11.1 years. This means that the probability of a hurricane with track 1 and a high maximum wind speed is estimated to be 576 years. Of course, one should consider the large uncertainty in this analysis. The lower bound not reaching higher values than 40 m/s represents the fact that in the previous analysis no probability of occurrence was found for combination 2.

Equation 6 - Joint probability of track 1 and maximum velocity

$$P(V > v_{high} \cap T = t_1) = P(T = t_1) * P(V > v_m \mid T = t_1)$$

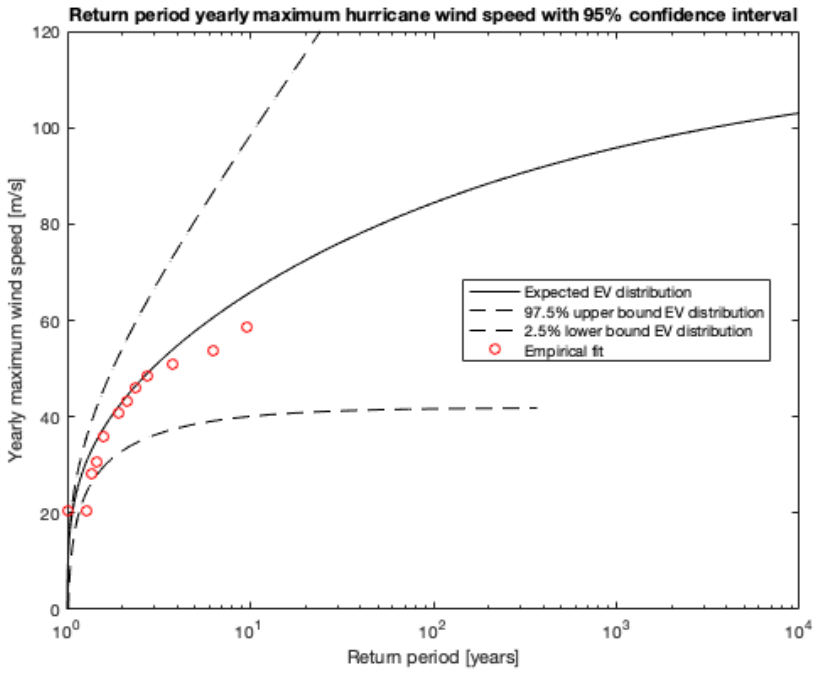

Figure 42 - Conditional extreme value distribution maximum wind speed

In order to come to a joint probability of a high maximum wind speed, a translational speed of 3 m/s and track 1, the formula that should be used for non-correlated variables can be found in Equation 7.

Equation 7 - Joint probability of high wind speed, low translational speed and track 1

$$P(V > v_{high} \cap V_{tras} = 3 \cap T = t_1) = P(V > v_{high} \cap T = t_1) * P(V_{tras} = 3 \mid V > v_{high} \cap T = t_1)$$

However, as was shown in Table 17, no combinations of such variables exist and therefore the conditional probability of a low translational speed and a high wind speed with track 1 is zero. In order to still get an estimate of the probability of occurrence, the calculation is adjusted as can be seen in Equation 8.

Equation 8 - Adjusted joint probability of high wind speed, low translational speed and track 1

$$P(V > v_{high} \cap V_{tras} = 3 \cap T = t_1) \approx P(V > v_{high} \cap T = t_1) * P(V_{tras} = 3)$$

The reason for this assumption is, that earlier it was found that the correlation between the translational speed and the maximum wind speed is close to zero.

The probability of a translational speed of about 3 m/s can be found by analyzing the empirical CDF of this variable. This can be found in Figure 43. The probability of this translational speed is found by taking the probability that the translational speed is between 1.5 and 4.5 m/s. This is range is chosen to allow for some deviation from the exact translational speed of 3 m/s. This calculation is shown in Equation 9.

Equation 9 - Probability of translational speed equal to approximately 3 m/s

$$P(1.5 < V_{tras} < 4.5) = P(V_{tras} < 4.5) - P(V_{tras} < 1.5)$$

The probability that is found from Figure 43 can be seen in Equation 10.

Equation 10 - Working out probability translational speed equal to approximately 3 m/s

$$P(1.5 < V_{tras} < 4.5) = 0.4250 - \ 0.0604 = 0.3646$$

Filling in Equation 8 means that the return period of combination 2 is about 1580 years.

Discussion

Quite some uncertainty is induced by adjusting Equation 7 and taking the expected conditional extreme value distribution of the maximum wind speed given in Figure 42. These assumptions were made to come to a return period which can be worked with, but it is in no way an accurate indication of the real-life return period. This uncertainty should therefore be considered for the design of the protection of the CTE.

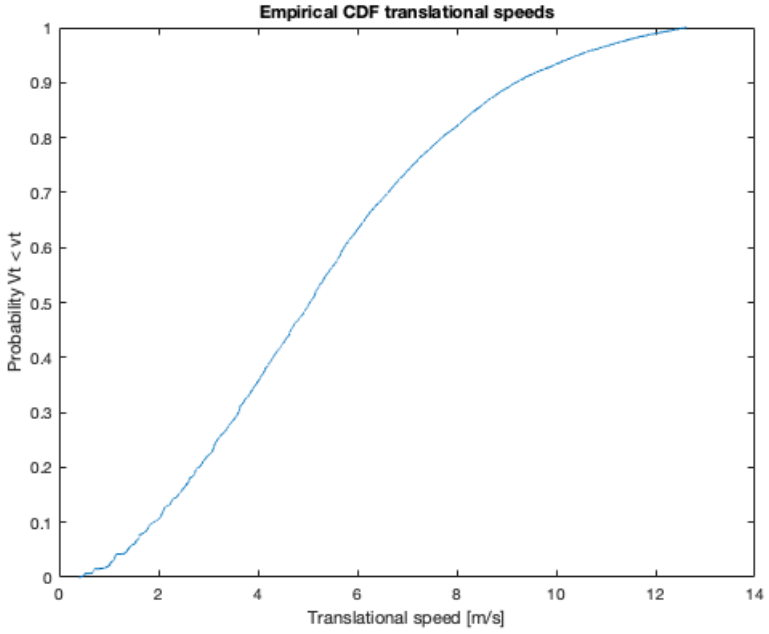

Figure 43 - Empirical CDF translational speeds

4.2.4 Conclusion probabilistic approach

The current design and the design proposal from this report should be based on a certain allowable probability of failure. In order to make a safe, but not over-dimensioned analysis and design, an allowable probability of failure over the lifetime of the structure of 0.01 is chosen as is mentioned earlier. This means that during the lifetime of 50 years, the probability of failure can be 0.01. Using the Poisson distribution, the annual probability of failure can be computed as shown in Equation 11. Here P_f is the probability of failure over the lifetime, T is the lifetime of the structure and f is the annual probability of failure that should be calculated.

Equation 11 - Poisson distribution

$$P_f = 1 - \mathrm{e}^{-\mathrm{fT}}$$

From Equation 11 one finds that the annual probability of failure of this structure may be equal to $2.0 * 10^{-4}$. Given that the probability of hurricane combination 2 is $\frac{1}{1580} = 6.3 * 10^{-4}$, the probability of failure during such a storm may be equal to $\frac{2.0*10^{-4}}{6.3*10^{-4}} = 0.32$. This probability of failure should be considered for the analysis of the current design and the design proposed in this report.

For section C, the probability of failure during a storm is allowed to be a bit higher, as there are no vital structures present behind this section of the sea defense. Hence, the acceptable probability of failure during a storm is set equal to 0.5. This means that the annual probability of failure of this section may be equal to $3.1 * 10^{-4}$.

Chapter 5

Modeling

5.1 Delft3D model

The set-up for the Delft3D model will be explained in this chapter. The following research question as defined in paragraph 2.2.1 can be answered with the use of this software: what are the hydrodynamic and meteorological effects of these extreme weather events?

To be able to answer this question correctly it is of utmost importance that the model is validated. This is done by comparing the output of the model with the observed data from stations located in the Caribbean area. By validating the model, it can be checked if it gives a result that is reliable and close to reality.

Delft3D is used because the program is able to couple FLOW and WAVE computations at a large scale. For the research it is important to run the computation with FLOW and WAVE coupled. This way the significant wave height and the water levels can be computed in more detail and the interaction between the two phenomena is captured. The project area consists out of the Caribbean Sea and a large part of the Atlantic Ocean, because Delft3D can work with large scale areas, this model is a good option. Next to this, Delft3D gives the possibility to recreate hurricanes close to as they would occur in reality, by giving the model a Spiderweb grid as input. Within this research, the possibility to create these hurricanes is vital, therefore it is chosen to work with Delft3D.

5.1.1 Computational Grid

Position of the grid

The computational grid is shown in Figure 44 and includes the Gulf of Mexico, Cuba, Haiti, the Florida peninsula the Bahamas and some other small island and countries. The grid covers this area for several reasons. The grid should cover enough area such that hurricane Irma always stays within the grid boundaries. Later, in this study, potential synthetic hurricanes are designed to test whether the coastal defense will be resistant to different types of hurricanes as well. The grid should also cover enough area such that these synthetic hurricanes may be modelled as well by staying within the grid boundaries. Also, the project area is situated at the northern coast of Cuba. Hurricane generated waves from the south do not result in large waves at the project area. Furthermore, hurricanes that arrive near Cuba are generated in the area above the equator. Irma and the majority of the synthetic hurricanes come from this area, namely the open sea of the Atlantic Ocean. The grid covers this area well.

Refinements of the grid

The computational grid consists of many grid cells. When grid cells in a certain area are made smaller, it is said that the grid is more refined in this area. A more refined grid gives more realistic and reliable output since more detail of the bathymetry is considered in the computations. The most refinement is desired around Cuba to get more detailed information at the area of interest, which is the CTE that is in the bay of Matanzas. On open sea less refinement is needed because this is far away from the area of interest and only the general propagation of the waves and surge is needed. Furthermore, extra refinements around the Bahama's and other islands in the Caribbean are desired as well. The bathymetry in this area in this area shows complicated patterns with the abundance of islands. Delft3D only recognizes small islands as there are refined cells. Such needs for refinements are tried to be incorporated in the designed grid

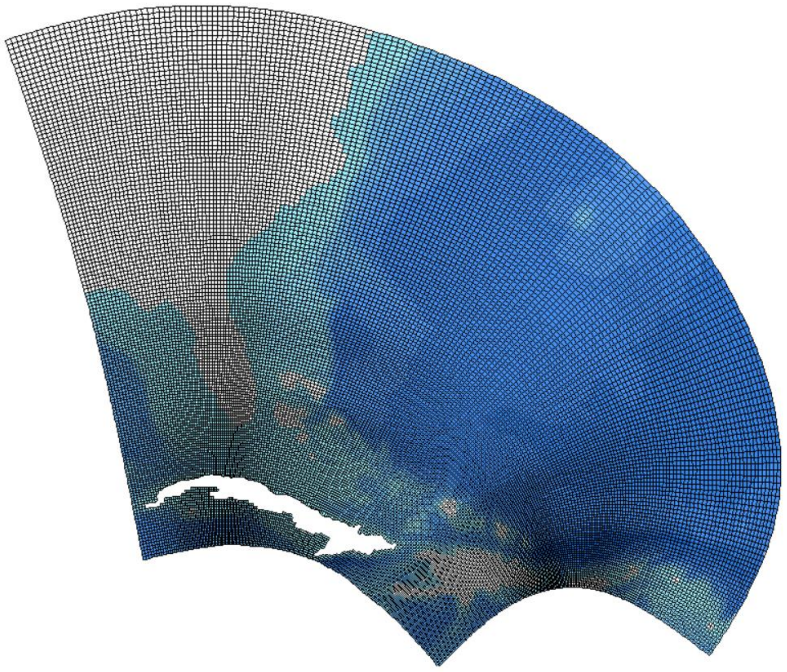

Figure 44 - Computational grid with bathymetry

Grid cell size

The cell sizes at the area of interest are on average 7 x 7 km in M and N direction respectively (see Figure 45 & Figure 46). At open sea the cell sizes are 22 x 33 km in M and N direction respectively (see Figure 45 & Figure 46). In the M-direction are the grid lines that follow the X-direction, in the N-direction are the grid lines that follow the Y-direction.

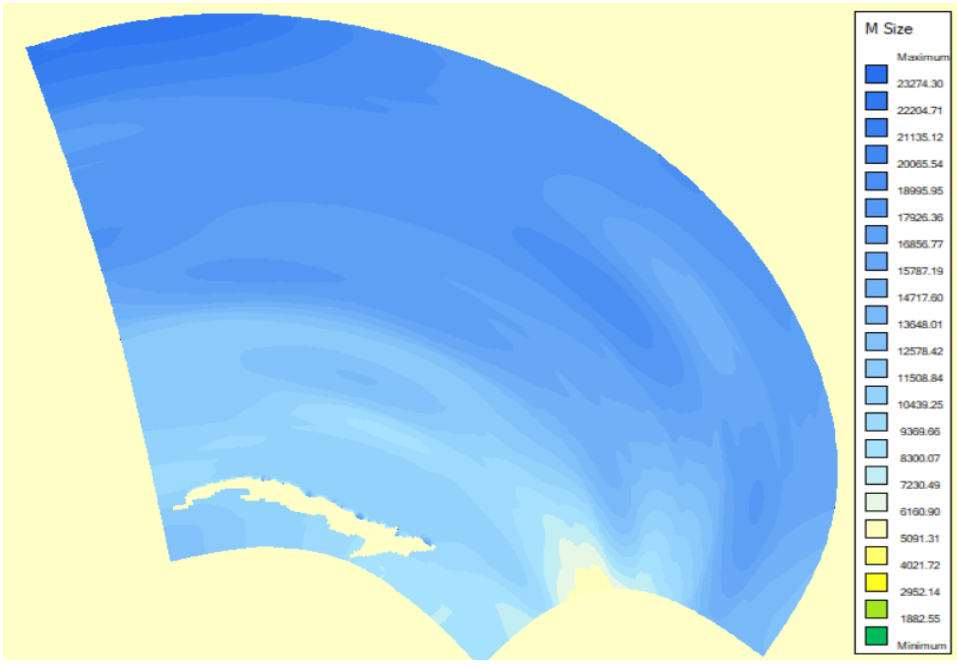

Figure 45 - Cell sizes M direction

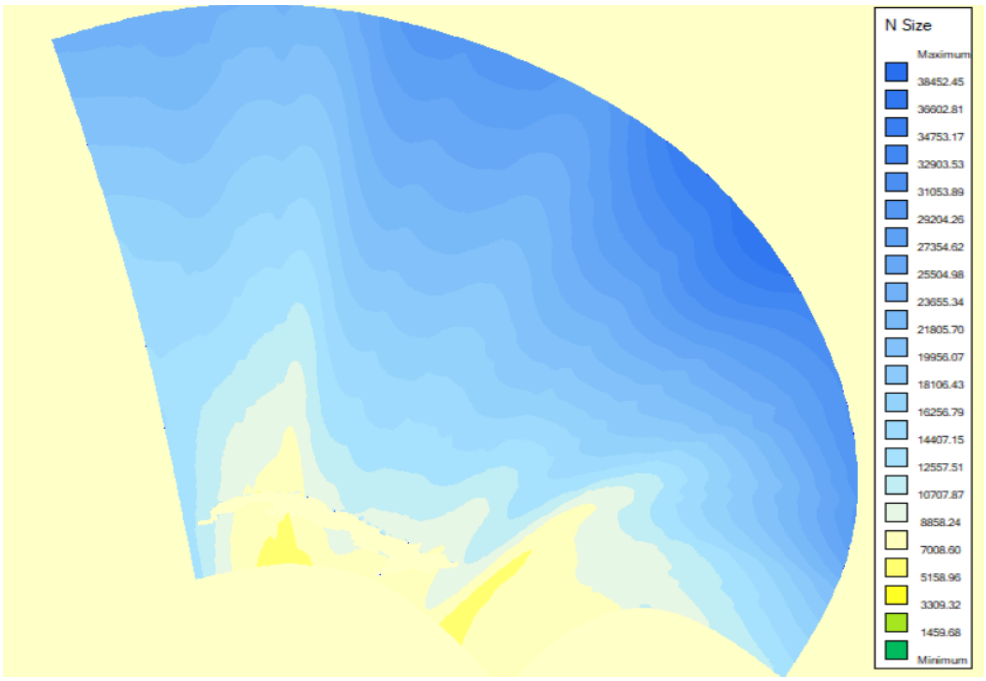

Figure 46 - Cell sizes N direction

Grid ratio

For Delft3D computations the grid cells need to be as close to squares as possible. The ratio between the size of the M and N cells, the aspect ratio, needs to be between one and two. As can be seen in Figure 47 this condition is met everywhere in the grid.

Figure 47 - Aspect ratio grid

Orthogonality

The orthogonality is an important property of the grid; it is a cell centered cosine value. When a cell is perfectly orthogonal the orthogonality value is zero. The error in the direction of the pressure gradient in Delft3D-FLOW is proportional to the deviation from zero. For this reason, the grid needs to be as orthogonal as possible. Near the closed boundaries, which is discussed later in this chapter, larger values can be tolerated.

This comes in handy at the land boundaries where many irregular shapes are present. As can be observed in Figure 48 that only along the southern open boundary and the northern coast of Cuba, there is a slight deviation from 0 but this is well within the acceptable range.

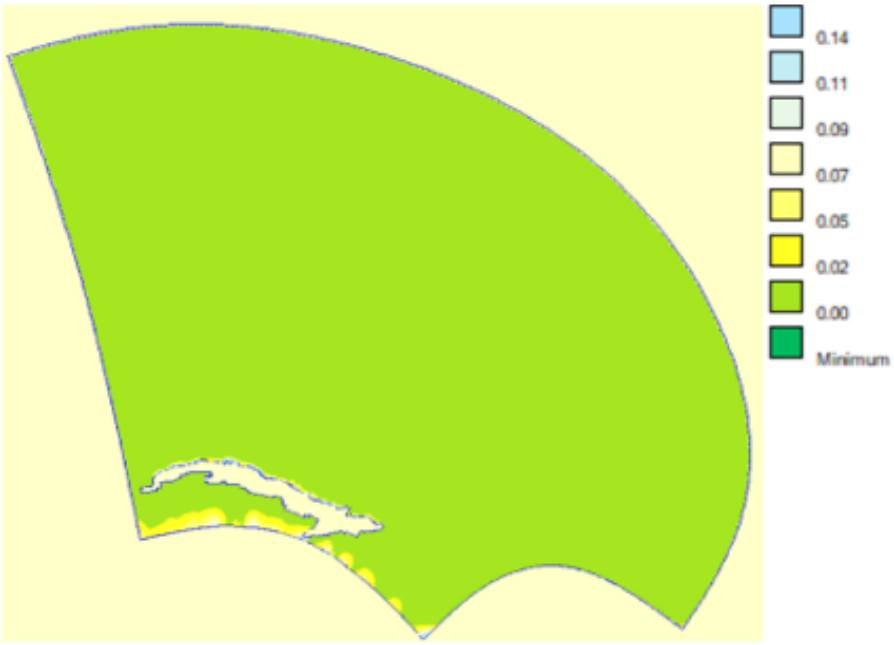

Figure 48 - Orthogonality property grid

5.1.2 Boundary conditions

Open Boundaries – Delft3D-FLOW

In this model there are multiple open boundaries. These open boundaries require some type of forcing of prescribed flow or gradient in order to represent the processes happening outside of the computational domain. The type of boundary conditions that are available in Delft3d-FLOW are: water level, velocity, Neumann (water level gradient), discharge or flux and Riemann.

In this model there is a very large sea domain and the only forcing that can be described to some extend realistically is the water level through tidal forcing. A difficulty in defining the water level is that there is a large correlation between water levels in neighboring points. An error in the prescription of the water level at a point must be compensated by the velocity component in another point, this effect influences the whole area. For this reason, the water levels are only useful boundary conditions when they are accurate. As a precaution the open boundaries are placed as far away as possible from the area of interest. The open boundaries are shown in Figure 49.

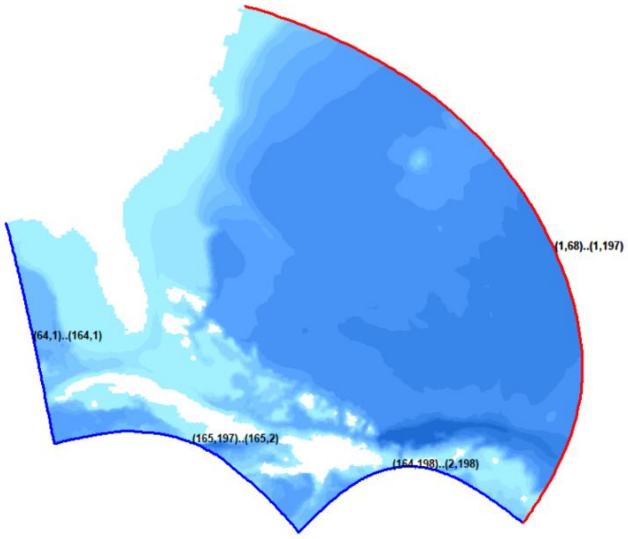

Figure 49 - Open boundaries

When imposing a water level at multiple open boundaries there is a risk that these values are not compatible and lead to unstable results. This again stresses the importance of the careful consideration of the water levels to be imposed at the boundaries.

The model covers a very large area and the tidal conditions are not constant over the curved open boundaries. An amphidromic point is located near Cuba where the tidal elevation and velocity are zero, this can be seen in Figure 50. A tidal wave rotates around this point. This means that the tide is variable both in time and space around all boundaries. The open boundaries could be subdivided into smaller boundaries over which the tide in space is constant. The smaller the spacing the less the velocity gradients are between boundaries caused by any discontinuities. The tide constitutes of astronomical components which are harmonics. A tide can consist of many components, which can be obtained from a tidal signal through Delft3D-TIDE or Delft3D-TRIANA (Science Kennesaw, sd).

Figure 50 - Amphidromic point Cuba (Science Kennesaw, sd)

To divide all open boundaries in smaller sections of e.g. 100 km and find tidal information for all these areas and decompose these with Delft3D-TIDE or Delf3D-TRIANA will be a very laborious task. Most likely it will have a substantial influence on the model, but the model does not necessarily become more realistic since the boundary conditions are very sensitive to errors and the data available at this moment does not have the desired accuracy. For this reason, it is chosen to not include tide in the Delft3D model, but rather add it later for the design. Since the aim of the study is to get a design that can withstand extreme weather

conditions, it must be designed for the case where the maximum wave and maximum surge and maximum tidal elevation occur simultaneously. With Delft3D the maximum wave and surge is modelled while the tide is retrieved from data. The open boundaries for the model will be set to water level with a tide of amplitude and phase 0. In this way the tide does not interfere with the other processes, no large gradients will occur, and all boundaries are compatible.

One very simplified method to include the tide in the model could be to only put the tidal range recorded at the CTE as a single harmonic at the upper open boundary. The other open boundaries are set to a water level of zero, so no complicated interference pattern occurs. This way the tidal signal at the CTE can be simulated, however it will not represent a realistic tidal pattern for the whole domain. Therefore, it is chosen to not do this. Using super positioning of the tide and the storm surge, the water level elevation at the CTE can be found.

The tidal characteristics of the Caribbean are based on the character of the Gulf of Mexico, which is seen as a fully enclosed sea. Therefore, a micro tidal regime can be found in the Caribbean Sea, which results in a mean tidal signal that is smaller than two meters. The character of this tidal regime is given by the diurnal and semi-diurnal amplitude components. The tidal regime is a combination of the two and results in a daily inequality.

Open Boundaries – Delft3D-WAVE

Delft3D-WAVE takes wave heights, directions and their respective period as input for the boundary conditions. Since the open boundaries cover a huge part of the east side of the computational grid it is difficult to generate clear boundary conditions that are valid for the complete boundary. Another way to generate wave heights that closely resemble reality is to change the initial conditions that have to do with the wind. By letting wind rushing over the model before starting the objected simulation, the wave field is already developed in the area of interest. These initial wave conditions can be generated by including a uniform wind in combination with a TC shown by wind vectors in Figure 51.

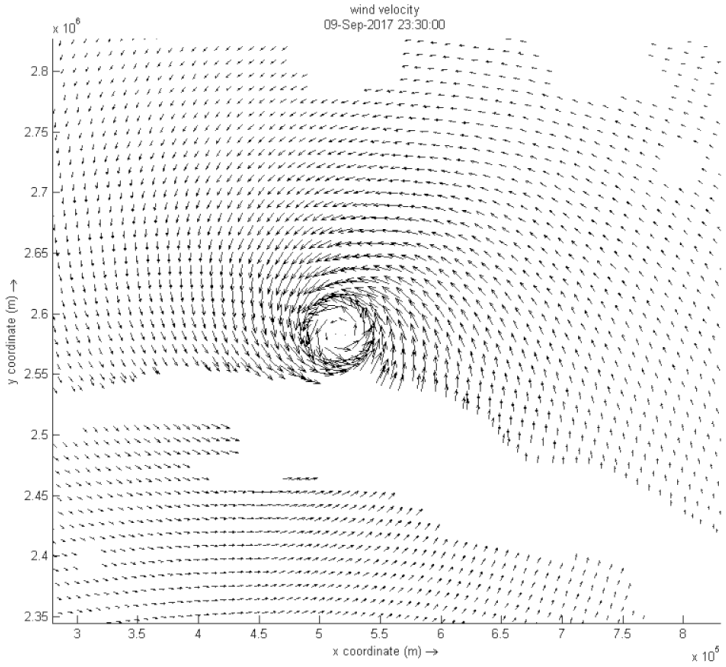

Figure 51 – Uniform wind vectors in combination with a TC

A uniform wind over the entire grid is added to the model to better simulate reality. Otherwise TC Irma is the only source of wave generation and in the absence of other boundary conditions, the sea would initially be perfectly smooth. A uniform wind is added two days before Irma starts her track in order to generate initial waves. It is assumed that the sea conditions after this period comes close to a fully developed sea state. Variations in this initial period with wind can be applied if this leads to better results. The wind velocity and

direction, used to design these initial wave conditions, are taken from buoys with measurements every 6 hours. These buoys have registered wind data in the area during the period of interest and are consequently used as input for the uniform wind.

In regions where the TC Irma is also active this results in a transition of the two wind fields at the edges of the TC, whether this is acceptable will be evaluated. The TC that is generated is based on actual measured wind data along the track and automatically includes all wind i.e. uniform and TCs. Adding another uniform wind value will therefore lead to a deviation from the actual wind velocities at the edges of the TC, since Delft3D projects a transition range between two different wind inputs. A limitation of the model is that uniform wind must be implemented over the entire grid and cannot be altered locally. An option that is evaluated is to let the wind blow normally for the 2 days before Irma, using uniform wind in combination with a still-standing TC (Figure 52), and afterwards reduce the uniform wind to 1 m/s. Far away from Irma this will lead to waves lower than in reality but around Irma the waves will be closer to reality, the results of this option are discussed later.

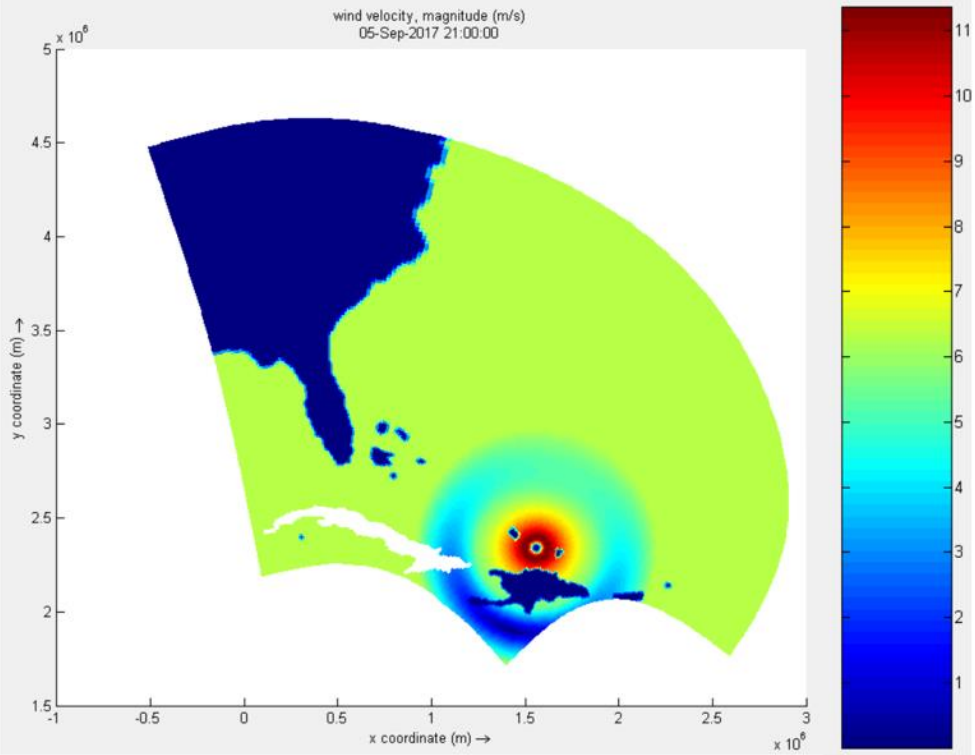

Figure 52 - Uniform wind in combination with. still-standing hurricane

Closed Boundaries

There are also closed boundaries present in the model, which are the boundaries of the land within the computational grid. One of the closed boundaries, Cuba, is enveloped by a land boundary. To make sure that Delft3D sees Cuba as land, the grid points within this land boundary, are removed and the grid cells around Cuba are attached to the land boundary. This way a high amount of detail can be found around the coast of Cuba. The other part of the closed boundaries including the tail of Florida as well as the Bahamas, Puerto Rico, the Dominican Republic and Haiti but also the other small island in the Caribbean Sea are generated using the bathymetry. The bathymetry gives information about the depth at a certain location. It uses point values that are scattered around the designated area, see Figure 53 and Figure 54.

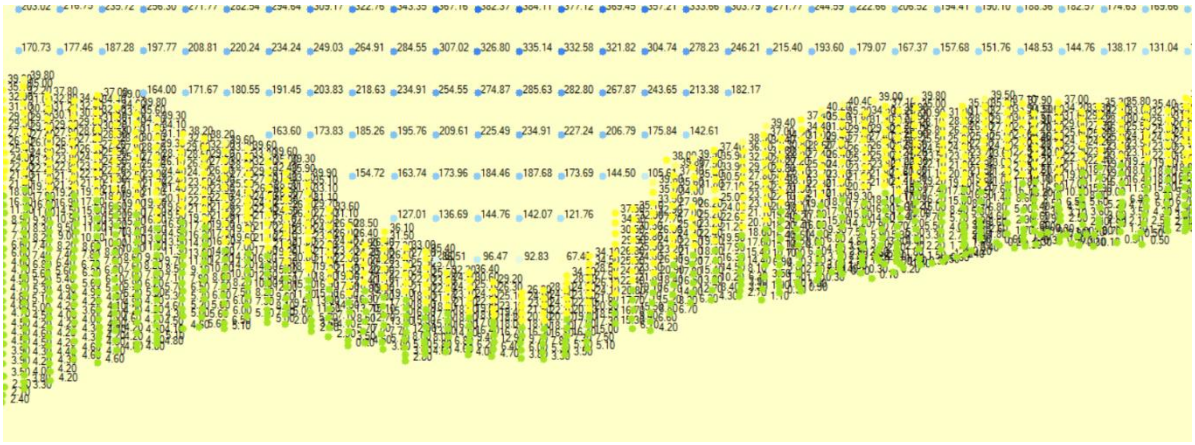

Figure 53 - Bathymetry zoomed in

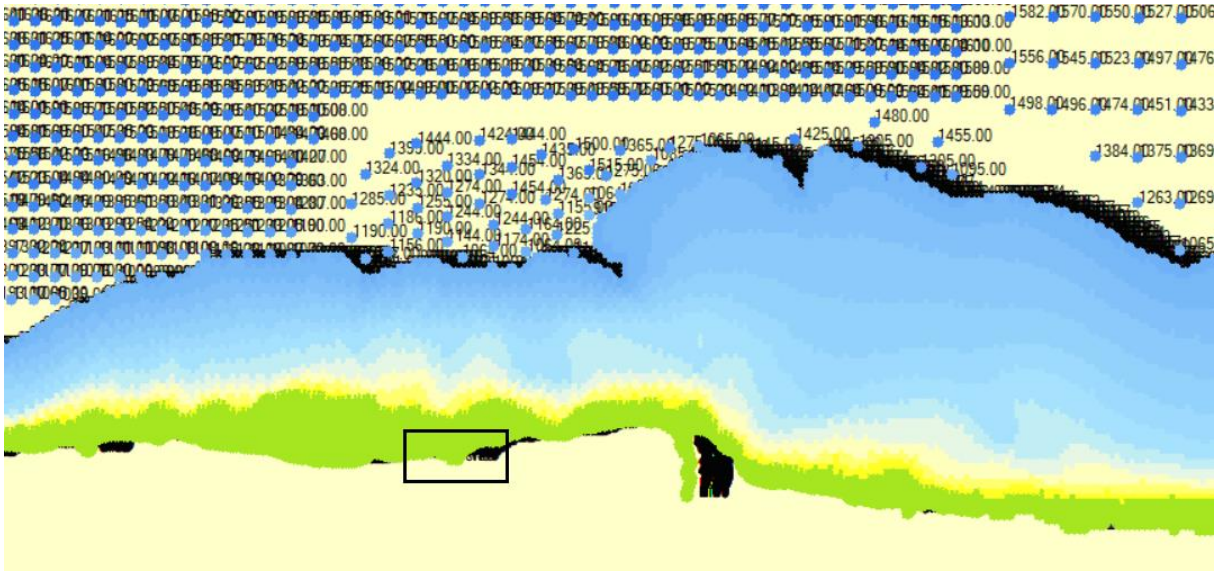

Figure 54 - Bathymetry zoomed out

For the area around Cuba there are a lot more point values available which results in better accuracy of the depth at these grid cells (see Figure 53). From these point values a depth file can be created using the grid in combination with the bathymetry. Delft3D takes this depth file as input in order to create the desired output. From the depth file the closed boundaries can be generated.

The grid cells that do not have enough bathymetry point values are projected as land. To be able to compute these closed boundaries as realistic as possible some tweaks are made while creating the depth file. Normally a minimum of four point-values is needed within a grid cell to create a value for the depth at that cell. However, since the North-East as well as the South-East part of the grid contain a small amount of point values, this is not enough. The program assumes that oceanic grid cells are land since it these cells are not given a depth value. To combat this problem the minimum required amount of point values is set to 1.

Next to this there is another parameter which is important to look at. The relative search cell for averaging which affects the area around the grid cell that is used to search for point values, this is set to 1.1 as a default. This value is set to 3 and in combination with the lowering of the amount of point values needed this resulted in a high enough detail to point out small island but a low enough detail to give all the oceanic grid cells a depth value.

It can be seen in Figure 55 that the tail of Florida, a large part of the Bahamas, Puerto Rico, Haiti, Turks-Caicos-islands and the Dominican Republic are present as closed boundaries. However, when comparing the closed boundaries to GOOGLE Satellite images, it is seen that some tiny islands are not depicted as closed

boundaries. The only way to also present these small islands in the model is to refine the grid substantially. This would increase the computation time x16 (Refining 2 times M and N, 4 by 4), which would result in computation times of a week, which in the short time span of this study is too long.

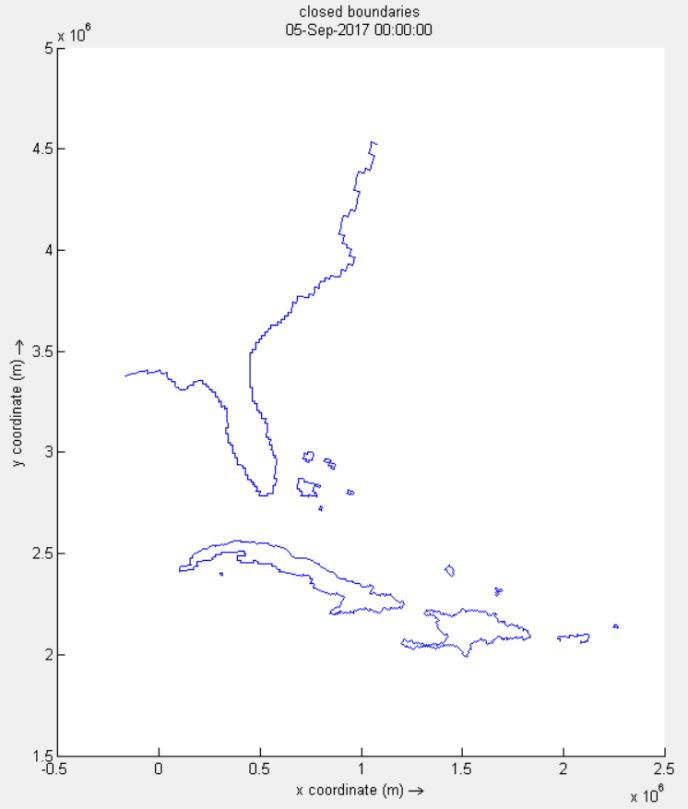

Figure 55 - Closed Boundaries

It is important to consider that these islands are present in the real situation since they influence the wave propagation as well as the storm surge as they create a barrier for the water to move around. Because of the very shallow bathymetry around these islands a lot of dissipation will occur, and waves will not be able to build up. The volume balance of the domain will be slightly off because these islands now can be flooded, but since their dimensions are so small relative to the grid cells, this influence will be only minor. Along the northern coast of Cuba there are also a lot of small islands which cannot be shown on the grid, here the same holds, the shallow water and islands function as a barrier that limit wave propagation towards the coast.

5.1.3 Input

Delft3D takes some more variables as input, some of them are not discussed yet above and are discussed in this paragraph.

Time frame

During the period of 31st of August 2017 06:00 till the 11th of September 2017 12:00 Irma was classified as a TC. Considering the computational time, not this whole-time frame is used. In total a period of 6 days will be used with time steps of 10 minutes. Making the time step smaller than this, increases the accuracy, but also greatly increases the computational time. The upper boundary of this time step is given by the Courant number. There is an upper boundary since the difference between the flow velocity and the size of the grid cannot be too large, else the flow would skip grid cells. By making an estimation of the trade-off between the computational time and the accuracy, the period from the 5th of September 20:00 till the 11th of September 20:00 will be used for the computations.

Physical parameters

The physical parameters can be divided into multiple categories; physical constants, bottom roughness, viscosity and wind.

Constants include the gravity, water density, air density and the wind drag coefficient. The standard values are used for gravity, water density and air density.

For the wind drag coefficient, however, a small study was made. To simulate the effect of surge by means of winds and water levels the traditional bulk relation is used, this relation is characterized by the wind drag coefficient. The magnitude of this coefficient is either constant or it increases monotonically with increasing surface wind speed. The drag coefficient levels off at wind speeds at the surface level of 30 m/s. If the wind speed is increased further, this drag coefficient starts to decrease. This is due to the saturation of the air above the sea surface elevation at wind speeds above 30 m/s. During a study from (Vatvani, Zweers, & al., 2012) some variations were tested. To give a good representation of the coefficient the Charnock drag formulation was extended with a correction term. The Delft3D storm surge model was tested using this Charnock's drag formulation and the improved Makin's wind drag parameterization. The tests resulted in the observation that the Makin's new drag parameterization is favorable over the original Charnock drag formulation (Vatvani, Zweers, & al., 2012).

According to this study, for the Delft3D-model the wind drag coefficients were taken from the blue line in Figure 56. For a windspeed of 0 m/s at a height of 10 m above the sea surface a value of 0.001 was taken, for 30 m/s a value of 0.003 and for 70 m/s a value of 0.0015 for the wind drag coefficients. Delft3D takes these three values as input and linearly interpolates between them. The wind drag coefficient depicts the amount of influence that wind has on the water surface. If the wind drag coefficient is high, there is a lot of surface tension, which results in the creation of higher waves due to wind.

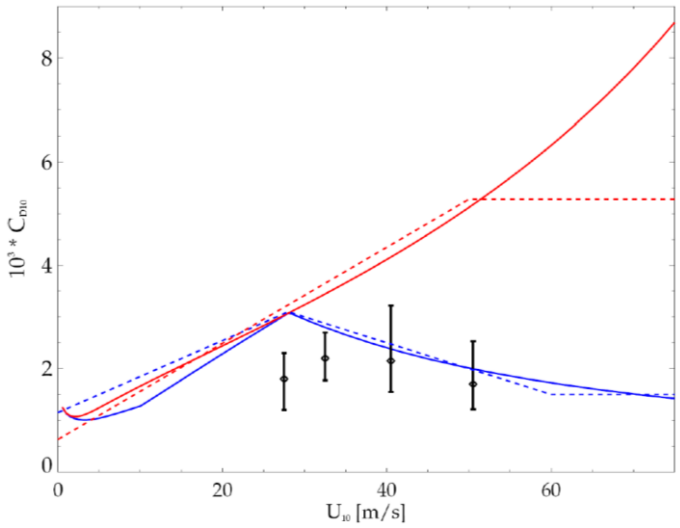

Figure 56 - Wind drag coefficients (Vatvani, Zweers, & al., 2012)

Output parameters

Since the model is run on a large scale and over a large period, the model is run in non-stationary mode. This captures the spatial and temporal propagation of both storm and swell waves in the computational region. Hence, the swell waves that propagate due to the TC and the uniform wind can be modelled correctly. This way the coupling between the FLOW and WAVE model is more accurate as well. Within the output parameters 2D spectra are generated at the location of interest. This 2D spectrum gives information that can be used in XBeach as input. More elaboration on this subject can be found in Chapter 5.2 about XBeach.

5.1.4 Setting up the Spiderweb grid

In order to input the wind and pressures induced by the TC into Delft3D, a so called Spiderweb grid is created. A Spiderweb grid is a radial set of axes where the grid is divided into columns and rows. The number of columns divides 360 degrees into equally large columns and the number of rows divides the total radius into equally large rows. In the figure below a graphical representation of such a Spiderweb grid can be found.

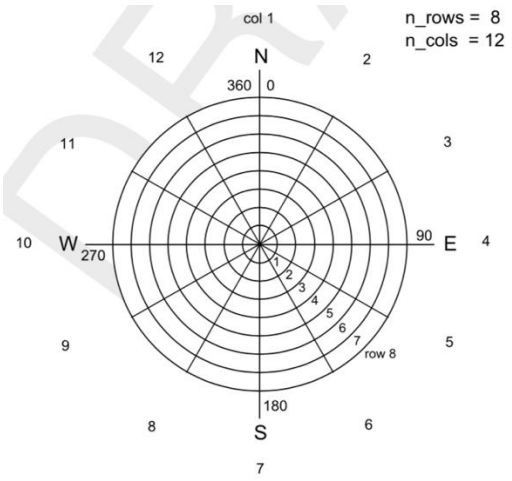

Figure 57 - Spiderweb grid set-up (Deltares, 2019)

To create such a Spiderweb grid, a Python script is created that takes as input the hourly best track of the TC, i.e. the spherical coordinates of the TC for each of the hours that are simulated. In addition, a choice needs to be made on how large the radius of the Spiderweb grid should be and in how many rows it should be divided. The consideration to be made is the run time of the scripts that generate the wind and pressure field, the size of the to be created Spiderweb input file and the precision with which the peak of the maximum velocity is presented in the Spiderweb wind and pressure file. By means of an iterative process, it is defined that a radius of about 600 kilometers gives wind velocities in the order of only 1 m/s at the edge of the wind field. To be able to still represent the maximum velocity inside the TC well, the number of rows is set equal to 200. This means that a pressure value and a wind speed value is given for about every 3 kilometers from the center of the hurricane. The number of columns should be large enough to realistically give a circular wind and pressure field that does not have too much spacing on the outside of the Spiderweb. Hence, the number of columns is set equal to 360. In earlier stages of the project it was found that a large spacing led to a 'beam'-like behavior of the waves that are generated. In Appendix E the according Python file may be found.

There are a few limitations to the Spiderweb grid that Delft3D takes as an input file. Firstly, the radius of the grid must be set equal for all time steps, but since the size of the TC takes different sizes during its course, optimally this radius would be varied for each time step. However, since this is not possible for Delft3D, the radius is kept constant in terms of longitude and latitude. Also, this is not exactly correct, since one-degree latitude is not the same distance in cartesian coordinates as one-degree longitude and this differs for each position on earth. This effect is reduced by containing the simulated TC largely within UTM zone 17N, which is shown in the figure below.

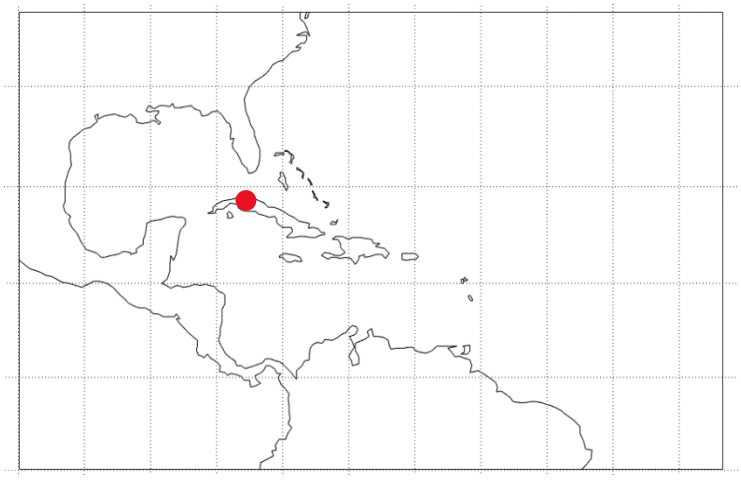

Figure 58 - UTM zones around Cuba

In the Figure 58 the different UTM zones are divided by the dashed lines. The CTE is indicated by the red dot and the zone that surrounds it is UTM zone 17N. The zone to the right of it, is zone 18N and this is also where Irma passes by, so the UTM coordinates are not completely correct. However, on the large scale of the TC this effect is negligible.

By scaling the maximum radius of the TC to the largest size of the TC in its path, the undesired effect that the TC is 'chopped off' at a place where still non-negligible velocities and pressures are present is prevented.

Creating wind and pressure fields

The Spiderweb grid that was created using the Python script, is loaded into a Matlab script that calculates the wind speeds and pressures for each of the grid points. This is done by means of the Holland formula (Holland, Belanger, & Fritz, 2010), which takes as input the Spiderweb grid and the best track of the TC. This best track consists of the location of the center of the TC in both spherical and cartesian coordinates, the translational velocities, the maximum velocities and the minimum pressure inside the center of the TC. As mentioned in Chapter 3.4, the Holland formula is divided into two parts; inward from the radius of maximum velocities and outward from this radius. The pressures within the TC decrease exponentially from outside inwards, with a minimum pressure in the center of the TC. This is also described in Chapter 3.4.

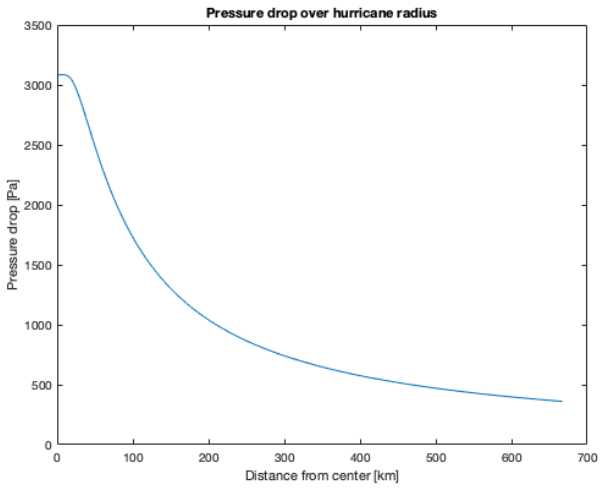

Figure 59 - Pressure drop over hurricane radius

In Figure 59 one can see how the pressure drop decreases from the center of the TC to the outside of the hurricane, where the pressure drop is close to zero and hence the total pressure closes to normal atmospheric pressure.

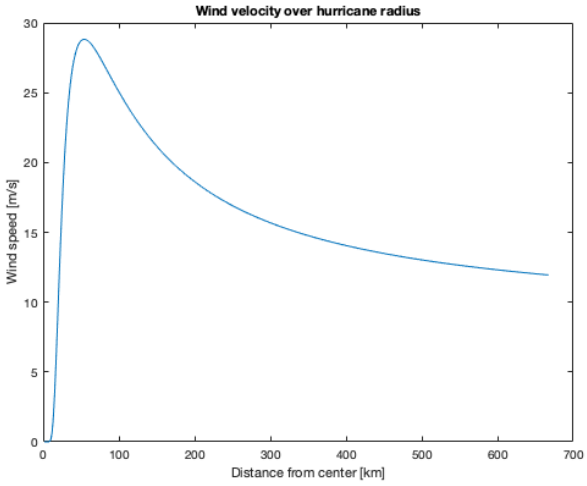

Figure 60 - Wind speeds over hurricane radius

In Figure 60 one can see how the wind speeds first increase from the TC center to the maximum velocity and then decrease with a decaying rate towards the outside of the TC wind field.

The third output that is created by this Matlab script is the wind direction of each grid point. The wind directions are given in nautical coordinates, so this means that 0 degrees gives a vector coming directly from the North, 90 degrees from the East, 180 degrees from the South and 270 degrees from the West.

All this information is written in a text file with the specific layout that Delft3D requires. In Appendix E the lay-out of such a Spiderweb input file can be found.

Using a Spiderweb grid as an input file for the wind in Delft3D gives the advantage that the wind velocities and the pressures are only calculated in the vicinity of the TC center and that no unnecessary information is calculated for regions far away from the TC.

Another advantage of not using for instance the Delft3D grid is that the Delft3D grid does not necessarily have a high resolution near the TC center and therefore the peak velocities might not be included in the wind field that is calculated by the Matlab script. A Spiderweb grid guarantees that the most grid points are created near the TC center; where the highest resolution is needed.

One should keep in mind that the high resolution around the Spiderweb grid is diluted by the smaller resolution of the Delft3D grid, since the values from the Spiderweb grid are interpolated and averaged over the computational Delft3D grid. However, the highest values from the Spiderweb grid are projected onto the computational grid and therefore the information is not lost.

5.1.5 Explanation of the output

There are several characteristics of the modelled hurricanes that stand out and should be explained in more detail. These phenomena are the non-perpendicular velocity vectors and the asymmetrical wind field.

Non-perpendicular velocity vectors

The first one is the increased rotation of the wind velocity vectors towards to outside of the hurricane. This means that close to the hurricane center; the wind velocity vectors are perpendicular to the radius of the hurricane and further away from the center the velocity vectors are pointed more in the direction of center. The factor that is used to describe this phenomenon is called ‘TE’ and it is illustrated in Figure 61.

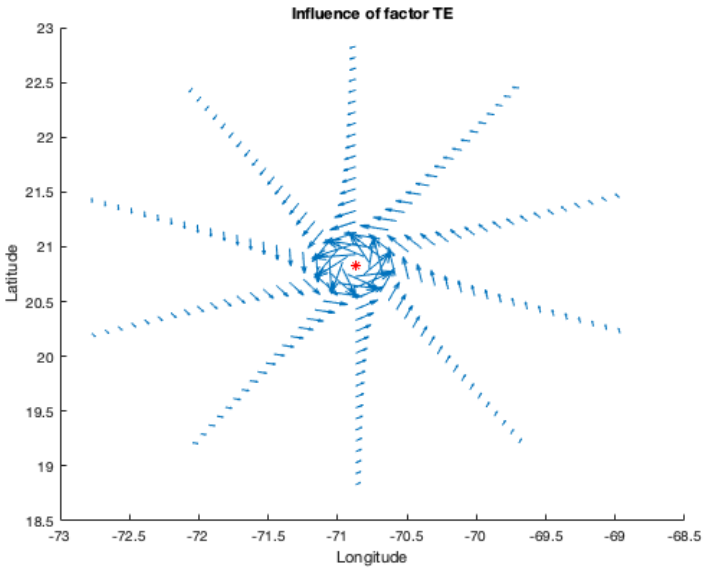

Figure 61 - Influence of factor TE

In Figure 61 one can clearly see that the vectors start to point more towards the center the further they get from this center. This is probably due mainly to the vertical up thrust at the wall cloud, leading to a pressure gradient in vertical sense and a more inward behavior of the velocity vectors in a horizontal sense. The exact phenomenon is not known (Senn & Hiser, 1959).

Asymmetrical wind field

The other phenomenon that stands out is the way that the wind velocity field is not symmetrical. Because the hurricane is moving with speeds in the order of 5 to 10 meters per second, the total wind velocity that is observed by the ocean water surface is higher than the velocity that is generated only by the low pressure inside the center of the hurricane. In Figure 62 one can see a wind field of hurricane Irma that is moving from the north coast of Cuba towards Florida. This means that the hurricane is moving North and since the air around the hurricane is moving anti-clockwise on the northern hemisphere, the velocities on the east side of the hurricane are larger than on the west side. A schematization of this can be found in Figure 63.

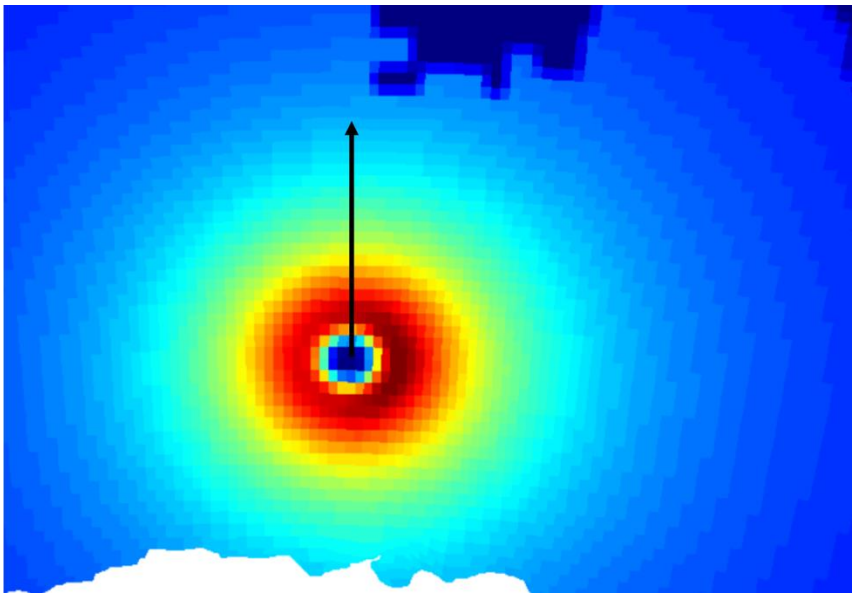

Figure 62 – Asymmetrical wind field

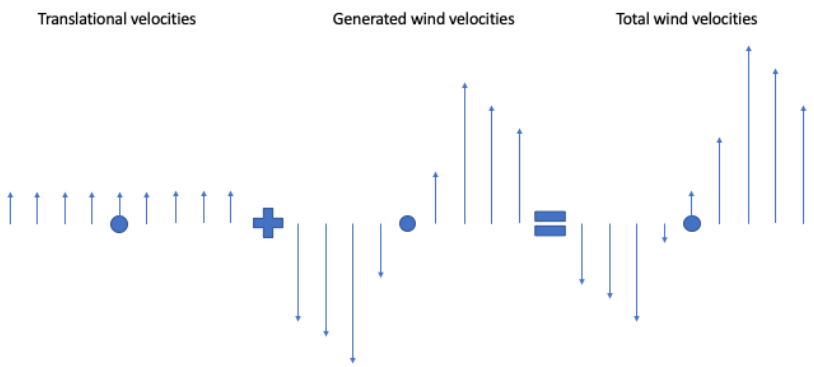

Figure 63 - Schematization of asymmetrical wind field

In Figure 63 one can observe the addition of the translational velocities and the generated wind velocities. The resulting total wind velocities clearly show that in the case of Irma moving towards Florida from the Cuban north coast, the velocities on the east side of the hurricane should be larger than on the west side.

5.1.6 Delft3D – FLOW and WAVE coupling

Delft3D has several modules to model hydrodynamic processes, in this model the FLOW module is used in combination with the WAVE module to simulate the processes during a hurricane. The advantage of running these two modules together is that they exchange information during the run. Every time FLOW runs, a WAVE run is also preformed, then FLOW resumes using the results of the latest WAVE run and so on. This way the hydrodynamic processes can be simulated more realistically since in real life surge, flows, pressures and waves also interact.

For TC modelling, the coupling of these two modules is especially important, since the input file to simulate this consists of space varying pressure and wind. Currently the space varying pressure can only be incorporated in FLOW, but by coupling the two the effect of the pressure will also be felt by WAVE.

5.1.7 Validation

Measuring stations

Close to the location of the CTE very limited data is available. To be able to validate the model, observation stations located near Key West are chosen. These stations, called 8723970 and 8724580 are show in Figure 64. The period of the TC Irma measurements of the recorded water levels are available for every 6 minutes. Virtual wave buoys are placed in the Delft3D model at the same locations as the actual wave buoys. The stations PLSF1 and KYWF1 are located near Key West and for these stations the wind speeds are measured every hour. The stations 41046 and 41043 are in the open ocean and measure wave heights every hour. These four stations are also placed in Delft3D as observation points (Figure 64). The results are compared to the measured data of NOAA.

Wind speed comparison

For the stations PLSF1 and KYWF1 the wind speeds are measured. These measurements are compared with the wind speeds from the Delft3D model. The Spiderweb from the Matlab script forms the input for the Delft3D-model. The generated wind fields can be observed for every timestep in the Delft3D-model. At the exact coordinates of the PLSF1 and KYWF1 the wind speed magnitude is extracted from the model. At these coordinates, observation points are placed to measure the different parameters like wave heights, water levels and wind speeds. Since the wind speeds are measured for every time step, a graph can be plotted for the whole duration of the run. This graph is compared to the graph that is made from the stations data.

Figure 64 - Observation points

At station PLSF1 a peak wind speed of 17 m/s is measured with the Delft3D-model (see Figure 66). In the observations however a peak wind speed of 35 m/s was measured (See Figure 67). At station KYWF1 a peak wind speed of 46 m/s is measured with the Delft3D-model (see Figure 65). In the observations however a peak wind speed of 32 m/s was measured (See Figure 67). The time when this peak wind speed occurs is similar, they occur at around September 10, 12:00. The difference in wind speed observed from the model and from real life observations is quite large, however. This is due to the path difference of the TC Irma in real life and the Delft3D-model. For the Delft3D-model the best track approximation for Irma is used. This means however, that the locations that Irma passes in the model are not the same as in reality.

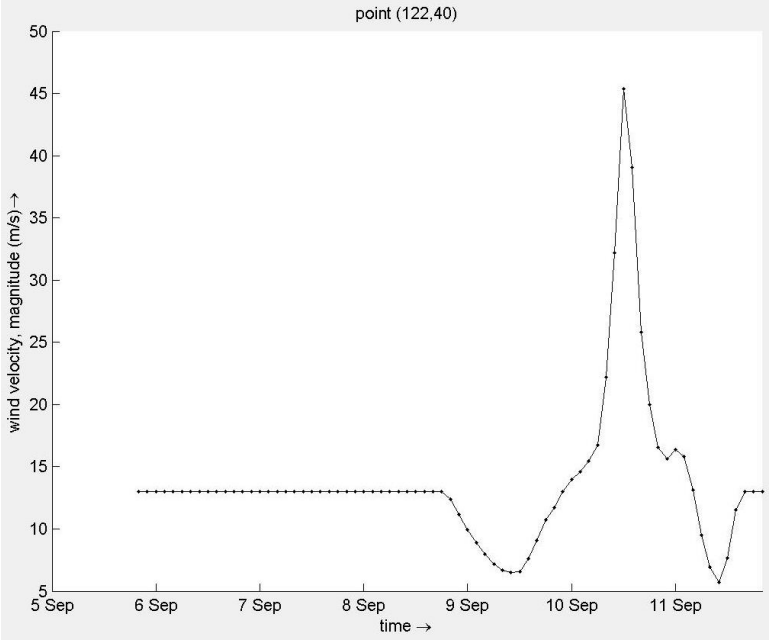

Figure 65 - Modelled wind speed station KYWF1

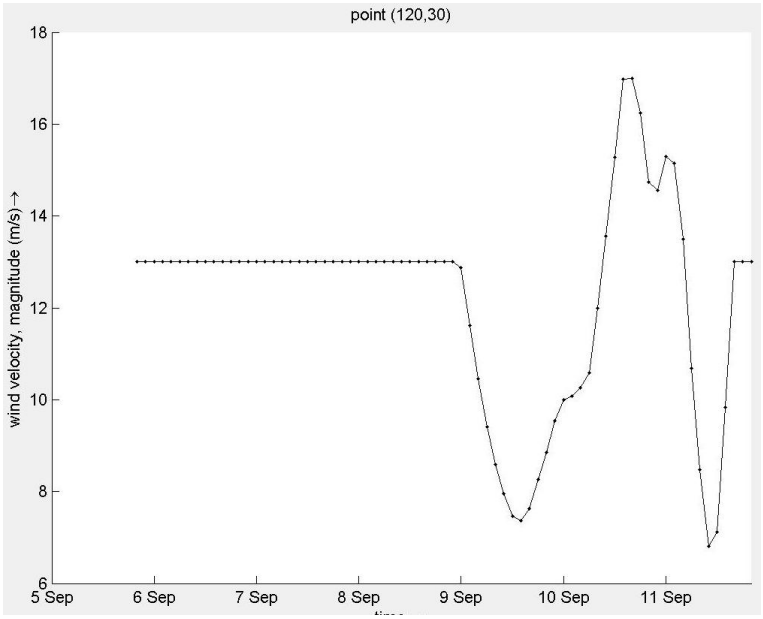

Figure 66 - Modelled wind speed station PLSF1

The TC Irma measured maximum wind speeds of 51 m/s at the 10th of September at 18:00 (P. & al., 2018). Because of the location difference of Irma, in the Delft3D model the observation station KYWF1 was located near the center of TC Irma. Therefore, the wind speeds measured in the model are the maximum wind speeds of the TC at that time. When the observed maximum wind speed of Irma at that time is compared with the modelled one, it is seen that they are similar, respectively 51 m/s and 46 m/s. This means that the model does generate the correct wind speeds, but that the location of Irma in the model does shift a portion from the exact location of Irma. Next to this the observation points cover one grid cell and therefore cover a larger portion of space than the station in reality does. The grid cells are around 10 km in length which means that a larger part of the TC wind speeds was measured, this also explains a deviation from the real number.

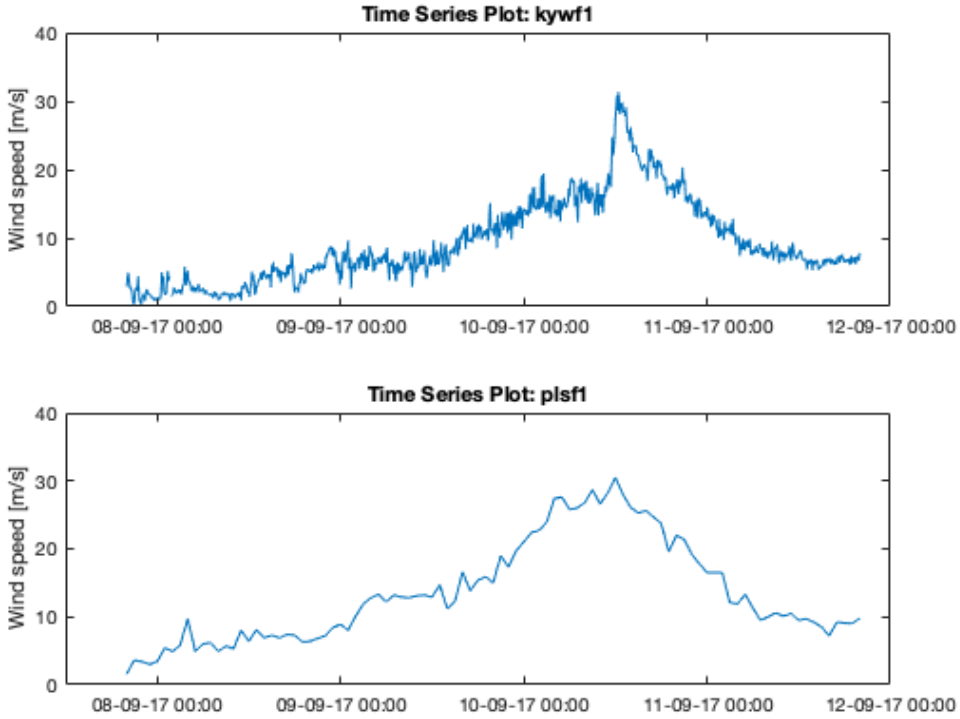

Figure 67 - Wind speeds observed at KYWF1 and PLSF1

Wave height comparison

For the stations 41046 and 41043 the wave heights are measured. These measurements are compared with the wave heights from the Delft3D model. These stations are in the open ocean and were at the time of TC Irma quite far away from the center (see Figure 68). Therefore, the measured and observed wave heights are not very high. For the validation of the model, not much wave height buoys are available. Hence, use needs to be made of buoys that were not located as close to the CTE as what would have been optimal.

Another factor that influences the validation of the generated wave heights of the model is the appearance of a second TC, called José in the same timeframe. In hurricane season it can happen that multiple TCs occur shortly after each other. For the validation process it is observed that TC José passes by the wave buoys in the area and therefore the time frame in which this happens is neglected. Since José resulted in observed wave heights that were of the order of 10 meters, this would have influenced the wave height graphs too much. Therefore, a time frame for the validation of the wave heights is chosen between 6 and 10 September. Considering that José entered the grid at around the 10th of September, this frame is assumed to be correct.

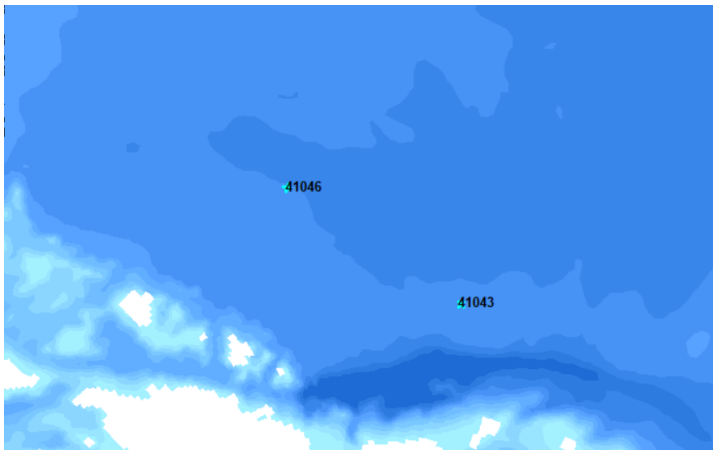

Figure 68 - Observation points open ocean

At station 41043 a peak significant wave height of 3.5 m is measured with the Delft3D-model (See Figure 69). In the observations a peak significant wave height of 6.8 m was measured (See Figure 70). At station 41046 a peak significant wave height of 3.6 m is measured with the Delft3D-model (See Figure 69). In the observations a peak significant wave height of 6.6 m was measured (See Figure 70).

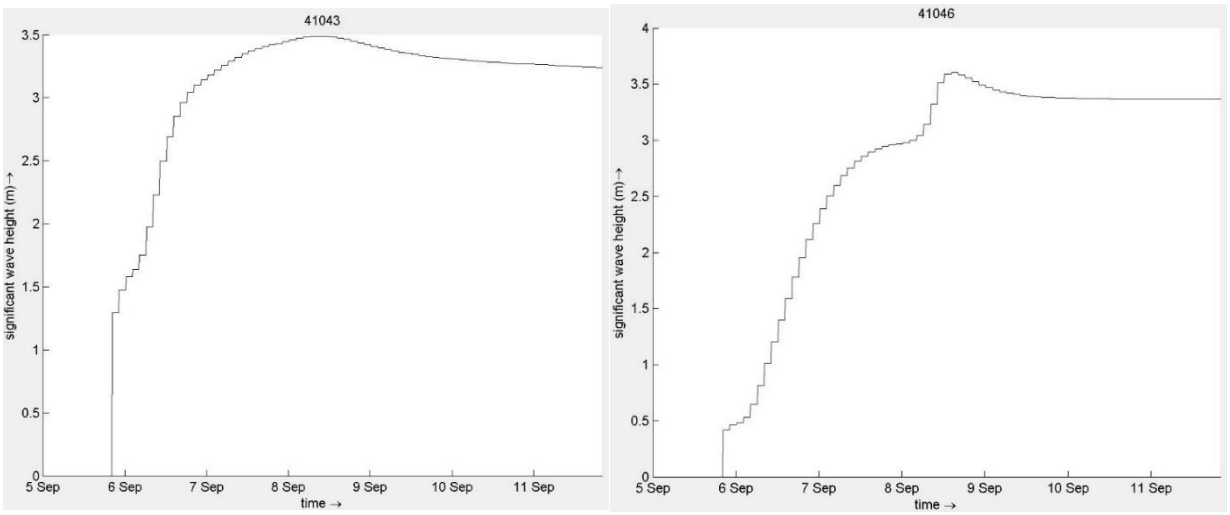

Figure 69 - Significant wave height 41043 & 41046

The peak significant wave height is reached at approximately the same time for station 41046 via the model compared to the real observations. They occur around September 8th. For station 41043 it can be concluded that the peaks are not observed at the same time. Also, it can be said that the gradients in the graphs are not alike. The waves that are measured at these observation points have wave directions of around 180 degrees, however the Delft3D gives the main wave direction in the order of 350 degrees. From this it can be concluded that the waves that were measured at the observation stations probably arose from a different source. Since there are no other wave buoys that can be used to validate the model, not a good estimation can be made whether the wave propagation from the Delft3D model is close to reality. Next to the use of wave buoys, use can be made of one-time observations during the Irma. This is less accurate since its only one value and not calibrated, however it still gives a good approximation for the recorded maximum wave heights. Therefore, it is chosen to compare the wave heights from the model to the observations during Irma at Cayo Coco.

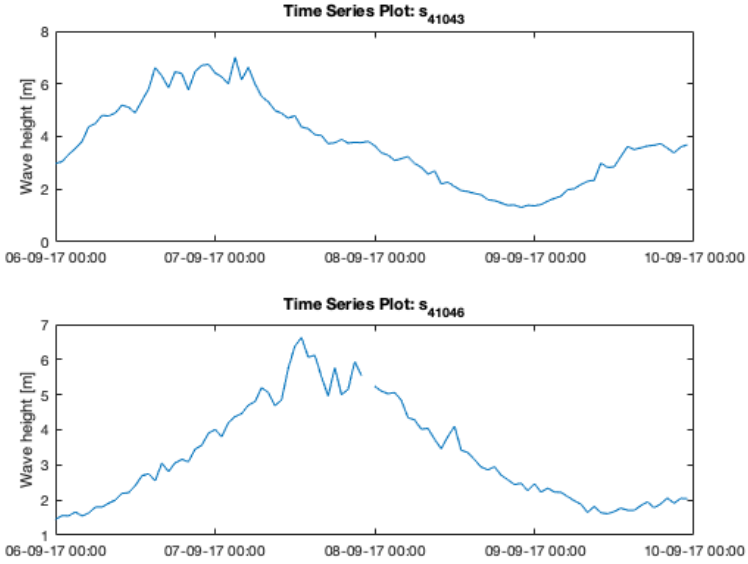

Figure 70 - Significant wave height 41043 & 41046

According to (P. & al., 2018) the maximum significant wave heights at Cayo Coco were estimated to be between 5 and 6 meters. As can be seen in Figure 71 the measured wave heights at Cayo Coco, are said to be between 5 and 6 meters for the Delft3D-model.

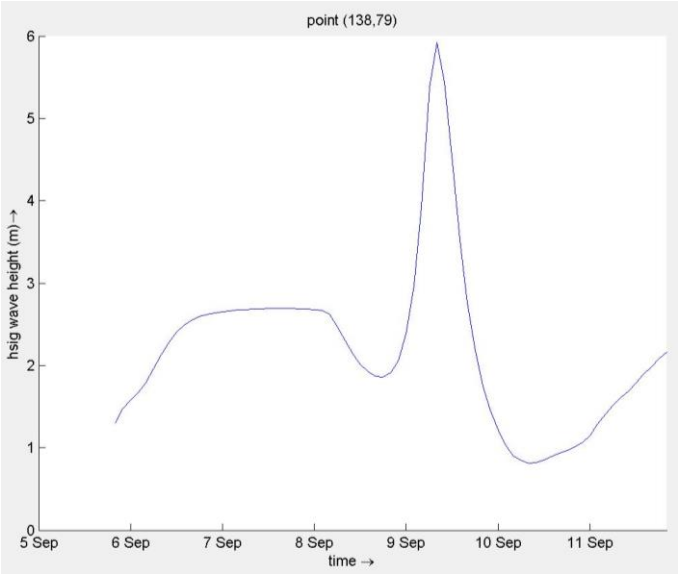

Figure 71 - Significant wave height Cayo Coco

Water level comparison

For the stations 8723970 and 8724580 the water levels are measured. These measurements are compared with the measured water levels from the Delft3D model. These stations are located near Key West (see Figure 64). For the observed water levels from the stations the tidal fluctuations were removed to generate a graph which has its x-axis located at MSL. This tide is removed, since in the Delft3D model has no tides inputted as boundary conditions. By removing the tidal signals, the water level graphs from the real observations and from the Delft3D model can be compared. First a least-squares tidal fit was applied to the dataset (see Figure 72 & Figure 73).

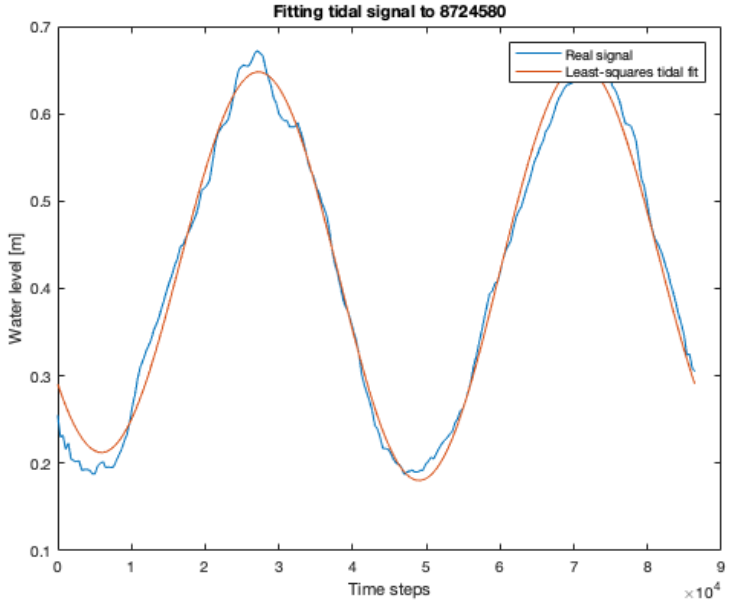

Figure 72 - Least-squares tidal fit to 8724580

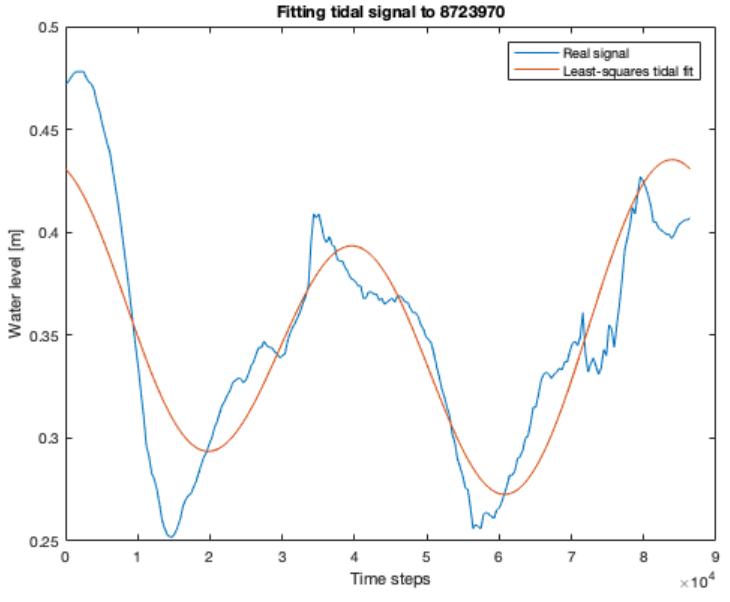

Figure 73 - Least-squares tidal fit to 8723970

To obtain the final dataset, which allows for comparison between the Delft-3D data and the observed data, this least-squares tidal fit was subtracted to the real data set (see Figure 74). For further elaboration on this topic, see Appendix E.

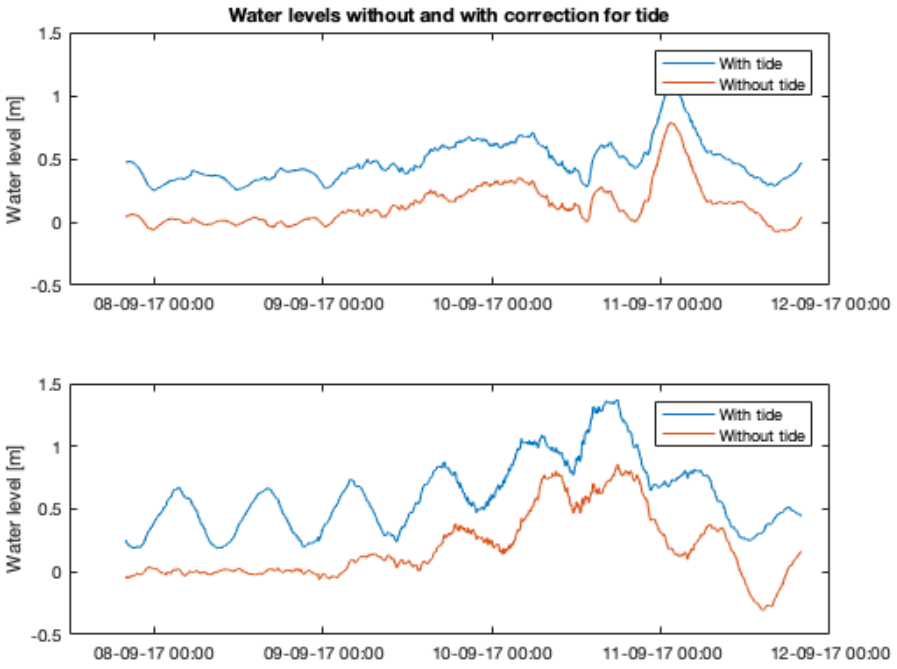

Figure 74 - Water levels with and without tide

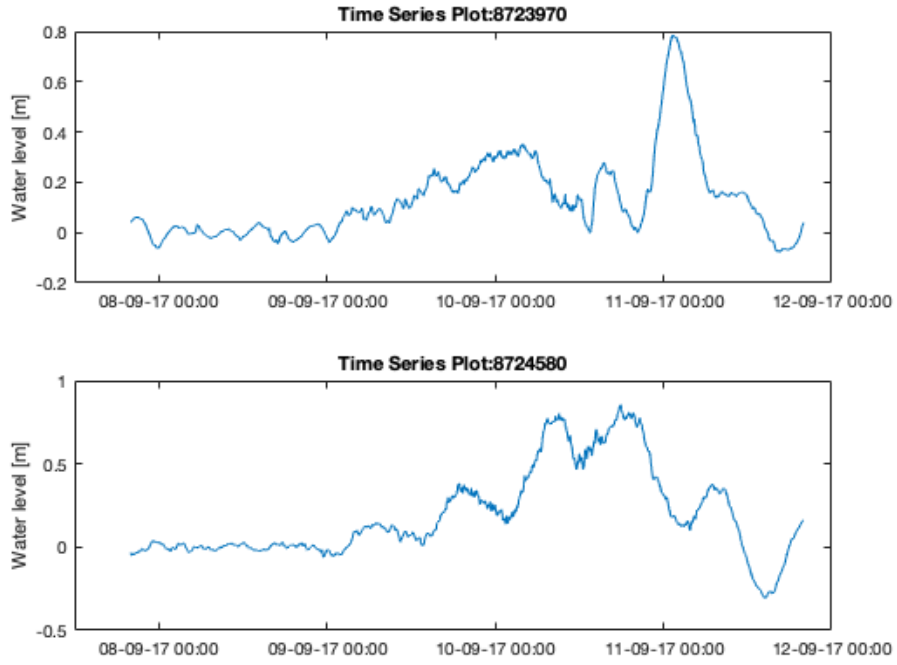

Figure 75 - Water levels stations 8723970 & 8724580 from observed data

At station 8723970 a maximum water level of 0.85 m is measured with the Delft3D model (see Figure 76). At station 41043 a peak significant wave height of 3.5 m is measured with the Delft3D model (see Figure 69). In the observations a peak significant wave height of 6.8 m was measured (see Figure 70). At station 41046 a peak significant wave height of 3.6 m is measured with the Delft3D model (see Figure 69). In the observations a peak significant wave height of 6.6 m was measured (see Figure 70).

In the observations a maximum water level of 0.8 m was measured (see Figure 75). At station 8724580 a maximum water level of 0.68 m is measured with the Delft3D model (see Figure 77). In the observations a

maximum water level of 0.75 m was measured (see Figure 75). The maximum water level is reached at around the same time for the model as well as for the real observations. For station 8723970 as well as station 8724580 the peak is reached at around September the 10th at 12:00.

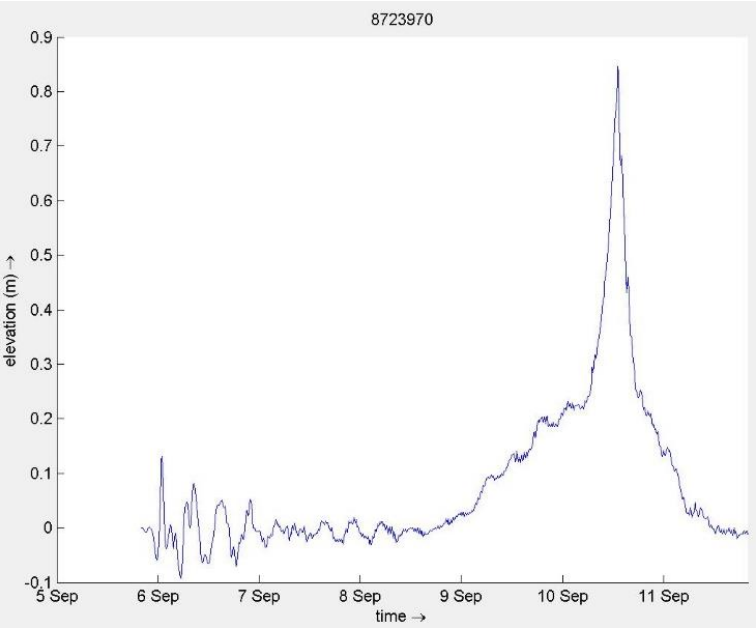

Figure 76 - Water level station 8723970

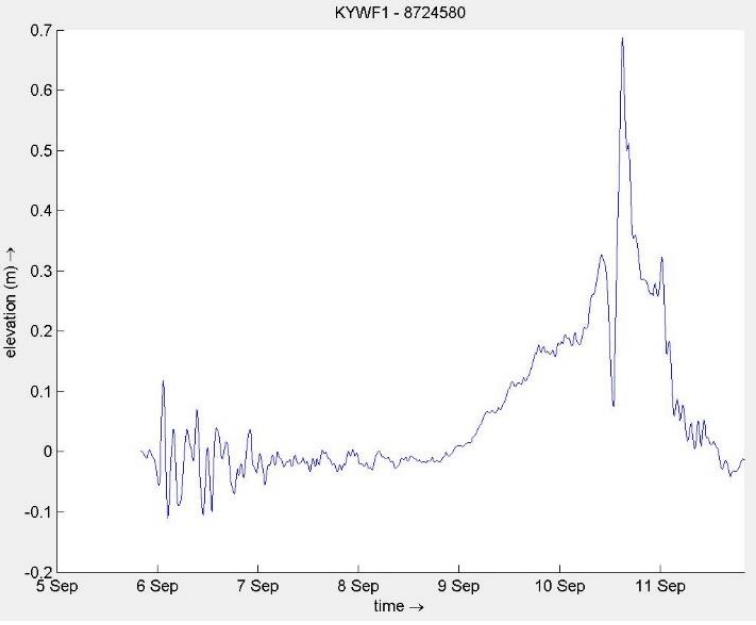

Figure 77 - Water level station 8724580

5.1.8 Conclusion

The focus of the Delft3D-model is to simulate the real hydrodynamic and meteorological effects of an extreme weather event at the location of interest, the CTE at the bay of Matanzas. Thus, it is important to check if the results of the model are similar to the real observations. However, the model has some limitations which makes it not possible to get the same results as in reality.

Firstly, the model has some limitations in its ability to simulate the wind and waves that are present in the Gulf of Mexico. The inputted uniform wind can only have a uniform value for the whole grid which can only vary over time and not in space, which is not the same as in reality. Also, the modelled uniform wind can only have a single direction over the complete domain. The TC that is generated via the Spiderweb also differs from reality in the fact that the radius is kept constant for the whole duration of the track, while the radius of the TC differs over time.

Secondly, stations located in the open ocean can observe waves that are not generated by Irma or the uniform wind, but by other sources that are not present in the model. These distortion in the wave buoys of influences outside the model are not to be modelled. These distortions will negatively influence the validation process.

Consequently, it can be concluded that the model works well enough to generate reliable wave heights and water levels, which can be used as input for the XBeach model. The Delft3D results will be used in XBeach to go more in depth into the location of interest and see what happens at the project location in detail.

5.2 XBeach model

The program XBeach, which is used to give more detail to the generated output by Delft3D is a numerical model that simulates hydrodynamic and morphodynamical processes with their corresponding impact on coastal areas with a small domain size. It includes the short- and long wave transformation and wave-induced setup. The morphodynamical processes are not considered in the scope of this project since bed load and suspended load transport for a rocky coast such as near the CTE for a short storm duration is negligible. Because erosion is not an issue in this situation the main interest is the wave propagation. XBeach can more accurately predict wave propagation and includes higher order processes in its simulation. For waves the following phenomena can be simulated in XBeach:

- Time-varying wave action balance including refraction, shoaling, current refraction and wave breaking
- A roller model, including breaker delay
- Wave amplitude effects on wave celerity
- Wave-current interaction
- Dissipation model for use in the nonstationary wave energy balance (Roelvink, 1993)
- Wave dissipation formulation for stationary wave energy balance (Baldock, 1998)

(Unesco-IHE institute for Water Education, Deltares, Delft University of Technology, 2010)

5.2.1 Computational grid

The computations made in XBeach are on a much smaller scale than Delft3D. A small cell sizes is needed to accurately model all wave processes. The variance density spectra that are given by Delft3D to the XBeach model give information about the wave climate. The narrower the spectrum and the more constant the wave climate (variance density spectrum does not change rapidly over time), the larger the wave grouping, the more profound long waves are. These long waves are the main contributors to for example overtopping, hence these need to be represented well. Less wave grouping means shorter long waves and therefore the grid needs to be refined even more.

A tradeoff had to be made between saving computation time and the size of the area of interest and cell sizes. The area of interest is 1440 m x 1200 m and all cells are 30 m x 30 m. In Figure 78 the grid is shown with the bathymetry. The location of the CTE is indicated with the purple dot. The wave input comes from the seaward boundary, in this case the north side of the grid (see section below), the orientation is such that the expected predominant wave directions are included.

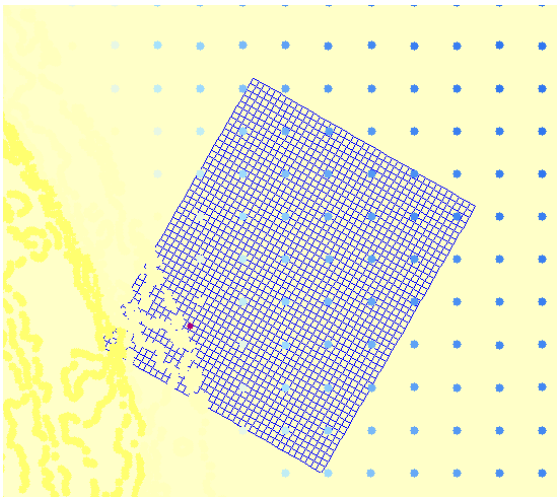

Figure 78 – XBeach grid with bathymetry and CTE indicated

5.2.2 Bathymetry

The bathymetry used is both of land and the seabed. Because of the high degree of refinement of the grid, only a few bathymetry points fall within the grid as can be seen in Figure 78. By loosening the requirements for grid cell averaging and using internal diffusion all points on the grid are given a depth value. However, this interpolation causes some deviations from the real situation.

5.2.3 Boundary Conditions

XBeach works with both flow and wave boundary conditions. Flow boundary conditions need to be specified on all sides of the domain. XBeach differentiates between offshore, lateral and landward boundaries. Wave boundary conditions only need to be specified at the offshore boundary.

Flow

The landward and offshore boundaries are set to absorbing generating (weakly reflective) boundaries in 2D. This boundary condition is based on the method of characteristic and needs to satisfy 2 conditions:

- The region outside the computation domain can influence the motion within the domain only through the incident (long) waves and through the currents along the boundaries
- The (long) waves propagating out of the computational domain must be allowed to freely propagate through the open-ocean offshore boundary with minimal reflection

(Unesco-IHE institute for Water Education, Deltares, Delft University of Technology, 2010)

The lateral boundary conditions are set to Neumann. This means that there is no change locally in surface elevation and velocities. In this way the lateral boundaries do not influence the results.

Wave

At the seaside boundary wave boundary conditions can be implemented. Delft3D can calculate 2D energy density spectra at selected locations. The 2D energy density spectrum contains information about the frequency spreading, directional spreading and the energy densities per frequency per direction ($J/m^2/Hz/degree$). XBeach uses this output from Delft3D as input at its boundaries and simulates the waves propagating from open water to shore.

Tide

No tide is used in the model, information available about the tide at the location is uncertain and will more likely distort the model results than add to it. As mentioned in 5.1.2, the tide is added separately in the design stage by means of super positioning.

Chapter 6

Results

6.1 Synthetic Hurricanes - Part 1

6.1.1 Set-up

Introduction

In this chapter the results of the synthetic hurricane run that were set up in Chapter 4 are discussed. When running the hurricanes and looking at preliminary results some adjustments to the runs had to be made, this will first be discussed. Afterwards the relevant output parameters are analysed and interpreted.

Model adjustments

Time step

The synthetic hurricanes are run with different time steps according to their duration. The synthetic hurricane combinations consist of different forward speeds and therefore, take a larger or smaller amount of time to cover the different tracks. Some of the hurricanes take 4 days to cross the grid, where others take 10 days. Thus, not the same time step can be used for all combinations, since the computational time would be too large for the hurricanes that take 10 days to cross the grid.

Next to this, it is observed that the hurricanes with a high forward speed need a small timestep in order to give reasonable results. It seems that when the time step is chosen too large (10 minutes), the hurricane skips steps in the track and does not generate waves at those steps. The hurricane 'jumps' over the waves and when the waves are not travelling with the hurricane, the generated waves are much smaller. This results in significant wave heights that are very small and cannot be true to reality (Figure 79).

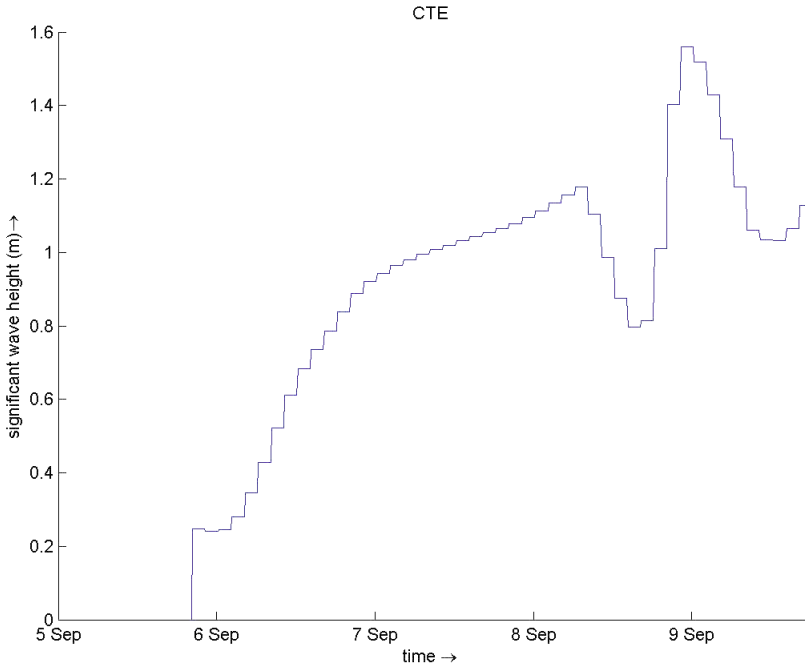

Figure 79 - Significant wave height at CTE, combination 1, large time step

Consequently, it is chosen to run the fast hurricanes with a time step of 1 minute and slow-medium hurricanes with a time step of 3-10 minutes.

Spiderweb

For every combination a Spiderweb should have been generated according with the desired wind speeds, locations and forward speed of the TC. Combinations 1 to 6 are supposed to have high wind velocities, 7 to 12 medium wind velocities and 13 to 18 low wind velocities (See Table 13). However, Figure 80 shows that for the different combinations the maximum wind speed at the CTE is not as they are supposed to be.

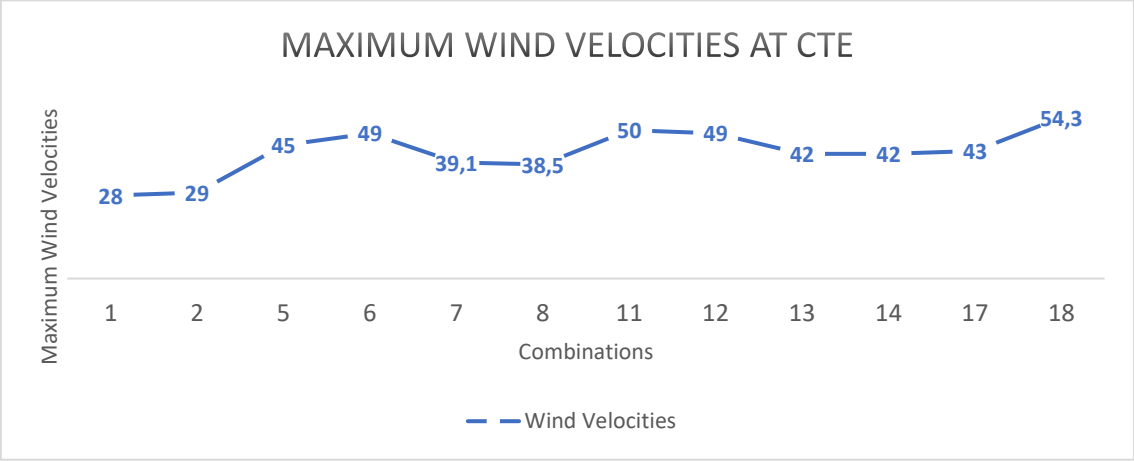

Figure 80 - Maximum wind velocities

Something went wrong with the generation of the Delft3D Spiderweb input files. It seems that this has to do with the approach of the Holland formula, which is used in the MATLAB script to create the Spiderweb input file. The wind speed input into this formula must be manipulated to resemble the different wind speed categories (Low, Medium, High). It seemed that the manipulation of this input created a discrepancy between the wind and central pressure. This most likely resulted in a ratio that was not accurate leading to the unexpected wind speeds.

A note should be made that this does not mean that the maximum velocity over the entire track cannot be higher than the maximum wind speeds given in Figure 80. The synthetic hurricanes are based on hurricane Irma, which did not have a constant speed over the entire track. Furthermore, since the forward velocity is altered the maximum wind speeds are observed at a different point along the track (Figure 81). Track 3 is the track of hurricane Irma but moved below Cuba 1.5 degrees to the south. This means that wind speeds that were originally observed overseas and near Florida are now over the CTE.

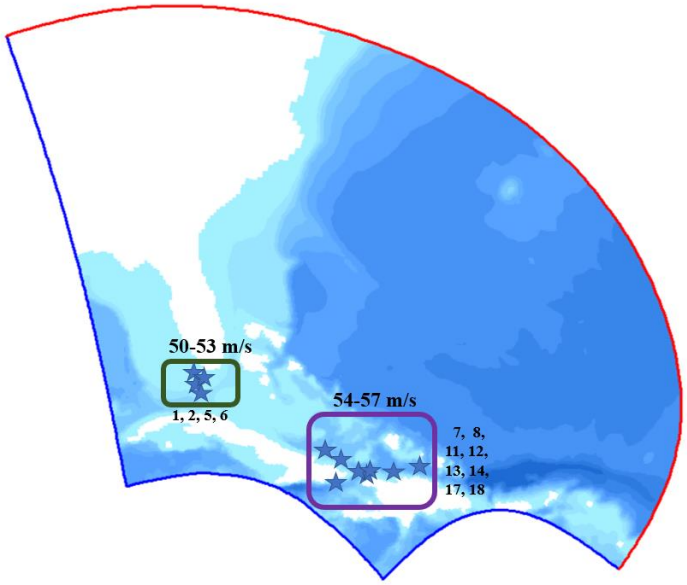

Figure 81 - Maximum recorded wind speeds for all combinations

In Figure 81, maximum record wind speeds are given for all the combinations. It can clearly be seen that combination 1, 2, 5 and 6 have their maximum wind speeds near Key West and have slightly lower maximum wind speeds than the other combinations.

Track 2 excluded

From Figure 80 it can also be seen that some combinations that have been discussed in Chapter 4.2 are missing. These observations, which all follow the second track, are left out on purpose, since they are deemed irrelevant. The probability of occurrence for hurricanes that follow the second track is significantly lower than the probability of occurrence of the first and third track. Next to this, also the wave height and water level results of the second track seemed to be significantly less normative than for the first and third track. As an example, the results of the third and fourth combination that follow the second track are given.

In Figure 82 the water levels and significant wave heights are given for combination 3 and 4 that follow the second track. From Delft3D the maximum storm surge is measured to be 0.17 - 0.19 m and the maximum wave height 1.2 - 1.5 m. These measured wave heights and water levels are negligible compared to the measurements from the combinations that follow track 1 and 3, as will be discussed in 6.1.2. The combinations 3, 4, 9, 10, 15 and 16 that follow track 2 are therefore not further assessed within this research.

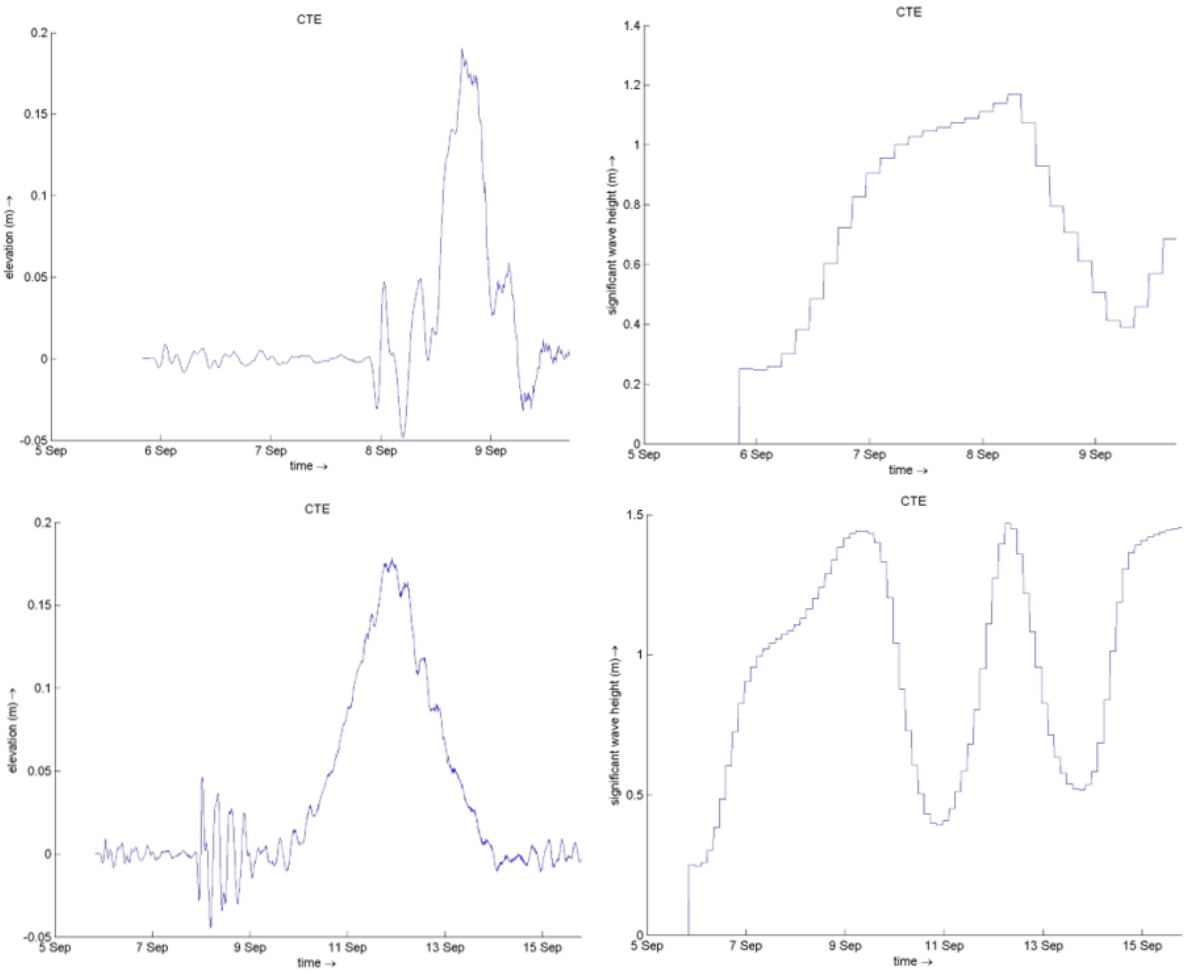

Figure 82 - Water levels and significant wave heights, combinations 3 & 4

Location specific output

The combinations are run in the Delft3D model. At the location of the CTE an observation point is placed to generate location specific output that is used to compare the combinations (see Figure 83).

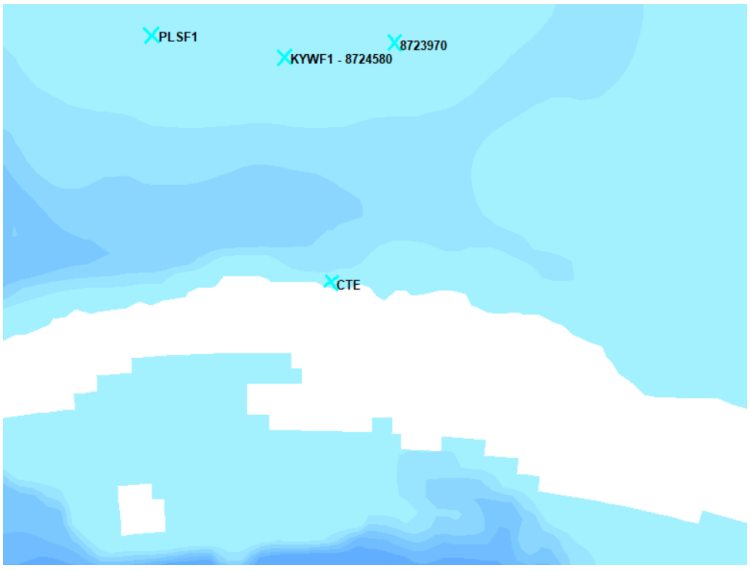

Figure 83 - Observation point CTE

New Grid Track 3

For combinations that follow track 1 and 2, the grid discussed in Chapter 5 is used. Track 3 follows a path that doesn't entirely fall into the original grid since it runs largely south of Cuba (see Figure 84). Extending the original grid to the south would create a lot of refined grid cells in an unwanted area and it would not be possible to capture the entire track. For this reason, an additional grid is created for this track.

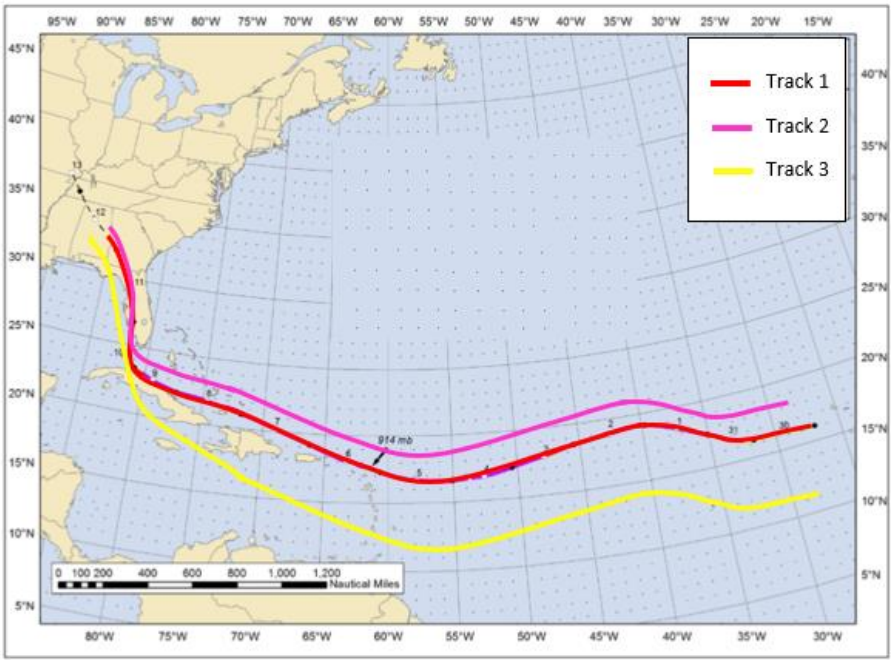

Figure 84 - Synthetic Hurricanes Tracks

The additional grid for track 3 is shown in Figure 85. The new grid has grid cells with dimensions of 15 by 15 km. It is not as refined at the area of interest as the original grid which has a resolution of 7 by 7 km at the area of interest. Because of limited time a trade-off has to be made between the refinement of the grid and the corresponding computation time. The results from Delft3D for the area around the CTE are analyzed in XBeach, which has a much higher resolution. The depth and boundary conditions are handled the same way as the original grid. This information can be found in Chapter 5.

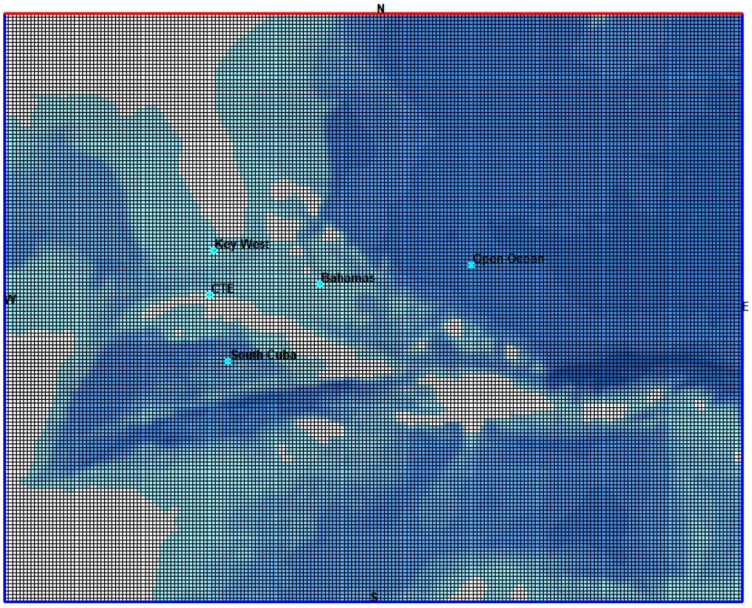

Figure 85 - Grid used for combinations on track 3

6.1.2 Delft3D results

Introduction

The results for all the combinations including track 1 and 3 are given in Table 18. The output of these runs is structured per combination. The output of Delft3D is given by graphs of the water levels, significant wave heights, peak wave periods, wave directions, wind velocities and wave lengths. The maximum values of these graphs are given in Table 18. In the analysis, special attention is given to each output parameter with respect to the significant wave height, forward speed and their corresponding track.

More elaboration on the following topics in relation with the background theory is given in the discussion and sensitivity analysis.

Results

Combination	Peak Wave Period [s]	Significant Wave height [m]	Water level [m]	Wave direction [degrees]	Wind Velocity [m/s]	Wavelength [m]	Forward speed [m/s]	Track	Wave group celerity [m/s]
1	8.4	4.8	0.47	350	28	108	13.3	1	6.43
2	9.8	7.5	0.44	350	29	147	3	1	7.5
5	6.5	4.3	0.84	350	45	66	13.3	3	5.08
6	7.6	5.95	0.84	305	49	91	3	3	5.99
7	10.6	9.5	0.57	350	39.1	177	10.2	1	8.35
8	10.95	9.1	0.55	350	38.5	184	3	1	8.40
11	10.5	11.7	0.84	305	50	169	10.2	3	8.05
12	10.5	11.1	0.83	350	49	171	3	3	8.14
13	11.9	12.1	0.58	350	42	220	7.8	1	9.24
14	12.2	13.7	0.56	350	42	246	3	1	10.08
17	9.3	8.2	0.85	340	43	138	7.8	3	7.42
18	11.8	14.1	0.85	305	54.3	209	3	3	8.86

Table 18 - Maximum values at CTE

Analysis

Wind velocity

As discussed in the introduction of this chapter, the wind velocities do not match the desired wind speeds that were theoretically designed to create the most likely normative TC. It is seen in Table 18 that the maximum wind velocities of the different combinations do not vary as much from each other as they should.

There is not a very clear correlation between the maximum wind velocities and significant wave heights, at the time that the TC passes the CTE.

The TCs that follow track 3 generate higher wind speeds at the location of interest than track 1. There is no trend observed between the wind speeds and the forward speed of the TC.

Significant wave height

From the results in Table 18 it can be concluded that according to the Delft3D model, there is a correlation between TCs with a low forward speed and TCs that generate large waves.

It can also be seen that there is no correlation between track 1 & 3 and the generation of waves. For some synthetic hurricanes where the forward speed for track 1 & 3 is equal, the significant wave height is higher for the hurricanes that cross track 1 and for others the generated waves for track 3 are higher.

Wave group celerity

The wave group celerity has not been extracted from the Delft3D model, but has been calculated from the peak wave periods, using deep-water conditions.

There seems to be a correlation between TCs that generate the largest waves and the group celerity of these generated waves, this group celerity tends to be higher when the generated waves are higher as well.

The TCs that follow track 1 and have the same forward speed as the TCs that follow track 3 seem to have a higher wave group celerity. When the forward speed of a TC is higher, the wave group celerity is lower. This holds for the TCs for track 1 as well as for track 3.

Water level

There is no trend observed between the significant wave height and the rise in water level.

Table 18 gives the water levels at the time that the synthetic hurricane passes the CTE. It is seen that for the synthetic hurricanes that follow the same track, the generated storm surge in relation to the rise of water level is equal. Therefore, according to the Delft3D-model, the forward speed of the synthetic hurricanes does not influence the amount of storm surge experienced by the CTE.

The generated storm surge for track 3 is higher than the generated storm surge for track 1.

Peak wave period

It can be seen that the peak wave periods increase as the wave height increases. A trend is also observed that higher forward speeds lead to lower peak wave periods. This is a logical trend as there is a maximum steepness that the waves can have. The differences however are small. Furthermore track 3 has lower peak wave periods than track 1 for the same forward speed.

Wave direction

There seem to be no correlations between the wave direction in relation to the tracks, forward speed and significant wave heights. The graphs also seem to be very similar for all the combinations.

Wavelength

From Table 18 it can be concluded that the wavelength is larger when the wave heights are also higher. The wavelengths seem to be slightly lower for the TCs that follow track 3 than the ones that follow track 1. Ultimately, lower forward speeds for the TCs seem to generate higher wavelengths, for all combinations.

6.1.3 XBeach results

Choice of combinations

The storm surge, as well as the significant wave height, can be calculated in more detail with the program XBeach. Since the time span of the project is limited, the XBeach calculation is only be applied to two normative combinations which caused the highest significant wave heights for the two respective tracks. Therefore, the combinations 14 and 18 are run again in more detail with a smaller timestep.

Model set-up

The Delft3D runs are run with a location file added to them. This location file contains the coordinates of a point at the boundary of the XBeach grid (Figure 86). At this location the energy density spectrum of the waves is calculated. This energy density spectrum is used as the boundary condition for XBeach.

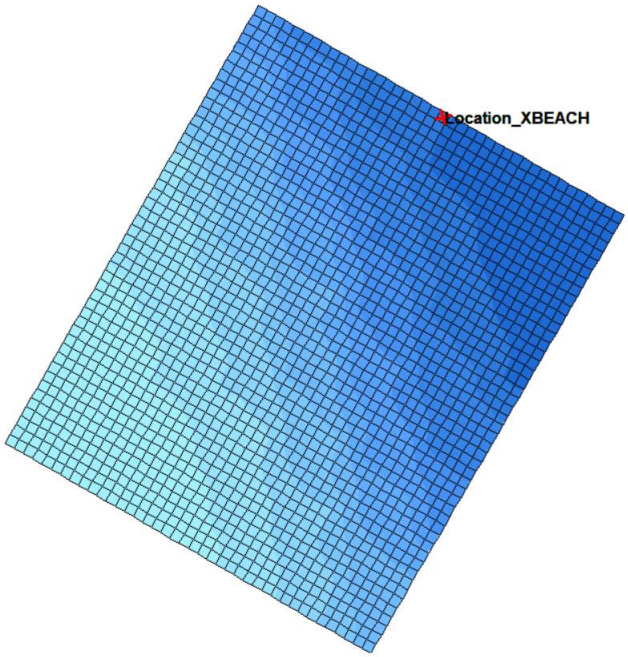

Figure 86 - XBeach Grid with Location Delft3D

For the XBeach model, the grid from Figure 87 is used with the corresponding bathymetry. The bathymetry data used for the XBeach depth file has more detail than the bathymetry used for the main grid, since it is focussed on the location of interest and consists out of more bathymetry points. As seen on Figure 87, the CTE is located on Cuba's mainland, therefore it is not possible to gain data for the significant wave height and storm surge at that location. Hence, a point is chosen that is located as close as possible to the CTE and is situated in the water. For this point (observation point "Closest-Shore" in Figure 87), the data (significant wave height & storm surge) generated via XBeach is given for the combinations 14 and 18.

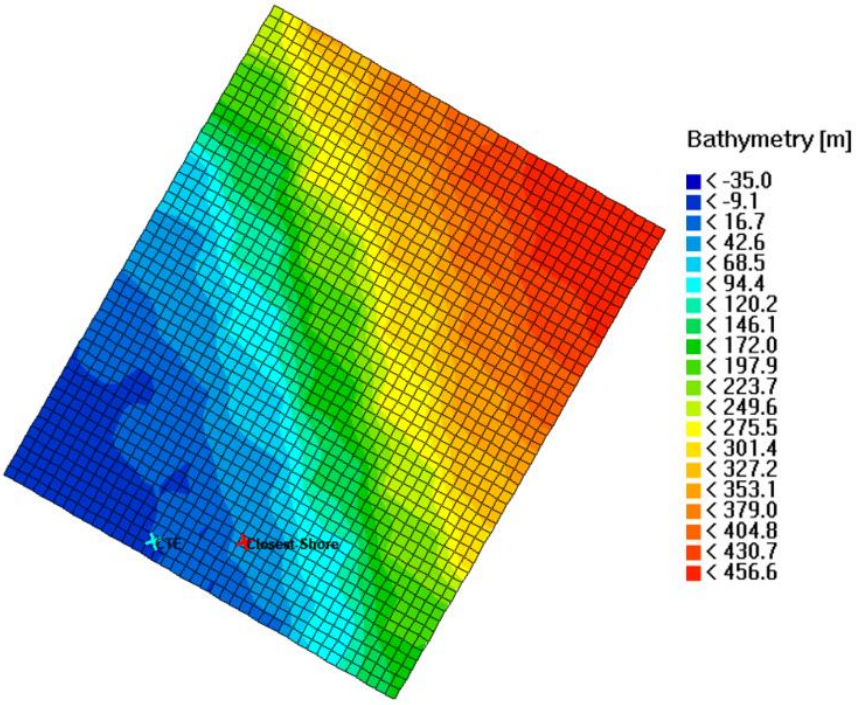

Figure 87 – XBeach Bathymetry grid and Observation point for significant wave height

The synthetic hurricanes from combinations 14 and 18 cover the time span from the 5th of September 2017 at 8 o'clock in the evening till the 15th of September 2017 at seven o'clock in the evening. This translates to almost 10 days. In order to give reasonable results, but not create unmanageable computational time, a duration of 24 hours is chosen to run XBeach. For each combination it is decided for which 24 hours the highest waves were created in the XBeach grid. This results in time steps 270 until 318 for combination 14 and time steps 302 until 350 for combination 18. With each time step being 30 minutes (output chosen for Delft3D), this translates to the period from the 11th of September 10:30 AM till the 12th of September 10:30 AM for combination 14. For combination 18 this translates to the period from the 12th of September 02:30 AM till the 13th of September 02:30 AM.

At the Observation point "Closest-Shore" on Figure 87, a file is extracted with the corresponding significant wave heights and water levels. From this, graphs are formed, that can be seen in Figure 88 and Figure 89. The same process is done for combination 18, resulting in graphs that can be seen in Figure 90 and Figure 91.

It should be taken into account that XBeach gives wave heights as H_{rms}. The significant wave height is about 1.4 times as large as the H_{rms} for a storm wave spectrum. In the following combinations this ratio is used to calculate the significant wave heights from XBeach.

Combination 14

For combination 14, a significant wave height of 9.7 m is observed from the XBeach computations (Figure 88). From Delft3D, a significant wave height of 13.7 m is observed. Since the XBeach model, as explained previously, is superior over the Delft3D-model in the shallow water-, coastal areas. The value of 9.7 m is used for the significant wave height that is created by synthetic hurricane combination 14 at the location of the CTE.

Next to this, a maximum storm surge of 1.6 m is measured via the XBeach model (Figure 89), where the Delft3D model predicted a maximum storm surge of 0.56 m.

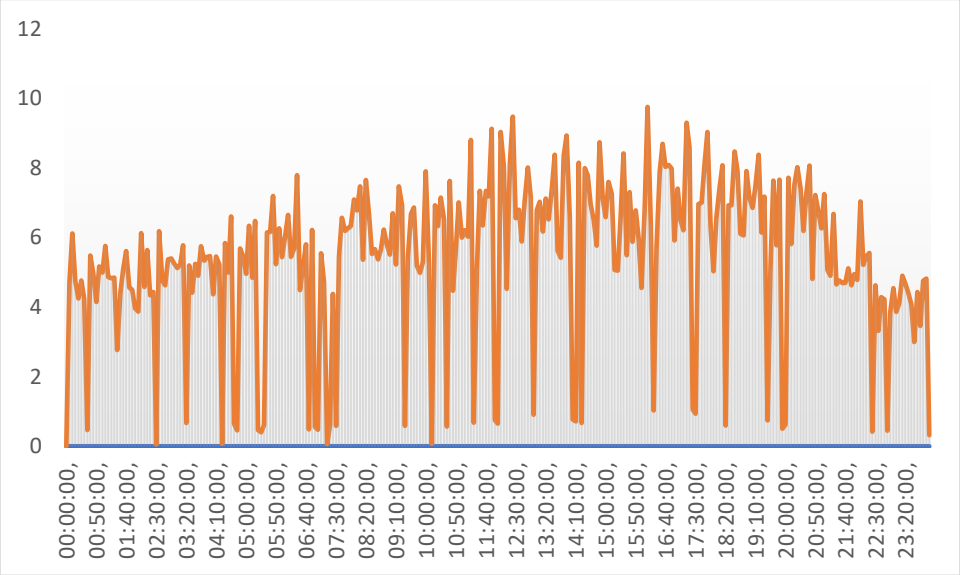

Figure 88 - Significant wave height, combination 14

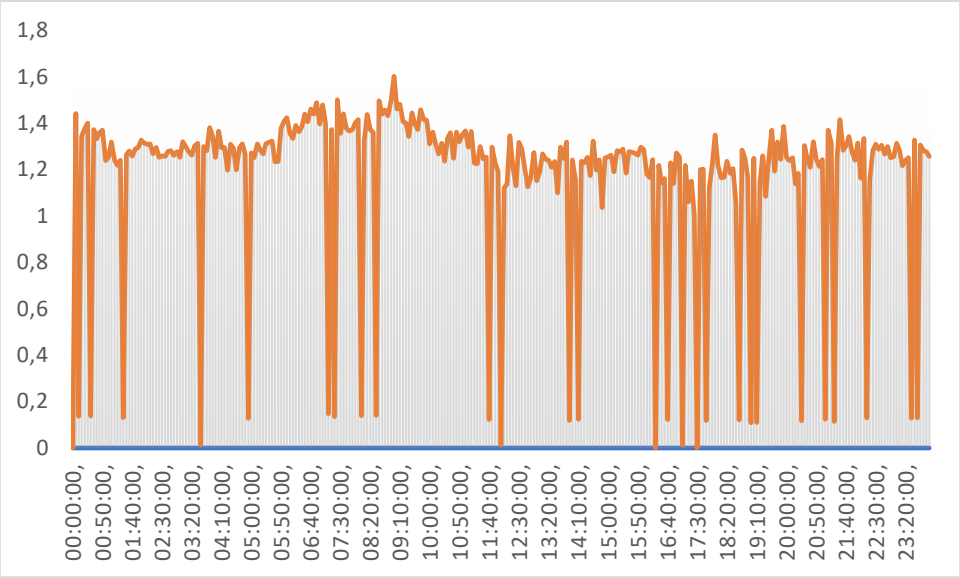

Figure 89 - Storm surge, combination 14

Combination 18

For combination 18, a significant wave height of 9.6 m is observed from the XBeach model (Figure 90). From Delft3D, a significant wave height of 14.1 m is observed. As explained before, the value of 9.6 m is used for the significant wave height that is created by synthetic hurricane combination 18 at the location of the CTE.

Next to this, a maximum storm surge of 1.5 m is observed via the XBeach model (Figure 91), where the Delft3D model predicted a maximum storm surge of 0.85 m.

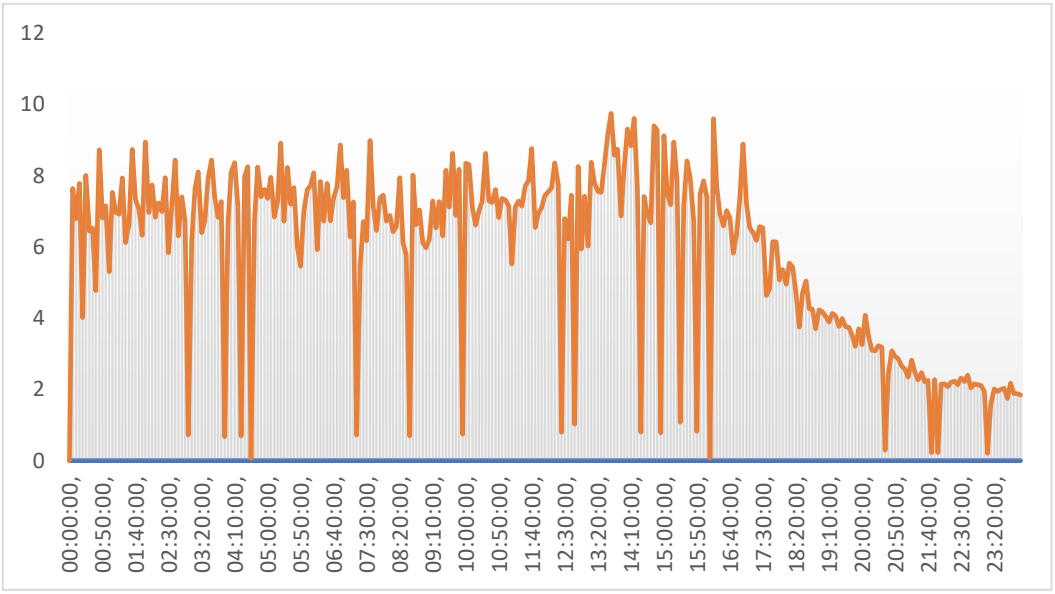

Figure 90 - Significant wave height, combination 18

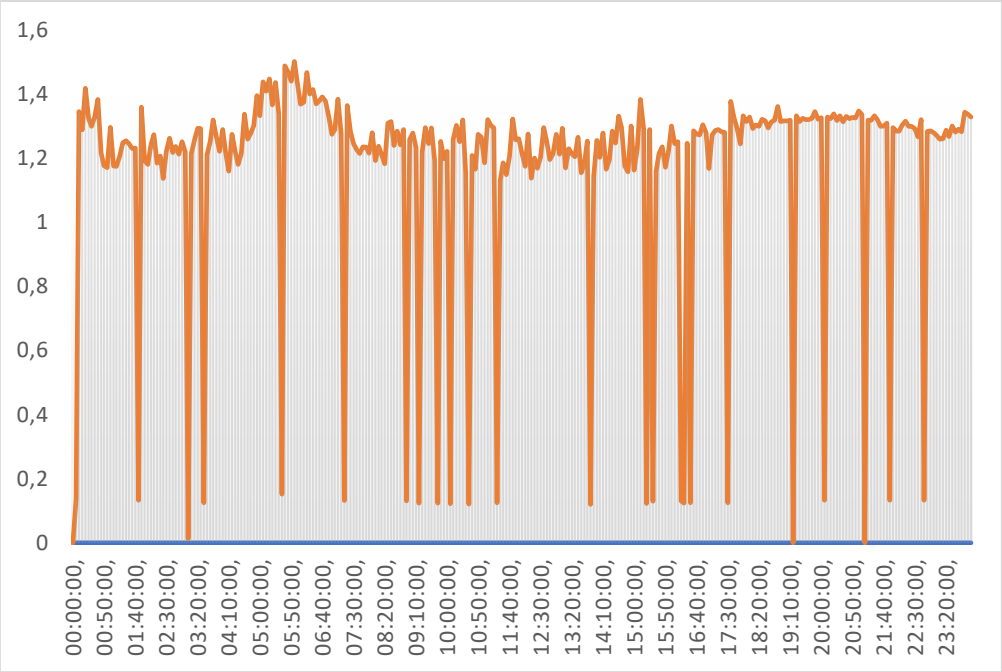

Figure 91 - Storm surge, combination 18

6.1.4 Discussion

Peak wave period

An observation from the Delft3D-model is that the significant wave height is high when the wave period is high. This wave period can be linked directly to the corresponding wavelength via Equation 12 for deep water circumstances.

$$L = \frac{g \cdot T^2}{(2\pi)}$$

Equation 12 - Deep water wavelength

From theory it is known that when the wavelength of a wave group is high, the corresponding waves can reach a greater height before the wave breaks. This is due to the wave steepness limit, which is defined according to Equation 13.

$$\frac{H}{L} \approx 0.142$$

Equation 13 - Wave steepness limit

The equation above gives the maximum value that a wave can reach before the wave breaks, when the wavelength is high the corresponding wave height can also be higher before the value of 0.142 is reached. Therefore, it can be concluded that the observed correlation between the peak wave period and the significant wave height is correct.

Another observation from the Delft3D-model is that higher forward speeds lead to lower peak wave periods. This wave period is directly linked to the frequency according with Equation 14.

$$f = \frac{1}{T}$$

Equation 14 - wave period to frequency

Since the peak wave periods are low, the corresponding frequencies are relatively high. Wave groups in deep water that have a high peak frequency travel slower compared to wave groups that have a low peak frequency.

Thus, according with the model outcomes, a fast traveling TC generates slow wave groups, and a slow travelling TC, generates fast wave groups.

When a TC is travelling slowly, the generated wave groups have more time to develop and more energy will be put into the waves. This will result in high energy waves, which is given by Equation 15. According to theory, a TC travelling with the group celerity would be best at creating large waves, but since the movement of the synthetic hurricanes is not continuous, it 'jumps' over the travelling waves, drastically reducing the wave height. Hence, from the Delft3D model results it is found that slowly travelling TCs generate higher waves.

$$E = \frac{1}{8}\rho g H^2$$

Equation 15 - Wave energy

From the wave energy equation, high energy waves, result in higher significant wave heights. As said previously, waves with a high significant wave height also have high wave lengths and thus high wave periods and low frequencies. This means that these wave groups travel relatively fast. The theory therefore confirms that slow travelling TCs result in the generation of fast wave groups and vice versa and the observations from the Delft3D model are, therefore, correct.

Furthermore, it is observed that track 3 has lower peak wave periods than track 1 for the same forward speed. Track 3 follows a path that crosses Cuba's landmass. When it moves north over Cuba it reaches the Gulf of Mexico, where the location of interest, the CTE is located. When it reaches the body of water again, it does not have enough time to put much energy into the generated waves, as is described above. The generated waves have little energy and their corresponding peak wave period is also lower. Track 1 does not cross a land mass as big as Cuba, therefore there is plenty of time for the TC to create waves with a high wave period. All in all, it can be concluded that the theory agrees with the observations and is consequently correct.

Wavelength

From the theory surrounding the peak wave period it can be concluded that the wavelength is higher when the wave heights are also higher. In addition, the same theory also confirms the fact that the wavelengths seem to be slightly lower for the TC that follow track 3 than the ones that follow track 1. Ultimately, the same theory also proves that TCs with a lower forward speed generate higher wavelengths.

Wave group celerity

The theory that is given with the peak wave periods concludes that fast TCs generate slow travelling wave groups. Since the wave groups travel with the group celerity, it can therefore be concluded that fast travelling TCs generate wave groups with a low wave group celerity. Theory about the peak wave period, confirms that TCs that follow track 1 have a higher wave group celerity and confirms the observation that a high wave group celerity is connected to a higher significant wave height.

Forward speed

The slow travelling hurricanes ultimately generate higher waves, this is not what was initially predicted. From Table 18 it is found that the group celerity that was predicted for the high wind velocities is not the group celerity that was calculated. This can be explained by the lower than expected wind speeds. Through iteration the forward speed and group celerity can be matched. Due to lack of time this is omitted.

Hurricane 17 has a group velocity that matches well with the forward speed; however, this cannot be compared to hurricane 18 since this hurricane has a larger maximum wind speed. Hurricane 13 and 14 have the same track and wind speed, and the forward speed of hurricane 14 lies relatively close to the group celerity of the waves. The wave heights are close together, but the slower forward speed generates higher waves. The theory cannot be proved or disproved based on these runs. It is likely that when the group celerity and forward speed are matched, and the model is run with a very small-time step this will generate large waves that could potentially be normative. However, due to the limited duration of the project it is not possible to run all the

combinations again. The results show that low forward velocities also generate very large waves. When the hurricane moves slowly it can transfer a lot of its energy to the waves at each location. The waves generated by the slow hurricanes are viewed as valid bases for the design of the seawall.

Water level

As discussed in the section about model adjustments, due to the change in wind velocity a discrepancy between pressure and wind caused unexpected results. It is unclear to what extend the pressure distribution in the hurricane was altered. Since surge and pressure are closely related this leaves a large uncertainty in the water levels near the CTE.

The observation that track 3 creates a larger surge also seems strange. Since the track 3 hurricanes approach Cuba from the south they also generate surge south of Cuba, this cannot reach the CTE since it is blocked by land. It could be that because the eye passes almost directly over the CTE this leads to the larger surge that is modelled. An under-pressure, which is associated with the eye of the hurricane, will cause the water to rise directly beneath it.

Track 1 vs Track 3

For some of the output parameters track 1 and 3 show different results. This is for the wind speeds (track 3 higher), peak periods (track 1 higher), wavelengths (track 1 longer) and water level (track 3 higher).

The differences can be attributed to several factors. The location of the track is very important, as mentioned before waves south of Cuba generated by track 3 are blocked by Cuba, while waves from track 1 can travel over a large distance to reach the CTE. But where track 1 passes near CTE track 3 passes directly over the CTE, this can certainly lead to different values.

The fact that track 3 crosses land would in theory mean that it will lose some of its energy. This could however not be modelled in the spider web grid due to time limitations. This means that the observed wind speeds and other parameters could be lower than shown in the model.

Another potential cause for the observed differences for the different tracks is that two different grids are used. The finer grid of track 1 is more accurate around the CTE. The results from track 3 therefore contain more uncertainty than the results from track 1. The values could lie closer together or further apart. It is however expected that these differences are not very large.

6.1.5 Sensitivity analysis

The sensitivity of the model to changes in different parameters is checked. A total of 18 different synthetic TCs are used as input for the Delt3D-model, this gives a good possibility to perform a sensitivity analysis on these TCs. The outputs of these different TCs need to be substantially different when the TCs used as input are very different, and consequently outputs need to be comparable when comparable TCs are used.

The setup of the synthetic hurricane runs is to vary one factor each time. However, as discussed before, the wind speeds of all hurricanes lie relatively close together. The average wind speed recorded at the CTE is 42 m/s with a standard deviation of 7 m/s. Nonetheless the results give a good view of the sensitivity of the model.

Hurricane 1 and 2 have all factors constant except for the forward speed, where hurricane 1 has a significantly larger forward speed of 13.3 m/s. The difference in significant wave height is 1.7 m. The difference in water level is only 3 cm.

Hurricane 1 and 13 also have the same conditions except for the wind velocity. The wind has a large effect on the significant wave height since it more than doubles. The water level differs 11 centimeters, considering the total water level increase this is a significant increase.

Hurricanes 6 and 12 have the same wind speed and the same forward speed at the CTE. The results, however, are entirely different. The time steps used for these 2 hurricanes are different. This could partly have led to a deviation of the results. Looking more closely at these runs, it becomes clear that the wind velocity field is

different for these two hurricanes. The maximum for combination 12 lies east of Cuba and for combination 6 lies near Key West. Also, the maximum wind speeds for combination 6 are lower than combination 12. This could explain, why combination 12 has higher significant wave heights.

A further sensitivity analysis is done in paragraph 6.2.1, since those result prove to be more reliable for the model analysis.

6.2 Synthetic Hurricanes - Part 2

6.2.1 Continuation Synthetic Hurricanes

As said before, something went wrong with the generation of the wind speeds earlier. Again, for computational purposes, there was no time to redo all the hurricanes, so a selection of five synthetic hurricanes was made. The five synthetic hurricanes are chosen to be combination 1, 2, 13 (slow wind speeds), 13 (high wind speeds) and 14. It is interesting to look at these hurricanes, since they are all on track 1. Additionally, from the probabilistic analysis it is concluded that there is a very small probability of occurrence for the hurricanes that follow track 3 (next to track 2, which has been concluded earlier in Chapter 6.1). Combinations 1 and 2 have high wind speeds and for those combinations it is interesting to see what impact the high wind speeds have on for example the significant wave height. From the probabilistic analysis it is also seen that combination 13 and 14 have the highest probability of occurrence and are therefore interesting to look at as well.

Next to the re-running of these synthetic hurricanes, also Irma is run with the XBeach model. This is because the synthetic hurricanes are originated from the hurricane Irma. It is interesting to look at the results of the newly run combinations with respect to Irma and compare the results. The synthetic hurricanes that have a high wind-speed are boosted with a factor according to the hurricane Irma. The synthetic hurricanes that have low-wind speeds, are originated from Irma with about half of the original wind speeds (Figure 93). What does differ for all combinations is the forward speed in relation to the forward speed of the original hurricane Irma. The original hurricane Irma had a forward speed which shifted between 2 and 8 m/s (see Figure 92), whereas the synthetic hurricanes have a constant forward speed.

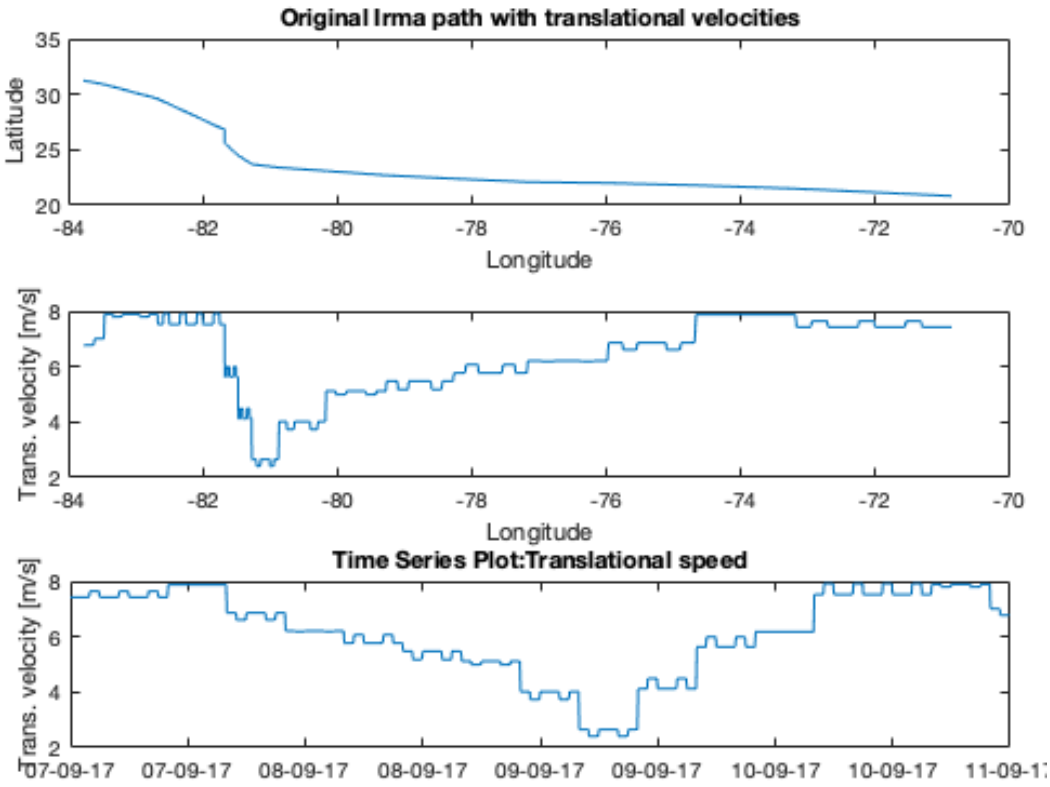

Figure 92 - Irma path with translational velocities

Figure 93 shows that the generation of the desired wind speeds in the Spiderweb grid worked this time. For the combinations 1, 2 and 13 (high wind speeds) that all have high wind speeds, the maximum wind speeds near the CTE peak out at around 68 m/s. For the combinations 13 (low wind speeds) and 14 the peak wind speeds near the CTE are around 25-29 m/s, which correspond with the desired low wind speeds. Hurricane

Irma, which has medium wind speeds, peaks at around 53 m/s near the CTE, this falls in line with the peak high and low wind speeds.

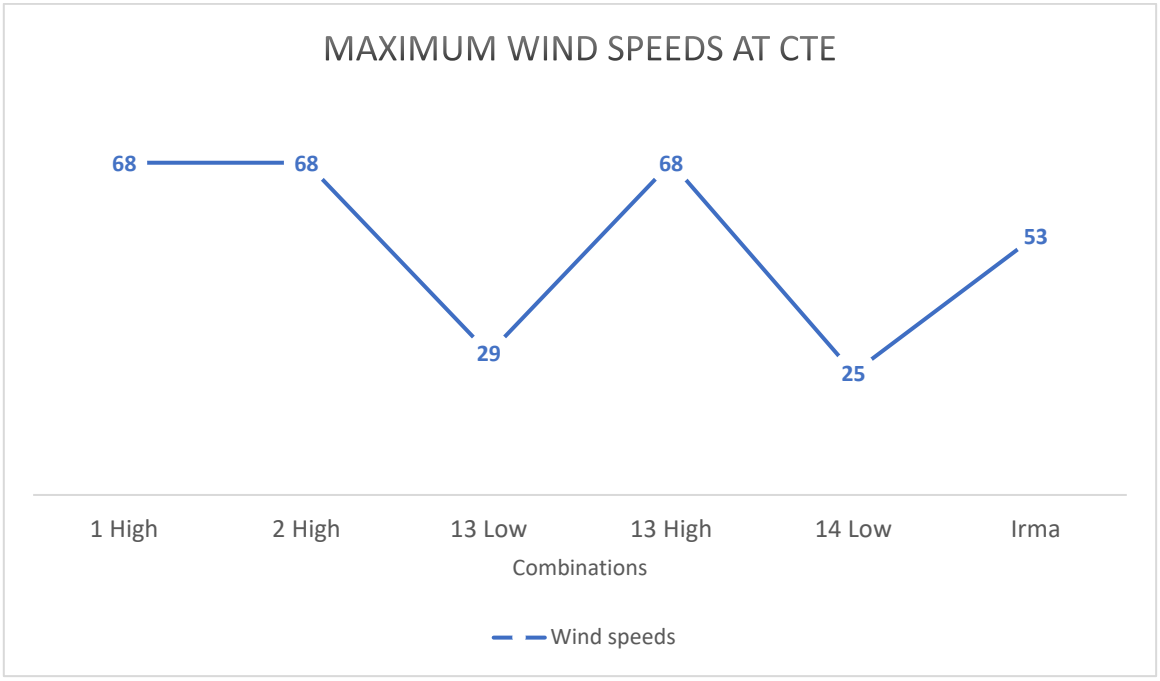

Figure 93 - Maximum wind speeds at CTE

The results of the combinations 1, 2, 13 (Low and High wind speeds), 14 and Irma are given in the following sections. They are given for the Delft3D-model as well as the XBeach model. The setup for the XBeach model is the same as explained earlier for combination 14 & 18.

However, for combinations 1 and 13 (Low and High wind speeds), a different XBeach grid had to be used. This has to do with the generated variance density spectra by the Delft3D-model that is used as input for the XBeach model. As explained earlier, XBeach takes the variance density spectra at a location at the boundary of the XBeach grid. These variance density spectra differ for all combinations, since different circumstances apply (wind speeds, forward speeds). To be able to run XBeach properly the grid should be refined enough so that no information gets lost and the program does not give errors. Combinations 1, 13 (High and Low wind speeds), have a faster forward speed and therefore cross the area of interest faster.

There seems to be a correlation between the rate of change of the variance density spectrum and the required grid refinement. The faster the synthetic hurricane the higher the rate of change of the variance density spectrum and the more refined the grid should be. This is because a changing spectrum is less narrow, leading to less wave grouping and hence shorter long waves. Since XBeach resolves its hydrodynamic equations for long waves, this means that for a wider spectrum more grid cells are needed.

Therefore, it is necessary for the combinations 1, 13 (High and Low wind speeds) to create a new more refined grid. This resulted in a longer computational time but also a higher detail in the results.

Combination 1 – High wind speeds

In the beginning of this chapter, it is mentioned that combination 1 is run with a different XBeach grid. The results from the XBeach run with this new grid seems to be right for the significant wave heights. However, the resulting water level rises that XBeach give as output look to be wrong. Thus, for combination 1, only the significant wave heights are considered.

Combination 1 is run with the original forward speed of 13.3 m/s. A significant wave height of 5.58 m is observed via the XBeach computations (see Figure 94). With Delft3D a significant wave height of 7.1 m is observed.

Originally combination 1 had a significant wave height of 4.8 m as a result of the Delft3D-model. The wind speed increased for combination 1 in relation to the original run combination 1. The resulting significant wave height of 7.1 m from Delft3D is higher than the original 4.8 m.

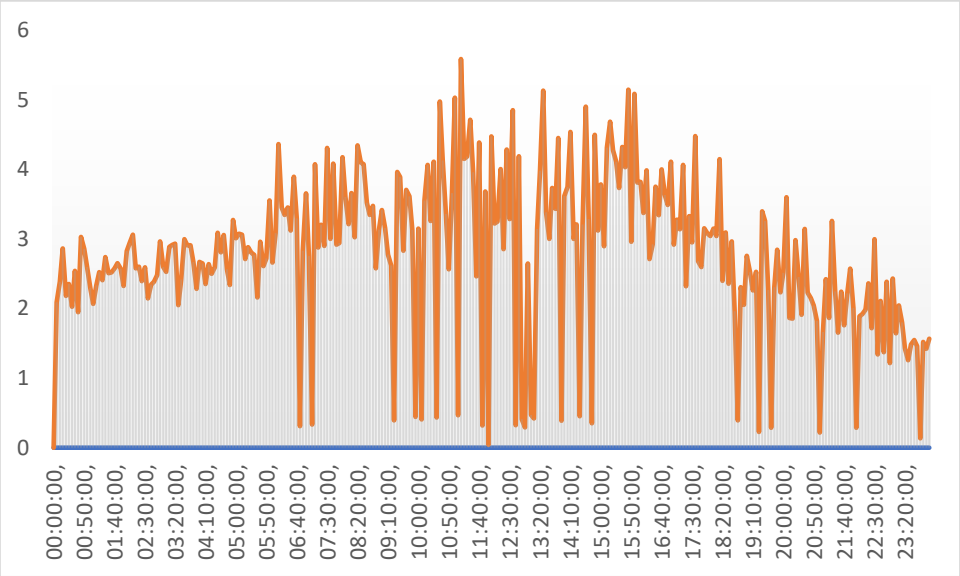

Figure 94 - Significant wave heights, combination 1

Combination 2 – High wind speeds

Combination 2 is run with the original desired high wind speeds and the corresponding forward speed of 3 m/s. For this combination a significant wave height of 8.8 m is observed via the XBeach computations (see Figure 95). With Delft3D a significant wave height of 12.1 m is observed.

A maximum storm surge of 1.61 m ix measured via the XBeach model (see Figure 96), where the Delft3D model predicts a maximum storm surge of 0.46 m.

Originally combination 2 had a significant wave height of 7.5 m and a maximum storm surge of 0.44 m as a result of the Delft3D model. It is seen that due to the increase in wind speeds, the significant wave height according to the Delft3D model increased from 7.5 to 12.2 m. For the storm surge apparently the increase in wind speed did not have a big influence. Combination 2 was originally not run with XBeach, so it cannot be compared with the original XBeach output.

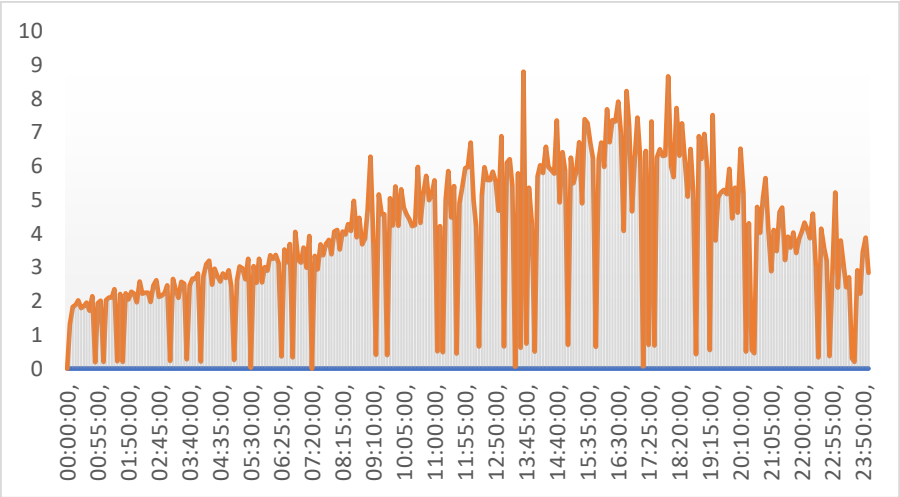

Figure 95 - Significant wave heights combination 2

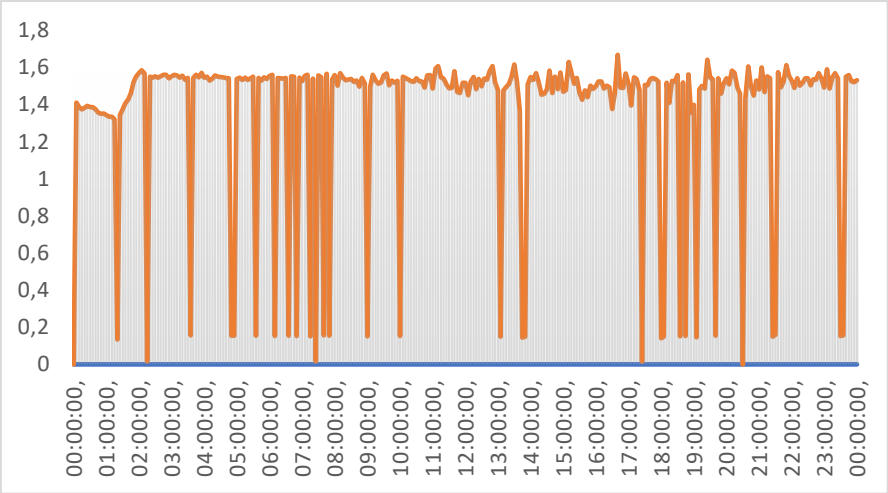

Figure 96 - Water levels combination 2

Combinations 13

As discussed in the beginning of this chapter, the combinations 13 (Low & High wind speeds) are run with a different XBeach grid. Looking at the results, the water levels seem to be wrong. Therefore, it is chosen to only look at the significant wave heights. For the combination 13 (Low wind speeds) a smaller period of about 10 hours was taken. This was done because the combination 13 (High wind speeds) had to run for more than 30 hours in order to give results for the chosen 24-hour time period. These 10 hours were taken right when the synthetic hurricane had the most impact on the location of interest.

Combinations 13 were both run with the original forward speed of 7.8 m/s. Originally combination 13 had a significant wave height of 12.1 m as a result of the Delft3D-model.

Low wind speeds

For this combination a significant wave height of 5.09 m is observed via the XBeach computations (see Figure 90). Delft3D gave a significant wave height of 5.9 m.

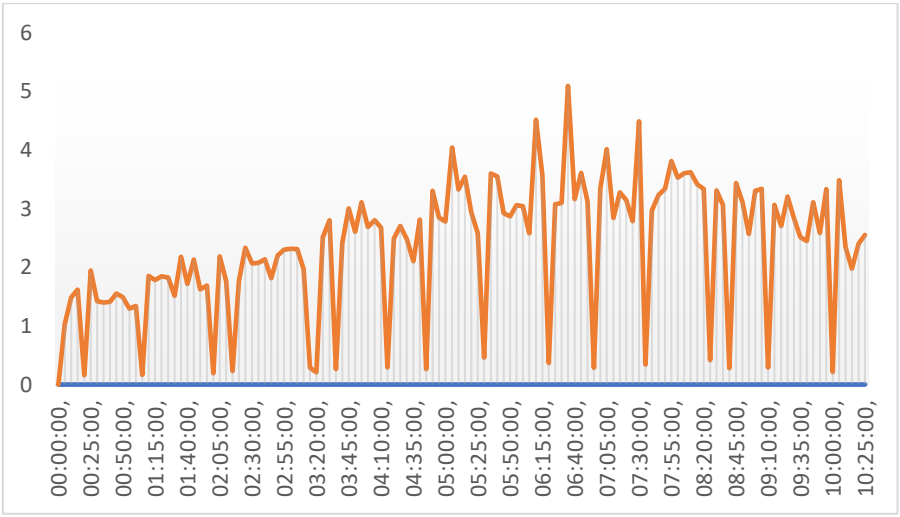

Figure 97 - Significant wave heights combination 13 (Low wind speeds)

High wind speeds

For this combination a significant wave height of 7.59 m is observed via the XBeach computations (see Figure 95). Delft3D gives a significant wave height of 10.2 m.

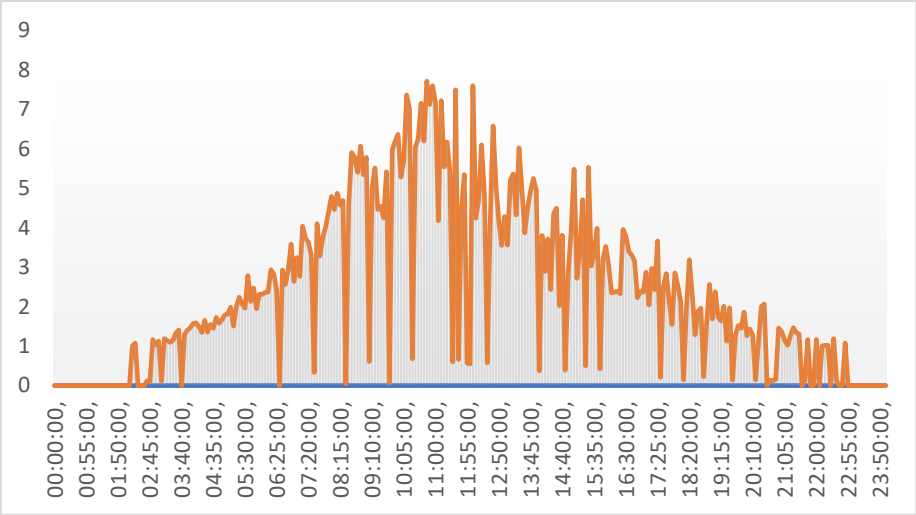

Figure 98 - Significant wave heights combination 13 (High wind speeds)

Combination 14 – Low wind speeds

Combination 14 is run with low wind speeds and a forward speed of 3 m/s. A significant wave height of 4.54 m is observed via the XBeach computations (see Figure 99). With Delft3D a significant wave height of 6.4 m is observed. A maximum storm surge of 1.58 m was measured via the XBeach model (see Figure 100), where the Delft3D-model measured a maximum storm surge of 0.32 m.

In the previous paragraph, where the wind speeds were not projected correctly, combination 14 had a significant wave height of 13.7 m and a maximum storm surge of 0.56 m as a result of the Delft3D-model. From the XBeach results for this combination, a significant wave height of 9.7 m and storm surge of 1.6 m was measured.

In relation to the earlier ran combination 14 with medium-high wind speeds, the combination is now run with low wind speeds. It is therefore logical that for Delft3D and XBeach the significant wave heights as well as the maximum storm surge decreases. Significant wave height decreased from 13.7 to 6.4 m for Delft3D and from 9.7 to 4.5 for XBeach. The maximum storm surge decreased from 1.6 to 1.58 m and from 0.56 to 0.32 m.

Due to the decrease in wind speed, the significant wave heights dropped drastically, where the storm surge barely changed. The storm surge in the XBeach model did change a lot due to the decrease in available wave energy to be transformed into a wave set-up.

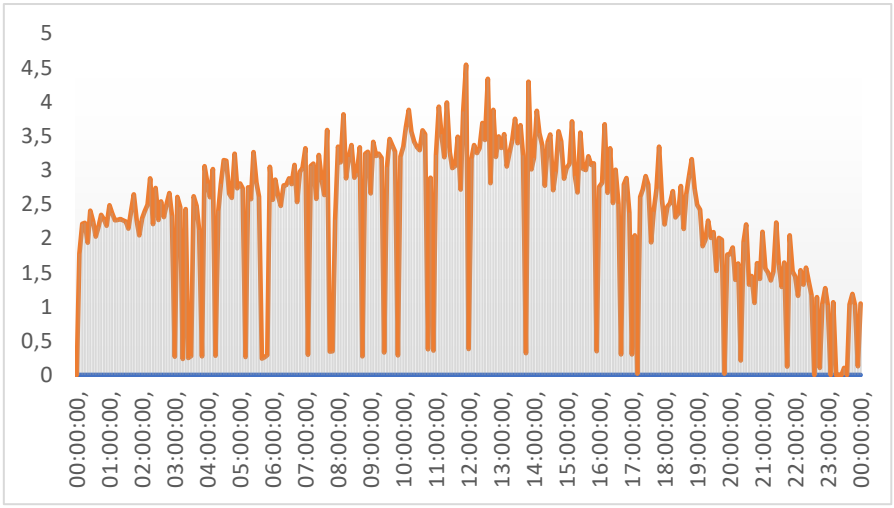

Figure 99 - Significant wave heights combination 14

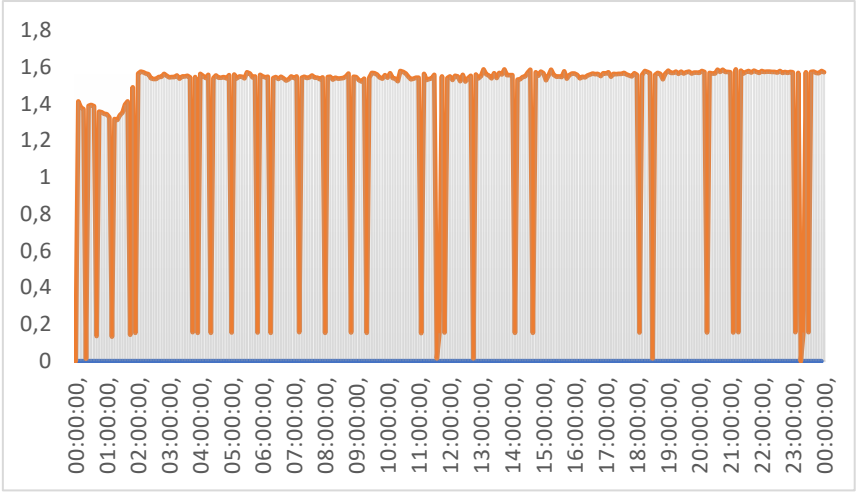

Figure 100 - Water levels combination 14

Irma – Medium wind speeds

The Delft3D-model used for the validation with the TC Irma is also run with the location for XBeach. The model is run with time steps of 30 minutes and runs from the 5th of September 20:00 PM till the 11th of September 20:00 PM. Again, for computational purposes, the XBeach model is run for 24 hours, which results in the period of the 9th of September 13:30 PM till the 10th of September 13:30 PM.

The XBeach run results in a significant wave height of 6.56 m at the CTE and a maximum storm surge of 1.61 m.

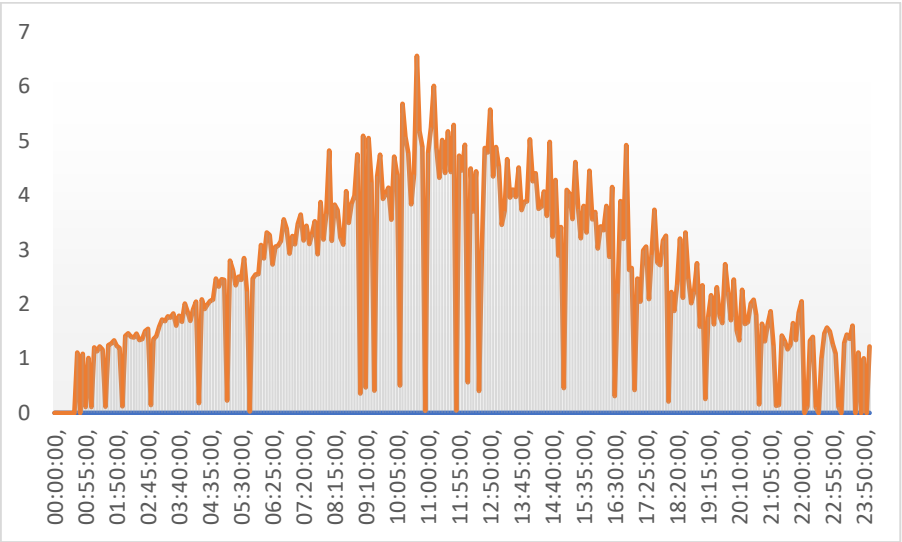

Figure 101 - Significant wave height Irma at CTE

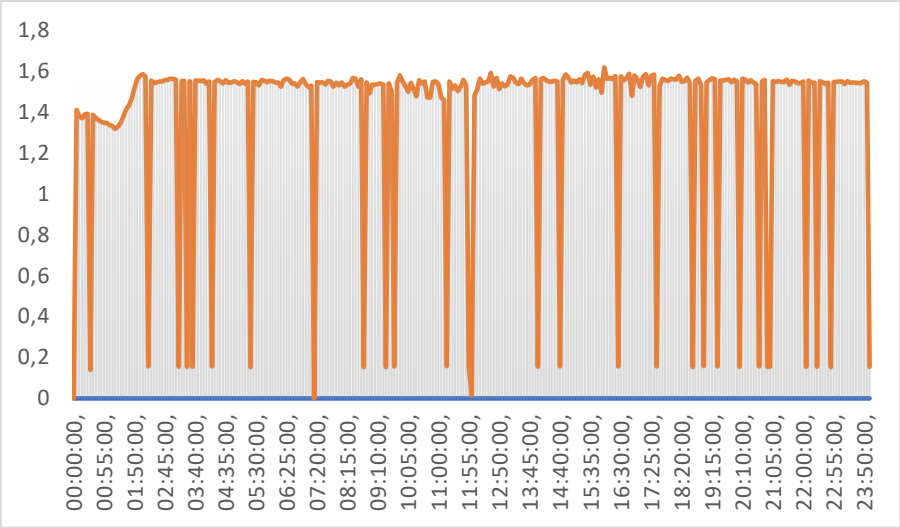

Figure 102 - Water levels Irma at CTE

6.2.2 Delft3D and XBeach Results

Introduction

The results for the combinations 1, 2, 13 (Low and High wind speeds), 14 and Irma are given below. Where Table 19 gives the XBeach results and Table 20 gives the Delft3D results. The output of these runs is again structured per combination. For the XBeach model, the significant wave height and storm surge are available. For the Delft3D model the peak wave period, significant wave height, water level, wavelength and wave group celerity are given. The maximum values of these parameters are given in the two tables below.

In the analysis, more in attention is given to each output parameter with respect to the significant wave height and the forward speed of the corresponding synthetic hurricane. More elaboration on the following topics in relation with the background theory is given in the discussion and sensitivity analysis.

Results

Combination	Significant Wave Height [m]	Storm surge [m]	Forward speed [m/s]	Track	Wind speed
1	5.58	-	13.3	1	High
2	8.80	1.61	3	1	High
13	5.09	-	7.8	1	Low
13	7.59	-	7.8	1	High
14	4.54	1.58	3	1	Low
Irma	6.56	1.61	2 - 8	1	Medium

Table 19 - XBeach results

Combination	Peak Wave Period [s]	Significant Wave height [m]	Water level [m]	Wavelength [m]	Forward speed [m/s]	Track	Wave group celerity [m/s]	Wind speed
1	10	7.1	0.46	157	13.3	1	7.85	High
2	12.5	12.1	0.46	244	3	1	9.76	High
13	9	5.9	0.32	126	7.8	1	7.02	Low
13	11.6	10.2	0.46	210	7.8	1	9.06	High
14	9.2	6.4	0.32	132	3	1	7.18	Low
Irma	10.6	8.9	0.44	176	2 - 8	1	8.27	Medium

Table 20 - Delft3D results

Analysis

Forward speed

From the new Delft3D results (see Table 20), it can be seen that slow travelling hurricanes generate higher waves. For example, combination 1,2, 13 (high wind speeds) all consist out of high wind speeds, follow the same track, however their forward speed differs. Combination 1, that travels the fastest, generates the smallest waves, where combination 2, that travels the slowest, generates the highest waves. The same can be concluded for combination 13 (low wind speeds) and combination 14.

From the XBeach results (see Table 19) it can be observed that for combinations 13 (low wind speeds) and 14 the slower hurricanes generate higher waves. Although it is only a small difference, it is contrary with the observations from Delft3D. However, for combinations 2 and 13 (high wind speeds), the slower hurricanes generate higher waves.

Wind speed

As a result, from Delft3D, it is observed that high wind speeds coincide with high significant wave heights. For the combinations that have the same forward speed, the hurricane with the higher wind speeds create higher waves. For example, combination 2 and 14, both have the same forward speed of 3 m/s, however, combination 2 has a high wind speed where combination 14 has a low wind speed. It can be seen that combination 2 has a significant wave height that is about twice as much as combination 14.

As a result of the XBeach computations it can be seen that for combinations 13 (Low and High wind speeds), the hurricane with the highest wind speeds generates the highest waves. The same conclusion can be made for the combinations 2 and 14.

Peak wave period & Wavelength

From the Delft3D results can be observed that higher peak wave periods coincided with higher significant waves. The faster hurricanes created waves with lower peak wave periods. The wavelengths increase, when the peak wave periods increase, consequently the same observations are made for the wavelengths.

Water level

From the Delft3D results, it can be seen that the hurricanes with a high wind speed generate higher storm surge than the hurricanes with a low wind speed. The combinations that have the same wind speed, but a different forward speed have the same water level rise. Thus, the change in forward speed does not create a difference in water level set-up.

For XBeach, the generated storm surge seems to be about the same for the combinations with a lower Delft3D storm surge as well as for the higher Delft3D storm surge. For combination 2 and 14, the difference in storm surge as a result of Delft3D was 0.14 m, due to XBeach, this difference reduced to only 0.03 m.

Significant wave heights

From the Delft3D as well as for the XBeach results the synthetic hurricanes that travel with the same forward speed and have high wind speeds result in higher waves than the synthetic hurricanes with low wind speeds. The hurricanes that travel with a slow forward speed and have the same wind speed generate higher waves than the synthetic hurricanes that have a high forward speed.

6.2.3 Discussion

Forward speed

A very important thing to keep in mind is that the synthetic hurricanes are run with a constant forward speed, where the hurricanes as they are present in the real world differ in translation speed over time as can be seen from Figure 92.

The CTE is located at -81.53 W, 23.1 N. As can seen from Figure 92, the forward speed of the hurricane Irma at that location was about 2.2 m/s. The hurricane Irma was at its slowest at around 2 m/s, and 8 m/s at its fastest. There was a large difference over time in the translation speed for the hurricane. This could create larger waves at the location of interest, when the hurricane is slower at that point. As explained earlier, if the hurricane has more time to generate waves, the resulting waves will be more significant.

The XBeach results show that for some combinations the slower hurricanes generate higher waves and for other combinations the slower hurricanes generate smaller waves. There does not seem to be a correlation between forward speeds of hurricanes and their corresponding wave generation. It must be noted though that for combinations 1 and 13 (Low & High wind speeds), the corresponding water levels were wrong. It could be that the modelled significant wave heights are slightly off as well due to the different grid used for these combinations. The generated significant wave heights seem to be realistic, but they can still be off by a small margin.

Water level

There is a big difference between the values for storm surge as a result from the XBeach and Delft3D runs. XBeach computes the flow with the combination of bed friction and viscosity. Where the bed friction is influenced by the dimensionless friction coefficient C_f. From Delft3D, a uniform water level is given as input for XBeach. This input is then interpolated to the simulation's local time step. XBeach processes the storm surge in combination with more factors than Delft3D does. Next to this, XBeach also does it on a very small scale with a lot of detail. This creates the big difference between the XBeach and the Delft3D model with respect to storm surge modeling. The main contributor of the extra storm surge is the wave set-up that is caused by the breaking of waves over the foreshore. As mentioned, the wave height largely reduces from the offshore (output Delft3D) to the nearshore (output XBeach) and this change in radiation stresses along the cross-shore profile causes a higher water elevation at the coast.

Significant wave height

There is also a difference between the generated values of the significant wave heights as a result from the XBeach and Delft3D runs. XBeach solves coupled 2D horizontal equations for wave propagation, for the varying spectral wave and flow boundary conditions. The XBeach model generates wave heights with their significance in more detail than Delft3D it does. The XBeach model also considers the variation of the wave height over time. This resolves the long wave motions, created by this variation. These motions are also known as surf beat.

The variance density spectrum that is output from Delft3D, is given as input to XBeach. With the more detailed bathymetry, this information is processed by XBeach and the resulting wave heights near the coast are therefore different. It must also be noted, that the measured wave heights from Delft3D are given at the observation point CTE (Figure 83), where the measured wave heights from XBeach are given at observation points Closest-Shore (Figure 87). The observation point for XBeach is located much closer to the coast than the observation point for Delft3D is. This is because the Delft3D model is a lot less refined than the XBeach model and it is therefore not possible to get an observation point that is located close to the land.

Irma

From the Delft3D as well as the XBeach results, the output seems very reasonable compared to the validated Irma run. The wind speeds of Irma are medium and with the observations made before, the significant wave heights as well as the storm surge should therefore fall between the synthetic hurricanes with high wind speeds and the low wind speeds. From Table 19 and Table 20, it can be seen that this holds for the significant wave heights as well as for the water levels. It can therefore be concluded that the results are viable and are ready to be used as input for the final design.

6.2.4 Sensitivity analysis

A second analysis can be performed on the synthetic hurricane combinations with a variation of wind speeds. This way the resulting wave heights and storm surges can be looked at with changes in not only the forward

speed but also in the wind speeds. These combinations are all following track 1. For the sensitivity analysis the Delft3D results as well as the XBeach results are examined.

Changing the forward speed

For combinations 1, 2 and 13 (High wind speeds) all the factors are equal except for the forward speed, where combination 2 has a low forward speed of 3 m/s, combination 13 (High wind speeds) has a forward speed of 7.8 m/s and combination 1 has a high forward speed of 13.3 m/s.

For Delft3D, this resulted in a difference between combination 2 and 13 (High wind speeds) in significant wave height of 1.9 m and no difference in water level. Between combination 1 and 13 (High wind speeds), this resulted in a difference in significant wave height of 3.1 m and no difference in water level.

For XBeach the same conclusion can be made for the combinations 1, 2 and 13 (High wind speeds). A difference between combination 2 and 13 (High wind speeds) in significant wave height was measured of 1.21 m. Between combination 1 and 13 (High wind speeds) a difference in significant wave height of 2.01 m was measured.

Combination 13 (Low wind speeds) and combination 14 both have the same low wind speeds and follow the same track, so the only difference is the forward speed. Combination 13 (Low wind speeds) has a forward speed of 7.8 m/s, whereas combination 14 has a forward speed of 3 m/s.

As a result of Delft3D, there is a difference in significant wave height for these combinations of 0.5 m, and no difference in water level.

For XBeach a difference in significant wave height is measured of 0.55 m between combination 13 (Low wind speeds) and 14.

For Delft3D, with respect to changing the forward speed, it can be concluded that the model is sensitive to a change in wave heights but not for a change in water level. When the model is run with higher wind speeds the difference in significant wave heights are bigger. Thus, increasing the model's input wind speeds creates a higher sensitivity for the change in wave heights, again the water level doesn't seem to be affected.

For XBeach, it can also be concluded that the model is sensitive for change in wave heights but not for change in water level.

Changing the wind speed

For combinations 2 and 14 the only factor that is changed is the wind speed. Combinations 2 and 14 both have a low forward speed of 3 m/s,

The Delft3D-model resulted in a significant wave height difference of 5.7 m and a difference in water level of 0.14 m.

The XBeach model resulted in a difference in significant wave height of 4.3 m between combination 2 and 14. And a difference in storm surge of 0.03 m.

For combinations 13 (Low wind speed) and 13 (High wind speed), the only factor that is changed is also the wind speed. These combinations both have a forward speed of 7.8 m/s.

The Delft3D-model resulted in a difference in significant wave height of 4.3 m and a difference of 0.14 m in water level.

The XBeach model resulted in a difference in significant wave height of 2.5 m between combinations 13 (Low and High wind speeds).

For Delft3D, as a result of only changing the wind speed, the model seems to be sensitive for the change in significant wave height as well as for the change in water level. The difference in significant wave height is bigger when the corresponding forward speed is lower, the change in water level is the same for the different

forward speeds. The model is therefore more sensitive to a change in significant wave height than it is to a change in water level.

As result from XBeach, with respect to only changing the wind speed, the model seems to be sensitive to changes in the significant wave height and not to a change in the water level. The XBeach model seems to be less sensitive though to changes in significant wave heights than the Delft3D model. The values seem to be closer for the combinations with the same forward speed and a difference in wind speed. It seems that those computed values are closer to reality.

6.2.5 Final Choice

It is chosen to take the synthetic hurricane 2 as the normative synthetic hurricane as a basis for the final design of the sea structure.

From the probabilistic computations in section 4.2.3 it can be observed that the return period of combination 2 can be calculated to be 1580 years. This value is obtained by some more assumptions, leading to some more uncertainty in the probability of occurrence than the original probabilistic computation, but it close to the correct value. Hence, it is taken that combination 2 can be used as the normative hurricane for which the final design is made.

Combination 2 is chosen since it has the highest significant wave height in Delft3D and in XBeach and therefore is normative. As explained earlier, XBeach works better in coastal areas. Therefore, the values that are generated from XBeach are used as input for the final design. For combination 2, a significant wave height is found of 8.8 m with a corresponding storm surge of 1.61 m. However, from Figure 95 it is seen that only 2 peaks are close to the value of 8.8 m. For the design it is more important to look at the significant waves that occur during a longer period or occur more often. It is chosen to take the mean significant wave height for the period between 14:40 and 19:10. This resulted in a mean significant wave height of 6.49 m with a standard deviation of 0.92 m. For the storm surge of combination 2, the value of 1.61 m will be taken, because this value is reached more than once during the period of the hurricane and the other values in the graph are close as well (see Figure 96).

Figure 103 shows that over the whole grid area waves are generated, due to the combination of uniform wind and the synthetic hurricane 2. A screenshot is taken where the synthetic hurricane has just passed the CTE. As shown in the figure, a large area between Cuba and Florida consist of waves that are larger than 5 meters.

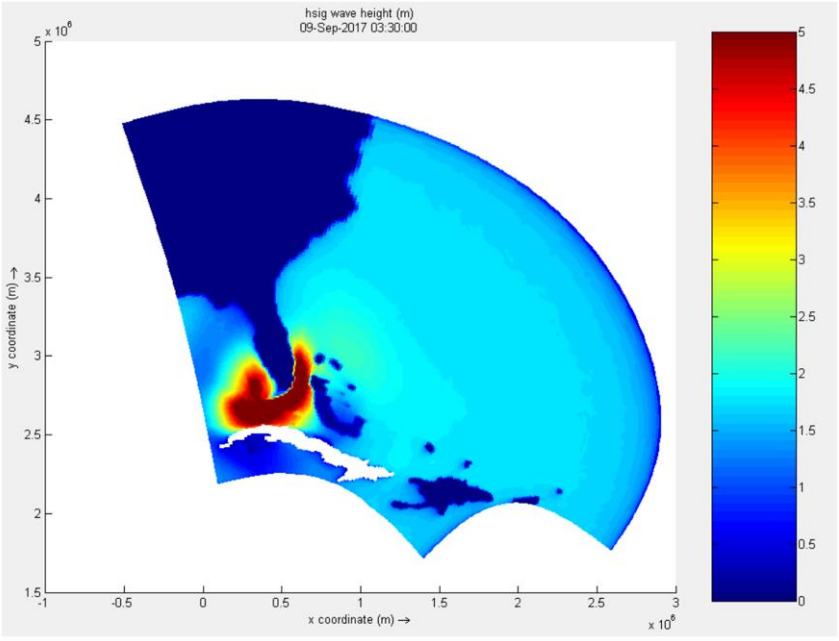

Figure 103 - Combination 2, distribution significant wave heights over the whole area

Figure 104 and Figure 105 give the significant wave heights and storm surges in XBeach. The screenshot is taken at 14:40, which is the start of the period which was taken to calculate the mean significant wave height. Figure 104 shows that significant waves with heights of 11 m enter the domain and decrease to a height of around 6 to 7 m near the coast. Figure 105 shows that the storm surge is maximum in the middle of the grid and decreases very near to the coast.

For the results of part 2 of the hurricane it should be noted that for the significant wave heights near the coast of the CTE, the H_{rms} values given by XBeach are used. This can be argumentized in the following way. The ground for this research is that there should be a correlation between the increase of the storm surge near the coast and the decrease of the significant wave height as XBeach can only produce wave set-up and no wind set-up. It is found that the storm surge increased by 1.15 meters in the XBeach output compared to that of Delft3D, whereas the significant wave height increased by 0.22 meters when taking $H_s = H_{rms} * 1.4$. However, this cannot be the case for an extra storm surge of 1.15 meters. Hence, dissipation near the coast must take place. The reason this analysis is done analytically and not by XBeach is because there are not enough data points near the coast for XBeach to recreate this phenomenon accurately.

Equation 16 - Set-up

$$\frac{\partial \eta}{\partial x} = \frac{\partial S_{xx}}{\partial x} * -\frac{1}{\rho g h}$$

Equation 17 - Radiation stress

$$S_{xx} = \left(2n - \frac{1}{2}\right) * \frac{1}{8}\rho g H^2$$

For deep water n is taken to be 0.5 and for the nearshore and therefore shallow water n is taken to be 1. The difference between the radiation stresses is assumed to be linear, meaning that equation Equation 16 can be approximated with the following formula.

Equation 18 - Linearized Set-up

$$\frac{\Delta \eta}{\Delta x} = \frac{\Delta S_{xx}}{\Delta x} * -\frac{1}{\rho g h}$$

From this follows that Δx can be eliminated from the equation, giving that the difference between the radiation stresses can be rewritten as follows

Equation 19 - Linearized radiation stress

$$\Delta S_{xx} = -\Delta \eta * \rho g h$$

Hence, combining equation Equation 17 and Equation 19 gives that the significant wave height at the coast of the CTE can be calculated using equation Equation 20.

Equation 20 - Significant wave height CTE

$$H_{s,CTE} = \sqrt{\frac{16}{3} * \left(\Delta \eta h + \frac{1}{16} H_{s,off}^2\right)}$$

For an average depth over the foreshore of the CTE of 4.5 meters, the significant wave height near the CTE should be equal to 8.8 meters if H_{rms} is taken equal to H_s. Filling in equation Equation 20 gives a significant wave height of 8.84 m, which means that taking H_s at the coast of the CTE to be equal to the H_{rms} values found by XBeach is a good estimation.

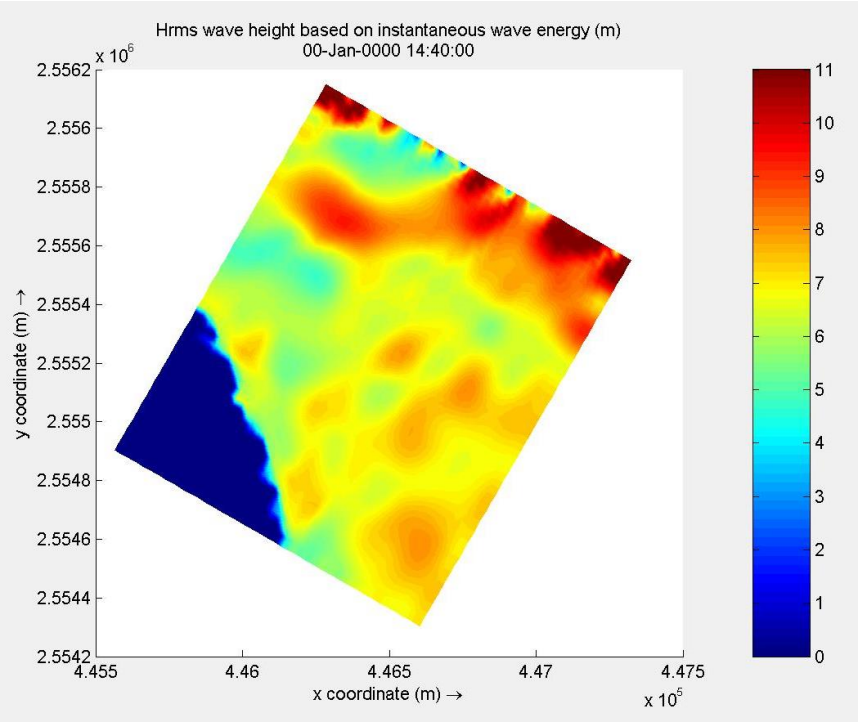

Figure 104 - Significant wave heights combination 2, XBeach

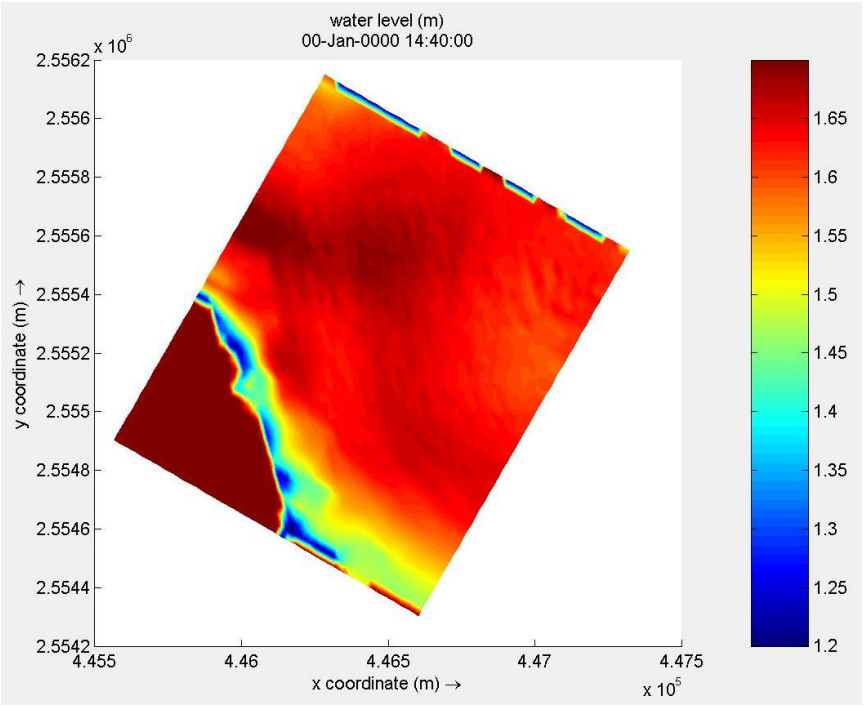

Figure 105 - Storm surge combination 2, XBeach

Chapter 7

The Design Solution

As a first step in the design process a study of the area is done, the subsoil will be analyzed and the amount of allowable overtopping at CTE Antonio Guiteras needs to be determined. The current design needs to be checked. Next, several variants will be explored that focus on the reduction of waves, minimizing overtopping and maximizing drainage capacity. The variants will be evaluated by means of a multi criteria analysis which will result in a definitive design which will be further elaborated.

7.1 Analysis project area

7.1.1 Subsoil

The CTE is located on a plain on a rocky coast. Behind the CTE are mountains and towards the sea there are cliffs. The rock is characterized as carsic and is a strong material with a large bearing capacity. This means that the new sea wall does not need any foundation, only proper anchoring. No settlements are expected at the site due to a new structure. The seabed is also rocky at this location and no erosion occurs, meaning that any structure placed on the sea bed would not require bed protection to prevent scouring.

7.1.2 Allowable overtopping

There is no clear limit to overtopping that can be established. However, an estimation can be made based on the size of the plant, the drainage capacity present and the return period. Extensive overtopping can cause damage to the defense structure with possible breaching and flooding, a direct danger to the people behind the sea defense and especially in the case of the CTE damage to property, infrastructure and operations of the defended area which can cause major disruption of economic activities.

The type of overtopping phenomena observed are dependent on the defense structure, in the case of a sloping sea wall. On a sloping structure the waves break before or on the structure and the overtopping process is relatively gentle. A vertical structure experiences much more of an impulsive breaker where overtopping flows are more sudden and violent. This can be accompanied by ‘white water’ i.e. non-continuous overtopping and or significant volumes of spray. Vertical structures can also cause more reflection of waves, reflecting waves may increase wave heights in neighboring areas and may initiate or accelerate local erosion which in turn can increase depth-limited wave heights.

Tolerable overtopping is related to the type of structure, the function and drainage capacity of the protected area and the wave height. A dangerous failure mechanism that can occur with a permeable protection during overtopping is erosion of the backside and a subsequent breach of the structure. In the case of the sea wall this is not a problem and there are no demands for the structure itself relating to overtopping. When the protected area has very poor drainage capacity this means that the water will pile up and significant damage can occur. In such a situation the tolerable overtopping is less than in the case of a well-drained area. Lastly, tolerable overtopping depends strongly on individual overtopping volumes which are related to the wave heights. Frequent small waves can give a same overtopping volume as a single or a couple of large waves. The mean tolerable overtopping discharge should thus be coupled to the wave height causing that discharge.

In the situation of the CTE there is already a drainage system present in the form of the outlet channel. It is estimated that through the outlet channel in the smallest cross section a maximum of 20.4 m^3/s. This channel runs over a width of 600 m, if this is efficient in draining the overtopping this results in a maximum allowable overtopping of 34 l/s/m. If a better drainage system is constructed combined with more pumping capacity this can allow for more overtopping.

7.2 Check overtopping current design

To check whether the current design is enough to withstand the design surge and wave, a schematization is made. The overtopping of the sea wall the conditions around the sea wall need to be established. The design approach depends on whether there is an influencing foreshore present, if there is a significant mound and whether the wall experiences impulsive or non-impulsive conditions.

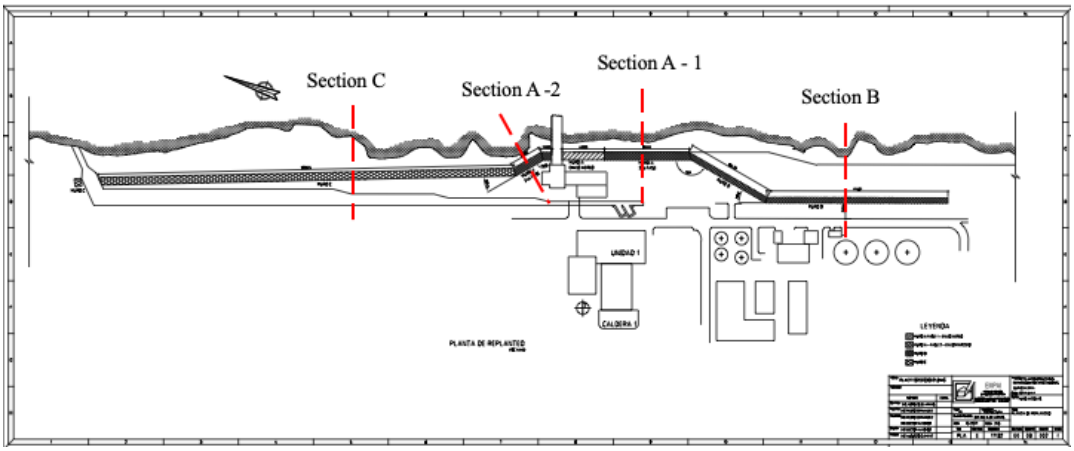

Figure 106 - Cross section determination different sections

In Figure 106 the cross sections for the different sections are given. Section A-1 is taken as the most common section A, which is taken as the main example to describe the overtopping calculations. Section A-2 is orientated more towards the North and, as will be discussed later, will have less oblique incoming waves. Section B and C have a different sea wall and are therefore discussed separately as well.

7.2.1 Schematization

The design contains many elements which need to be combined. Schematizations are necessary to be able to calculate the overtopping. Correction factors are applied for relevant schematizations. Figure 107 shows the cross-shore profile at the location of the CTE, there is a steep cliff present which is schematized as being vertical.

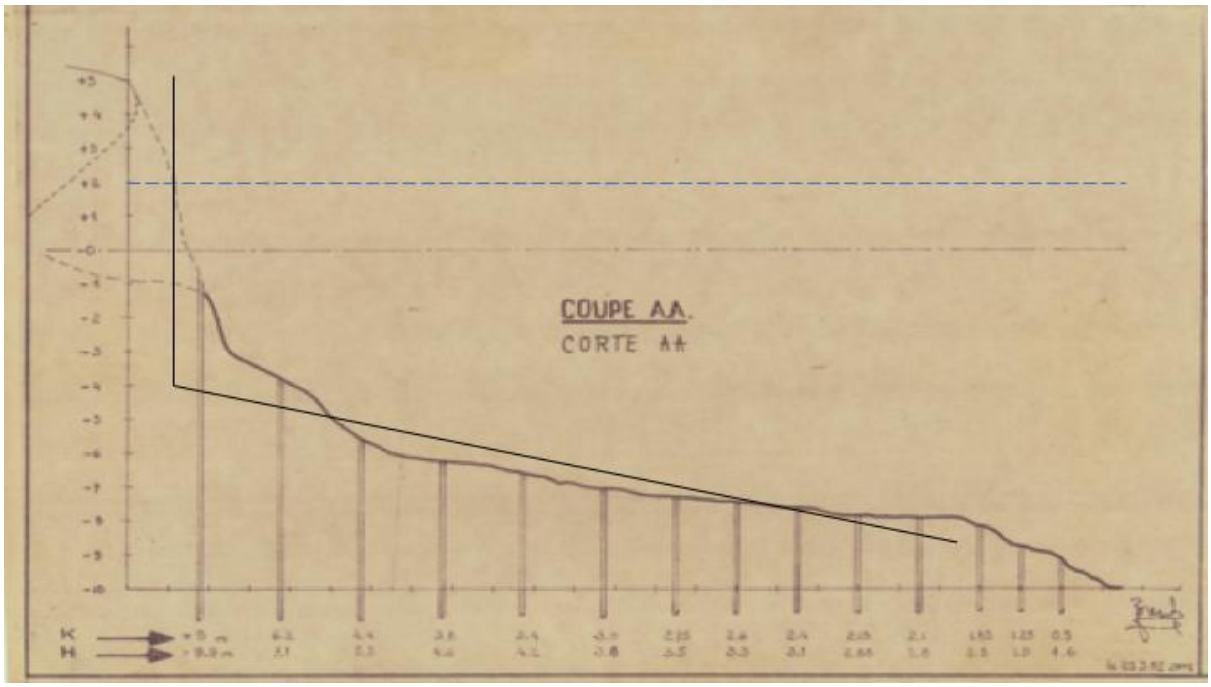

Figure 107 - Cross shore profile CTE with schematization

The cliff and sea wall are of different slopes and have been combined by viewing them as one chamfered vertical wall, where the sea wall is a large parapet ($\alpha > 0$). This is shown in Figure 108. On top of the sea wall a bullnose is present ($\alpha < 0$) which is included separately by means of correction factors.

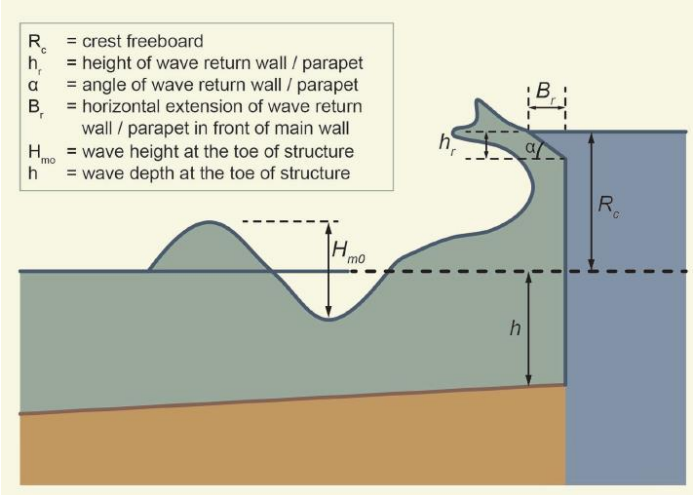

Figure 108 - Vertical wall with parapet (EurOtop, 2018)

The horizontal spacing between the cliff and the sea wall is schematized as a berm which is included in the design also through correction factors. The overall schematization is shown in Figure 109.

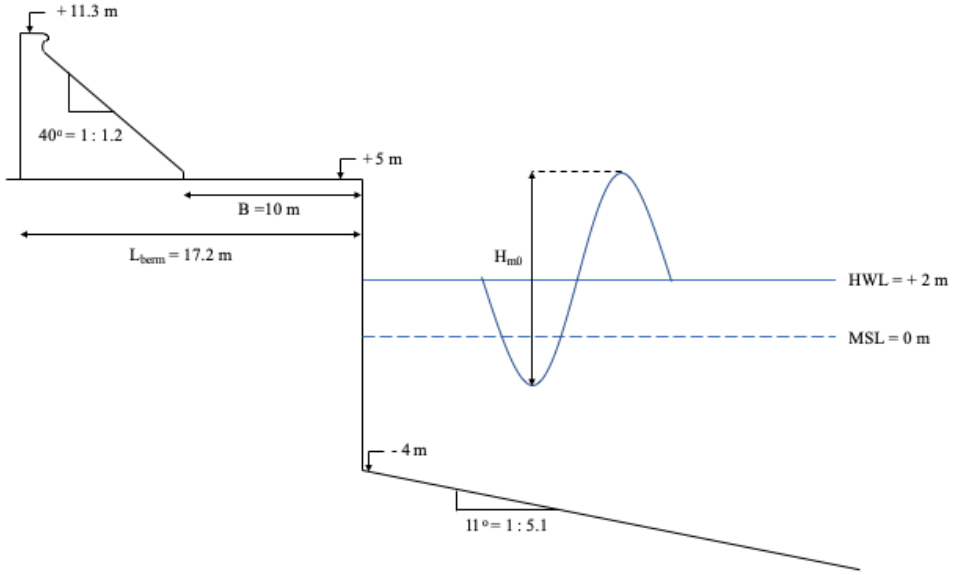

Figure 109 - Schematization current design section A-1

7.2.2 Foreshore

In practice an influencing foreshore means that there is intermediate or shallow water depth at the toe. In this situation the deep-water waves are transformed by the near shore processes such as shoaling and refraction. An influencing foreshore means that impulsive conditions can occur.

The peak wave period for hurricane Irma was 12.5 seconds. The water depth is 6 m. The wavelength at this depth 78.4 m, the resulting d/L = 0.07, for $0.05 < d/L < 0.5$ the depth is classified as intermediate. It can be concluded that there is an influencing foreshore. There is no significant mound present.

7.2.3 Impulsive conditions

Since there is an influencing foreshore the possibility of impulsive overtopping needs to be explored. If the conditions satisfy the equation below, the waves are impulsive.

Equation 21 - Check for impulsive conditions

$$\frac{h^2}{H_{m0}L_{m-1,0}} \leq 0.23$$

In this case the outcome is 0.07 < 0.23. It can be concluded that there are impulsive conditions.

7.2.4 Uncorrected overtopping

The overtopping for a vertical wall can be calculated. This will be used as a starting point and will be adjusted with correction factors to closer resemble the situation at hand.

For impulsive conditions two situations are distinguished: low relative free board and high relative free board. Overtopping of relative lower free boards can be approximated with an exponential decay where for high relative free boards a power law is used. High relative free board starts from $R_c/H_{m0} > 1.35$, which is the case for this situation ($R_c/H_{m0} = 1.38$)

Equation 22 - Uncorrected overtopping

$$\frac{q}{\sqrt{gH_{m0}^3}} = 0.0014 \left(\frac{H_{m0}}{h\, s_{m-1,0}}\right)^{0.5} \left(\frac{R_c}{H_{m0}}\right)^{-3}$$

7.2.5 Parapet

The parapet correction factor is larger than zero as it allows for more overtopping. (EurOtop, 2018) gives a range for the correction factor for α > 100 degrees under non impulsive conditions. The factor $\gamma_{parapet}$ has a range between 1.05 and 1.10. However, since this is for non-impulsive waves, a correction needs to be made. This correction factor is found by comparing the design overtopping discharge for impulsive waves and non-impulsive waves.

Equation 23 - Overtopping vertical wall non-impulsive waves

$$\frac{q}{\sqrt{gH_{m0}^3}} = 0.062 \exp\left(-2.61 * \frac{R_c}{H_{m0}}\right)$$

Using the formulation of overtopping for non-impulsive waves in Equation 23 an overtopping discharge of 0.08 $m^3/m/s$ is found. This means that the ratio between the overtopping discharges is 2.4. The final parapet correction factor is found using Equation 24.

Equation 24 - Parapet correction factor for impulsive waves

$$\gamma_{parapet,imp} = (\gamma_{parapet} - 1) * \frac{q_{imp}}{q_{non,imp}} + 1$$

Finally, this gives a range of parapet correction factors between 1.12 and 1.24.

7.2.6 Berm

As can be observed in Figure 109, a berm is present in the current schematization that is not yet considered for the overtopping discharge calculation. Hence, for the berm also a correction factor must be determined. The correction factor for the berm can be calculated using Equation 25. Here the two partial factors r_B and r_{db} are defined in Equation 26 and Equation 27.

Equation 25 - Berm correction factor (EurOtop, 2018)

$$\gamma_b = 1 - r_B(1 - r_{db})$$

Equation 26 - Partial factor r_B (EurOtop, 2018)

$$r_B = \frac{B}{L_{berm}}$$

Equation 27 - Partial factor r_{db} (EurOtop, 2018)

$$r_{db} = 0.5 - 0.5\cos\left(\frac{\pi d_b}{R_{u2\%}}\right)$$

The distance from the top of the cliffs to the toe of the sea wall or *B* is 10 meters. The berm length is calculated by finding the intersect of the 'ground' surface on the lines 1 H_{m0} below and above the berm. On the seaside there is no intersect and on the landside this line intersects with the crest of the sea wall. Hence the berm length L_{berm} is 17.2 meters.

The runup $R_{u2\%}$ for vertical walls can be calculated with Equation 28 and the berm height d_b is equal to the cliff level +5 m minus the water level during storm conditions.

Equation 28 - Runup for vertical walls (EurOtop, 2018)

$$R_{u2\%} = 1.8H_{m0}$$

The final value for the berm correction factor is hence equal to the lower bound value of 0.6. Since the value of the berm reduction factor from the calculations is quite smaller than the lower bound, no uncertainty for this reduction factor is considered.

7.2.7 Bullnose

The bullnose is a relatively small structure that is overhanging seaward at the crest of the coastal defense (Allsop, et al., 2018). The idea of the bullnose is to deflect back the impulsive waves seaward. Impulsive waves that break on coastal defenses will release their impulse into an upward splash. This upward splash may become very large with large impulsive waves. For water moving upward and parallel to the sea wall to release its impulse, a bullnose comes in handy and effective to prevent much of the overtopping. The bullnose will deflect the water back to the sea to prevent the water to fall onto the crest of the defense.

Figure 110 – Effective bullnose at Cascais, Portugal (Allsop, et al., 2018)

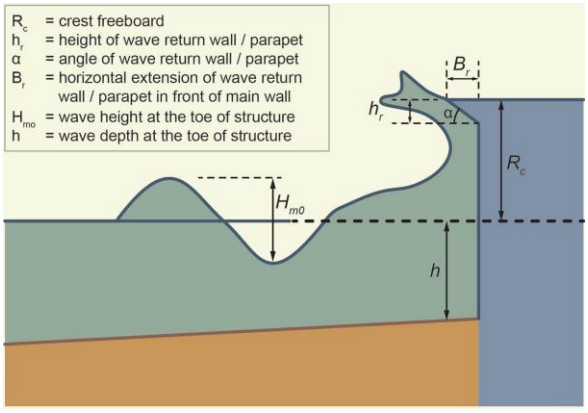

Figure 111 – Schematic figure of the parameters that determine the bullnose effectiveness.

The bullnose effectiveness is a complicated process which is tried to be modelled with a set of formulas. The formulas are displayed in a decision chart drafted by (Pearson, Kortenhaus, Bruce, & Allsop, 2003) in the EuroTop manual. The effectiveness is strongly depended on the seawall's crest freeboard. The bullnose needs that water to be moving freely upward and parallel to sea defense wall to bend this impulsive waterflow back sea. If the crest freeboard is too small for a bullnose to work, then the waves will disturb this deflection process and water will still be able to overtop like a bullnose is not present. This description describes the regime in which the bullnose is not working. If the crest freeboard is in the intermediate regime for a bullnose to be effective, then the waves break to the sea defense below the bullnose. However, some waves will still influence this deflection process and still cause for overtopping. In the high-freeboard regime, the bullnose

effectiveness will not be disrupted by incoming breaking waves anymore, and the bullnose is in small geometries already effective. The effectiveness will be purely be depended on the geometry of the bullnose. A bullnose that has smaller angles are more effective.

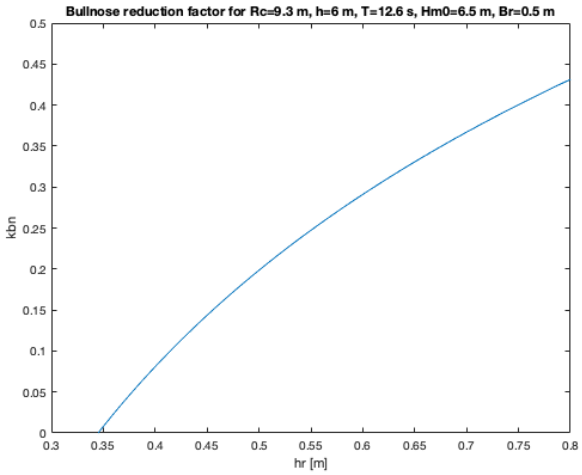

Figure 112 – A plotted bullnose reduction factor versus the height of the bullnose for a relatively large crest freeboard situation.

Figure 112 shows the relation of the bullnose effectiveness with respect to the height of the bullnose. The relation shows that smaller heights will lead too much more effective bullnose designs. This strong dependency is only visible for relatively large crest freeboards.

In short, the bullnose design becomes very effective if the bullnose is placed on a crest with a relatively large freeboard. The bullnose will work even better as the height of the bullnose will be reduced to a small value.

Current design

The bullnose dimensions of the current design are $h_r = 0.6\ m$ and $B_r = 0.2\ m$. Following the flow chart, one finds that the bullnose reduction factor k_{bn} is calculated using Equation 29, where the intermediate reductions R_0^* and m^* can be calculated using the bullnose dimensions and the freeboard.

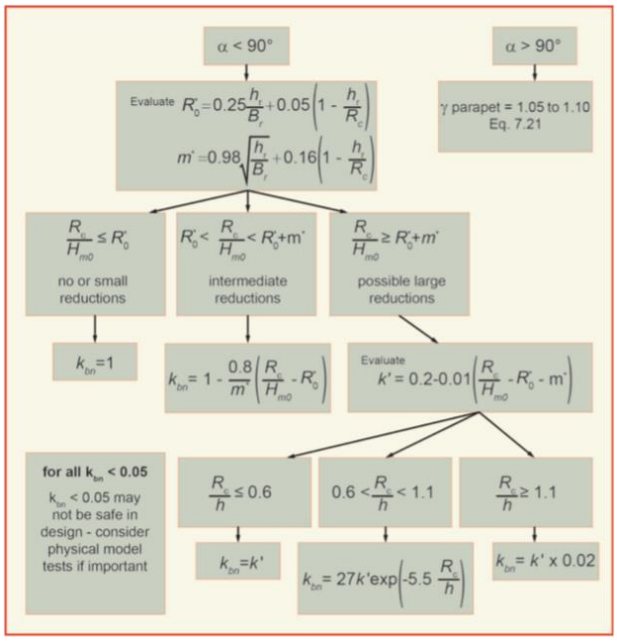

Figure 113 - Bullnose reduction factor flow chart (EurOtop, 2018)

Equation 29: Bullnose reduction factor (EurOtop, 2018)

$$k_{bn} = 1 - \frac{0.8}{m^*}\left(\frac{R_c}{H_{m0}} - R_0^*\right)$$

The bullnose correction factor is finally estimated to be 0.73 with some uncertainty induced by the uncertainty of the equations used in the bullnose reduction factor flow chart and the estimation of the bullnose dimensions.

7.2.8 Obliqueness

The obliqueness of the incoming waves is defined by the shoreline orientation and the peak direction of the waves. From Figure 114 one can find the wave directions. These directions seem to vary a lot, but in reality, the values stay between 350 to 10 degrees in nautical terms, which means that they come from the North in the early morning of September 10th, 2017 when the wave heights were at their maximum. This gives that the angle that the incoming waves make with the normal of the shoreline is 70 degrees, as is schematized in Figure 115.

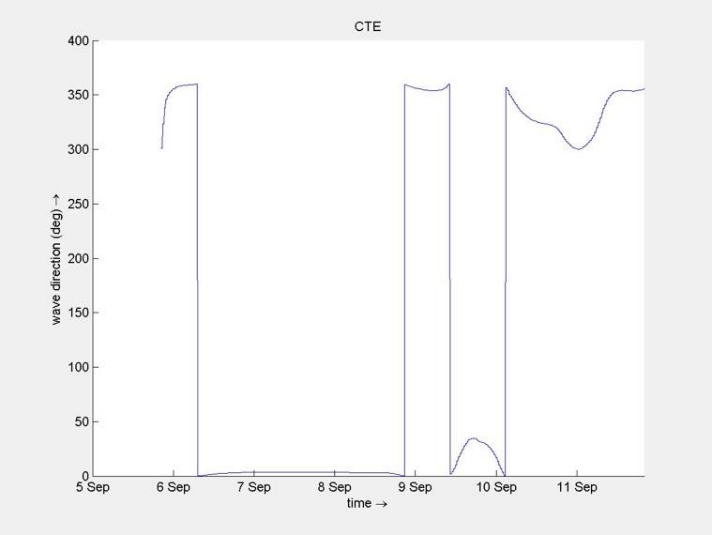

Figure 114 - Wave directions at CTE

Figure 115 - Overview coastline orientation and peak direction waves

The obliqueness correction factor is defined in Equation 30 to have a constant value for wave angles with the shoreline normal that are larger than 45º. This means that the small deviation of the wave direction during the storm does not have any influence on the correction factor, since the angle of incidence is always larger than 45º.

Equation 30 - Obliqueness correction factor (EurOtop, 2018)

$$\gamma_\beta = 0.72 \qquad for\ \beta \geq 45^o$$

7.2.9 Total overtopping

The total overtopping can be defined as a product of all the correction factors that have been discussed and the overtopping discharge for the uncorrected case of a vertical wall with a foreshore. In Equation 31 one can find the corrected design overtopping formulation with the discussed correction factors.

Equation 31 - Corrected overtopping (EurOtop, 2018)

$$q_{overtopping} = \gamma_{parapet} k_{bn} \gamma_{berm} \gamma_{oblique} 0.002 \sqrt{g H_{m0}^3} \left(\frac{H_{m0}}{h\, s_{m-1,0}}\right)^{0.5} \left(\frac{R_c}{H_{m0}}\right)^{-3}$$

Section A-2, B and C

The overtopping for sections A-2, B and C is calculated in the same manner as for section A-1, but the current designs differ a bit and the orientation for these sections may differ somewhat from section A-1.

Section A-2

Section A-2 has the same schematization as A-1 and can be seen in Figure 109. The overtopping calculation of section A-2 differs from A-1 in the fact that A-2 has a different orientation to the waves. From Figure 106 one can estimate that the coastline at this section turned 30° towards the north, hence decreasing the obliqueness of the waves from about 70° to 40°. For such an obliqueness, the Equation 30 does no longer apply and Equation 32 is used.

Equation 32 - Obliqueness correction factor for $\beta < 45°$ (EurOtop, 2018)

$$\gamma_\beta = 1 - 0.0062\beta$$

Now the estimated correction factor for the obliqueness of the waves is 0.75 instead of 0.72, slightly increasing the impact of the waves arriving at the sea wall. This value does however contain an uncertainty since it may differ for different coastline orientations and wave directions.

Section B

Section B has a lower crest and a larger berm than section A-1 as can be seen in Figure 116.

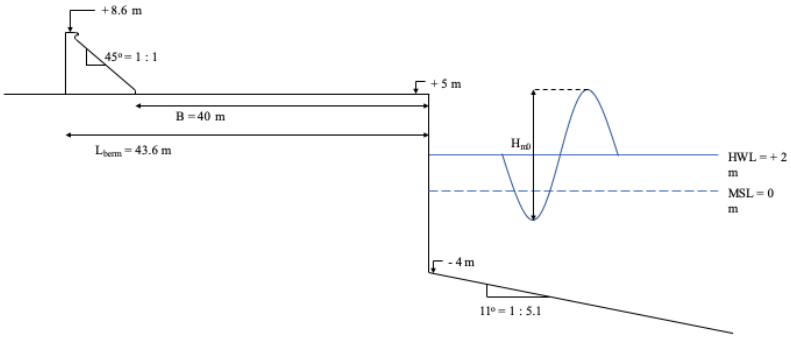

Figure 116 - Schematization section B

The lower crest causes this section to be in the 'low relative free board' regime (R_c/H_{m0} = 0.95). The overtopping equation that should be used according to (EurOtop, 2018) is given below.

Equation 33 - Overtopping equation

$$\frac{q}{\sqrt{g\ {H_{m0}}^3}} = 0.011\sqrt{\left(\frac{H_{m0}}{h\ s_{m-1,0}}\right)}\exp\left(-2.2\frac{R_c}{H_{m0}}\right)$$

Following Equation 25 one should conclude that the lower bound of the berm correction factor is found and equal to 0.6. However, the berm that is present for section B gives a correction factor of about 0.23. Even though the lower bound is equal to 0.6, it is unlikely that a berm of 10 meters gives the same overtopping reduction as one of 40 meters. This assumption is made because the main overtopping mechanism is spray overtopping, which is highly dependent on the distance of the sea wall from the shore.

In the current schematization this correction factor of 0.23 gives overtopping discharges that are much too large. This means that the berm reduction factor equation for section B does no longer apply. Especially since

the crest of the sea wall is much smaller than that of section A-1 and A-2, the overtopping discharges are disproportional. Hence, the correction factor for the berm is set equal to 0.03. This is based on a non-ideal schematization for this section.

Since the crest of section B lies quite a bit lower than that of section A-1, the overtopping for the non-corrected case calculated with Equation 23 is much higher, namely about 0.53 m^3/m/s. The freeboard that is available also has influence on the bullnose correction factor and the parapet correction factor, namely that the bullnose becomes less effective and the parapet increases the overtopping less than for a larger freeboard since the difference between impulsive and non-impulsive conditions becomes smaller. This influence can be seen in Equation 24.

In the end this leads to a k_{bn} of 0.90 and a $\gamma_{parapet}$ of 1.20.

Section C

Section C is, just as section B, located further away from the shore than section A-1 as can be seen in Figure 117. Even though the crest level is the same, a second berm is designed on top of the sea wall which must be considered for the overtopping calculation. The crest level is the same as that of section A-1.

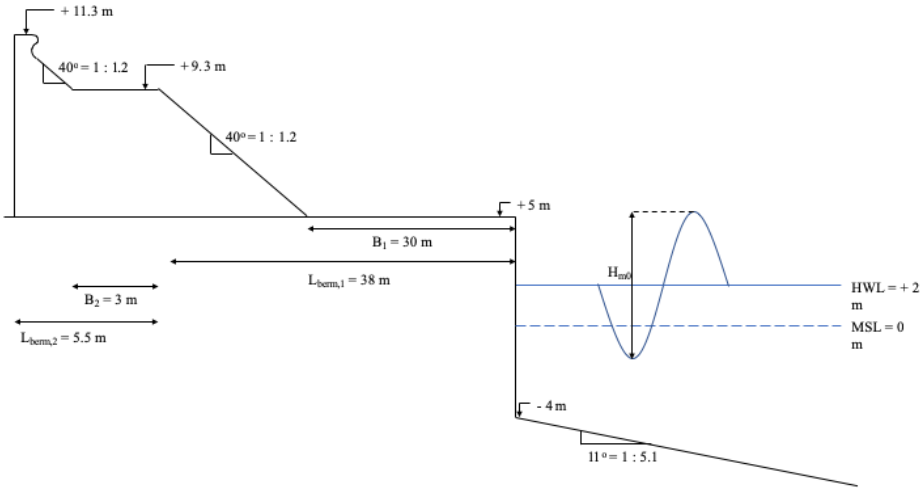

Figure 117 - Schematization section C

The berm influence is therefore the only change compared to section A-1. Firstly, the berm in front of the sea wall considered. On average the distance from the toe of the structure to the cliff is about 30 meters, which means that with a wave height in the order of 6.5 meters, the berm length is 43.6 meters. Again using Equation 25 one can find that γ_b is equal to 0.33. However, again just as for section B, the berm is much larger than for section A-1 and A-2 and therefore the schematization of the situation is not completely correct anymore. That is why γ_b is reduced to 0.10 for this situation.

For the second berm on top of the sea wall a similar calculation is done. This berm, being much higher above the HWL gives a much smaller reduction. As can be seen in Figure 117, the berm is located at +9.3 meters. Using Equation 25 one can find that the correction factor for this berm is about 0.83. The total berm correction factor is found by multiplying both correction factors giving a γ_b of 0.083.

7.2.10 Probabilistic calculation overtopping

There is quite some uncertainty in some of the parameters and in the schematization. For this reason, a deterministic calculation will not suffice but a probabilistic calculation will be done. In this stage a FORM (level II) calculation is done in order to facilitate parametric reliability calculations.

When it is assumed that the maximum allowable overtopping is q_{max} is 34 l/s/m a limit state function can be constructed. The mean value equation for impulsive overtopping will be used. The limit state function is as follows for sections A-1, A-2 and C

Equation 34 - limit state function sections A-1, A-2 and C

$$Z = q_{max} - \gamma_{parapet}\gamma_{bullnose}\gamma_{berm}\gamma_{oblique}0.0014\sqrt{gH_{m0}^3}\left(\frac{H_{m0}}{h\ s_{m-1,0}}\right)^{0.5}(\frac{R_c}{H_{m0}})^{-3}$$

For section B the limit state function is given as follows:

Equation 35 - Limit state function section B

$$Z = q_{max} - \gamma_{parapet}\gamma_{bullnose}\gamma_{berm}\gamma_{oblique}0.011\sqrt{g\ {H_{m0}}^3}\sqrt{(\frac{H_{m0}}{h\ s_{m-1,0}})}\exp(-2.2\frac{R_c}{H_{m0}})$$

All relevant parameters are given a distribution and spread. An overview is given in Table 21 Some elaboration will be given about the chosen distributions.

Parameter	Distribution	Mean A-1	Standard Deviation A-1	Mean A-2	Standard Deviation A-2	Mean B	Standard Deviation B	Mean C	Standard Deviation C
constant	Normal	0.0014	0.0006	0.014	0.006	0.014	0.006	0.0014	0.0006
g	Deterministic	9.81	N.A	9.81	N.A	9.81	N.A	9.81	N.A
Hm0	Normal	6.49	1.35	6.49	1.35	6.49	1.35	6.49	1.35
Tpeak	Normal	12.6	1	12.6	1	12.6	1	12.6	1
Surge	Normal	1.6	0.16	1.6	0.16	1.6	0.16	1.6	0.16
Tide	Normal	0.3	0.05	0.3	0.05	0.3	0.05	0.3	0.05
Top of Structure	Deterministic	11.3	N.A	11.3	N.A	8.6	N.A	11.3	N.A
Sealevel rise	Normal	0.47	0.047	0.47	0.047	0.47	0.047	0.47	0.047
gamma parapet	Normal	1.17	0.117	1.17	0.117	1.16	0.116	1.17	0.117
gamma bullnose	Normal	0.73	0.073	0.73	0.073	0.9	0.045	0.73	0.073
gamma berm	Normal	0.6	0.06	0.6	0.06	0.3	0.045	0.27	0.027
gamma oblique	Deterministic	0.72	N.A	0.75	N.A	0.72	N.A	0.72	N.A

Table 21 - Overview parameters and their distributions per section

As discussed in the previous section there is uncertainty in the correction factor for the parapet since no equation is given for impulsive conditions. To account for this a standard deviation of 10% is applied.

Since the dimensions of the bullnose had to be estimated and the exact shape influences the effectiveness of the bullnose, this correction factor also contains uncertainty. To account for this a standard deviation of 10% is applied.

The correction factor for the berm also contains uncertainty because of the schematization that had to be done for the vertical wall on one side which is not the classical case for a berm. A standard deviation of 10% is given to this parameter.

The constant for high relative free boards 0.014 is based on scale models and is not exact, the standard deviation 0.006. The constant for low relative free boards 0.011 similarly has a standard deviation of 0.0045. (EurOtop, 2018)

Since the Delft3D and XBeach model are also based upon assumptions and simplifications the output contains some uncertainty. Figure 118 shows the peak wave periods modelled at the CTE by Delft3D. The maximum period is 12.5 s and there is a sharp peak. It is assumed that the peak period has a standard deviation of 1 second.

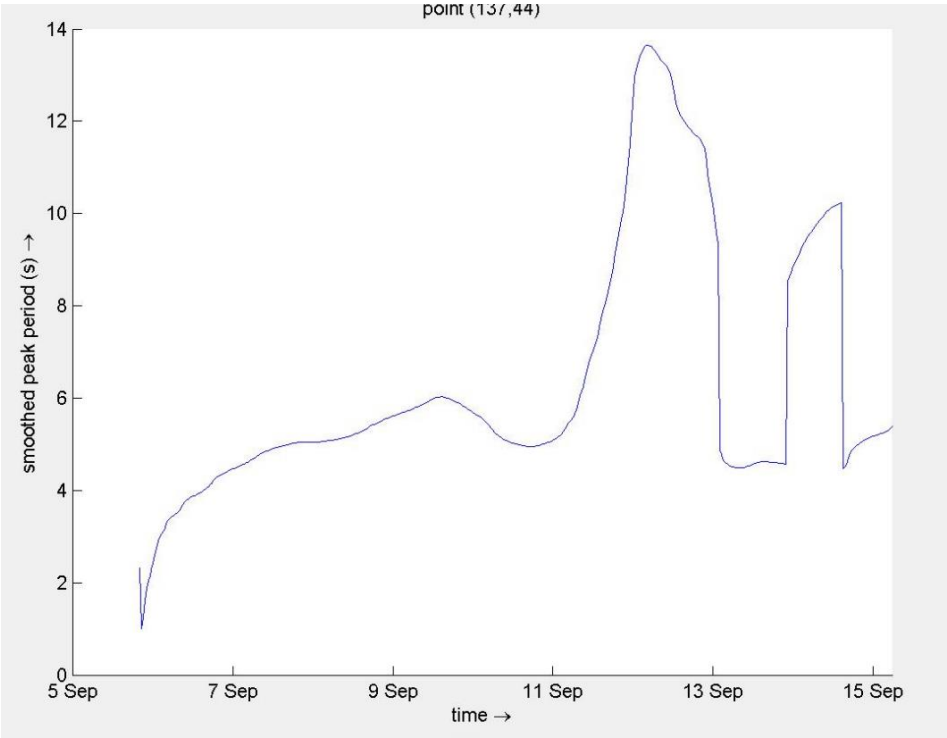

Figure 118 - Peak period at CTE

The significant wave height has been modelled in XBeach and is shown in Figure 119. Over the period from 14:40 till 19:10 the largest waves are observed, and they are fairly constant. The downward peaks are removed, and the mean and standard deviation are calculated, $\mu = 6.5$ m and $\sigma = 0.91$ m. This is the variation within the model while in fact the model is also where the uncertainty lies. It is however assumed that with the relatively large standard deviation (14%) this is accounted for.

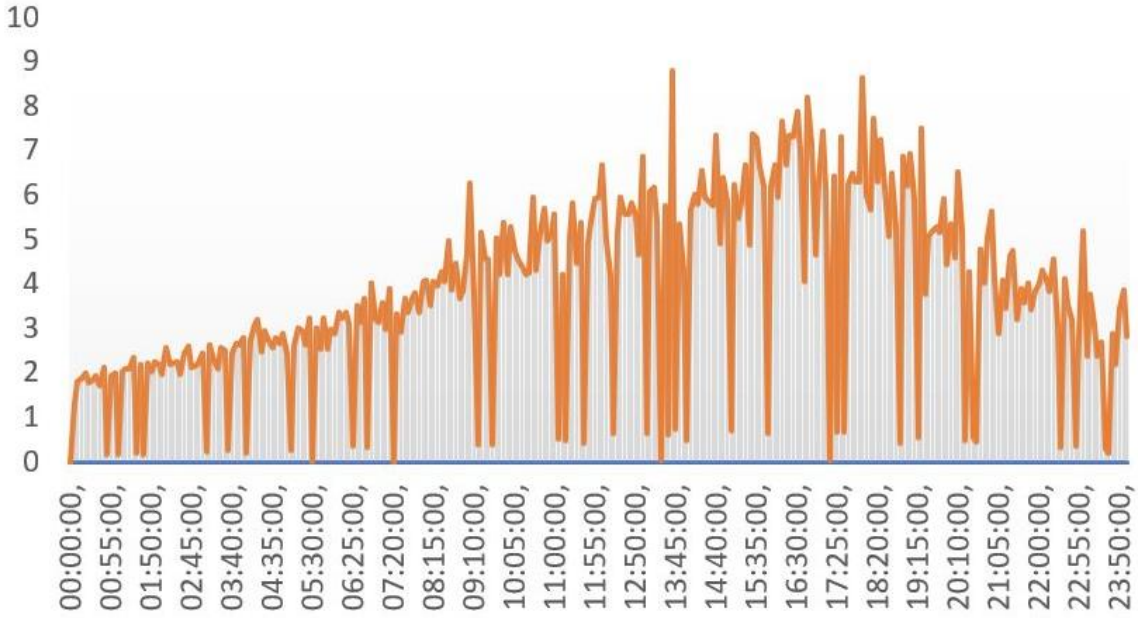

Figure 119 - Significant wave height Irma XBeach

Looking at the XBeach results in Figure 120 the water level is quite constant over the time. It is chosen to use 1.6 as the mean and add a standard deviation of 10% to account for the model uncertainty.

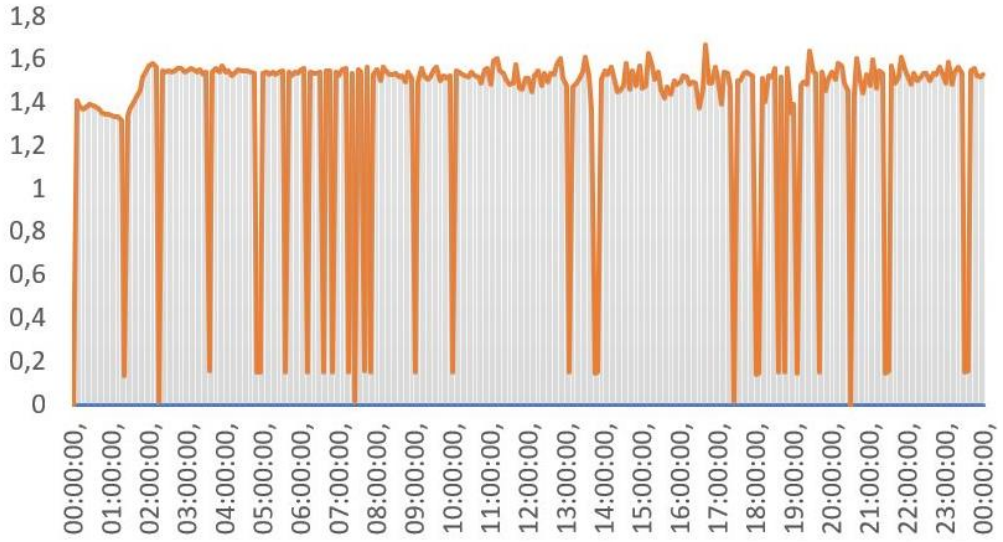

Figure 120 - Water level Irma XBeach

The sea level rise is discussed in Chapter 3. Since this is a projection this is not a fixed number and contains uncertainty. This is assumed to be 10%. It is important to note that the mean value is chosen as the value at the end of the 50 years. This is a rather conservative choice.

Because of the limited data on the tide this is also given an uncertainty.

7.2.11 Conclusion overtopping check

Section A-1

The probabilistic analysis shows that for section A-1 the CTE experiences unacceptable overtopping as the probability of failure is 90%. Given the return period of the design hurricane the target probability of failure is 30% as was discussed in Chapter 'Probabilistic approach for synthetic hurricanes'. The most likely overtopping for this section with these dimensions is 105 l/s/m.

Section A-2

For this section the failure probability is also 91%. The most likely overtopping for this section with these dimensions is 110 l/s/m.

Section B

This section the probability of failure is 94.7% for the current design. The most likely overtopping for this section is 130 l/s/m.

Section C

In this section the probability of failure is 65.6 %. The most likely overtopping for this section is 45 l/s/m.

Overall

Sections A-1, A-2 and B all have an unacceptable failure probability. For these sections adjustments to the current design need to be made. These will be discussed in the remainder of this chapter. The probability of failure of section C is lower yet still too high, the overtopping discharge is closer to the maximum allowable overtopping, some adjustments might be necessary for this area as well.

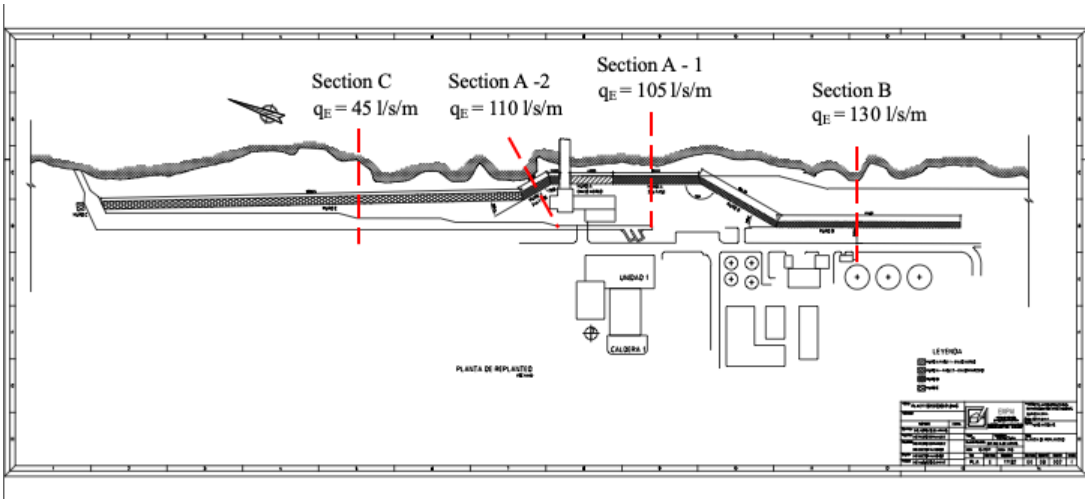

Figure 121 - Overview expected overtopping discharges

7.2.12 Discussion overtopping check

There are a few variables and correction factors that should be discussed. The first one being H_{m0} that has a very large influence on the probabilistic method. This variable has an α equal to -0.83, which means that about 69% of the uncertainty is induced by the significant wave height. As one can see in Figure 119, the wave height differs a lot during the time that Irma passes the CTE, which might cause the standard deviation of the wave height to be overestimated. However, since the standard deviation equals about 14%, it is still used for the probabilistic calculations. Another reason why not more about the significant wave height has been changed is because the wave height is dominant in the overtopping mechanism. Hence, a high α factor is to be expected and one should be careful not to overestimate the precision of the XBeach and take model uncertainties into account.

The berm correction factor γ_b is very small for sections B and C. While in literature a recommended minimum value of 0.6 is used, for these sections correction factors in the order of 0.3 were applied. The reason for doing so is the combination of an extremely large berm and the fact that the uncorrected overtopping is calculated using a schematization of a vertical wall. By doing so, section A-1 and A-2 have been schematized as such that a reliable overtopping discharge can be calculated, but the schematization is less correct for the other two sections. There is a limitation in the concept ‘berm’ when the berm exceeds certain lengths. In this case, the berm is so large that spray overtopping caused by the cliff is very unlikely to travel the full extent of the berm and thus will not cause overtopping at the site. Especially with a sea wall present. The berm can dissipate most of the wave energy over such a long distance.

7.3 Check current drainage channel

At the location of the CTE there is a drainage channel present which is used to discharge warm cooling water into the Gulf of Mexico. This channel is simply gravity based and increases in width from the start near the power plant to the outlet into the sea. In Figure 122 one can observe a top view of the CTE with the drainage channel highlighted in a light blue color.

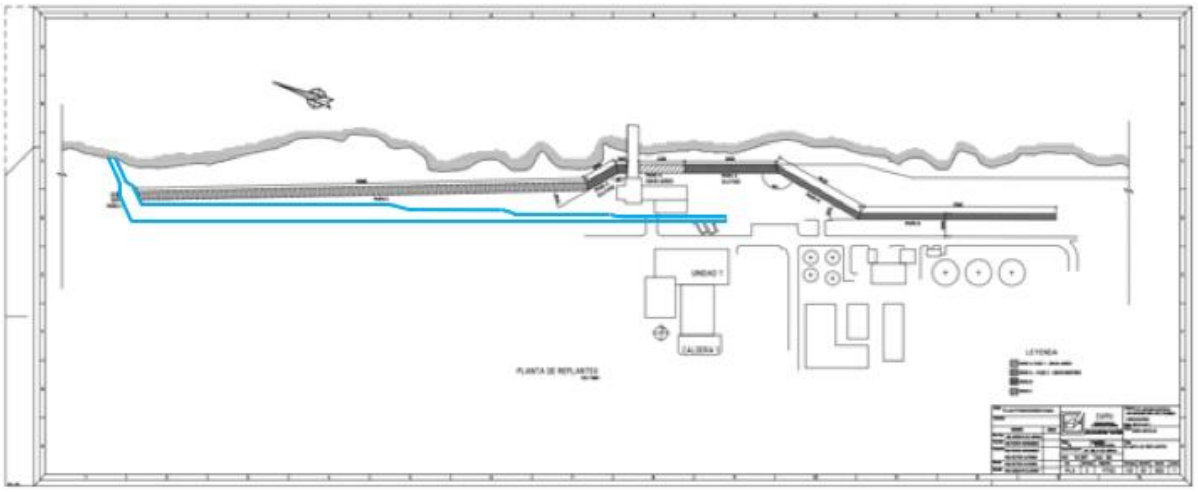

Figure 122 – Top view of the CTE with highlighted drainage channel

7.3.1 Normal conditions

Since the drainage channel has been built to discharge cooling water, the channel has a slope that makes it able for the water to flow in the desired direction. Based on aerial photographs it is estimated that the bottom of the end of the channel is located 1 meter lower than the start, hence leading to a gravitational forcing on the water mass.

In Figure 123 a schematization of the drainage channel under normal conditions can be found. This means that a constant Q is discharged into the channel and eventually let out into the sea. Since the channel is made of several segments with different widths, the equilibrium depth in the channel changes as well. The equilibrium depth in each of these segments can be calculated with Equation 36. Here c_f is a friction factor, which is about 0.005 for medium rough concrete. The slope i_b is about $\frac{1}{600}$ for this case, q is the specific discharge in $m^3/s/m$ and g is the gravitational acceleration in m/s^2.

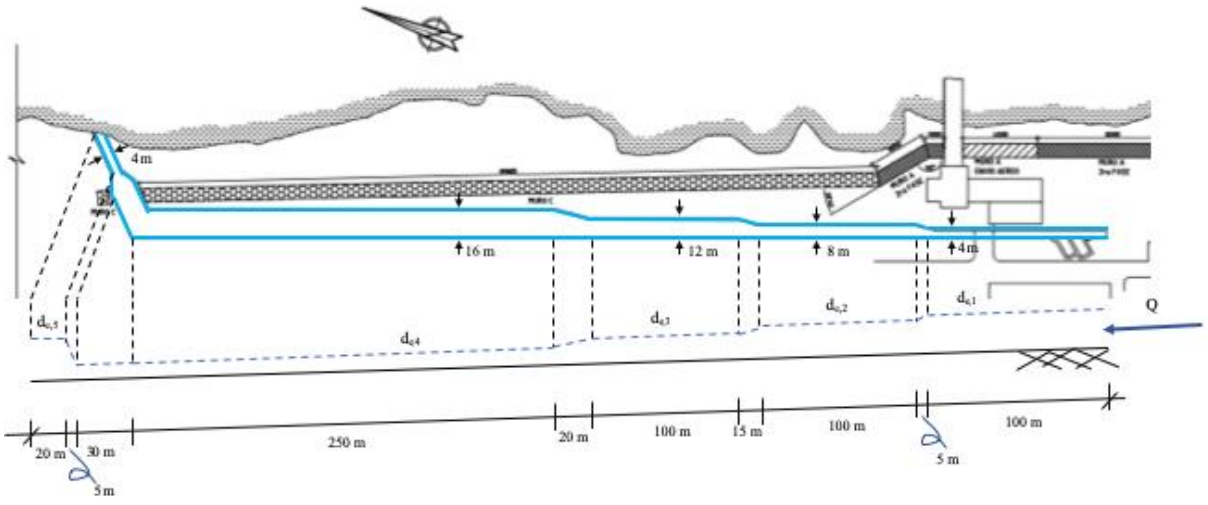

Figure 123 – Drainage channel under normal conditions

Equation 36: Equilibrium depth in open channel

$$d_e = \left(\frac{c_f}{i_b}\frac{q^2}{g}\right)^{\frac{1}{3}}$$

The CTE Antonio Guiteras has a potential to generate about 250 MW (Jesús, 2019). According to (Jones, 2008) it takes about 95 liters of water to produce 1 kWh of electricity. This water is mainly used as cooling water. This means that in order to generate 250 MW, the CTE Antonio Guiteras needs about 6.6 m^3/s to keep the plant at a correct temperature during maximum production.

This leads to the following equilibrium depths during high production, but no storm conditions.

Segment	***B (m)***	***q ($m^3/s/m$)***	***d_e* (m)**
1	4	1.65	0.94
2	8	0.83	0.60
3	12	0.55	0.45
4	16	0.41	0.37
5	4	1.65	0.94

Table 22 – Equilibrium depths normal conditions

In Table 22 one can see that the equilibrium depths decrease for larger widths of the channel, which is of course logical. It should be noted that in this case the discharge through the channel is constant, whereas during storm conditions it could maybe be varied.

Storm conditions

During storm conditions the drainage system behaves much different than during normal conditions. First thing to note is that the water that must be drained towards the sea is in this case not only cooling water, but also water that enters the site as (spray) overtopping and overland flow due to rain. These influxes depend on the magnitude of the storm and the hydraulic works that prevent overtopping and guide the overland flow.

Overland flow

The maximum rainfall intensity of a common hurricane could lead to a discharge of about 50 m^3/s, which is freely flowing over the hill surface (Chapter 3). In the current design this water can freely flow over the project area (flooding the plant) and into the drainage channel. Assumed is that the complete rain discharge of the area is captured by a drainage channel, and that it is equally distributed over the segments. The total discharge due to rainfall is as stated in Table 23, assumed is that it will enter the channel at the beginning of each segment. This represents a more critical situation then in reality.

Segment 5 is located behind the defense wall. Therefore, no overland flow will be able to reach this segment. For this reason, the rain discharge in this segment can assumed to be zero.

Segment	**Lenght**	**Total rain discharge m^3/s**	
1	102.50	Q1rain =	8.23
2	110.00	Q2rain =	8.84
3	117.50	Q3rain =	9.44
4	292.50	Q4rain =	23.49
5	22.50	Q5rain =	0
Total			50

Table 23 – Rain discharge per segment

(Spray) overtopping

The following assumption is made concerning the water entering the channel due to overtopping; the amount of water due to overtopping is summed up per segment and will enter the channel at the beginning of each segment. This represents a more critical situation then in reality.

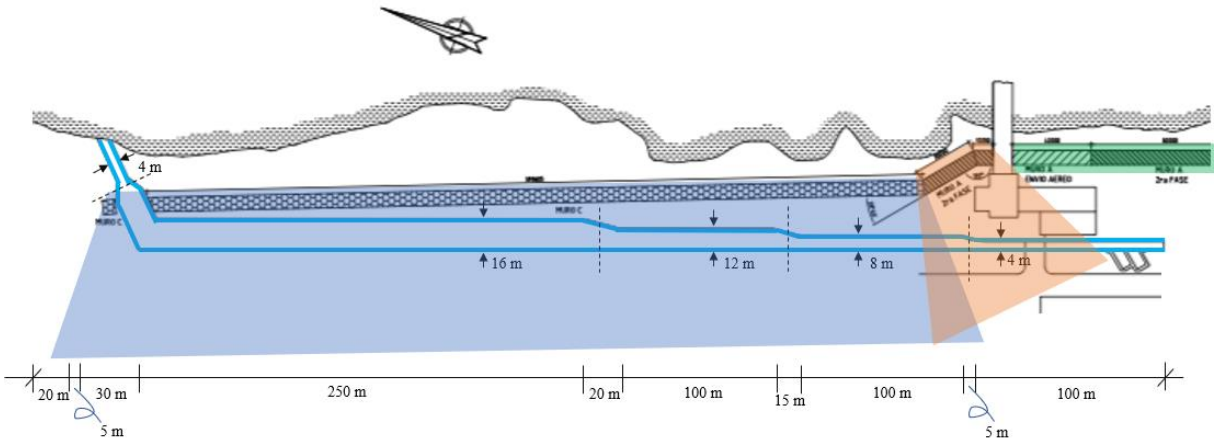

Figure 124 – Distribution of the overtopping

The blue area represents an overtopping of 45 l/s/m. The orange area represents an overtopping of 110 l/s/m. These overtopping values are calculated in the previous chapter.

Segment 5 is located outside of the defense wall; therefore, the calculated overtopping values will therefore not be accurate. The segment functions as an outlet pipe to guide the water out the drainage channel and make sure seawater does not flows back in. For this reason, this segment is very short. The discharge due to overtopping will be relatively small compared to the discharge flowing through the segment from the previous segments. Therefore, the discharge due to overtopping in this segment will be assumed zero.

The defense wall in the green area is rather far away from the drainage channel. For this reason, the overtopping discharge will be based on the blue and orange overtopping areas. The total discharge due to overtopping per segment is determined by estimating the lengths over which the different intensities of overtopping apply. Then the overtopping volumes are summed up per segment.

Segment	**Length of segment in this area**		**Total overtopping m^3/s**
	Blue	Orange	
1	0	61.5	Q1overtopping = 6.77
2	96.25	27.5	Q2overtopping = 7.36
3	117.50	0	Q3overtopping = 5.29
4	292.50	0	Q4overtopping = 13.16
5	0	0	Q5overtopping = 0

Table 24 – Total discharge volumes per segment

Total discharge

The discharges that enter the drainage channel can be seen in Figure 125. The Q of the segments consist of the rain discharge and the overtopping discharge added up.

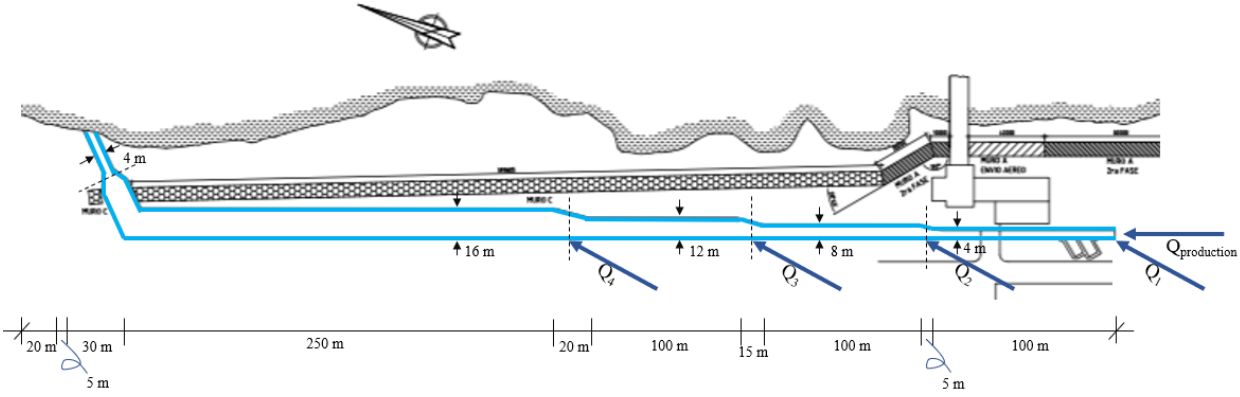

Figure 125 – Distribution of the discharge due to overtopping

This gives a total discharge per segment during storm conditions, shown in Table 25.

Segment	Discharge composition	Storm discharge in m^3/s
1	Q production + Q1rain + Q1overtopping	6.6 + 8.23 + 6.77 = 21.60
2	Q1 + Q2rain + Q2overtopping	21.60 + 8.84 + 7.36 = 37.79
3	Q2 + Q3rain + Q3overtopping	52.51 + 9.44 + 5.29 = 52.51
4	Q3 + Q4rain + Q4overtopping	89.17 + 23.49 + 13.16 = 89.17
5	Q4	89.17 = 89.17

Table 25 – Discharge composition throughout the drainage channel

In total this means that about 89.17 m^3/s should be able to be discharged through the main drainage channel during storm conditions. Since the situation is a storm, the flow in the channel is not able to reach exact equilibrium depths. For such large discharges it takes quite some time for the equilibrium depths to be reached. However, since there will also be influence of backwater curves, there are large uncertainties in the inflows and the fact that the inflow is never constant, this non-exact equilibrium flow is neglected, and an equilibrium flow is assumed.

Using the same principle as for normal conditions, the equilibrium depths for each of the segments are calculated. In one can find the equilibrium depths during storm conditions for each segment.

Segment	B (m)	q ($m^3/s/m$)	d_e (m)
1	4	5.40	2.07
2	8	4.72	1.90
3	12	4.38	1.80
4	16	5.57	2.12
5	4	22.29	5.34

Table 26 – Equilibrium depths storm conditions

The maximum equilibrium depths can be found in the narrowest segments. A depth of 5.34 meters means that the channel needs to have this same depth, to not overflow at the edges.

The sea wall next to the end of the drainage channel is situated at +5 MSL. This means that a drainage channel with a depth of 5.34 meters would not have a free outflow with or without storm surge. During storm conditions a storm surge of about 2 meters is present, meaning that the sea surface induces a backwater curve on the drainage channel. Also waves from the sea can partly travel through the channel. Since the last segment of the channel is much smaller however, the waves are partly damped.

In Figure 126 one can see the influence of the storm surge on the outlet of the channel. The drainage channel currently has a depth of 2 meter. In Figure 126, the drainage channel in the current situation is projected. It is seen that the drainage channel currently has free outflow into the sea. The difference between the bottom of the drainage channel and the HWL which includes the storm surge is 1 m. Therefore, it would be possible to deepen the drainage channel by 1 m and still create free outflow.

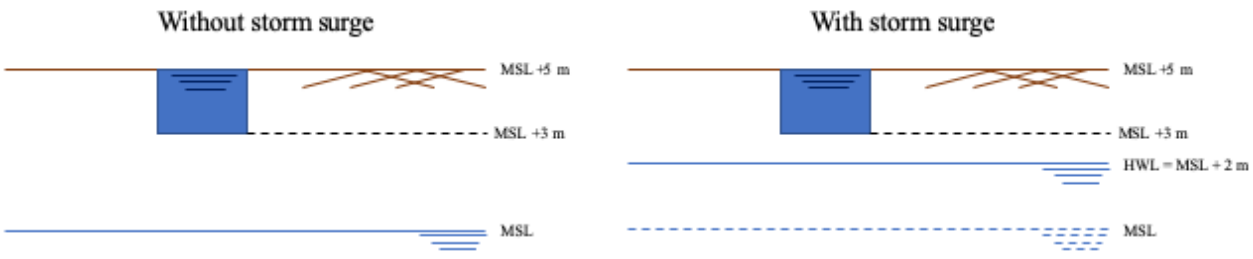

Figure 126 – Deep channel without and with storm surge

7.3.2 Influence outflow on water depths

As a way of induction, it is set that the outflow of the drainage channel will be free flow and therefore the flow over the exit is critical. The critical depth of the flow during storm can be calculated in the same manner as the equilibrium depth. Alternatively, it is not dependent on the bottom friction and the slope of the channel. The Froude number is equal to 1 and therefore the critical depth d_c is defined as in Equation 37.

Equation 37: Critical water depth

$$d_c = \left(\frac{q^2}{g}\right)^{\frac{1}{3}}$$

This means that for the outlet of the channel the critical water depth during storm conditions is equal to 3.7 meters. Now it is important to calculate the maximum depth at each of the channel segments during storm conditions by means of defining the half lengths of the backwater curves that are created.

The backwater curves are defined using the empirical fit of Bresse. The half lengths will be calculated with Equation 38:

Equation 38: Half length

$$L_{1/2} = 0.24\frac{d_e}{i_b}\left(\frac{d_0}{d_e}\right)^{\frac{4}{3}}$$

The maximum water depths during storm conditions will be calculated with Equation 39:

Equation 39: Empirical fit

$$d(x) = d_e + (d_0 - d_e)2^{\frac{x-x_0}{L_{1/2}}}$$

The results are shown in Table 27. The d_e is calculated in the previous paragraph for each segment. For $x\text{-}x_0$ the distance is taken between the beginning of each segment till halfway the change of channel width to the next segment. With this the half-length can be calculated and the maximum water depths during storm conditions can be determined. The d_0 is the water depth at the start of the segment i.e. the d(x) of the previous segment.

Segment	**d_e**	**d_0**	**$x\text{-}x_0$**	**$L_{1/2}$**	**d(x)**
5	5.34	3.70	22.50	471.57	3.76
4	2.12	3.76	292.50	654.46	3.16
3	1.80	3.16	117.50	548.79	2.94
2	1.90	2.94	110.00	490.68	2.77
1	2.07	2.77	102.50	438.73	2.65

Table 27 – Empirical fits according Bresse

The schematic representation of the backwater curves is shown in Figure 127. The figure is not scaled, so that the backwater curve types can be clearly distinguished.

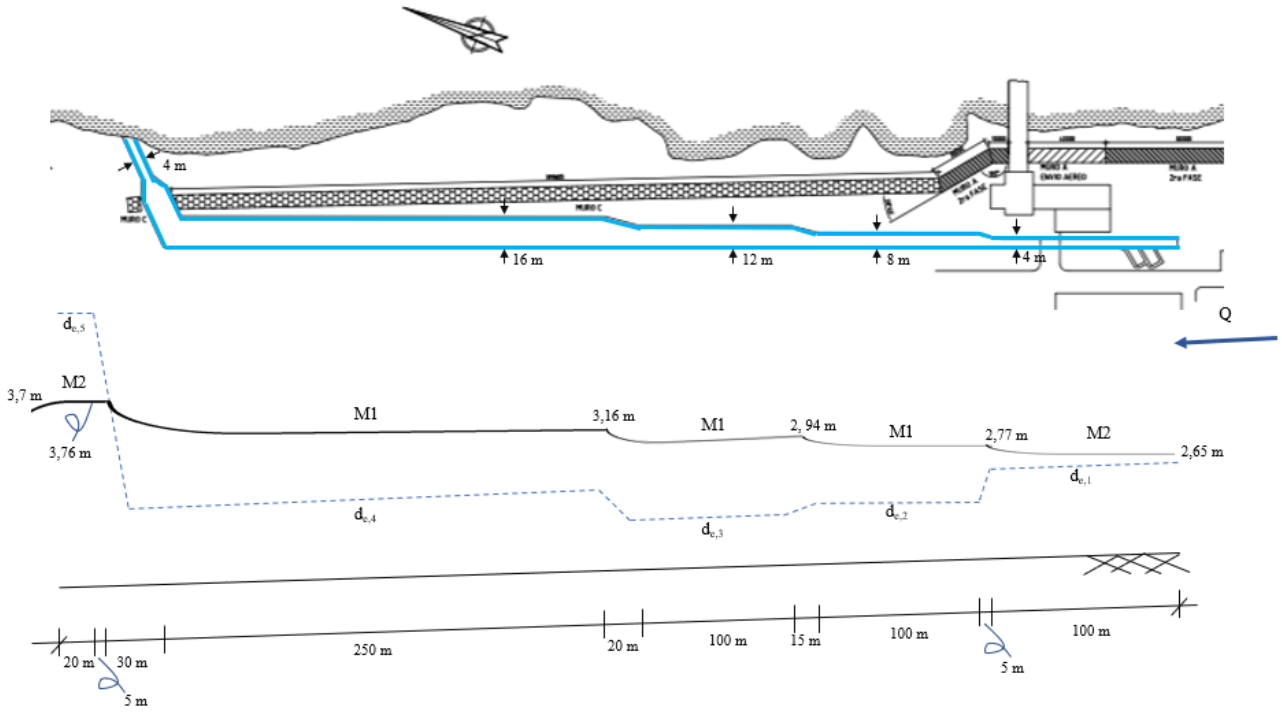

Figure 127 – Backwater curves

The maximum water level in the drainage channel during storm conditions takes place in segment 5 and is 3.76 meters. To make sure the channel has a free outflow, a channel with a depth of 3.80 meters would be enough. The channel which is present has an approximate depth of 2 meters and thus does not meets this requirement. The segments will flood and therefore water from the drainage channel will run towards the power plant.

7.4 External stability of current design

In checking the stability of a structure with respect to its environment, three types of stability should be considered: horizontal, vertical and rotational stability. Vertical stability can easily be guaranteed, due to stone type subsoil. It can be safely assumed that this type of subsoil will be able to resist for the vertical forces of the coastal defense and the vertical forces of the water in stormy environments.

7.4.1 Horizontal stability

In most cases, the horizontal stability needs to be guaranteed by the ratio of the weight of the structure and the friction coefficient between the structure and the subsoil. This ratio should be smaller than the horizontal pushing force. A teeth-like structure is used in the design and is part of the structure to prevent for horizontal instability. These teeth are sticking in the stony subsoil. The structure needs to be lifted in order to allow for horizontal movements. These massive types of structures are not able to float or to be moved by other types of pressures. The structure will always vertically stay in its place. This teeth type of drag system generates a fictive unlimited large friction coefficient. Even without a downward force, this teeth type system generates enough resistance to prevent for horizontal instability. This horizontal stability will only be guaranteed as long as there is internal stability at all times. In other words, the teeth need to stay connected to the structure. This analysis focusses on macro stability and always assumes internal stability. The internal stability will be checked in the next paragraph.

7.4.2 Rotational stability

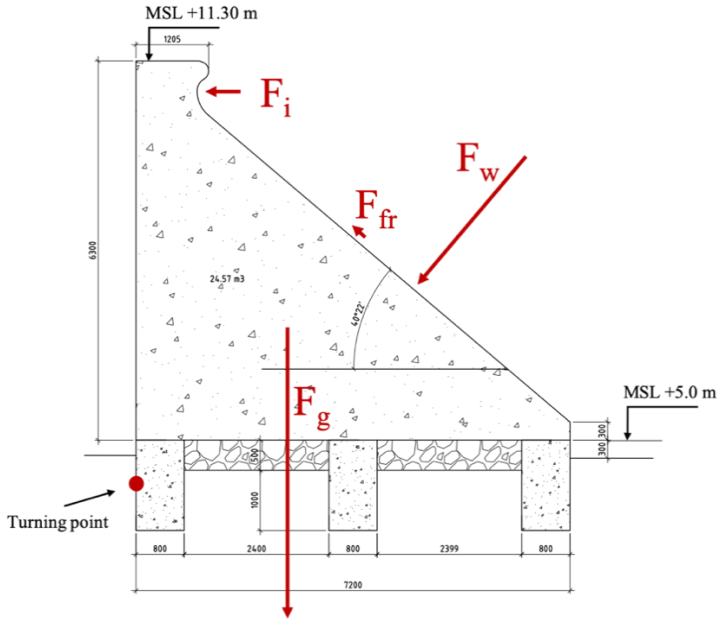

Figure 128 - Cross section of coastal defense part A in which the relevant forces for a stability analysis are displayed

Figure 128 shows a cross section of coastal defense part A to help analyzing the rotational stability, the only type of macro stability that is not analyzed yet. The relevant forces that are needed for a rotational stability analysis are displayed in this figure.

- *Turning point*: Initially, the turning point should be determined to know around which point will be used for the sum of moments. The water forces are pushing to the left, and the gravity forces are pushing downward. Hence, the turning point will be defined in the lower left corner of the drawing. The turning point is placed in the middle of the lower left tooth. In case overturning will happen, then the concrete and/or stone material will plastically deform. By placing the turning point in the middle of a tooth, both materials need to plastically deform a bit upon the turning the structure.
- *Water pressure:* The water pressure force is represented with the "F_w". This force acts perpendicular to the sloped wall. The slope of the wall is less steep than 1:1. The force of the water may act in the middle of this slope but is more prone to act on lower parts of the slope due to low waves and the course of the hydrostatic pressure. Hence, the water pressure force will always contribute to a rightward overturning moment and will not lead to rotational instability. In other words, the water pressure line of force will always run through the base of the structure and will not lead to rotational instability.

Gravitational force: The gravitational force due to the self-weight of the structure is represented with the "F_g" in

- Figure 128. It is clearly visible that this force will contribute to a rightward overturning moment and will not lead to rotational instability. Also, this line of force will always run through the base of the structure and will not lead to rotational instability.

Friction force: The friction force of the water that runs upward onto slope is one of the forces that is acting on the structure as well. This force may be found in

- Figure 128 with "F_{fr}". However, this force has an order of magnitude that is much smaller than the other forces. This force can be neglected in this analysis.

- *Impulsive force*: This force is in the notch of the bullnose and is to be viewed in the figure with "F_i". The waves will run up the slope and smash into the bullnose. This force could contribute to an overturning moment that would lead to a rotation instability.

A quick calculation that checks for just one-meter wide section of the cross section will help to see how the forces are balanced. The calculation below will show what realistic impulsive forces could initiate rotational movements. In the calculation below, only the gravitational force is taken into account to compensate for force on the bullnose. The hydrostatic force has a small lever arm to the turning point and will therefore have a small overturning moment.

Equation 40 - Sum of moments for rotational stability check

$$M_r = V \cdot \rho \cdot g \cdot r = 24.5 \cdot 25 \cdot 9.81 \cdot \frac{7.2}{3} = 14420\ kNm$$

Equation 41 - Needed impulsive wave force

$$F_i = \frac{M_r}{r} = \frac{14420\ kNm}{6.5\ m} = 2220\ kN$$

This impulsive water force can be converted to a water pressure force to get a sense of the order of magnitude of the pressure. The height of the bullnose is maximum 1 meter high. The water pressure that acts on the bullnose area will then be 2220 kPa. This pressure would be equal to the hydrostatic water pressure of a column of 2220 meters. This is an impossibly large pressure to have generated by such impulsive waves. For this reason, rotational stability is always ensured.

7.4.3 Defense design B and C, compared to design B

The external stability of sea defense B and C will always be maintained as well. Sea defense B and C have more or less the same design of structure as defense A. Sea defense B and C can be viewed in respectively Figure 129 and Figure 130. The slope facing the water of defense B and C is less than 1:1. The slope of defense A is less than 1:1 as well, which resulted in stability of the structure. Also, the teeth in the foundation of the structures is to be found back at sea defense B and C. These criteria are the basis for the statement that the external stability will always be maintained.

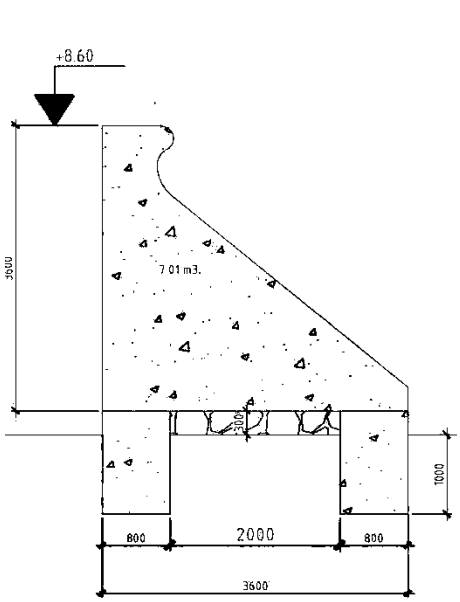

Figure 129 – Sea defense design B

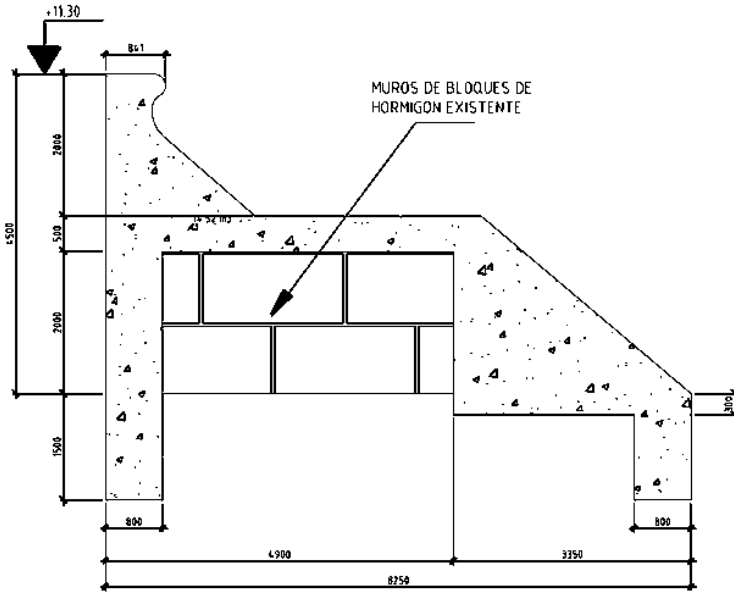

Figure 130 – Sea defense design C

7.4.4Conclusion External stability

The current designs are stabile in vertical, horizontal and rotational directions. The subsoil offers much stability for the structure. Furthermore, the design of the sea defense has a few basic ideas that give much

stability in the horizontal and rotational directions. However, these stabilities can only be guaranteed if the internal stability is always maintained. The next chapter will look into this internal stability.

7.5 Internal stability of current design

The design has proven to be stabile on macro scale. The sea defense will stay in place with the extreme hydrodynamic conditions. However, this stability will only be guaranteed as long as the structure is internally stable at all times. This section will dig into the internal stability of the structure.

A rough approach will be taken in this analysis to perform some basic first checks in the internal integrity. The maximum design surge and the maximum wave height will be the basis for the hydrodynamics used for the calculation. First, the outer forces will be quantified in the sense of its magnitude and its direction. Based on those results of the forces, the internal integrity will be checked. For internal instability a few types of failures will be considered, and a quick consideration will be made to see whether the type of failures could be relevant for the structures.

Vertical forces exceed the concrete pressure capacity: Concrete compressive strength is large enough to resist for the vertical forces of its own weight. The water pressures due to a wave that runs up the defense will not lead to significant pressures that would exceed the compressive strength of the concrete. This type of failure will not be considered.

Horizontal forces exceed the shearing capacity: The horizontal pressures due to the waves will lead to a shear force in the concrete. The horizontal forces of the waves need to be transferred to the subsoil. The model assumes that the horizontal forces will be transferred through the teeth that stick into the concrete. The critical cross section for the shear capacity will be just at the joint of those teeth on the structure. These critical cross sections are marked with dashed lines in Figure 131. These sections will be checked for concrete shearing capacity later.

Moment forces exceed the moment capacity: The cross section has a surface area of 24.53 m^2. A large moment capacity will come along with this large cross-sectional area. Moment forces due to the waves are not going to be an issue for this cross section concerning the internal stability.

7.5.1 Shear capacity of the teeth sticking into the subsoil

The shear capacity of the teeth that stick into the subsoil will be critical in this internal stability study as is discussed before. Figure 131 shows the system to be analyzed. The concrete has a compressive strength of $f_{ck} = 20\ MPa$.

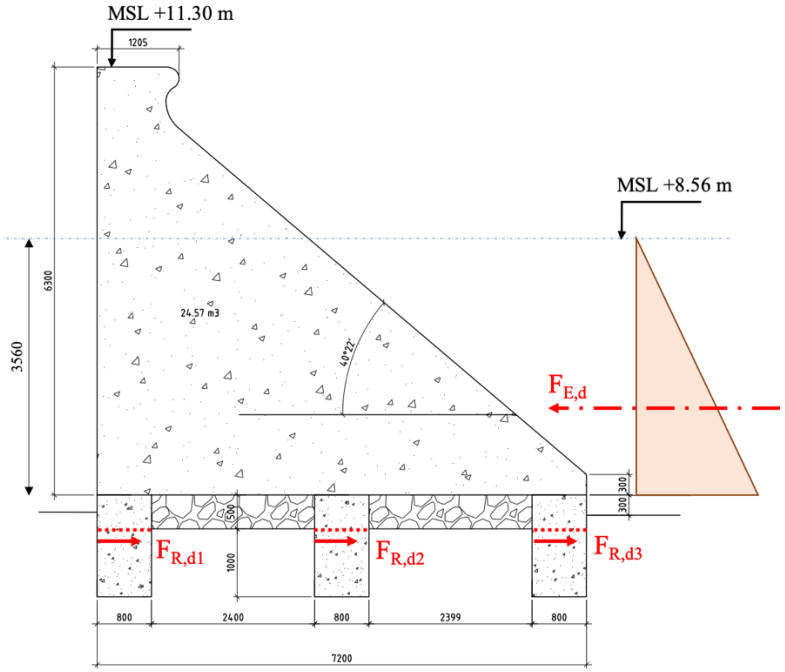

Figure 131 – Forces that could lead to internal instabilities

The teeth contribute to the resistance for horizontal displacement of the complete structure. The width of one tooth is d=800 mm. There is a compressive strength on the teeth due to the self-weight of the structure, therefore, the complete width may be used for a resistance capacity calculation. The resistance capacity of these three teeth in total can be calculated with Equation 42 and Equation 43.

Equation 42 - resistance capacity shear stress cross section

$$v_{rd,c} = 0.035 \cdot k^{\frac{3}{2}} \cdot \sqrt{f_{ck}} \cdot 3 = 0.035 \cdot \left(1 + \sqrt{\frac{200}{800}}\right)^{\frac{3}{2}} \cdot \sqrt{20} = 0.29 \frac{N}{mm^2}$$

Equation 43 - resistance capacity shear force cross section

$$V_{rd,c} = v_{rd,c} \cdot b \cdot d \cdot 3 = 0.28 \cdot 1000 \cdot 800 \cdot 3 = 690\ kN$$

The force will be induced by the waves. The maximum wave height will cause the governing force that can cause internal loss of integrity. The horizontal force due to this maximum wave height is:

Equation 44 - top of wave

$$top\ of\ wave = surge + tide + \frac{1}{2} H_{max} \approx 2 + \frac{1}{2} \cdot H_s \cdot 2 = 2 + 6.56 = 8.56\ m$$

Equation 45

$$h_{wave\ on\ structure} = 8.56 - 5.00 = 3.56\ m$$

Figure 131 shows the course of this hydrostatic pressure acting on the structure.

Equation 46 - hydrostatic pressure

$$F_{E,d} = \gamma_E \cdot F_{E,d} = 1.2 \cdot \frac{1}{2} \cdot rho \cdot g \cdot h_{wave}^2 = 1.2 \cdot \frac{1}{2} \cdot 1025 \cdot 9.81 \cdot 3.56^2 = 76.5\ kN$$

The forces of impulsive waves have been calculated earlier in the report. This impulsive force was in the order of magnitude of 20 kN/m. The shear capacity is still large enough to resist for the hydrostatic pressure force and the impulsive forces. Hence, the internal integrity will be maintained at all times. There is no need for reinforcement in the structure to enhance structural strength.

7.5.2 Defense design B and C, compared to design B

Sea defense design B and C have the same structure with teeth as foundations. Earlier analysis showed that this part of the structure might be vulnerable to internal integrity problems. Sea defense B and C have two teeth instead of three teeth. The width of each separate teeth is similar in every design. To make a rough guess of the resistance capacity due to shear forces, the total resistance capacity of design A can be multiplied by two thirds. The shear capacity can be calculated to be 460 kN. This shear capacity is still enough to resist the hydrostatic pressures and the impulsive forces of the maximum existing wave height.

In short, the current designs of the sea walls have enough shear capacity to resist for the shear forces induced by the waves. The designs have enough shear capacity, even without reinforcement. Hence, the designs will have internal structural strength for all load cases.

7.6 Design Functionality

For each function of the sea defense several alternatives are possible. Four functionalities can be distinguished and will be discussed separately. These are wave reduction, barrier, gap protection and drainage capacity. This is done to get an idea of what the possibilities for a design are, which will be used as input for the variants.

7.6.1 Wave reduction

Wave reduction means that the wave energy needs to dissipate so that waves will lose their height and have less impact. Wave reduction measures can be used stand alone or in combination with another sea defense. Some options for wave reduction are emerged/submerged rubble mount breakwater, emerged/ submerged caisson breakwater, floating breakwater, pile screens or a shallow foreshore.

Rubble mount breakwater

A breakwater forces waves to break and therefore dissipating energy and limiting the transmission of wave energy. A submerged breakwater can force waves to break but there will be still transmission of wave energy, the higher the breakwater the more waves it will stop but the more costly the breakwater will also become. An optimum in cost and efficiency is when the breakwater is at water level, the wave height is halved and only 25% of the wave energy is transmitted.

Because the CTE is located near a steep cliff into the water placing a rubble mount breakwater can be very costly because of the large depth directly in front of the coast. A rubble mount breakwater of such a height would also take up a lot of space because of the slope needed for the breakwater to be stable.

Caisson breakwater

A caisson breakwater works from the same principle as the rubble mount breakwater. The advantages of a caisson are that it can be placed with more precision and will take up less space. Production of a caisson would have to be in either a dry or floating dock, and the caisson(s)to be transported to the site. A caisson could prove to be more expensive than the breakwater but would not be subjected to spatial limitations.

Floating breakwater

A floating breakwater has the advantage that it can be used at large depths; it only needs to be anchored to the sea floor and floats at water level. The dimensions of the floating breakwater need to be in the order of

magnitude of the wavelength in order to be effective. The design wave for this area has a wavelength of 70-80 m, which means that a breakwater of very large dimensions would be needed.

Pile screens

Pile screens can be installed in front of the CTE to attenuate the waves. Wave energy is dissipated because it is forced to flow around and through the piles causing turbulence. The pile has to be firmly in the ground to withstand the wave forces. The top of the piles would need to be a few meters above the water level since most water movement will occur there in extreme conditions. The feasibility of the pile screen is dependent on the subsoil and available equipment to transport and drive piles into the bed from sea.

Shallow foreshore

A shallow foreshore causes energy dissipation due to bed friction and the wave heights are depth limited and will break sooner. In this case because of the very large depth in front of the CTE very large volumes of sediment would be needed as a nourishment to create such a foreshore. This sediment will erode away so many nourishments would be needed to maintain the shallow foreshore. This would be a very costly and maintenance intensive measure.

Barrier

The barrier directly in front of the CTE is meant to stop the waves and limit overtopping. In this situation a seawall is the most suitable option. The barrier needs to be high enough so that only a limited amount of waves overtop with an acceptable volume. It also needs to be stable against the wave impact. By varying with the slope of the barrier the manner and amount of overtopping can be influenced. The way in which individual blocks are attached to each other and the ground can also be varied.

Slope of the wall

As can be seen in Figure 132 the slope of the wall has a large influence on the amount of overtopping, for the same relative freeboard the overtopping for a vertical structure with no influencing foreshore can be half of the overtopping of a wall with steep smooth slope, cot alfa = 2.

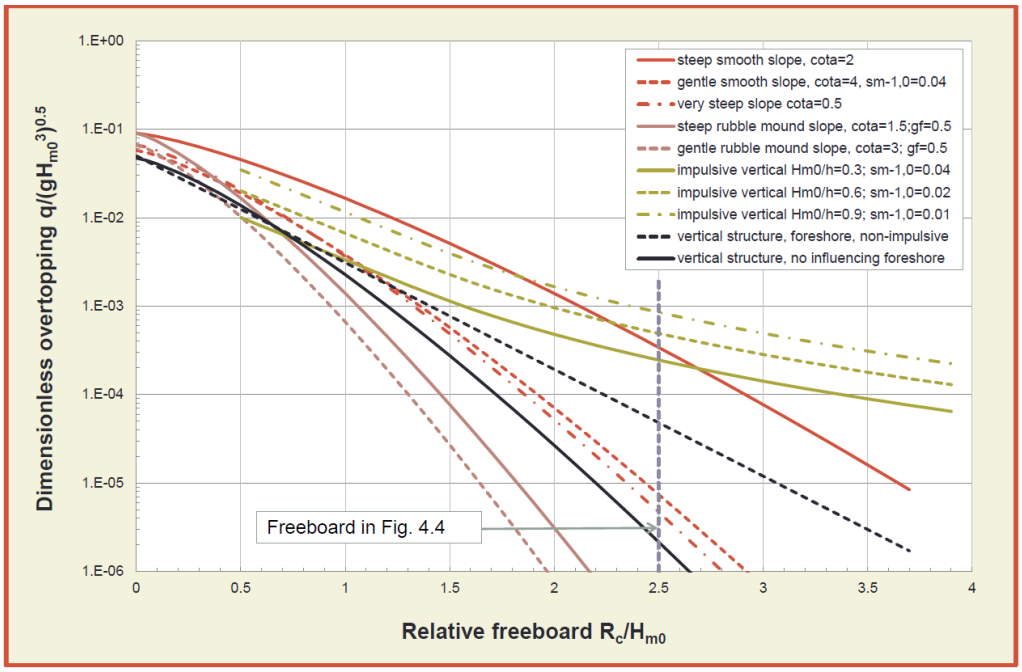

Figure 132 – Comparison of wave overtopping formulae for various kind of structures (EurOtop, 2018)

As mentioned in previous paragraphs impulsive waves cause sudden and violent breaking and water is thrown high in the air, so overtopping can occur even for very high structures. Gentle waves act as plunging breakers, which greatly reduces overtopping.

A vertical structure is the most space efficient design. In the case of no influencing foreshore and thus no impulsive waves this is also a very effective design as a low relative free board is needed to reduce dimensionless overtopping. In the case of impulsive waves however, a high vertical structure will have little effect on the water thrown into the air caused by the violent breaking. A measure against this could be to have an overhanging structure on top of the wall that will block this splash.

A gentle slope could also be implemented although this would require more space which might not be available. However, since such a measure would greatly reduce overtopping this structure would not have to be as high. For gentle slopes the wave period is of influence on the overtopping.

A rubble mount slope is the most efficient in reducing overtopping because of the more gentler breaking and the energy absorption due to the rough material. The stability of the rubble mount breaker is however questionable considering the type of waves to be expected. Very large rocks or for example tetrapods would have to be placed.

Gap protection

The inlet channel for cooling water proves a difficult element in the design. Cooling water needs to be available for the CTE to use at any moment. In normal conditions an open channel to sea does not provide a problem, during a storm however large amounts of water can flood in and the barrier can be damaged at this location. A solution needs to be sought that allows the continuous flow of water but more safety against flooding during an extreme storm condition.

Wave attenuation channel

An option would be to create obstacles in the channel, the water needs to flow around these obstacles and the turbulence caused by this will dissipate energy. The attenuated waves will do less damage to the cooling water basin and cause less overflow.

Gate

A steel gate could be placed in front of the gap which could be completely or partially closed during storm conditions. The gate could also be of a lower height than the surrounding protection, so a ‘controlled’ amount of overtopping occurs in the channel, so enough water stays available during the storm. However, the gate will have to withstand very large wave impacts, this means that the thickness will have to be very large. The gate is therefore an expensive alternative.

Pipeline

An option would be to close the channel and instead use a pipeline from sea for inflow of cooling water. The pipeline would have to have a large diameter to have the same discharge as the inflow channel. Construction of a pipeline can also be very costly.

Sea wall across the gap with walls around the channel and basin

The sea wall can be extended over the channel, this way the overtopping is reduced. The walls of the channel and the cooling basin can also be heightened so that water from the basin will not flood the whole plant. Because of the relatively narrow and shallow channel the water will lose a lot of its energy due to friction. For this reason, the walls of the basin do not have to be of the same caliber as the sea wall, they just need to retain the water.

Do nothing

Another option would be to accept that there is a weak point in the barrier and that there will be excessive water inflow during extreme storm conditions. Mitigation measures can be taken such as moving important structures away from this area or improving drainage or pumping capacity at this location.

7.6.2 Drainage structures

Improving the drainage of the area of the power plant gives the advantage that water that enters as either precipitation, overtopping or overflow can be carried out of the area and hence make sure that vital parts of the power plant are not flooded and are therefore damaged less or not at all. There are several options to improve the drainage of the area. It can be done by diverting the water by means of drainage channels or by pumping away the water using one or several pumping stations.

The area of the power plant is a rocky area with large height differences, which makes water that enters as precipitation convert to low-lying areas. This kind of flow is uncontrolled and can therefore pose large threats to the power plant. As mentioned before, the water that enters the area as overtopping from waves can be trapped behind the seawall and also flow towards the low-lying areas. The waves generated by hurricane Irma showed large volumes of overtopping water that then flooded the area of the power plant. Hence it is important to take both factors into account for the design of the drainage structure and take into account the topography of the area.

Drainage channels

Using only drainage channels, the topography of the area needs to be used to convert the water to a less flooding-sensitive area. For instance, the water could be diverted away from the power plant towards an area that can flood, the inlet channel for the cooling water or it can be diverted directly towards the sea.

Using drainage channels means that the drainage system only uses gravitational flow and no pressured flow. Hence, water is only able to flow downwards, and a well-structured system is therefore a must. To design a gravitational drainage system well, the topography of the area must be analysed thoroughly.

Pumping station

A pumping station has the advantage over a regular drainage system that a pressured flow is able to overcome height differences and therefore water can be collected at almost any location and diverted from there. Using a combination of several pumps, a desired head difference and discharge can be created by assorting them in parallel and series set-ups.

By putting two similar pumps in a parallel set-up, the discharge from this pumping station is doubled and by putting them in a series set-up the head difference is doubled. However, since the pump curves that come with these pumps must fit the system curve (curve created by the attached system of pipes), the discharge and head difference is not doubled, but lies somewhere in between the situation of 1 pump and 2 pumps.

7.7 Variants

7.7.1 General

Looking at these functionalities the most promising interventions are further elaborated in different variants. The variants are all extremes where only one functionality is explored to determine the influence one intervention has on the overtopping. For the final design most likely a combination of variants will be chosen so that the interventions are less extreme, and some redundancy is included in the design.

The protection of the inlet channel and the protection against overtopping are separate items that can be combined in multiple way. In order to assess all items separately the variants relating to overtopping will be numbered 1, 2 and 3, while the variants relating to the inlet channel will be labelled A, B and C. A complete design consists of a combination of the two, e.g. variant 2-C. Rough dimensions will be given, only for the final design a full calculation is done.

7.7.2 Variant 1: Current design with wave reduction

It is most cost efficient and sustainable if the current design is maintained where possible. A parametric analysis of the probability of failure vs the wave height has been performed in Appendix F. In the section A-1 and A-2 the waves need to be reduced by about 1.7 m in order to limit the overtopping to an acceptable amount. In section B by 2.1 m, in section C the waves need to be reduced 0.7 m. A viable option is to do this by means of pile screens.

To reduce the waves before they reach the structure a pile screen will be placed in front of the sea wall. The piles will be placed away from the wall for effect, but close enough so that the depth is still limited. If the piles are placed all along the area that needs to be protected a very large number of piles will be needed. The closer together they are placed the less the transmission of energy will be, however the more expensive it will also be. Even though different sections need a different amount of wave reduction it is unpractical to use different piles. The piles can be prefabricated or produced on site and a high repetition factor means that the cost per pile are reduced. If the piles are prefabricated, they need to be transported over water. The piles need to be driven into the ground also from the water, equipment needed for this will be expensive.

The piles will be most effective when the orientation is perpendicular to the wave propagation direction. A problem however is that the bathymetry around the plant is uneven and shows a steep decline in some areas making it difficult to place uniform piles.

In order to reduce the height of the incoming waves a pile screen can be constructed. The effectiveness of a pile screen depends solely on the spacing of the piles given they stand high enough above the water line. In this case high enough means that the piles need to stand 2 meters above the high-water level. In Equation 47 one can find the transmission factor for a pile screen.

Equation 47 - Transmission factor pile screen

$$K_T = \sqrt{1 - W}$$

In this equation the factor *W* is the relative blockage of the pile screen. In Figure 133 one can see that the height of a dam, or in this case a pile screen, influences the transmission factor largely. It should therefore be considered that the difference between the transmission factor imposed by the spacing does not vary too much from that imposed by the relative crest height. Using a pile screen that stands 2 meters above the high-water level for waves in the order of 6.5 meters gives a transmission factor of about 0.35.

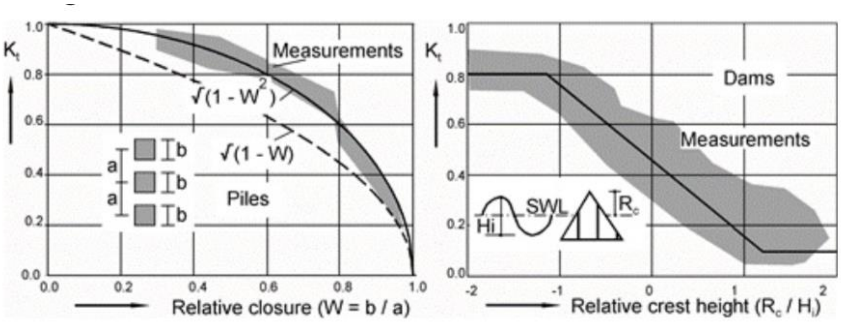

Figure 133 - Pile screen wave reduction

Section A-1

For section A-1 the wave height needs to be reduced to 4.8 meters, meaning the transmission coefficient can be 0.74. Filling in Equation 47 gives that the relative blockage of the pile screen should be 0.45. This means that the gaps between the pile of 1-meter diameter can be $W = \frac{b}{a} = \frac{1}{1+space} = 0.45$. Hence the spacing between the piles can be 1.2 meters.

Section A-2

For section A-2 the wave height needs to be reduced to 4.8 meters, meaning the transmission coefficient can be 0.74. Filling in Equation 47 gives that the relative blockage of the pile screen should be 0.45. This means that the gaps between the pile of 1-meter diameter can be $W = \frac{b}{a} = \frac{1}{1+space} = 0.45$. Hence the spacing between the piles can be 1.2 meters.

Section B

For section A-1 the wave height needs to be reduced to 4.4 meters, meaning the transmission coefficient can be 0.68. Filling in Equation 47 gives that the relative blockage of the pile screen should be 0.54. This means that the gaps between the pile of 1-meter diameter can be $W = \frac{b}{a} = \frac{1}{1+space} = 0.54$. Hence the spacing between the piles can be 0.85 meters.

Section C

Since the wave height for section C needs to be reduced only to 5.8 meters, the construction of a pile screen is not feasible since the costs of mobilization are too large to set up such a marginal pile screen.

Figure 134 and Figure 135 show a rough design for section A-1.

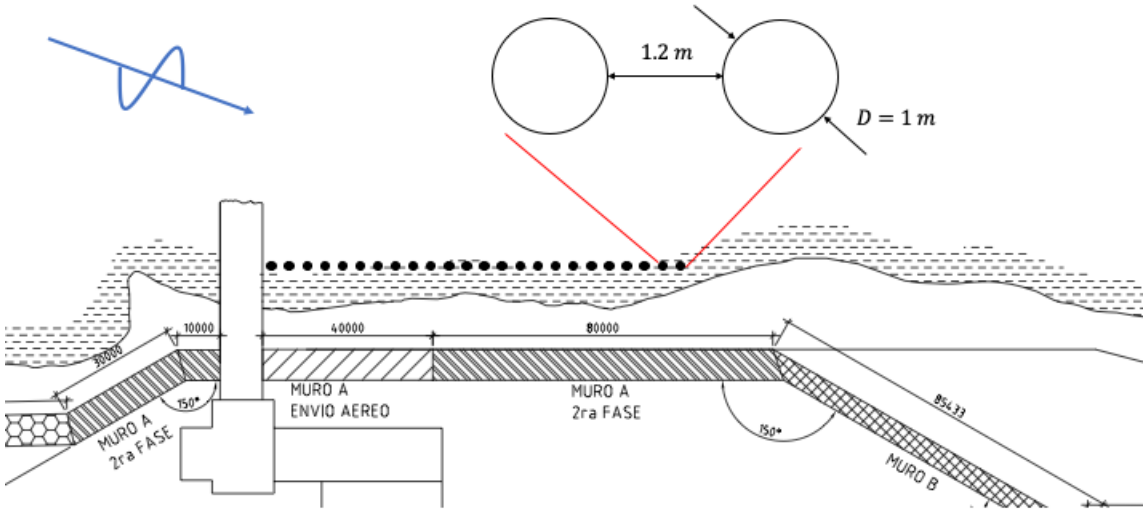

Figure 134 - Section A-1 pilescreen lay out

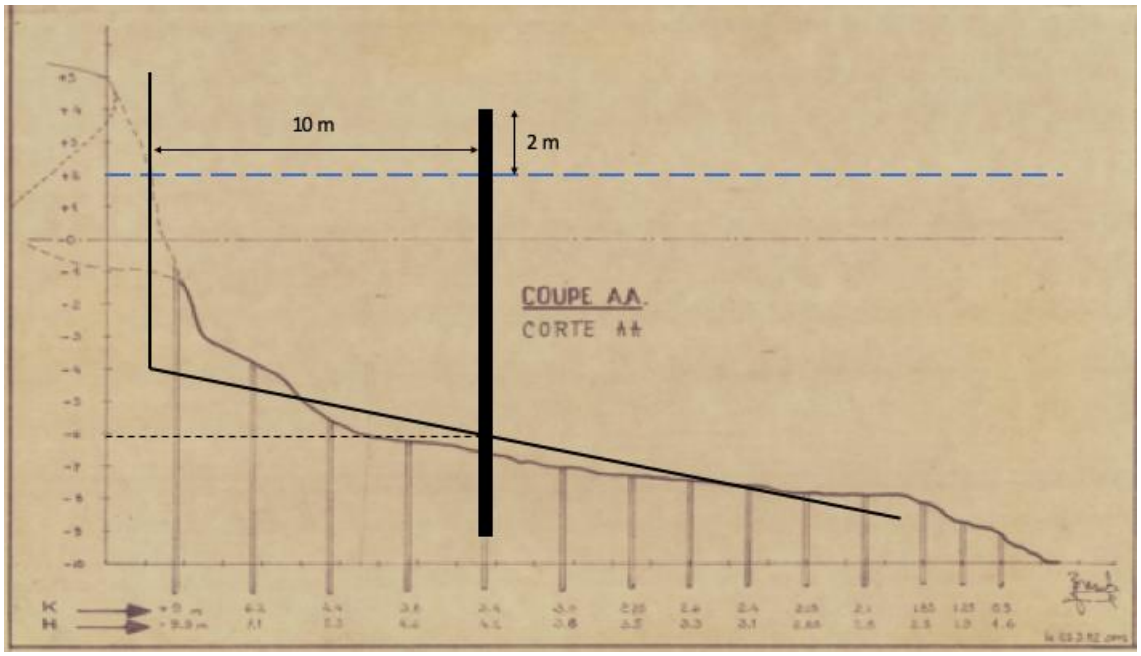

Figure 135 - Section A-1 cross section pile screen

7.7.3 Variant 2: Current design with pumping and drainage channel

For section A-1 the drainage capacity needs to be increased to 145 l/s/m in order to prevent flooding by overtopping. For section A-2 the drainage capacity needs to be 150 l/s/m. For section B 175 l/s/m is needed and for section C 65 l/s/m in order to meet the target failure probability.

By allowing some overtopping over the different sections of the sea wall, one could prevent the heightening of the sea walls. This means that the allowed overtopping is more than the limit of 34 l/m/s. If the overtopping over the sea wall exceeds this value, some measure needs to be taken. For this variant this excess overtopped water is discharged by means of pumping and/or improving the existing drainage channel.

For sections A-1 and B there is no drainage system already present and because of the high density of important systems in these sections there is also no space to construct a new system. Hence this is not a feasible solution for these sections and therefore there will be no elaboration about these sections in the variant.

During storm conditions the drainage system behaves very differently than during normal conditions. First thing to note is that the water that must be drained towards the sea is in this case not only cooling water, but also water that enters the site as (spray) overtopping and overland flow due to rain. These influxes depend on the magnitude of the storm and the hydraulic works that prevent overtopping and guide the overland flow.

Rainfall discharge

The maximum rainfall intensity of an average hurricane could lead to a discharge of about 50 m^3/s, which is freely flowing over the hill surface (see Chapter 3). To protect the power plant from flooding due to this rain discharge, a low wall is built around the power plant. Assumed is that the rainfall is equally distributed over the surface and the total rain discharge flows towards the power plant. The total length of the power plant area is estimated be 400 meters wide, so the rain flow will reach a depth of $\frac{50}{400} = 0.125$ meters. This means a wall of 0.2 meters would be enough.

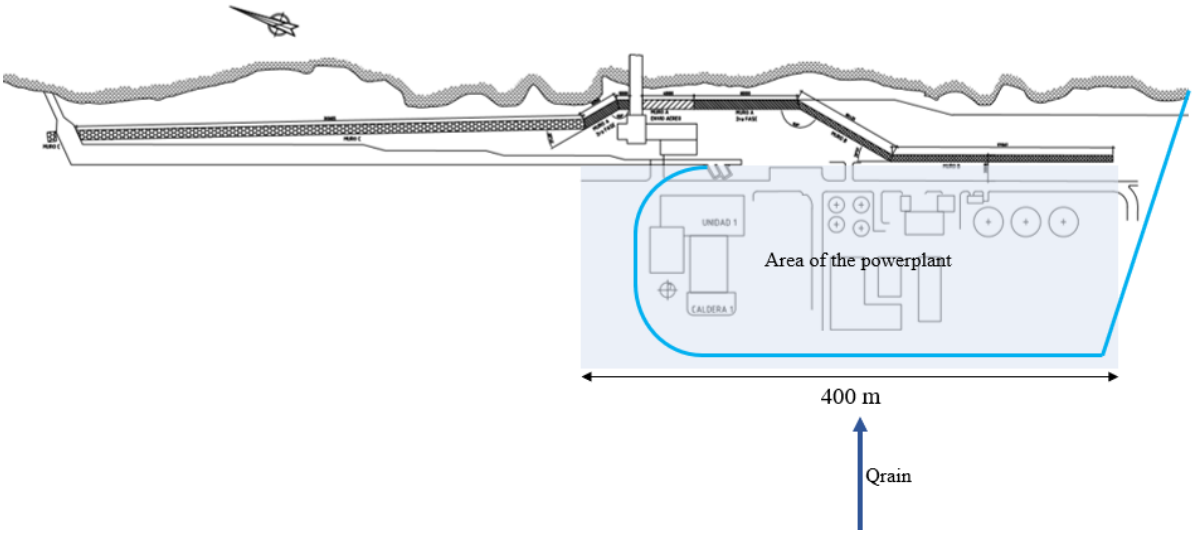

Figure 136 - Drainage wall

The rainfall is led into the channel via the drainage wall. The wall ends in the beginning of the channel, therefore in the schematization of the discharge the rainfall discharge enters the channel in segment 1 (Figure 136). This is an overestimation of reality, since a part of the rainfall can also flow into the other segments. However, for designing purposes this is a good simplification, because it represents a more critical situation then in reality.

Overtopping

The following assumption is made concerning the water entering the channel due to overtopping; the amount of water due to overtopping is summed up per segment and will enter the channel at the beginning of each segment. This represents a more critical situation than, hence it is a conservative schematization.

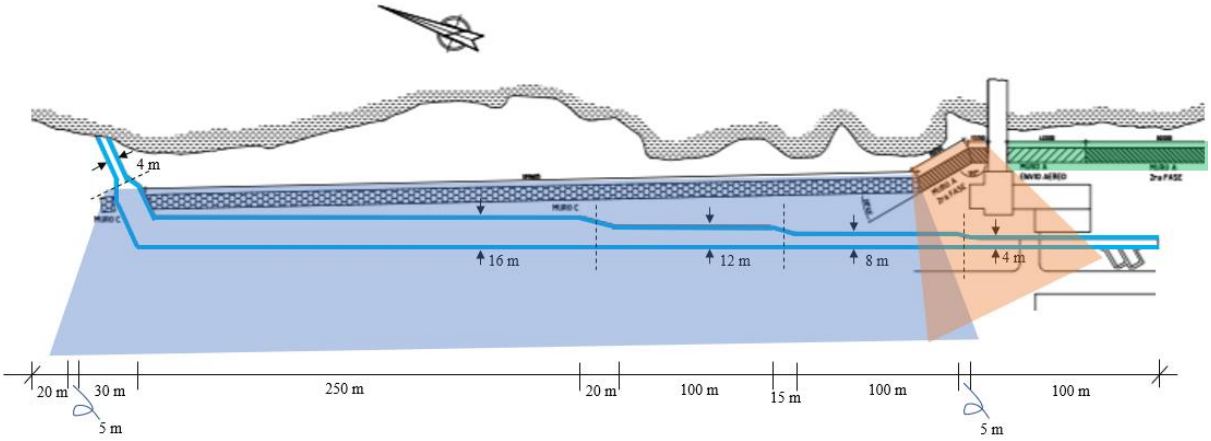

Figure 137 – Distribution of the overtopping. The blue area represents an overtopping of 45 l/s/m. The orange area represents an overtopping of 110 l/s/m.

Segment 5 is located outside of the defense wall; therefore, the calculated overtopping values will therefore not be accurate. The segment functions as an outlet pipe to guide the water out the drainage channel and make sure seawater does not flows back in. For this reason, this segment is very short. The discharge due to overtopping will be relatively small compared to the discharge flowing through the segment from the previous segments. Therefore, the discharge due to overtopping in this segment will be assumed zero.

The defense wall in the green area is rather far away from the drainage channel. For this reason, the overtopping discharge will be based on the blue and orange overtopping areas.

The total discharge due to overtopping per segment is determined by estimating the lengths over which the different intensities of overtopping apply. Next, the overtopping volumes are summed up per segment.

Segment	Length of segment in this area		Total overtopping m^3/s
	Blue	Orange	
1	0	61.5	Q1= 6.77
2	96.25	27.5	Q2= 7.36
3	117.50	0	Q3= 5.29
4	292.50	0	Q4= 13.16
5	0	0	Q5= 0

Table 28 – Total discharge volumes per segment

These overtopping volumes enter the drainage channel at the beginning of each segment, as can be seen in Figure 138.

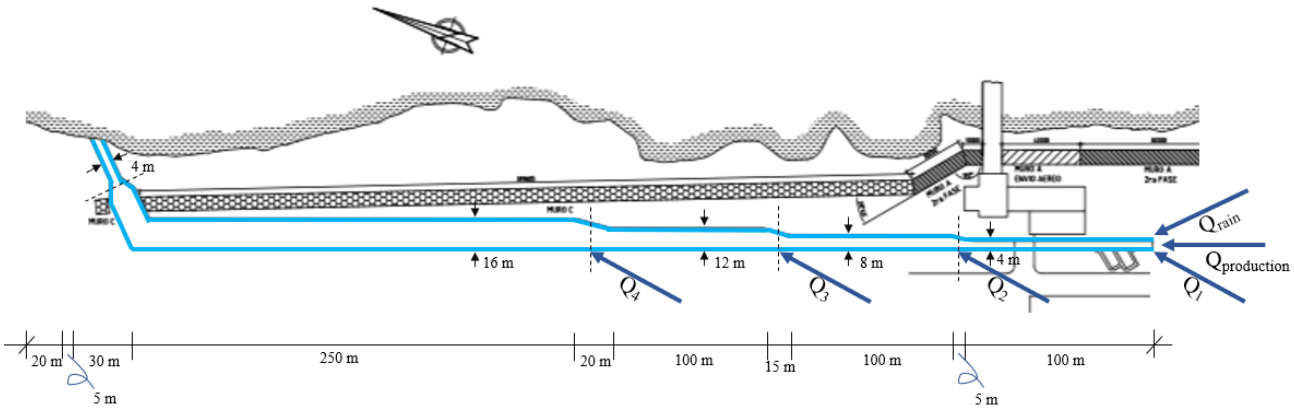

Figure 138 – Distribution of the discharge due to overtopping

This gives a total discharge per segment during storm conditions, shown in Table 29.

Segment	Discharge composition	Storm discharge in m^3/s
1	Q production + Q rain + Q1	6.6 + 50 + 6.77 = 63.37
2	Q production + Q rain + Q1 + Q2	63.37 + 7.36 = 70.72
3	Q production + Q rain + Q1 + Q2 + Q3	70.72 + 5.29 = 76.01
4	Q production + Q rain + Q1 + Q2 + Q3 + Q4	76.01 + 13.16 = 89.17
5	Q production + Q rain + Q1 + Q2 + Q3 + Q4	89.17 + 0 = 89.17

Table 29 – Discharge composition throughout the drainage channel

In total this means that about 89.17 m^3/s should be able to be discharged through the main drainage channel during storm conditions given that the power plant is still in operation. Since the situation is a storm, the flow in the channel is not able to reach exact equilibrium depths. For such large discharges it takes quite some time for the equilibrium depths to be reached. However, since there will also be influence of backwater curves, there are large uncertainties in the inflows and the fact that the inflow is never constant, this non-exact equilibrium flow is neglected, and an equilibrium flow is assumed.

Using the same principle as for the normal conditions of the current drainage system in paragraph ‘Current design channel’. the equilibrium depths for each of the segments are calculated. In Table 30 one can find the equilibrium depths during storm conditions for each segment.

Segment	B (m)	q ($m^3/s/m$)	d_e (m)
1	4	15.84	4.25
2	8	8.84	2.88
3	12	6.33	2.31
4	16	5.57	2.12
5	4	22.29	5.33

Table 30 – Equilibrium depths storm conditions

The maximum equilibrium depths can be found in the narrowest segments. A depth of 5.33 meters means that the channel needs to have this same depth, to not overflow at the edges. Influence outflow on water depths

Using Equation 38 and Equation 39 the half-lengths and maximum water depths ($d(x)$) during storm conditions can be determined. These are shown in the table below.

Segment	d_e	d_0	$x-x_0$	$L_{1/2}$	d(x)
5	5.33	3.70	22.50	471.76	3.75
4	2.12	3.75	292.50	654.18	3.16
3	2.31	3.16	117.50	505.31	3.01
2	2.88	3.01	110.00	440.26	2.99
1	4.25	2.99	102.50	382.44	3.24

Table 31 – Empirical fits according Bresse

The schematic representation of the backwater curves is shown in Figure 139. The figure is not scaled, so that the backwater curve types can be clearly distinguished.

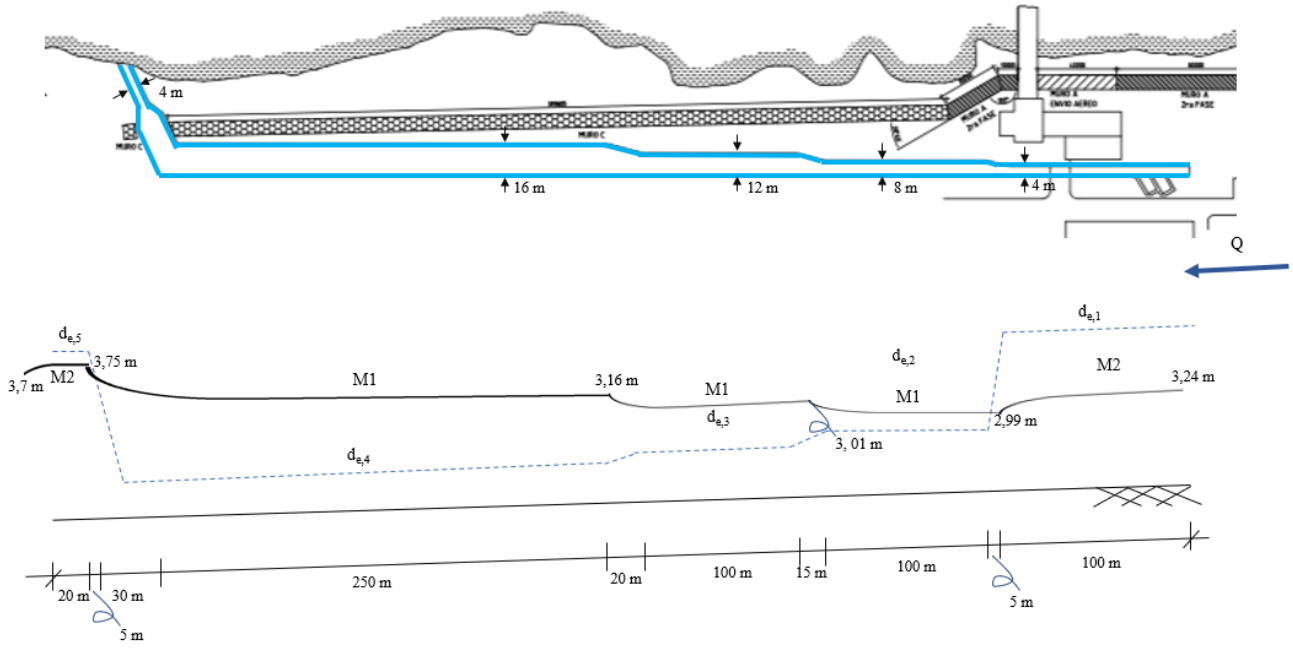

Figure 139 – Backwater curves

The maximum water level in the drainage channel during storm conditions takes place in segment 5 and is 3.75 meters. To make sure the channel has a free outflow a channel with a depth of 4 meters would be sufficient. The channel which is present has an approximate depth of 2 meters and thus does not meets this requirement. First, a study will be made, to research if a pumping station is possible to reduce the water levels in the drainage channel. Next to this, a study will be made if the deepening and/or widening of the drainage channel would be a good solution.

Pumping station

In order to discharge the excess of water that is accumulated by (spray) overtopping and overland flow due to rainfall accumulated from the area uphill, a pumping station could be used. The essence of such a pumping station is that it can use a combination of pumps in either parallel and/or series setup and hence come to a sufficient discharge and potential head to keep the power plant operational.

Pump discharge

The discharge capacity of the pumps depends on the amount of water which needs to be pumped out of the drainage channel during storm conditions. This consists of the rainfall, the overtopping and the normal discharge from the production of the powerplant.

The channel is 2 meters deep, so this is the maximum equilibrium water depth of the segments. The maximum specific discharge can be determined with Equation 36. The water which needs to be pumped away, is the water which will cause flooding of the channel. This is the difference between the storm discharge and the maximum discharge the segment can take.

Segment	Q_{storm}	B	$Q_{max} = q*B$	$Q_{pump} = Q_{storm} - Q_{max}$
1	63.37	4	20.44	42.93
2	70.72	8	40.88	29.84
3	76.01	12	61.32	14.69
4	89.17	16	81.76	7.41

Table 32 – Excessive discharge per segment

Table 32 shows that the maximum discharge is exceeded in all segments. This means that from the beginning of the channel water needs to be pumped out. If water is pumped out at the beginning of the channel, less water needs to be pumped out further on.

Pumping system

The most common pumps used for flood dewatering are centrifugal pumps. This is due to their very high flow rate with very low head. The flowrate for these kinds of pumps differ between 19 and 757,080 liters per minute (lpm) (Pumpscout, 2019). However, the pumps that can handle a capacity of 100,000's of liters per minute, generally are very large and expensive. Therefore, it is important to try and see if it is possible to create a cost-efficient set-up with multiple smaller pumps that are placed in series or parallel. This will be elaborated in the following sections. A conclusion could also be that it would be too expensive to pump the required amount of water from the drainage channel. Then a different solution would have to be looked at.

If pumps are placed at different points along the drainage channel, the total flow rate can be varied, and dry pumping can be avoided by turning on and off pumps. Another advantage of placing the pumps at multiple locations is, that when the discharge distribution of the overtopping and the rain intensity differ from the design situation, the system is adaptable. This way the pumping system can also be used for extreme weather events of different intensities.

Pumping away water at the beginning of the channel, lowers the water level further on in the channel. For this reason, placing a pump system with a high total flow rate at the start of the channel would be the best option. Segment 1 is also the most critical one, so at this location larger amounts of water need to be extracted. At segment 1 a pump combination would have to be placed with a maximal total flow capacity of around 42.93 m^3/s. This location has a big advantage because this part of the defense wall is constructed with high safety margins, so the pumps will be protected during extreme weather conditions. The location of this pumping station is also optimal for keeping the length of the outlet pipe to a minimum and so reducing the total amount of wall friction. The outlet pipe can be constructed next to the inlet channel for the cooling water, this way the length of the pipe is kept to a minimum.

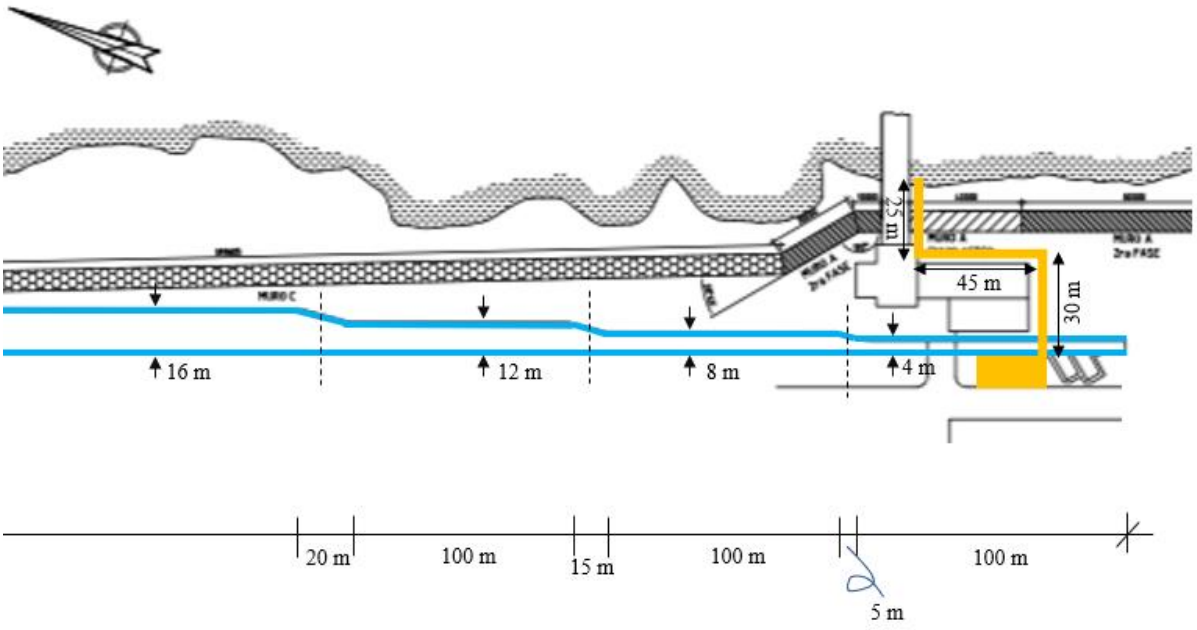

Figure 140 - location pumping system and outflow pipe

Pump curve

The discharge (Q) and the potential head (H) are the two variables of a pumping station. By putting two pumps in a parallel setup such as in Figure 141, the total discharge is doubled, whereas the potential head is equal as for a single pump.

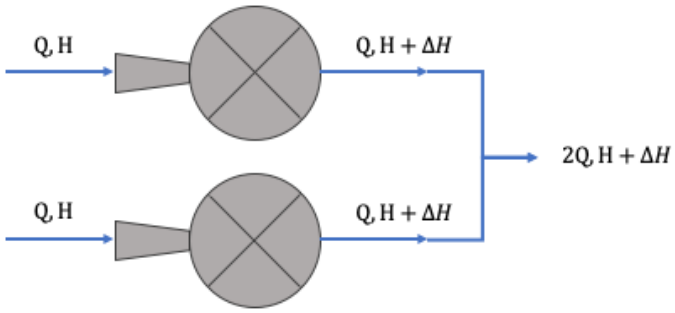

Figure 141 – Pumps in parallel

The potential head can be increased by putting two pumps in a series setup. In Figure 142 such a setup can be observed. Here the added potential head is doubled by putting the two pumps in series.

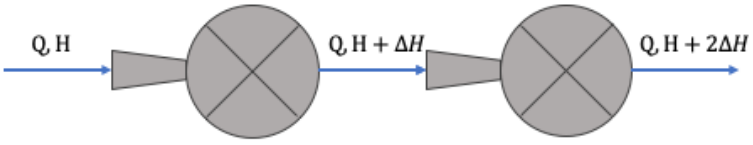

Figure 142 – Pumps in series

Of course, there is a possibility to make a combination of such setups to acquire the desired Q and H. Also using different types of pumps can give some room for optimization of the pumping station. The potential head that the pump can provide for different discharges or the so called 'pump curve' can hence be determined with the setups.

Head

The discharge and potential head that can be delivered by a certain pumping station is however not only determined by the pump curve. The pipes that are connected to the station and are in place to transport the water towards a more convenient location generate a friction force that decreases the potential head generated by the pumping station. For pressure flow inside such pipes, the dynamic head loss in terms of meters water column is calculated by the Darcy-Weisbach formula in Equation 48.

Equation 48: Darcy-Weisbach dynamic head loss

$$\Delta H_d = f * \frac{L}{D} * \frac{u^2}{2g}$$

The equation can be rewritten in terms of Q by assuming circular pipes and full pressured flow inside these pipes.

Equation 49: Darcy-Weisbach dynamic head loss rewritten

$$\Delta H_d = f * \frac{L}{D^5} * \frac{8Q^2}{\pi^2 g}$$

From Equation 49 is clearly seen that the head loss inside the pipes is quadratically dependent on the discharge inside the pipes and that the head loss is inversely proportional on the pipe diameter to the power 5. By choosing a pipe diameter, pipe length and type of pipe (PVC, concrete, etc.), a formula is obtained that relates the head loss inside the pipes directly to the flow through the pipes. Additionally, it should be considered that the pumping station is designed to transport the water to some location that is either located higher or lower. This is called the static head and it should be added to the dynamic head loss. In order to capture the total head needed, also the local losses need to be incorporated, which is in this case the sum of the inflow and outflow losses, namely equal to the total velocity head. This is shown in Equation 50.

Equation 50: Local head loss

$$\Delta H_l = \frac{u^2}{2g}$$

The total head that is required to be delivered by the pumping station or the system curve is formulated in Equation 51.

Equation 51: System curve

$$H = H_{static} + \Delta H_d + \Delta H_l$$

System curve

In Figure 143 an example of a pump and a system curve can be found. The point at which the two intersect is the so called ‘duty point’ at which the pumps will operate.

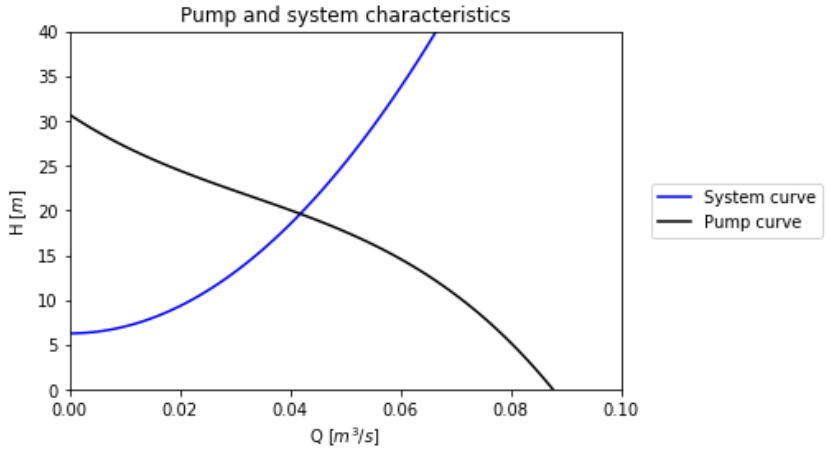

Figure 143 – Pump and system curves

As explained, the pumping station will have to work at a certain discharge when connecting it to a pipeline and setting a certain static head that is needed. However, every pump is most efficient at different discharges, hence it is important to consider that it is unadvisable to let a pump work at an inefficient point for too long.

However, since the pumping station for the CTE is designed for storm conditions and hence for short periods of time. The electrical power and/or diesel that can therefore be saved is relatively small and larger investments to shift the duty point more towards the best efficiency point (BEP) are not quickly feasible.

Choice of pump

Pump curve

To reach the requested discharge capacity of around 40 m^3/s one or multiple pumps with very high flow rates is/are necessary. The pump with the highest flow rate and with a corresponding pump curve found, is the BA700G. This is an 'Ultra High Flow Dewatering Pump', with a maximum flow of 7800 m^3/hour. The corresponding pump curve of the BA700G is shown in Figure 144. It is very costly, so if a pump with a higher flow rate is available, it will even be more expensive. (BBA Pumps, 2019)

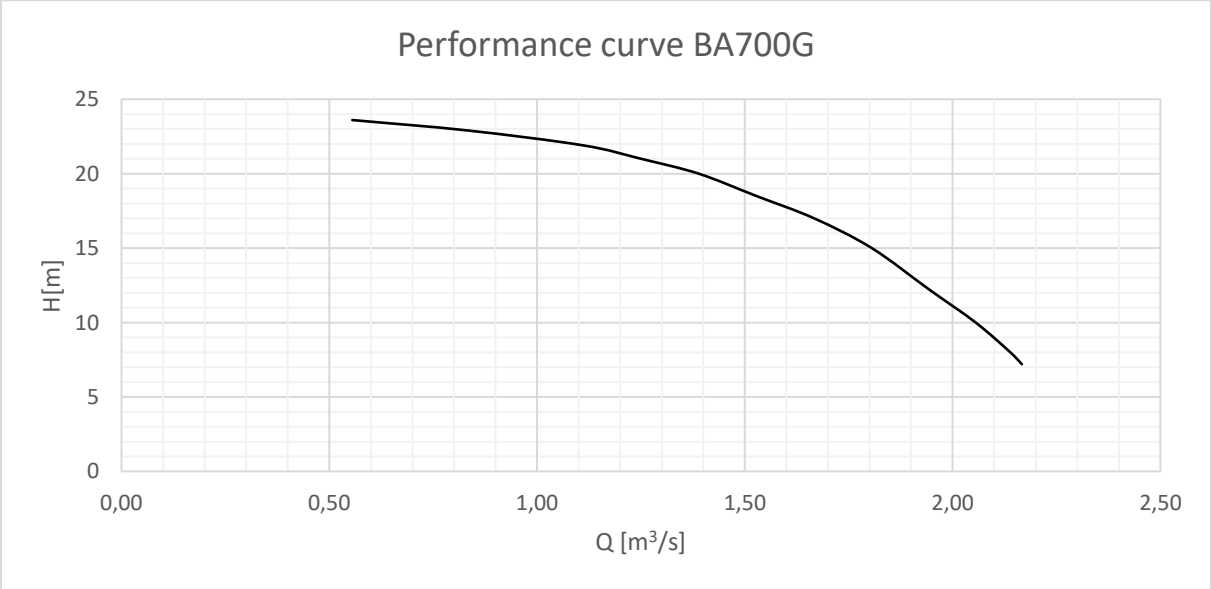

Figure 144 – Performance curve BA700G

One pump will be insufficient to provide the 40 m^3/s discharge, so multiple pumps are necessary. A high potential head is not necessary because the water does not have to be pumped over a large vertical distance.

The length of the pipe will be moderate, so the head loss due to friction will also be few. Therefore, a parallel system is chosen to increase the flow rate. The number of pumps needed in parallel, can be determined with the system curve.

System curve

The amount of pumps and the diameter of the outlet pipe are iteratively determined to obtain a duty point near the requested 40 m^3/s. Equation 51 needs to be written in terms of Q to plot it against the pump performance curve.

The pump needs to pump water from the drainage channel to the sea at the location of the inlet channel. The inlet of the pipe is located at surface level assuming the water level in the drainage channel is the maximum water depth of 2 meters. The outlet of the pipe can consider to be at surface level. The lack of height difference between the in- and outlet of the pipe gives a static head of 0 meters. However, a margin of 0.50 meters is assumed in case the ground is not completely flat or that the pipe needs to be supported at some places. The system curve can be plotted according Equation 52.

Equation 52: system curve rewritten

$$H = 0.5 + \left(f * \frac{8L}{D^5 \pi^2 g} + \frac{8}{\pi^2 g D^4}\right) * Q^2$$

The diameter is determined in an iterative way. The length of the pipe is 100 meters. The friction factor can be determined with Equation 53. For a concrete pipe, k is 0.0015.

Equation 53: friction factor

$$\frac{1}{\sqrt{f}} = 2\log\left(3.71 * \frac{D}{k}\right)$$

After this follows the iterative process to determine the number of pumps and an assumable diameter. If a second pump is added, the discharge capacity doubles while the potential head remains the same due to the parallel set up. By adding more pumps, the diameter of the outflow pipe needs to increase. For the pump system to reach a capacity of 40 m^3/s 20 pumps are necessary. To create a duty point near 40 m^3/s discharge, a total of 30 pumps are necessary. The corresponding diameter of the outlet pipe in this scenario is 4.5 meters. The pump and system curve are plotted in Figure 145.

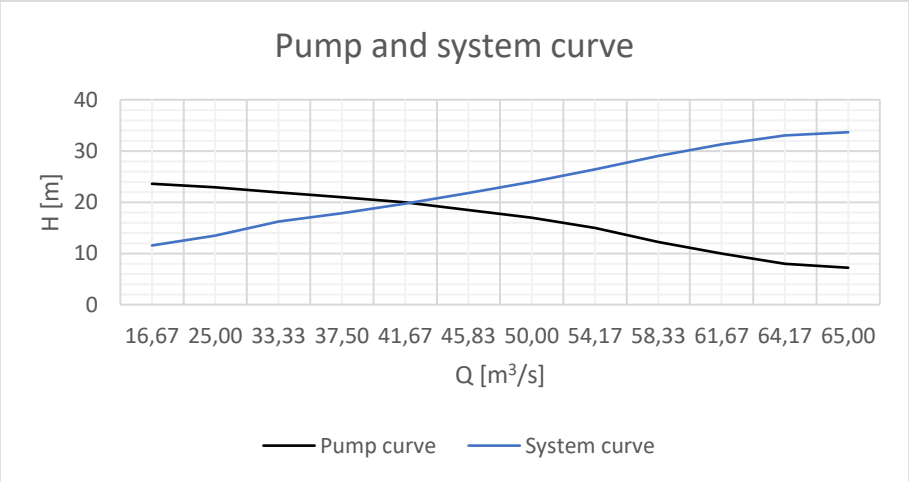

Figure 145 - Pump and system curve

This large number of pumps is very unfeasible due to investment costs and space requirements. The diesel which needs to be provided for this number of pumps is not sustainable and will also attribute to the costs. If

pumps with higher flow rates are available, a pumping system would still be a cost intensive solution and not realistic considering the limited space at the project site.

Deepening of the drainage channel

A more feasible solution would be to deepen and widen the existing drainage channel. A new gradient can could be created that improves discharge capacity. By expanding the cross section of the channel, the discharge is also automatically increased. It needs to be considered that the channel cannot be further deepened then 1 meter in segment 5 because of the free outflow. Also, to reduce the costs of excavating, it would be feasible not to deepen and widen the channel over long distances. The new dimensions of the drainage channel will be further elaborated on in the final design.

7.7.4 Variant 3: Current design with adjustment wall

A parametric study of the top of structure vs probability of failure has been done for all sections, this can be found in Appendix F. This is only a crude estimation as the exact geometry of the wall will have an influence on the amount of overtopping. It is found that the height of section A-1 needs to be increased to approximately 17 m and A-2 to 17.2 m. The structure needs to be increased to 14.8 m for section B and 14 m for section C. in order to get acceptable amounts of overtopping.

Another option is to alter the bullnose. By increasing the dimensions of the bullnose, the reduction factor can be increased and this can also be effective in reducing the overtopping to an acceptable amount. In Appendix F a parametric analysis of the bullnose correction factor versus the probability of failure was done. This shows that the correction factor needs to be about 0.15. This corresponds to dimensions hr = 0.45 and b = 0.5. A sketch of the current design with enhanced bullnose is shown in Figure 146.

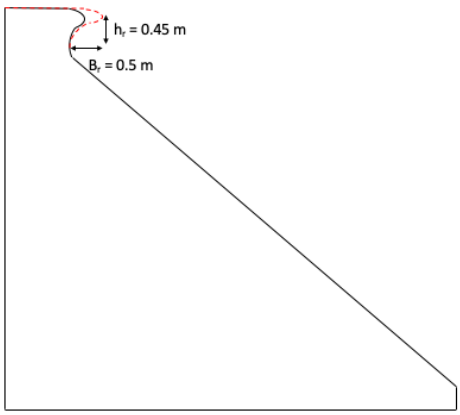

Figure 146 - Enhanced bullnose

If it is not desirable to rely entirely on the bullnose, it could also be chosen to combine a higher wall with a enhanced bullnose. A larger overhanging structure can also achieve a large reduction of the overtopping. This in turn means that the top of structure does not need to be as high. A parametric study was performed of the bullnose factor in combination with top of structure height increase versus the failure probability (Appendix F). For section A-1 and A-2 when a large bullnose is applied that has a large reduction effect of 0.3, the wall would only need to be increased to 13.3 m. hr = 0.6 m en b = 0.5 m. For section B with a bullnose correction factor of 0.27 the wall needs to be increased to 10.6 m.

An added benefit of a configuration where a higher wall is placed in front of the original structure is that a stilling basin is created that will already catch some of the overtopping, when an outlet with a valve is added to the design the water in the catchment can be discharged back to sea. It is estimated that the allowable overtopping is increased to 100 l/s/m by this intervention. With this increased overtopping the height of the wall can be reduced. A parametric study of the top of the structure vs the failure probability is done in the Appendix F. For section A-1 and A-2 the height of the wall in front of the original structure must be 10.1 m

and for section B 7.6 m. In case the stilling basin is entirely filled with water due to overtopping water, the water will spill towards the sea.

By means of struts connecting the wall to the current design global stability is ensured. Internal stability could be at risk when the impulse of the waves becomes too large, this is left to the final design to establish exact dimensions necessary. The configuration of such a solution is given in Figure 147.

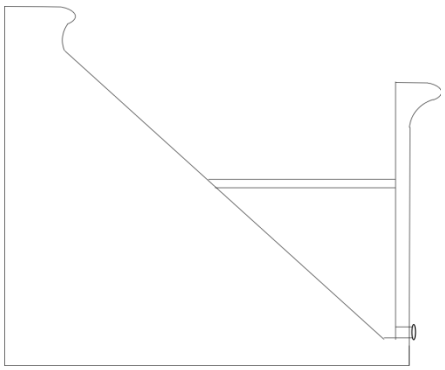

Figure 147 - Configuration wall and bullnose

7.7.5 Variant A

The wave attenuation channel will reduce the wave energy flowing into the cooling channel. This is achieved by placing concrete walls in the channel, the water needs to flow around these, and the waves will lose their energy. They need to be of enough thickness to withstand the wave impact. In Figure 148 a layout is given of the channel.

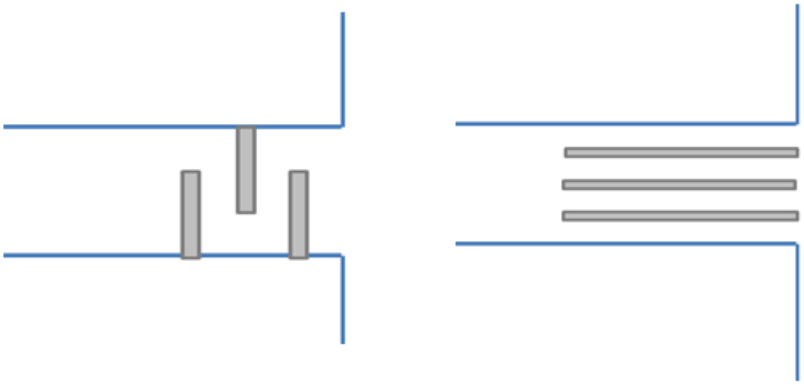

Figure 148 – Possible lay out of the wave attenuation channel

7.7.6 Variant B

The inlet channel can be protected by a gate. The gate that is installed in front of the inlet channel needs to be designed well enough to be able to withstand the incoming waves and still secure the intake of ocean water for the cooling system. This can be done by either let water flow over the gate and create a submerged gate, a gate which acts as a culvert or a regular gate that can partly open in horizontal direction. The gate dimensions will have to be substantial and will therefore be very costly. Possible designs for the gate are given in Figure 149.

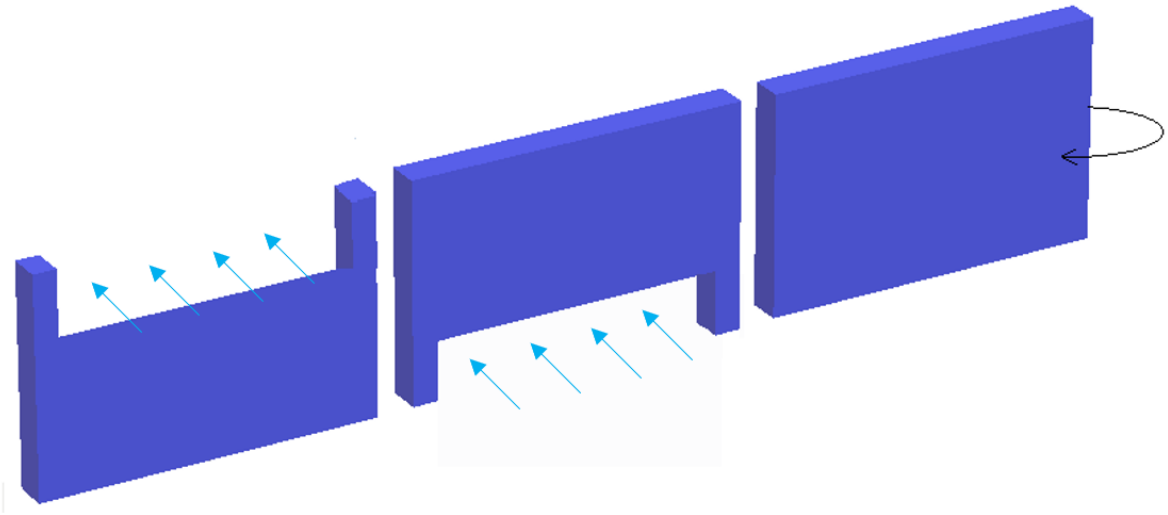

Figure 149 – The three types of gates, from left to right: submerged gate, culvert gate, regular gate

7.7.7 Variant C

An extension of the seawall can also be placed over the channel. This means that the wall will stop high waves, but water can still flow into the channel. The walls of the cooling channel will need to be heightened a few decimeters since the water level in the channel and basin will be elevated during the hurricane.

7.8 MCA

In order to come to a final design, a Multi Criteria Analysis (MCA) is performed. The MCA is divided into 5 parts, namely section A-1, A-2, B, C and the inlet channel. For the different sections, variant 1, 2 and 3 are analyzed and for the inlet channel variants A, B and C are analyzed.

The MCA evaluates four criteria of each of the variants, namely the effectiveness, costs, constructability and maintenance. Below each of these criteria are briefly explained. Each of the criteria has a weight factor between 0 and 5.

7.8.1 Criteria

Safety

The primary function of the design is to prevent flooding of the CTE. A design is only viable when it meets this criterion. When a design has some redundancy in the form of secondary defense systems this further increases the safety. This is the most important criterion and will be given a weight of 3

Costs

Factors that influence the costs are the materials used, the construction method used, overhead costs and man-hours. Materials that are not readily available in Cuba will need to be imported which will greatly increase the costs of the project. The equipment used for construction will also influence the costs, as well as labor intensive methods. In Cuba man-hours are relatively cheap compared to the use of expensive equipment, for this reason preference is given to more labor intensive but basic methods. When the project duration increases the overhead costs also increases. The costs of the project will be given a weight of 2.

Constructability

The design needs to be executed correctly. Therefore, it is important that the right materials, equipment and expertise are available. Furthermore, enough space is needed to execute the design i.e. 2 meters operating room is unrealistic. The constructability has a weight of 1.5.

Maintenance

Preferably the maintenance on the project is minimal. The more maintenance needed the higher the costs. A design that requires minimal maintenance during its lifetime is preferred. Maintenance has a weight of 0.5.

All in all, it means that the effectiveness of the variant is valued the most and the maintenance is least important.

7.8.2 Sections

For each of the sections an MCA is performed. The weight factors are all taken the same.

Section A-1

From Table 33 it is evident that for section A-1 the best variant is variant 3. Especially variant 2 shows a lack of effectiveness and the costs are also way too high if it were to be applied. This is mainly because there is no room for a drainage structure behind section A-1 and therefore very large pumps would need to be applied, which is not economically feasible.

Variant 1 also does not have a very high weighted average, especially because of the large costs of the variant. The piles of the pile screen would need to have a length of about 12 – 15 meters depending on the required foundation depth to assure that the piles have a good foundation. This would need to be done in a rocky bottom and with a relatively small spacing. Hence, this variant performs badly in its costs and constructability leading to a low weighted average.

Finally, it can be concluded that variant 3 shows the best prospects and is therefore chosen as the final design.

	Effectiveness	**Costs**	**Constructability**	**Maintenance**	**Weighted average**
Weights	3	2	1.5	0.5	
Variant 1	3.5	1	2	3.5	2.5
Variant 2	0	0	1	2	0.4
Variant 3	4	3	2.5	4	3.4

Table 33 - MCA section A-1

Section A-2

For section A-2 the same MCA is performed and therefore the arguments used in that section also count for this section. The results are shown in Table 34. Hence, also for section A-2 variant 3 is chosen.

	Effectiveness	**Costs**	**Constructability**	**Maintenance**	**Weighted average**
Weights	3	2	1.5	0.5	
Variant 1	3.5	1	2	3.5	2.5
Variant 2	0	0	1	2	0.4
Variant 3	4	3	2.5	4	3.4

Table 34 - MCA section A-2

Section B

Variant B has almost the same MCA as variants A-1 and A-2 and the only difference is that variant 1 shows a lower performance as the effectiveness of the pile screen is lower for this section as a relatively large pile screen needs to be constructed compared to the pile screen that would need to be constructed for variants A-1 and A-2.

	Effectiveness	Costs	Constructability	Maintenance	Weighted average
Weights	3	2	1.5	0.5	
Variant 1	3	1	2	3.5	2.3
Variant 2	0	0	1	2	0.4
Variant 3	4	3	2.5	4	3.4

Table 35 - MCA section B

Section C

The MCA is very different than that of variant A-1, A-2 and B. The result of the MCA is shown in Table 36. The current overtopping for section C is already quite a bit smaller than the other sections and therefore variant 3 means that the sea wall does not need to be heightened and only the bullnose has to be adjusted slightly. The costs of this variant are therefore a bit lower and also the constructability is higher since no extra wall and strut needs to be constructed. Hence, the higher score for variant 3.

Variant 1 gives a lower performance for section C, because section C is stretched for about 600 meters giving it larger costs and the effectiveness of such a pile screen would be lower as the required wave reduction is relatively small. Constructing a pile screen is therefore not very efficient as it is a very large operation for such a small required reduction.

Variant 2 shows the greatest promise with a weighted average of 4.3. In all criteria it scores high as already a drainage channel is present and the only intervention needed is to widen this drainage. The widening of the channel would only mean for the current channel to be demolished, some rock to be removed and a new concrete channel to be constructed. Therefore, for section C variant 2 is chosen.

	Effectiveness	Costs	Constructability	Maintenance	Weighted average
Weights	3	2	1.5	0.5	
Variant 1	2	0.5	2	3.5	1.7
Variant 2	4	4.5	4.5	4	4.3
Variant 3	4	3.5	3.5	4	3.8

Table 36 - MCA section C

Inlet channel

The variants for the inlet channel are different than those of the different sections. For the inlet channel variants, A, B and C are analyzed.

From the MCA in Table 37 one can find that variant B gives the smallest weighted average. This variant is a gate that is situated at the seaside of the inlet channel. This gate performs worst mainly because of the high costs that are involved. The gate should be able to resist large wave impacts, it should be attached to the channel which is more complex for a movable gate than a wall and lastly the gate needs to be able to be operated by means of a control system. This control system needs to be foul proof; especially during storm conditions and therefore the costs will go up significantly. A gate also requires more maintenance as it is more prone to blocking and the movable parts are more prone to wearing out and corrosion.

It is inconvenient that variant A and C have the same weighted average in this MCA. Each score different in each of the criteria, but they come to the same outcome. Finally, it is decided that because of the fact that the physics behind the attenuation channel are not completely clear and little information is present about such structures. Also, the sea wall at section A is already analyzed and the wall sections have been constructed already. Hence, it is easier to recreate these sections to be put around the inlet channel than to design an attenuation channel for which probably large uncertainties will spoil the design.

	Effectiveness	Costs	Constructability	Maintenance	Weighted average
Weights	3	2	1.5	0.5	
Variant A	3.5	3.5	4	2	3.5
Variant B	4	1	2	1	2.5
Variant C	4	3	3	4	3.5

Table 37 - MCA inlet channel

7.9 Final Design

From the variants and multi criteria analysis it shows that for the several sections different solutions are most suitable. Section A-1 and A-2 will have the same solution, section B will have a similar solution as section A-1 and A-2 only with a lower wall. Section C will have a solution that is focused entirely on improving the drainage of this area.

A sketch of the solution for A-1 and A-2 is given in Figure 150. The dimensions for the thickness of the wall and strut, armoring of the wall strut will be elaborated in the paragraphs below.

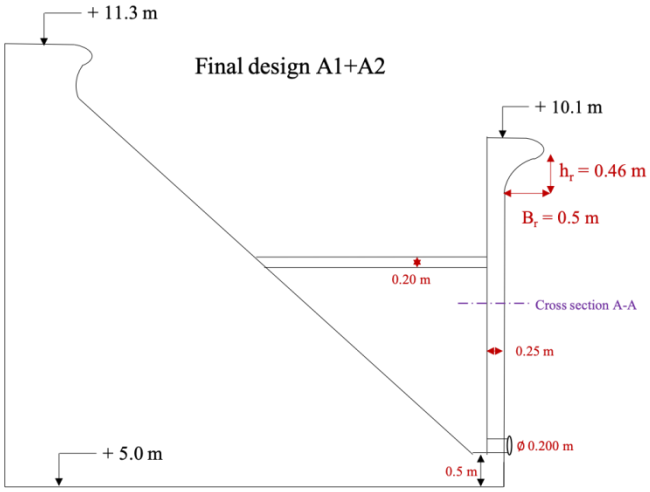

Figure 150 - Final design cross section A-1, A-2

As discussed in variant 3 the final design uses an enhanced bullnose to greatly reduce overtopping. The strut is added for stability and will be spaced every 2 meters. Because of the presence of the stilling basin a greater amount of water can overtop, and the wall can be lowered to 10.1 meter. Pipes with valves will be installed in the wall to discharge the overtopping water for which an optimization is applied.

Since the wall is combined with the old design global stability will not be an issue. This was discussed earlier and will not be checked here.

A sketch of solution for section B is given in Figure 151. This design has the same rationale as section A-1 and A-2. The height of the walls in this section is lower. Since the steps and calculations for this section are the same as for A-1 and A-2 this will not be worked out any further in this report.

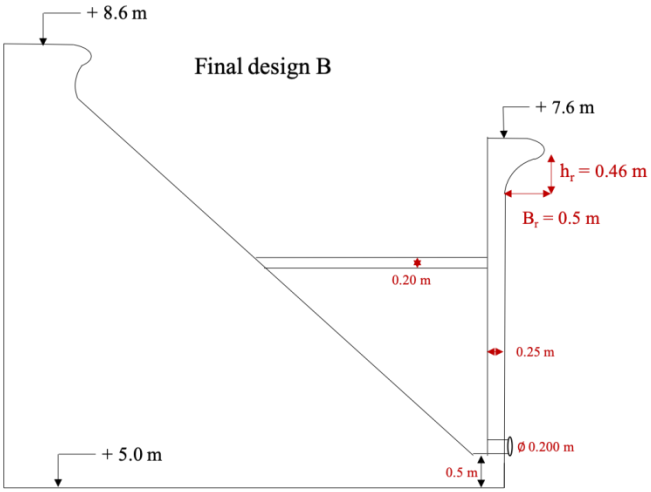

Figure 151 - Final design cross section B

For section C the drainage channel will be deepened to handle the full amount of overtopping. The dimensioning of the new channel and the possibility of pumps is investigated in paragraph 7.7.4.

For the inlet channel variant, A was chosen, the wall is extended over the channel and the small walls are placed behind the sea wall around the channel. This will be further worked out later.

7.9.1 Loads

The exact dimensions will be based on the governing loads. The loads that will be mapped are the impulsive force of the breaking wave and the force due to hydrostatic pressure. Since these forces occur simultaneously, they will be combined. Other loads such as the winds are considered negligible compared to these forces.

Serviceability limit state versus ultimate limit state

The coastal defense will be designed for the ultimate limit state (ULS). The ULS is about the strength and stability of the structure in extreme conditions. In this design, the largest loads possible and the minimum resistance will be evaluated. These loads and resistance will be compared with each other in a unity check. In theory, structures fail if the unity checks exceed the value of 1 in ULS. The serviceability limit state (SLS) is about deformation and safety of structures. The safety factors used in this design are adapted of the ULS design rules (TU Delft, 2019). The used load factors are:

Variable load factor	$Q = 1.5$
Resistance factor for steel	$\gamma_s = 1.15$
Resistance factor for concrete	$\gamma_c = 1.5$

Impulsive force

The wall will be loaded by breaking waves. Breaking waves cause high impulsive forces that only last for a very short time (about 0.01 s). This force is not normative for the overall stability of the structure but can cause very high loads locally and thus is important for internal stability. (TU Delft, 2019)

There are several methods available to model the impulsive pressure caused by the impact of breaking waves, though this is still difficult to approximate. Figure 152 gives an overview of wave forces calculated for 4 different methods for a fixed configuration. Quite large fluctuations are observed, for this design it is chosen to use the Minikin method even though this gives the lowest forces. In this the berm will influence the breaking process and reduce the forces. Since it is not possible to include this directly into the model a lower bound method seems appropriate.

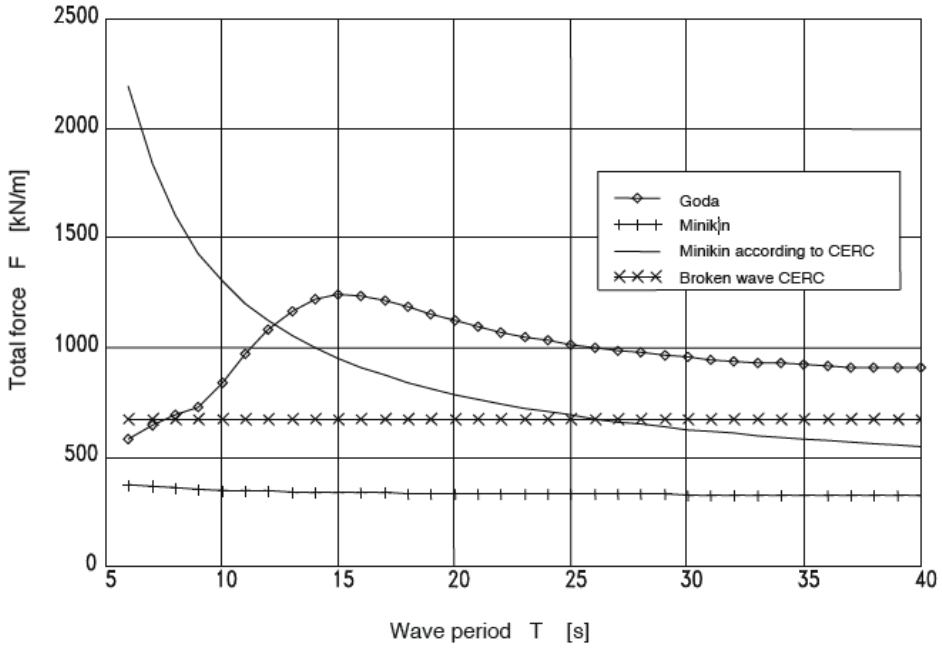

Figure 152- Comparison methods impulsive wave forces (TU Delft, 2019)

Figure 153 shows the schematization of the method by Minikin. The pressure due to the presence of waves is divided into a dynamic and hydrostatic component. The dynamic component represents the impulsive pressure.

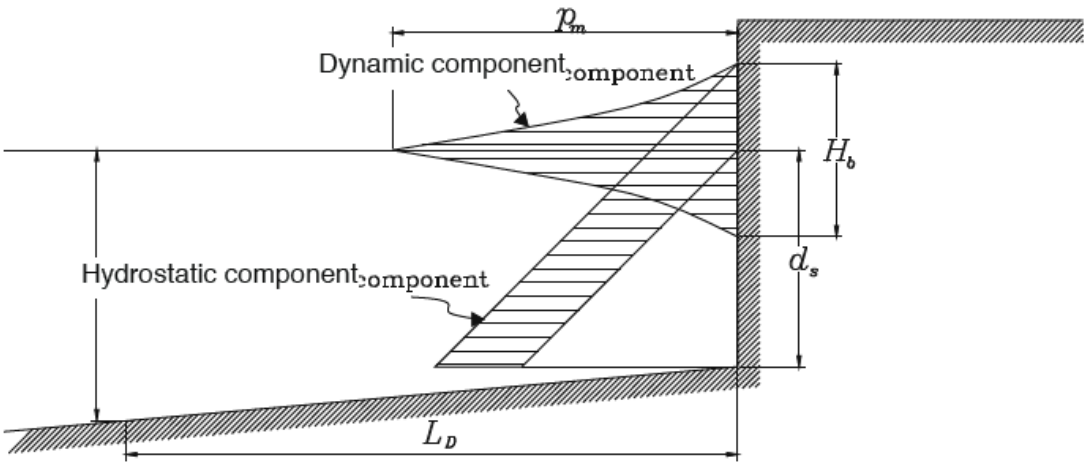

Figure 153 - Method Minikin broken waves pressure (TU Delft, 2019)

When assuming that the highest wave will be $2H_{m0}$ = 13.12 m. In this configuration the highest point of the wave reaches till 8.92 m. The force on the wall will be the integral of the wave pressure from 5 m till 8.92 m. The pressure distribution is schematized as linear, this will lead to slightly higher forces, but this is acceptable since it is a lower bound method. The equation below gives the maximum pressure.

Equation 54 - Maximum pressure impulsive wave Minikin

$$p_m = \frac{1}{2} C_{mk} \pi \rho g \frac{H_b}{L_D} \frac{d_s}{D} (D + d_s)$$

With C_{mk} the coefficient of impact, H_b the breaker height, d_s the depth in front of the wall, D the wavelength one wavelength away from the wall. L_D the wavelength at depth D.

The resultant force on the wall is 48 kN. This is a relatively low value, but it is consistent with the theory, only a small portion the wave impacts the wall and the largest pressures occur at the center of the wave which does not hit the wall.

Hydrostatic pressure

The hydrostatic pressure is schematized in Figure 154. Hydrostatic pressures need to be taken into account both for the seaside and the stilling basin side. It is assumed that the stilling basin can be filled to a maximum. When the basin is filled to the top the water will spill towards sea since this is lower than the wall on the side of the CTE.

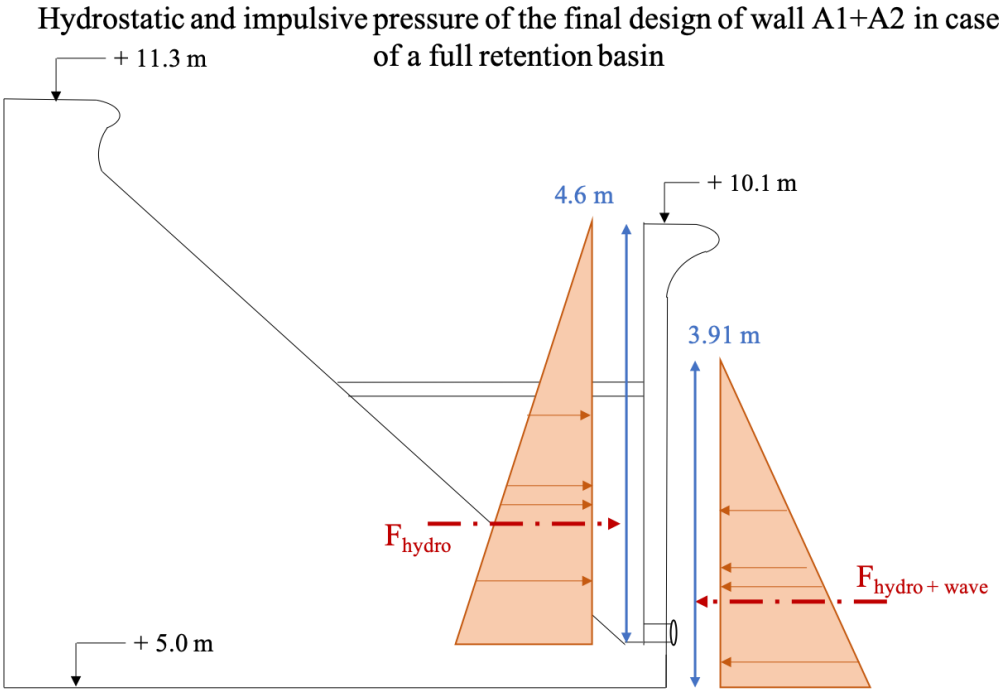

Figure 154 - Schematization hydrostatic pressures

The resultant force due to hydrostatic pressure on the seaside 77 kN, and 131 kN on the side of stilling basin.

Force on Bullnose

The bullnose reduction factor is assumed to have a value of 0.3. This means that 70% of the overtopping is prevented by the bullnose. The bullnose dimensions can be calculated with the decision chart of Figure 113. Most of the parameters in the bullnose decision chart are dependent on the situation. Only two parameters can be chosen by the designer. The overhang of the bullnose (Br) and the height of the bullnose (hr). The bullnose reduction factor is chosen such that it is variable of the height of the bullnose. The height of the bullnose is a parameter that can easily be changed, and it is a parameter that has a large effect on the bullnose reduction factor. A quick estimation showed that a bullnose overhang of 0.5 meters would result in realistic bullnose height values and bullnose reduction factors. Figure 155 shows the relation between the bullnose reduction factor and the bullnose height. The formula of the graph calculates that the height of the bullnose is 0.46 meters to result in the objected bullnose reduction factor of 0.3 (Allsop, et al., 2018).

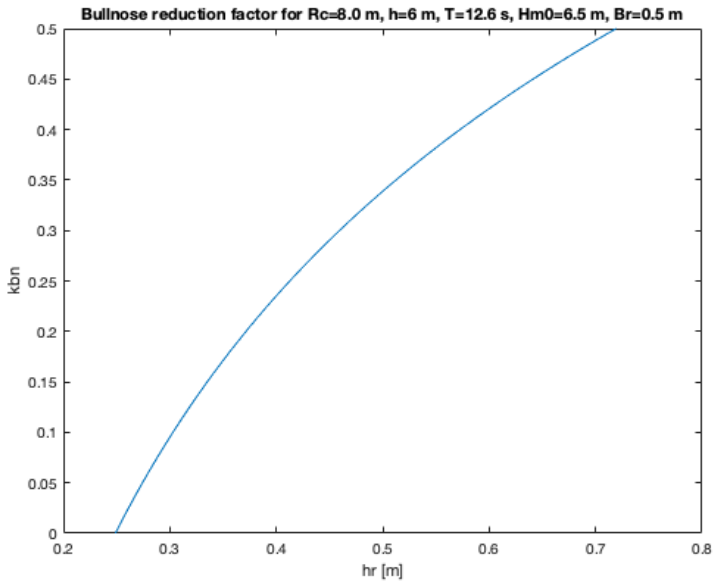

Figure 155 – Bullnose reduction factor versus the bullnose height for the parameters of the coastal defense at cross section A

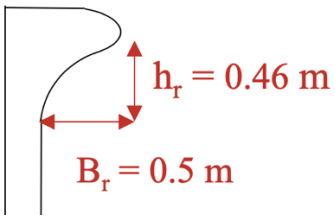

Figure 156 – Bullnose geometry

The waves that collide with the vertical protective wall are of the impulsive type. The impulse of the wave will partly resolve in an upward splash that will hit the bullnose. This upward splash will result in forces onto the bullnose. These forces may be calculated with the use of the momentum balances. The maximum splash is estimated to be of a flow that has a discharge of $Q = 3\ m^3/s$ and a thickness of 0.3 meters. These estimates would give a water velocity of v = 10 m/s. The forces due to the splashing water against bullnose can be found in the formulas below. Figure 157 shows the schematization of the balances of impulses:

Equation 55

$$\theta = \tan^{-1}\left(\frac{50}{45}\right) = 48°$$

Equation 56

$$F_y = \sin(\theta) \cdot \rho \cdot Q \cdot v = \sin(48) \cdot 1027 \cdot 3 \cdot 10 = 22.9\ kN$$

Equation 57

$$F_x = (1 - \cos(\theta)) \cdot \rho \cdot Q \cdot v = (1 - \cos(48)) \cdot 1027 \cdot 3 \cdot 10 = 10.2\ kN$$

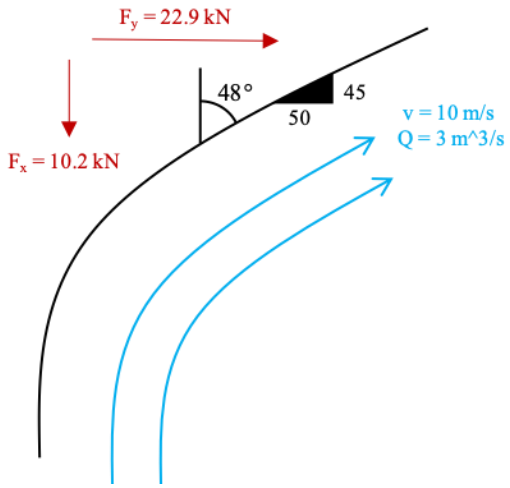

Figure 157 – Schematization of the forces on the bullnose due to the splashing water

7.9.2 Load cases

Three load cases will be evaluated which could be normative. These are given in Figure 158, Figure 159 and Figure 160. The own weight of the structure is also included in all load cases. All internal forces, moments and stresses are calculated with the program Matrixframe.

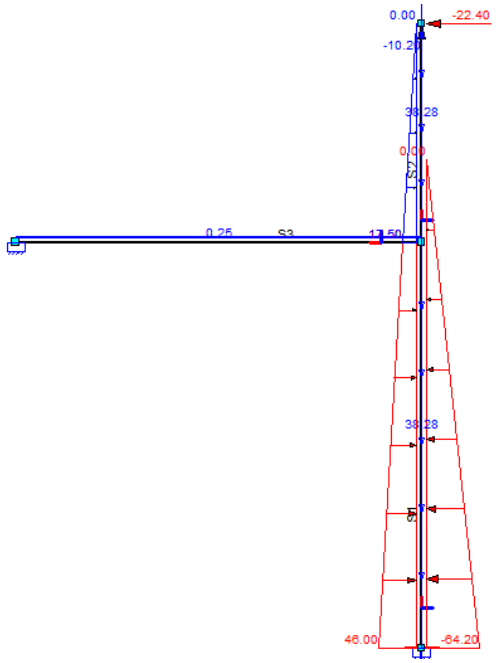

Figure 158 - Load case full stilling basin and full wave impact

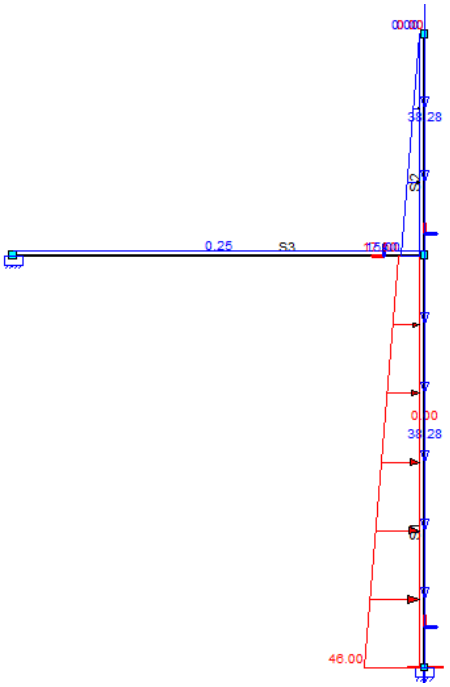

Figure 159 - Load case full stilling basin no wave impact

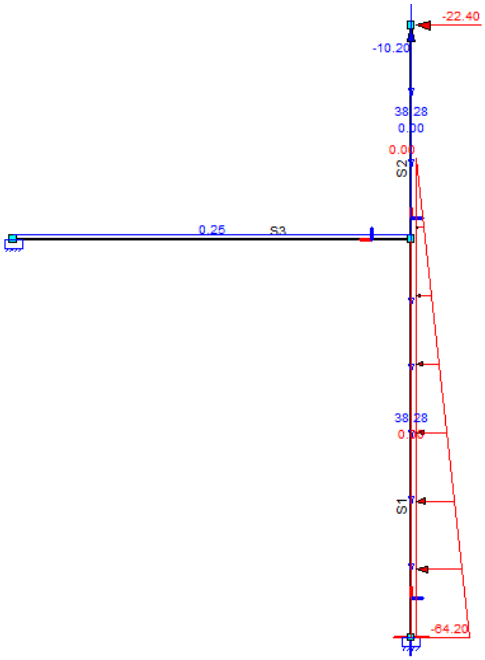

Figure 160 - Load case empty stilling basin full wave impact

The normative situation for all stability checks showed to be the case with an empty stilling basin (except for the moment distribution of the strut load case all forces). For this situation the normal and shear force diagrams are given as well as the moment distribution. In Appendix G the results for the other load cases can be found. In Table 38 and Table 39 the design values are given for the wall and strut respectively.

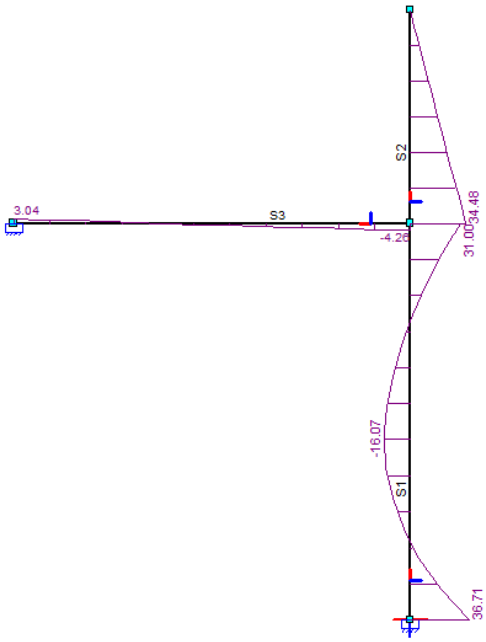

Figure 161 - Moment distribution empty tank, full wave impact

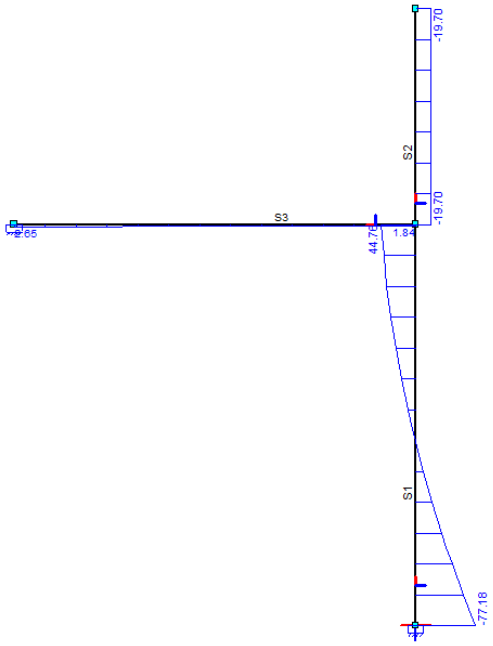

Figure 162 - empty basin with wave impact

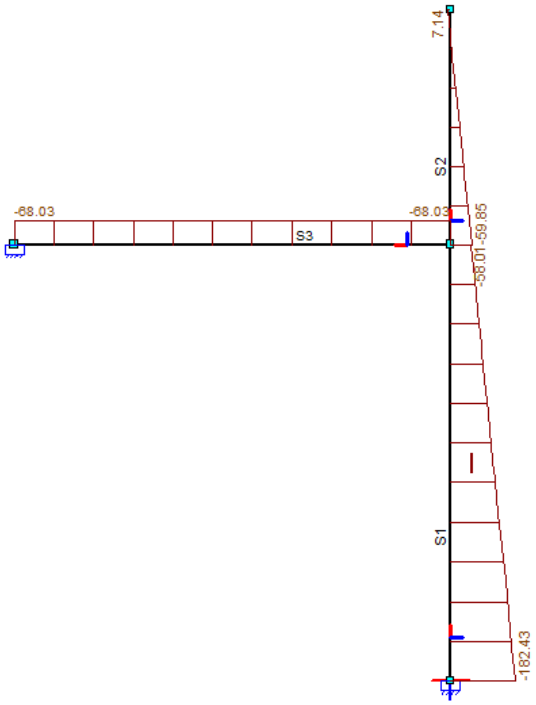

Figure 163 - Normal force, empty basin full wave impact

Wall	Result	Design value
Mmax [kNm]	36.71	55.1
Vmax [kN]	77.17	115.8
Nmax [kN]	182.43	273.6

Table 38 - maximum forces and moments wall normative load case

Strut	Result	Design value
Mmax [kNm]	9.46	14.2
Vmax [kN]	5.05	7.6
Nmax [kN]	68	102.0

Table 39 - Maximum forces and moments strut normative load case

7.9.3 Design of the wall and strut

In this section the dimensions of the cross sections are outlined which will be checked in following paragraphs.

Concrete cover

The exposure class is of importance in defining the minimum concrete cover. The salty conditions have negative consequences to the reinforcement steel and a good thick layer of concrete is necessary to protect the steel for corrosion. The Eurocode 2 describes the exposure class of the coastal defense to be XS3. This class is found by using the following two statements: 1. the coastal defense is exposed to salty water, and 2.

the concrete is not submerged in the water at all times. These conditions make the structure to be of exposure class XS3 (TU Delft, 2019).

The matching concrete cover of exposure class XS3 is 45 mm. This concrete cover is almost one of the largest that is described in the Eurocode 2. The Eurocode 2 requires a minimum cover to be added to the exposure class cover of 5 mm for deviations in the construction phase. The total cover will be found to be 50 mm. This cover will be used for the design of the sea defense (TU Delft, 2019).

Dimensions of the wall

The dimensions of the new coastal protection need to be sufficient for the moments, shear and normal forces on the structure. Quick checks before designing the initial dimensions showed that the shear force will be governing in the design. Shear reinforcement is greatly undesirable in such wide slabs. The construction method of such reinforcement is a laborious process. In general, it is more economical to make the slab wider, which has been done in this design as well.

Furthermore, the coastal protection is constructed with prefabricated slabs that have the height of the coastal defense (10.1 m – 5 m = 5.1 m) and a width in the order of 3 meters. The calculations will assume a unit width of one meter. The amount of reinforcement repeats every meter and a unit's width can therefore be assumed. The dimensions that are chosen are as follows and can also be viewed in Figure 164.

- Height: 250 mm;
- Width: 1000 mm;
- Reinforcement: B500 on both sides of the cross section with a diameter and relative distance of 16-200;
- Concrete class: C20/25.
- Bullnose: The overhanging width is 0.5 m and the overhanging height is 0.46 m.

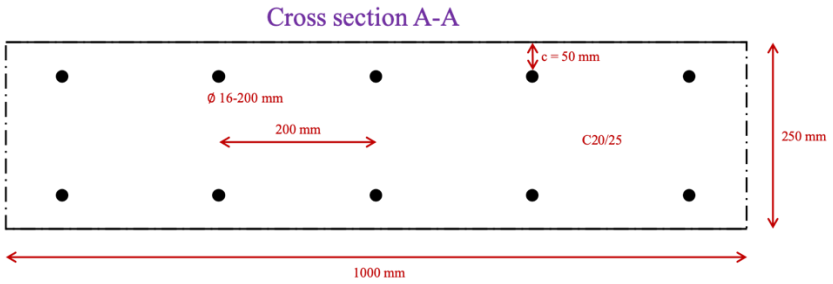

Figure 164 - Cross section of a unit width of 1000 mm wide of the coastal protection

Dimensions of the strut

The struts will be placed every other meter. The forces for two-unit section will be combined to one cross section. The cross-section dimensions are tried to be kept minimal to save for costs. Therefore, the strut will have outer dimensions of 200 x 200 mm. The same cover will be applied in the design of the strut. The cross section can be found in Figure 166.

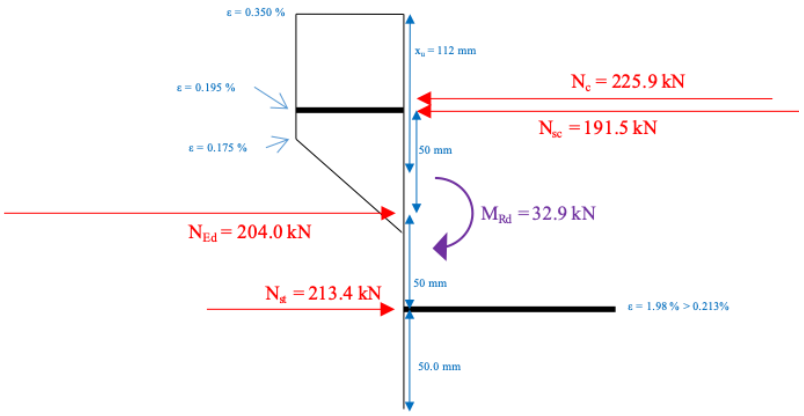

Figure 165 – Cross section with its forces of the strut

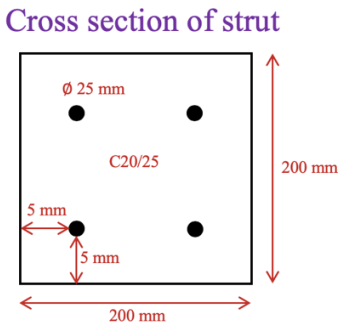

Figure 166 - Cross section of the strut

7.9.4 External stability check

The macro stability of the old design has been discussed earlier in the report. The old design is found to be stable if the internal integrity is maintained. The macro stability can be subdivided in three types of stability: vertical, horizontal and rotational stability. The stone subsoil gives much support to the design to be vertically stable. The teeth structure that stick into the subsoil prevent for horizontal stability failures. Furthermore, the old design was inherently stable for rotational failures, due to the slope on the seaside that was smaller than 1:1.

The new design is mounted to the old design and conclusions about the vertical and horizontal stability may be adapted to the new design as well. The rotational stability of the new design has become slightly different due to the different orientation of the water retaining wall. Figure 167 shows how the rotation point is placed in the lower left corner again. The hydrostatic water pressure and the wave impulse force lead to a combined force of 147.82 kN that has a lever arm of 1.3 m. The restoring moments are generated by the self-weight of the old sea defense design. This force has a magnitude of 6008 kN and a lever arm of 2.1. The restoring forces and lever arm are both larger than the overturning forces with its lever arm. Hence, the new design will be stable for the largest forces that may occur.

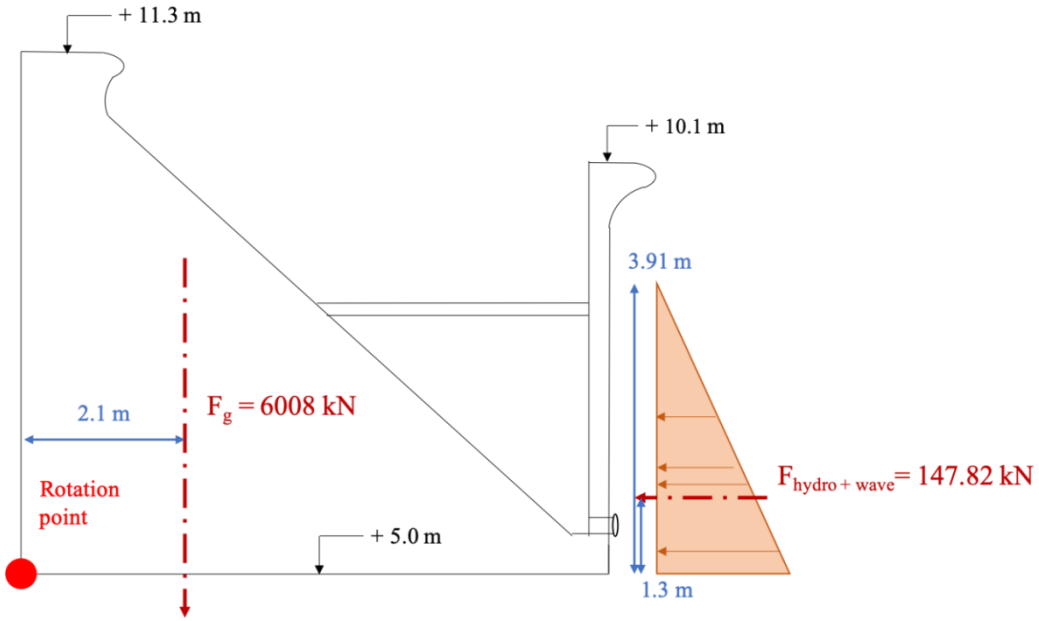

Figure 167 – Rotational stability of the new design

External stability of design B

The forces of the rotational stability calculation of the sea defense design B will look slightly different from the forces presented above. However, the massive poured concrete old design will generate much restoring moments and also design B will not have a slight chance to be rotated by the water forces. Furthermore, the spilling basin between the old design and the new design will fill up due to overtopping. The water in this basin will generate even more restoring moment forces. Hence, the new design will be safe for instabilities.

7.9.5 Internal stability checks

Wall

Quick checks showed that the shear force will be governing in the dimensions of the cross section. Hence, this factor will have the highest unity checks.

Moments

The cross section that has the largest normal forces, should be analyzed to find the maximum moment resistance capacity. This resistance capacity can be calculated using a figure of the cross section in which all forces are displayed (Voorendt & Molenaar, 2019). Figure 168 shows this cross section together with the magnitudes of the different forces acting on the cross section. There are four forces acting on the cross section.

1. N_{Ed}: This force is found by the known loads.
2. N_{st}: This is the tension force in the steel on the tension side of the cross section. The steel is yielding in this region and the maximum steel force of $N_{Ed} = A_s \cdot f_{yd}$ will be applied. The steel is yielding 2.06%. Reinforcement steel B500 may yield 4.5% before it breaks.
3. N_{sc}: This is the compression force in the steel on the compression side of the cross section. This force is dependent on the strain of the steel. The strain of the steel is dependent on the position of the x_u. The x_u describes the position in the cross section where tensions are equal to 0 N/mm^2. The N_{sc} and the x_u is unknown yet.
4. N_c: This force represents the concrete compressive force. The force will have a magnitude of $N_c = \alpha \cdot b \cdot x_u \cdot f_{cd}$. The α has a fixed value of 0.75, the b has a value of 1000 mm that represents the width of the strip that is checked and $f_{cd} = 13.333\ N/mm^2$. The N_c and the x_u are both unknown.

There are three unknowns and three equations which can be used to solve the unknowns N_c, N_{sc} and x_u. With the results to these unknows, the design value of the resisting bending moment can be calculated. This design value of the resisting bending moment is 87.6 kNm. The unity check of the bending moment will then be:

$$UC_M = \frac{M_{Ed}}{M_{Rd}} = 0.62$$

The forces parallel to the main axes are displayed in Figure 168. The summation of these forces will add up to 0 kN. The forces result in a bending moment together that will serve as the design resisting moment.

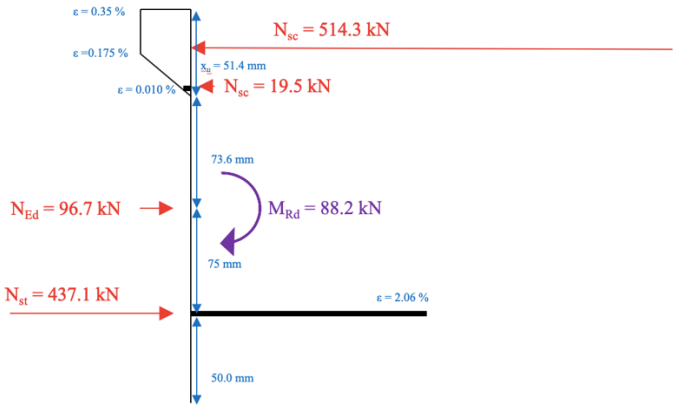

Figure 168 – Moment resistance capacity of cross section at the governing normal force

Normal Force

The unity check of the normal force is to be found below. The unity check has a very low value, since hardly vertical forces are acting on the structure.

Equation 58 – UC normal force

$$UC_N = \frac{N_{Ed}}{N_{Rd}} = \frac{N_{Ed}}{A_c \cdot f_{cd}} = \frac{89800}{250000 \cdot 13.33} = 0.027$$

Shear Force

The maximum shear force occurs at the base of the structure in the scenario that the basin is empty and there is a full wave impact. For construction reasons it is undesirable to have shear reinforcement in such a wall, for this reason the cross thickness of the slab will be adjusted so that it can resist the shear forces. The expression for the occurring shear force and the shear resistance of a cross section are given in the equation below.

Equation 59 – Shear capacity

$$v_{rd,c} = -1.2k(100\,\rho_l f_{ck})^{\frac{1}{3}} \geq v_{min}$$

Equation 60 – Minimum shear capacity

$$v_{min} = 0.035\,k^{3/2} f_{ck}^{1/2}$$

Equation 61

$$k = minimum\left(1 + \sqrt{\frac{200}{d}}; 2\right)$$

Equation 62 – Effective height

$$d = h - c - \phi_{sr} - \frac{1}{2}\phi_{lr}$$

Equation 63

$$V_{ed} = V\,\gamma$$

Equation 64

$$v_{ed} = \frac{V_{ed}}{bd}$$

Equation 65

$$UC = \frac{v_{ed}}{v_{rd,c}}$$

With ρ_l the density of longitudinal reinforcement in the cross section, f_{ck} the compressive strength of the concrete, c the concrete cover (50 mm), γ (1.5) a safety factor to get to a design load. The cross section can resist the shear force if the unity check is larger than 1.

In Appendix G the shear force diagrams for the 3-load combination are given. The maximum load occurs for the load case when the basin is empty, and the wall experiences a full wave impact. The calculation result for the maximum shear stress is given in the table below.

h [mm]	400
b [mm]	1000

c [mm]	50
d [mm]	342.5
k	2
vmin [N/mm2]	0.366767
vrdc [N/mm2]	0.167603
ved [N/mm2]	0.338015
UC	0.921606

Table 40- Calculation results shear force bottom slab

If the whole wall is 400 mm this is quite thick for the top sections, for this reason it is investigated what would be a better thickness of the slab for the upper section. For construction reasons it is chosen not to make the slab too slender, so as a starting point 250 mm was chosen.

h [mm]	250
b [mm]	1000
c [mm]	50
d [mm]	192.5
k	2
vmin [N/mm2]	0.44
vrdc [N/mm2]	0.19
ved [N/mm2]	0.35
UC	0.79

Figure 169 - Calculation results shear force at height strut

Next it was investigated at what height above the bottom of the slab 250 mm would suffice, this is plotted in Figure 170. After 40 cm the unity check is below 1 and the cross section is thus sufficient, it is chosen to create some extra margin and extend this to 50 cm above the bottom. For construction this is easy to achieve since it only requires that extra concrete is poured between the wall and the original structure.

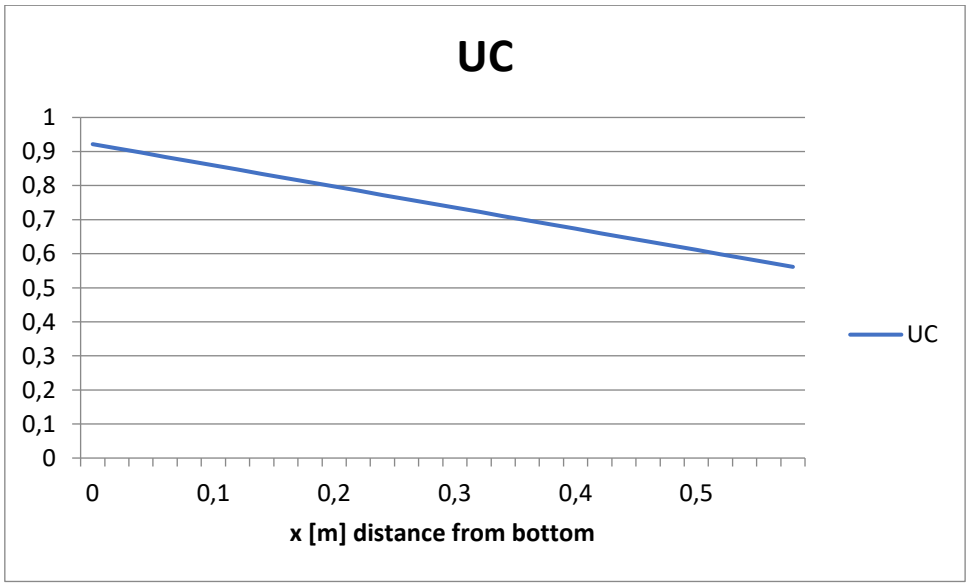

Figure 170 - Unity check vs distance from bottom, h = 250 mm

Transversal reinforcement in the wall

Initially, it is assumed that the loads would be transferred through the wall with solely the longitudinal reinforcement as described before. The load transfer would be of the beam model. However, to minimize the number of struts, the struts are placed every other meter. The assumption that the load transfer can be

modelled following the beam model, will lose its validity with the design change of the struts. The distance between the struts has become larger and the forces in the struts become larger as well. The wall gets more similarities of a slab than it has before. An idea of transfer loads in a two-way slab applied in the coastal wall is to be found in Figure 171.

A two-way slab has a load transfer that is in both directions of the slab. In case of the wall, the load transfer will be mostly of the one-way slab type, which is similar to the used beam model. However, it would be wise to add transversal reinforcement for the transversal load transfer that will take place in the wall. Due to the small distance between the struts, the wall does not need to be designed as a two-way slab. However, some transverse reinforcement is always good to apply in slabs. A good rule of thumb would be to add 20% of the longitudinal reinforcement which will be applied in the wall.

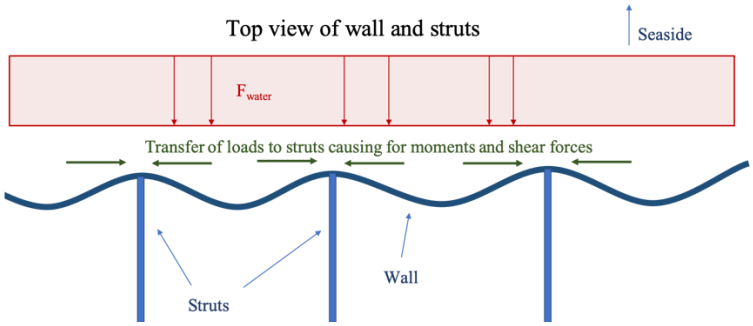

Figure 171 - Example of transfer loads in the sea defense

Strut

Moment capacity

In the paragraph about the moment capacity of the sea defense wall a way of calculating the moment capacity is used, that will be used for the cross section of the strut as well. This method is based on the fact that three unknowns will be resolved with three equations. The results of these forces and strains can be observed in Figure 166. The moment capacity of the strut is calculated to be 32.9 kN. The unity check is:

Equation 66 - UC moment capacity strut

$$UC_m = \frac{M_{Ed}}{M_{Rd}} = \frac{18.9}{32.9} = 0.58$$

Normal force

The unity check of the normal force looks as follows:

Equation 67 - UC normal force strut

$$UC_N = \frac{N_{Ed}}{N_{Rd}} = \frac{204}{A_c \cdot f_{cd}} = \frac{204}{200^2 \cdot 13.33} = 0.38$$

Shear force

For the shear force in the strut the normative situation is when all forces are applied simultaneously. Vmax = 5.05 kN. For the cross section of 200 mm x 200 mm, no shear reinforcement needed.

h [mm]	200
b [mm]	200
c [mm]	50
d [mm]	144
k	2
v_{min} [N/mm2]	0.44

v_{rdc} [N/mm2]	0.19
v_{ed} [N/mm2]	0.26
UC	0.59

Table 41 - Calculation result shear reinforcement strut

Buckling of the struts

The struts may fail on buckling due to the large normal forces in the strut. However, the unity checks of the struts show that the struts will not be loaded to the limits of the strut. There is still some capacity left to generate some redundancy for construction failures and design failures. The design of these struts will be sufficient to prevent for buckling.

Punching

Since a strut is placed against the wall the construction also needs to be checked against punching. The equations that can be used are the same as the ones for shear strength. The only difference is that the design load is applied over a smaller area (basic control perimeter) directly around the strut thus locally causing higher stresses.

Equation 68

$$v_{ed} = \frac{V_{ed}}{u_0 d}$$

Equation 69

$$u_0 = 4(4d + c)$$

The basic control perimeter is shown in Figure 172.

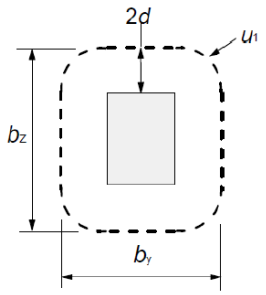

Figure 172 - Sketch basic control perimeter

The normal force that in the strut is the shear force that is applied to the slab at this location. Tension will be accounted for by the reinforcement, for these calculations only pressures are relevant. Figure 161, Figure 162 and Figure 163 show the normal force diagrams for all load cases. The normative situation is when the basin is empty and full wave impact hits, i.e. the normative load is 68.03 kN. Since the struts are spaced 2 meters apart 2 times this load goes to each strut. The calculation results are shown in Table 42, as can be seen no additional reinforcement is needed for punching.

h [mm]	250
u0[mm]	4072
c [mm]	50
d [mm]	192
k	2
vmin [N/mm2]	0.44

vrdc [N/mm2]	0.19
ved [N/mm2]	0.26
UC	0.59

Table 42 - Calculation overview punching

7.9.6 Pipes

As mentioned earlier the design will include pipes to discharge the water back into the sea. The pipes need to have a strong profile so that they can resist the moments and forces where they are placed. Otherwise there is a weak point in the wall and local failure can occur.

For the moment capacity, shear force capacity and punching capacity the load case where the basin is empty is normative. It can therefore be reasoned that it is favorable for the design if there is some water in the basin for structural stability. This will be used for the dimensioning of the drainage pipes.

The relation between the filling of the basin and the discharge back to sea is complicated since overtopping will not be constant and the discharge will also be dependent on the height of the water column in the basin. It is assumed that no losses will occur over the pipe because of the short length. For this reason some assumptions need to be made. A constant overtopping discharge will be assumed based on the most probable overtopping. The calculation can be found in Appendix F, the discharge is 70 l/s/m. The water height will remain constant if the discharge through the pipes is equal to the overtopping discharge.

A lowering of the water level directly results in an increase in the shear and normal force and the maximum moments for the load case of a filled basin and wave impact. For the case of a filled basin and no wave impact the opposite is true. The Matrixframe result for the load cases of wave impact and water level of 4 m are given, together with the results for h = 3 m with and without wave impact are given in Appendix G. Since these are both well below the normative case it is opted to increase the water level to about 3 m.

In figure 3 the discharge through the pipe is plotted for each height in the basin, when the Qin (the overtopping discharge) intersects with the Qout, this means that the water level is stable at this point. The spacing of the pipes and the diameter of the pipes can be adjusted in order to reach a desired height.

The combination chosen is diameter pipe = 0.2 meters, spaced every 3.5 m.

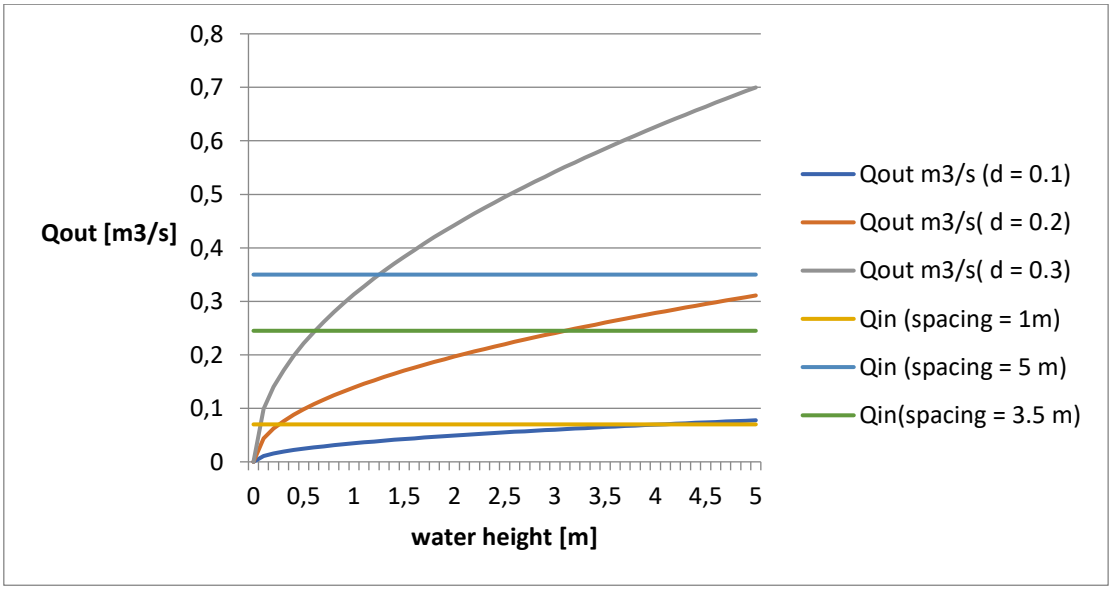

Figure 173 - Discharge vs water height

7.9.7 Widening drainage channel

Chosen is to increase the drainage capacity of the area by building a drainage wall around the project area as described in the variant. Furthermore, the existing drainage channel will be widened and deepened.

For the segments 1 to 5 the storm discharge was calculated in the paragraph pumping station. Those storm discharges are given in Table 43. With the use of Equation 36 the widths are computed for which the storm discharges can be processed by the drainage channel.

Changing the width

For the computations, firstly a depth of 2 meters is used; this is the original depth of the drainage channel. Next to this, also a depth of 1.9 meters is used to calculate the width; this is done to give a safety margin on the channel. This way, if the storm discharge must flow through the channel, there is still some capacity for extra water to flow into the drainage channel. The corresponding widths are given in Table 43.

Changing the width & depth

In Figure 126 one can see the influence of the storm surge on the outlet of the channel. During storm surge the water level at sea is 1 meter above the bottom of the drainage channel. It is therefore possible to deepen the drainage channel by a maximum of 1 m to a depth of 3 m. The corresponding widths for a depth of 3 m are given in Table 43.

Segment	Minimum width (2 m depth)	Width (1.9 m depth)	Width (3 m depth)	Storm discharge [m3/s]
1	12.4	13.5	6.75	63.37
2	13.9	15	7.6	70.72
3	14.9	16.1	8.1	76.01
4	17.5	18.9	9.5	89.17
5	17.5	18.9	9.5	89.17

Table 43 - New drainage channel widths

For the measures including the widening for the 2, 1.9 and 3 m depths, Table 44 gives the number of meters that the drainage channel has to be widened with respect to the original width.

Segment	B	Widening (2 m depth)	Widening (1.9 m depth)	Widening (3 m depth)
1	4	8.4	9.5	2.75
2	8	5.9	7	-
3	12	2.9	4.1	-
4	16	1.5	2.9	-
5	4	13.5	14.9	5.5

Table 44 - Number of widening meters necessary

It is logical that the channel with a higher depth of 3 m would need less widening than the channel with only 2 m depth. What can be seen, is that for segment 2, 3 and 4 no widening is necessary. It is important to find a good balance between the widening and the deepening of the channel.

With a depth of 3 m, it is beneficial for segments 2, 3 and 4, since the channel does not have to be widened in this area. However, deepening the channel with 1 m, costs a lot of money. Next to this, the channel of segments 2, 3 and 4 could even be less wide than the original depth. It is better to find a width for these segments that at least is as big as the original, otherwise these segments are overdesigned. Therefore, it might be better to deepen the channel a little less. If the channel would be deepened by 50 cm, this would result in a bit of widening in segments 1 and 2. No widening in segments 3 & 4. And quite a bit of widening in segment 5 (Table 45).

Segment	Width (2.5 m depth)	Widening (2.5 m depth)
1	8.9	4.9
2	9.9	1.9
3	10.7	-
4	12.5	-
5	12.5	8.5

Table 45 - Widening of drainage channel

For the most cost-effective design, it is important to look at the lengths of these segments. The lengths are given in Table 46. It would be best if segment 4 would not have to be widened. For segment 5 it is not important if that has to be widened quite a bit more, since the channel is relatively very short.

Segment	Length
1	102.50
2	110.00
3	117.50
4	292.50
5	22.50

Table 46 - Lengths of the segments

Looking at the lengths of the segments, the ratio between the deepening and widening the best combination would be to deepen the channel by 40 cm, which results in the widening of the segments 1 to 5 according with Table 47.

Segment	Width (2.4 m depth)	Widening (2.4 m depth)
1	9.5	5.5
2	10.6	2.6
3	11.3	-
4	13.3	-
5	13.3	9.3

Table 47 - Widening of drainage channel

Deepening the channel by 40 cm, secures free outflow at the end of the drainage channel, since it is still 60 cm above the water level with storm surge. The new situation with the widened segments 1, 2 and 5 are given in Table 47.

Orientation segment 5

As the width of segment 5 is made much larger than for the current design, the influence of incoming waves becomes much larger during a storm. Therefore, it is chosen to change the orientation of this segment with respect to the current situation. To minimize the possibility for waves to propagate through the drainage channel, segment 5 is orientated towards the south as can be seen in Figure 174below.

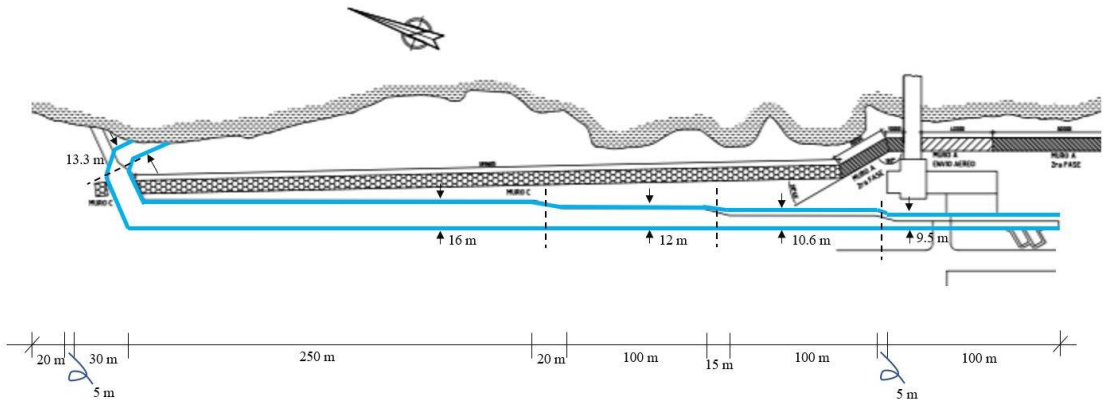

Figure 174 – Change of orientation segment 5

7.9.8 Inlet channel

The wall will be extended over the inlet channel; however, it cannot be supported on the old design. There is a large concrete sill over the channel already present. The struts will be directed downwards and, in this way, the global stability will still be ensured. A sketch of the situation is shown in Figure 175 and Figure 176.

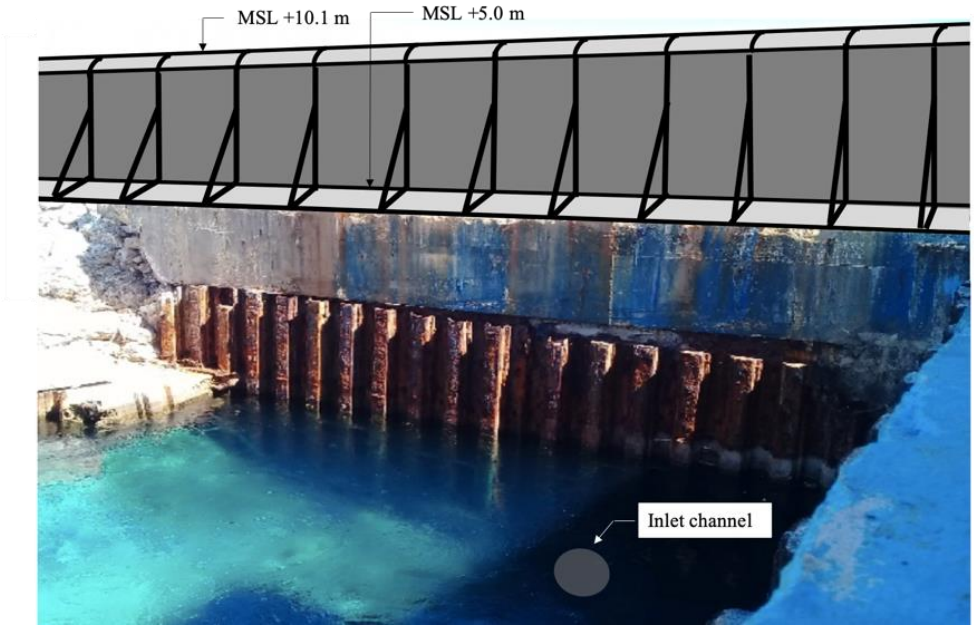

Figure 175 - Visualisation of the sea defense on top of the inlet structure

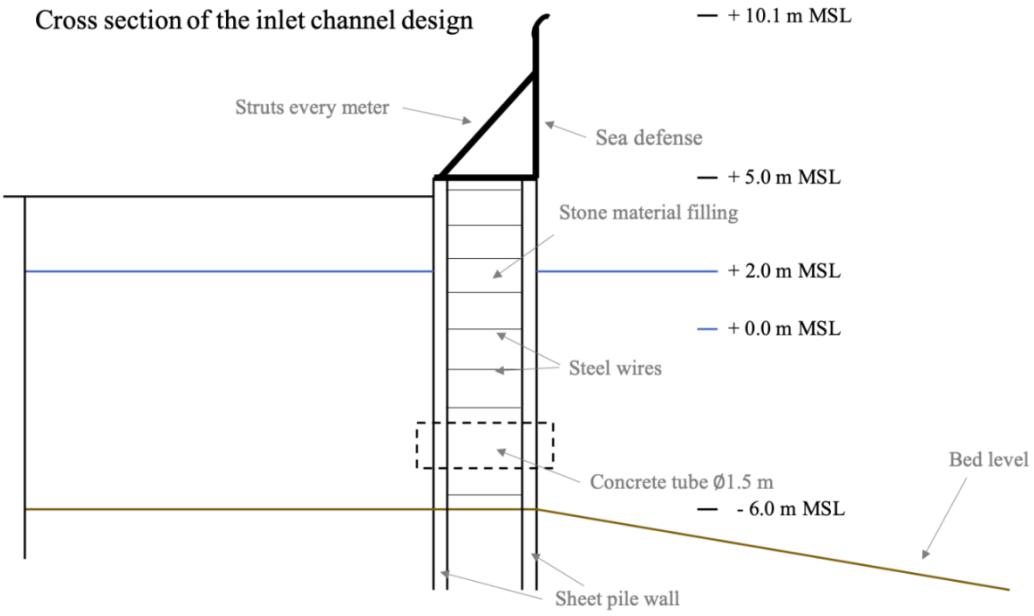

Figure 176 – Schematic cross section of the inlet channel with explanatorily notes

In front of the inlet channel the berm is removed, for this reason the waves will have more energy and there will be more overtopping. Since the berm reduction factor in area A-1 was 0.6, it is assumed that there will be 40% more overtopping at all times. The Minikin method for the impulsive wave force does not include a factor for the berm so these factors will be unchanged. It could be reasoned that a method could be used which yields higher forces since Minikin is a lower bound method which was justified by the presence of a berm. The increased overtopping over the wall is not seen as a complication because of the large discharge capacity of the channel.

Because the struts are now inclined the force and moment distribution in the construction changes. The normal and shear force diagrams as well as the moment distribution is given in Appendix G. The new governing loads are given in Table 48 and Table 49.

Wall	Result	Design value

Mmax [kNm]	39.2	58.8
Vmax [kN]	75.51	113.3
Nmax [kN]	106.96	160.4

Table 48 - Design loads wall inlet channel

Strut	Result	Design value
Mmax [kNm]	9.46	14.2
Vmax [kN]	5.05	7.6
Nmax [kN]	104.51	156.8

Table 49 - Design loads struts inlet channel

The normal force in the wall is significantly decreased, the normal force in the strut is significantly increased. The slab needs to be checked against punching and potentially a larger cross section is needed or more armoring if the moment capacity is decreased by too much.

The drainage capacity of the channel is very large because of the large cross section. The discharge to sea is directly proportional to the cross-sectional area and the height in the channel. It is estimated that the rise in water will be no more than 1 meter. Therefore, walls will be placed around the channels that reach 1 m above construction level. (6 m above MSL). There will be no waves in the channel; the walls will only need to withstand the hydrostatic pressure. No detailed calculation of these walls will be given in this report.

7.9.9 Construction method

In this paragraph the construction method of the final design will be described.

Wall and struts

Because of the limited space at the CTE it is desirable to prefabricate as many elements as possible. Formwork is costly and takes up a lot of space and needs experienced workers, prefabricated elements are faster and can be executed with more precision in specialized factories. For this reason, it is chosen to use prefabricated slabs for the wall and beams for the struts. The prefabricated elements need to be transported to the site either by road or by boat. The prefabricated slabs including bullnose will we 3 m x 5.1 m x 0.25 m when transported by truck, or 5 m x 5.1 x 0.25 m when transported by boat. The struts can easily be transported by truck since their dimensions are 5 m x 0.2 x 0.2 m. There will still need to be a concrete plant on site to pour concrete to connect all the elements.

As discussed in section 7.9.5 the walls are not uniform since the bottom is 0.4 m thick and the upper part is 0.25 m. The prefabricated walls will however be of uniform thickness, 0.25 m. The bottom part will gain its additional thickness by pouring concrete into the crease between the original structure and the wall.

To put the walls in place lifting cranes will be needed. If there is not enough space at the site, then the cranes will have to be placed on pontoons at the sea. When this is the case the weather conditions need to be calm during the placement of the walls. Reinforcement bars will be put at the bottom of the original structure, and material will be left out in the wall where these reinforcement bars connect with the wall. Formwork will be used to keep the walls in place while concrete is poured to connect the walls to the original structure and during the hardening process. The amount of formwork needed is much less than when the whole wall would be constructed on site.

The struts will be attached by putting reinforcement bars into the original structure and the wall which will be sticking out. In the strut material is left out where the bars fit into the strut. The connection is made by pouring concrete around the strut and filling the voids in the strut. It is important that first the strut is attached to the original structure; it’s then supported by a temporary structure until the wall is attached.

Drainage channel

The drainage channel needs to be deepened and widened. First the concrete cover of the channel needs to be removed. This can be done by drilling. Because of the hard subsoil normal digging machines will not be

suitable, instead large drills will be used. Rubble can then be removed by trucks. A concrete cover is desired to minimize friction over the channel so a maximum discharge can be achieved. Furthermore, if there is no cover there is a risk of eroding chunks of rock which will ultimately block the channel. The drilling will need to be done a little

7.10 Maintenance plan

Throughout the lifetime of the structure maintenance will be performed to ensure the functionality of the sea wall and drainage channel. The maintenance approach that is used in this project is reliability centered. This means that the focus lies on the function of different elements and making sure they can remain operational.

Elements which are subject to repeated loads and harsh environments will need maintenance. This is the case for the sea wall and struts. Maintenance can be corrective or preventive, depending on the consequences of failure of an element, how predictable this failure is and if the element can be easily inspected.

In this case when a wall element fails this creates a weak spot in the defense which can cause global failure in extreme cases. For this reason, preventive maintenance can occur. The failure of the defense can be predicted quite well, with the saltwater environment the concrete decay can be predicted. After heavy storms the sea wall can be damaged as well. The walls can be easily inspected since they are very accessible. A yearly inspection of the walls will take place before the hurricane season, in this manner any maintenance operation that needs to be done can be done before the hurricanes hit. Furthermore, after an extreme weather events an inspection of the wall will be done to see if there is any damage.

It is assumed that most repairs to the wall can be done by locally repairing damaged area and that not a whole wall element will need to be replaced. However, if extreme damage occurs 5 spare wall and strut parts are stored on site, which can be used to replace damaged sections of the wall and struts.

The drainage channel will need less inspection during the year, the most important thing is that there is nothing blocking the channel so that the discharge through the channel is optimal. For this reason, before an extreme weather event is expected the channel will be cleared and cleaned and debris around the channel is also removed so that this does not flow into the channel.

7.11 Costs and planning

Costs

The costs of the project are estimated by taking into account direct costs (material, construction and construction material costs), indirect costs (site office, facilities, design, etc.) and the overhead and additional costs. The costs are closely related to the duration of the project; the man-hours that are needed to reach a certain duration and the rental costs of equipment.

A 70 percent cost value is estimated to be in the region of 2.0 million USD or about the same value in CUC. This 70 percent value is obtained by assuming that the estimated cost is the most probable cost of a triangular distribution and the minimum and maximum costs are estimated by subtracting and adding 50 percent of the estimated costs. The 70 percent value is found between the estimated costs and the maximum costs.

Description	**Quantity**	**Unit**	**Unit price**	**Unit**	**Costs (1000$)**
Direct costs					
Materials					
Concrete walls + struts	301	m^3	120	$/$m^3$	36
Reinforcement steel	9	ton	1000	$/ton	9
Construction prefab walls			0.2	$/$	7
Concrete drainage channel	2151	m^3	120	$/$m^3$	258
Concrete drainage wall	250	m^3	120	$/$m^3$	30

Construction					
Formwork	50	m^2	20	$/$m^2$	1
Support formwork	50	m^2	50	$/$m^2$	3
Man-hours	19276	hours	10	$/hour	193
Construction equipment					
Crane rental + setup and removal	15	weeks	40000	$/week	608
Drilling equipment	11	weeks	6250	$/week	69
On-site concrete plant	15	weeks	15000	$/week	228
Indirect costs					
Site office	18	weeks	1000	$/week	18
Site facilities	18	weeks	500	$/week	9
Site preparation	3	weeks	1000	$/week	3
Design	7	weeks	4000	$/week	28
Total costs					1,500
Overhead and additional costs					
Overhead costs			5.0	%	75
Risk			5.0	%	75
Insurance			1.0	%	15
Total + overhead and additional costs					1,665
Find P70 (triangular distribution)					
Minimum costs -50%					832
Maximum costs +50%					2,497
P70					1,998

Table 50 – Total costs of the project

The costs should be considered to be a very rough estimated, since many of the costs are estimated. Additionally, many values are based Dutch values and norms. For this reason, a large uncertainty is used in the P70 value.

Planning

The project is estimated to take about 7 months. In Figure 177, Figure 178, Figure 179 and Figure 180 one can find the planning of the project, which is made up from 10 global stages. The red bars represent the critical path that leads to the total time needed to complete the project.

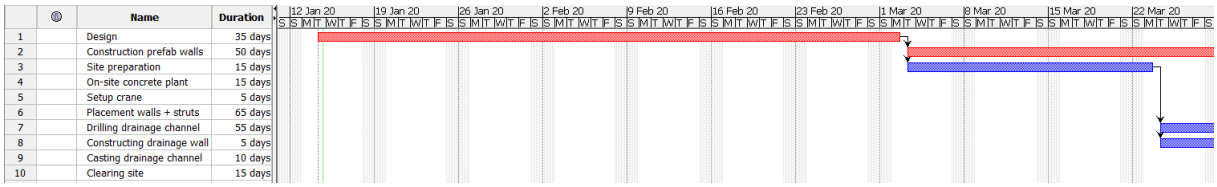

	Name	Duration
1	Design	35 days
2	Construction prefab walls	50 days
3	Site preparation	15 days
4	On-site concrete plant	15 days
5	Setup crane	5 days
6	Placement walls + struts	65 days
7	Drilling drainage channel	55 days
8	Constructing drainage wall	5 days
9	Casting drainage channel	10 days
10	Clearing site	15 days

Figure 177 – Planning part 1

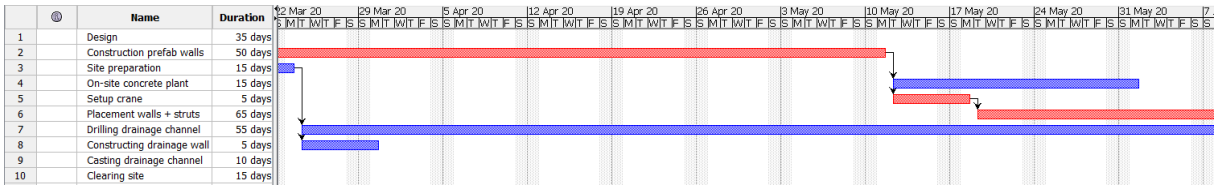

	Name	Duration
1	Design	35 days
2	Construction prefab walls	50 days
3	Site preparation	15 days
4	On-site concrete plant	15 days
5	Setup crane	5 days
6	Placement walls + struts	65 days
7	Drilling drainage channel	55 days
8	Constructing drainage wall	5 days
9	Casting drainage channel	10 days
10	Clearing site	15 days

Figure 178 – Planning part 2

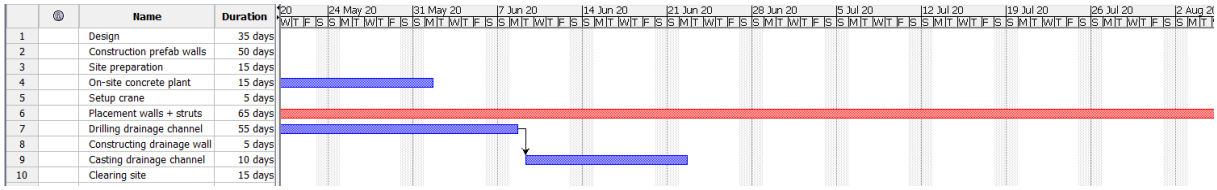

	Name	Duration
1	Design	35 days
2	Construction prefab walls	50 days
3	Site preparation	15 days
4	On-site concrete plant	15 days
5	Setup crane	5 days
6	Placement walls + struts	65 days
7	Drilling drainage channel	55 days
8	Constructing drainage wall	5 days
9	Casting drainage channel	10 days
10	Clearing site	15 days

Figure 179 – Planning part 3

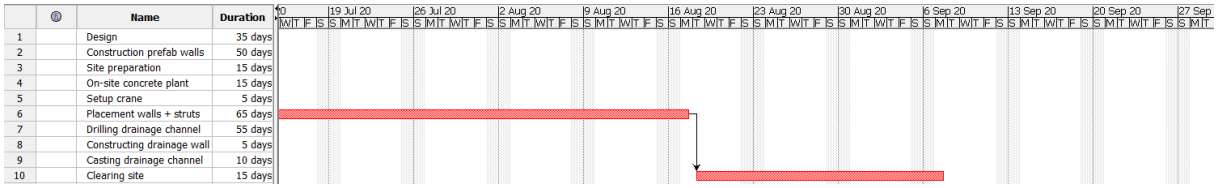

	Name	Duration
1	Design	35 days
2	Construction prefab walls	50 days
3	Site preparation	15 days
4	On-site concrete plant	15 days
5	Setup crane	5 days
6	Placement walls + struts	65 days
7	Drilling drainage channel	55 days
8	Constructing drainage wall	5 days
9	Casting drainage channel	10 days
10	Clearing site	15 days

Figure 180 – Planning part 4

Chapter 8

Conclusion

Hurricane Irma caused major damage to the Central Thermo Electrico Antonio Guiteras (CTE) in Matanzas. The sea defense at the time of the hurricane did not manage to withstand the waves and water level that was generated and large portions of the site were flooded, leaving the power plant unable to supply electricity to the surrounding area.

At the moment of writing this report, a new sea defense has being constructed. There is however little known about the effect of extreme weather conditions around the new sea defense. This report focuses on the main question: *"To what extend is the power plant protected during extreme weather conditions and what improvements are needed to ensure that the power plant can remain operational during these extreme weather conditions?"* In order to answer this question correctly, four sub-question were formed, that first will be answered in this chapter.

Firstly, the question: *"Which extreme weather events are of importance in the scope of this project?"*, is answered. It is found that in the scope of our project, it is of importance that two of these types of events are analyzed, namely tropical cyclones and cold fronts. Cold fronts can generate maximum wind speeds that correspond to category 3 tropical cyclones, meaning that category 5 tropical cyclones such as Irma can generate wind speeds that are much higher than that of a cold front. The cold fronts do have a much higher probability of occurrence. However, the cold fronts that are generated north of Cuba, arrive from the North-West, leading to waves being generated from the same nautical direction. Since the coastline where the CTE is located is perpendicular to the North-East, waves from such cold fronts have little influence on the project site. Hence, only tropical cyclones have been assessed in this report.

As Irma significantly damaged the CTE site, this tropical cyclone is taken as the basis for all hurricanes to be assessed. From the 18 synthetic hurricanes that have been created only hurricanes along track 1 and 3 are modeled. Track 2 hurricanes are excluded from the computations. From theory it is deduced that these hurricanes cause less damage, since their center is located further away from the CTE which causes the corresponding waves and storm surge to be less. The hurricanes that follow track 2 were also found to have a very low probability of occurrence. Furthermore, these hurricanes of importance are modeled with different combinations of wind speeds and forward speeds based on an approximation of the resulting group velocity of the generated wind waves. From the probabilistic calculations it is concluded that the probability of occurrence of most of these synthetic hurricanes is zero with the exception of hurricanes 6, 9 and 10. In an adjusted and a less precise probabilistic approach the return period of hurricane 2 is estimated to be 1580 years. This hurricane is taken as the normative extreme weather event in the scope of this project. However, also the other synthetic hurricanes have been modeled to gain insight into the hydrodynamic and meteorological effects.

Secondly, the question: "*What are the hydrodynamic and meteorological effects of these extreme weather events?*", is answered. It is concluded that only tropical cyclones are assessed within the scope of this project and therefore the effects of the synthetic hurricanes and the tropical cyclone Irma are researched. The main hydrodynamic effects of a hurricane are storm surge accompanied with waves being generated by the high wind velocities and the corresponding low central pressures in the hurricane center. Based on wind speeds, wave heights and water levels the Delft3D model has been validated to an accurate enough model to physically approach hurricane Irma and to be used as input for the XBeach model. Based on these models and running them for all the different synthetic hurricanes it can be concluded that tropical cyclones with large wind speeds, low central pressures and low translational velocities create the largest waves.

There is however no evidence for a correlation between the translational velocity and the water level near the coast of the CTE. It can be concluded that track 1 hurricanes create a smaller storm surge, higher peak wave

periods and larger wave lengths. There is no clear influence of the track on the significant wave height, wave group celerity and wave direction.

From the XBeach results of combinations 1, 2, 13 (low), 13 (high), 14 and Irma it can be concluded that combination 2 results in the largest maximum significant wave height of 8.8 meters with a storm surge of 1.6 meters. This means that the wave height near the coast of the CTE decreases, since the input from Delft3D gives a maximum significant wave height of 12.1 meters. The significant wave height for combination 2 that is used in the design steps of the report is calculated to be 6.5 meters with a standard deviation of 0.9 meters for a significant period of 3.5 hours. The storm surge has a constant value of 1.6 meters during this period.

Meteorological effects of tropical cyclones are mainly large wind speeds and high amounts of precipitation. The large wind speeds lead to an increase in spray overtopping as water splashing on the sea wall is sprayed over. Precipitation amounts of combination 2 are based on known rainfall data from past hurricanes. Due to limited data however no extreme value analysis can be performed and a total rainfall amount of 25 inches during the hurricane is taken as the design value. This value corresponds to a 30-year return period. Based on maximum observed precipitation rates from hurricane Harvey in Houston the maximum precipitation rate to work with is chosen to be 100 mm/h.

Thirdly, the question: "*What are the possible failure mechanisms related to these extreme weather events and their respective consequences?*", is answered. The flooding of the CTE can occur due to either a failure of the sea defense or a failure of the drainage system.

The sea defense can fail due to four different mechanisms, namely extreme overtopping, loss of structural integrity, construction and design errors and external and internal stability. Each of these failure mechanisms may lead to flooding of the CTE, where the degree of flooding depends on the degree to which this failure mechanism occurs. This counts for extreme overtopping, loss of structural integrity and construction and design errors as the severity of these failure mechanisms and therefore the consequences can vary largely with their respective causes. These are the hydrodynamic and meteorological state of the event and the state of the sea defense. There are three failure mechanisms within external and internal stability. These are horizontal sliding of the wall and soil, tilting of the structure and the anchorage breaking off. These events are always normative when they occur as they completely undermine the water-retaining function of the sea defense.

The drainage system can fail due to either a failure of the drainage channel or the pumping system. In the current situation the drainage channel can handle a maximum discharge of 21 m^3/s and 82 m^3/s for the narrowest (segment 1) and widest segment (segment 4) respectively. This discharge consists of cooling water, overland flow and (spray) overtopping. During storm conditions a maximum discharge of 63 m^3/s has to be drained through segment 1 and 89 m^3/s through segment 4, which results in flooding of both segments. To combat this excess discharge the drainage channel can be deepened and/or widened, or this discharge can be pumped by a combination of pumps situated at one or multiple locations along the drainage channel. For segment 1 the pump discharge needs to be 42 m^3/s and for segment 4 it should be able to discharge 7 m^3/s.

The last sub-question: "*What are feasible protection solutions to minimize the impact and probability of occurrence of these failure mechanisms?*", is answered. The four cross-sections of the current sea defense fail the overtopping requirement of 34 l/m/s with higher probabilities than the tolerable 30%. Cross section A-1, A-2, B and C fail with a probability of failure of 90%, 91%, 95%, and 66% respectively. Furthermore, the current drainage system and channel cannot process the storm discharge. This storm discharge consists of cooling water, (spray) overtopping and overland flow.

The four variants are: a wave attenuation solution, a pump solution, a channel deepening solution and a sea defense design adjustment solution. The wave attenuation variant has a screen of piles with a diameter of 1 and a core to core distance of 2.2 meters placed at a depth of 6 meters. The pile screen is a feasible solution that could decrease overtopping; however, the screen is expensive and has an unsatisfactory constructability. The second variant presents pumps to remove the storm discharge through a pipe to sea. Pumps at segment 1 of the channel work physically the most efficient. Large or many smaller pumps are needed for this solution which makes the variant economically less attractive.

The third variant has a discharge channel with increased dimensions. An iterative process between widening and deepening solutions shows that deepening channel section 1, 2 and 5 with 40 centimeters leads to a sufficient discharge capacity. The fourth method is a sea defense design change. The sea defense may be changed in the top of the structure height, the bullnose geometry, the installation of a stilling basin, or the application of a combination of the presented solutions to reduce te overtopping.

An MCA has been conducted on the variants for each different cross section separately. The MCA shows that cross section A-1, A-2 and B will get a different sea defense design with an allowable failure probability of 30% which comes with an overtopping of 100 l/m/s. This inventive design has a spilling basin with return flow situated between the new sea wall and the original design. This basin reduces the 100 l/m/s overtopping to less than 34 l/m/s, which has been the set overtopping criterium.

Analysis shows that an increased drainage channel dimensions solves the overtopping problems around cross section C and the storm discharge problem of the project site. The solution incorporates a drainage wall around the CTE to prevent overland flow over the project site. The probability that the costs of this complete solution are smaller than 2 million USD is of 70%.

Finally, the main question: "*To what extend is the power plant protected during extreme weather conditions and what improvements are needed to ensure that the power plant can remain operational during these extreme weather conditions?",* is answered.

Tropical cyclones are the type of weather conditions causing hazards for the CTE. Tropical cyclones with large wind speeds, low central pressures, low translational velocities and a close track to the CTE, have the largest probability of endangering the power plant's operational capacity.

The failure probability of the original situation concerning the overtopping discharge is 90% for passing tropical cyclones like Irma having return periods around once in 1580 years. The probability that the original situation fails once in the lifetime of 50 years is 3%. The original situation takes into account that overland flow due to extreme precipitation causes problems in the project area as well.

The renewed design has a failure probability of 30% for an Irma-like passing tropical cyclone. The new probability of failure becomes 1% that the new design fails once in its complete lifetime. Furthermore, the new design integrates overland flow problems, which ensures the power plant's complete operational capacities at all times.

The new design consists of an adapted sea defense for cross sections A-1, A-2, and B with a lower top of structure and a stilling basin with a return flow back to sea. The new design also incorporates a drainage wall around the project area to prevent overland flow problems and a deepened drainage channel. The drainage channel discharges the overtopped water and this overland flow back to sea by a gravity forced flow.

Chapter 9

Discussion

9.1 Problem definition

9.1.1 Fault tree

The fault tree is set up by combining failure mechanisms that are most likely to be normative in order to not broaden the scope of the project too much. For example, failure mechanisms such as ship collision and erosion of the foreshore are not taken into account. This could lead to an underestimation of the failure probability of the sea structure.

The two failure mechanisms that lead to a failure of the drainage system, namely the failure of the pumping system and the failure of the drainage channel, are influenced by two possible situations that are bound by an AND-gate. This means that the single occurrence of one of these situations cannot cause a failure of either the pumping system or the drainage channel. This could lead to an underestimation of the failure probability of these failure mechanisms.

The extreme overtopping failure mechanism is influenced by high waves and a water level rise. These are in turn bound by an AND-gate. This means that the sole occurrence of high waves or water level rise cannot lead to extreme overtopping. This might lead to an underestimation of the probability of occurrence, however since the physical causes of these events are mostly similar, they are largely correlated and happen simultaneously in differing severities. Therefore, the underestimation is marginal.

9.1.2 Coastal analysis

The bathymetry used for the coastal analysis has a relatively high resolution around the bay of Matanzas compared to the bathymetry used for the Delft3D simulations. However, the project is still very small compared to this higher resolution, which results in interpolation of bathymetry points creating a bathymetry and topography that is not completely true to reality.

In order to find the level at which the sea defense is located, use is made of available videos, bathymetry data and reports. The drawings of the new sea defense are limited and lack clearly specified heights. Hence, the heights that are used are deduced largely using visual observations and rules of thumb. The videos are of low resolution, making it hard to correctly observe the wave heights and the topography of the CTE including the sea wall. In addition, assumptions are made about the tides that were present at the bay of Matanzas. The tide is assumed to be equal to that in Varadero at the same time. It is unknown if the cross section that is used as the basis for the overtopping computations is located at the exact location of the CTE and if there is a large spatial variability in this cross section.

The rainfall amount and intensity that may occur during tropical cyclones is based on only 10 measured hurricanes that came close to Matanzas in the past and the rainfall intensity that hurricane Harvey produced in Houston. This is a very limited dataset from which the rainfall extrapolation has to be based on. Therefore, the rainfall amount and intensity that is used for the analysis in this report has a large margin of error. Additional to the uncertainty in the rainfall analysis, there is also a lack of data about the topography and soil composition of the catchment area. Because of all these uncertainties the use of a lumped model is preferred over a computer model that needs to be validated and requires a complete dataset.

9.1.3 Probabilistic approach

In the probabilistic approach it is assumed that there is no correlation between the hurricanes from the NOAA dataset. This means that for example hurricane Irma had no influence on the maximum velocity, central

pressure, translational velocity and the track of hurricane José which followed a few days later. However, since hurricanes are created by the atmospheric conditions around the same latitude, it is very probable that the formation of Irma had an influence on the formation of hurricane José as they were formed by largely the same atmospheric conditions. However, since this correlation could lead to an under- and overestimation of the marginal extreme value distributions, this feedback mechanism is neglected.

Another assumption is that there is no trend of increasingly intense hurricanes over the time span of the dataset. There is however a trend of hurricanes becoming more extreme over the past decades over the Atlantic Ocean, which means that some distortion affects the marginal extreme value distribution. Since this trend has not been quantified in this report, the amount of distortion is unclear, but it is assumed that it is within reasonable margins.

9.1.4 Synthetic hurricanes

In order to recreate the rough initial sea conditions, which is used for the synthetic hurricane combinations, use is made of uniform wind. In reality, the wind speeds differ at certain locations within the area, especially since this consists of a large part of the North-Atlantic Ocean, the Gulf of Mexico and the Caribbean Sea. This means that the rough sea state that is created differs from reality, which can result in slightly unrealistic results for the synthetic hurricanes.

The hurricanes from the dataset that were analyzed were categorized into different tracks by means of a certain margin. This margin allows for some different variations of the track; however, this might overestimate the probability of occurrence of the specific track. Hence, the tracks that were created for the synthetic hurricanes do not completely resemble the ones that have been found in this analysis.

In order to make easier probabilistic computations, correlations close to 0 are assumed to be exactly 0 and correlations close to 1 are assumed to be exactly 1. This may lead to some inaccuracies of the probabilistic approach. However, this effect is probably very small as the computed correlations are very close to 0 and 1.

In order to capture hurricanes with translational speeds of a certain value, it is needed to create a certain range for which the probability can be captured. In case of the translational speeds this range is taken to be 0.5 m/s. This means that the probability of a hurricane moving with a mean translational speed of 3 m/s is not exactly equal to the calculated value, which may lead to bias in both directions. Hence, this effect is assumed to be negligible.

In the additional probabilistic calculation for combination 2, a new extreme value distribution is fitted for the maximum velocity of the hurricane. However, in this case it is a conditional extreme value distribution meaning that a lot of data points have been disregarded. Hence, the uncertainty of the distribution is much larger than for the original EV distribution.

Since many combinations of a maximum wind speed, track and translational speed have not been observed until now, the conditional probability cannot be calculated and is therefore 0. In order to still capture the probability of occurrence of combination 2, an assumption is made that the conditional probability of a translational speed of 3 m/s given a high maximum wind speed and track 1 is equal to the probability of a translational speed of 3 m/s. Hence, one can imagine that some bias is therefore introduced into the calculations.

9.1.5 Modelling

For the Delft3D grid only one single grid is used, since the use of nesting was not accomplished. This results in quite large grid cells, since the grid covers a very large area. If the grid would be more refined the computation time would be too large within the time frame of this project. Since the grid is not very refined, the information that can be gathered from the grid is less detailed. The observation points are placed at one single grid cell and gather all information from this grid cell. The output (2-D spectrum) that is taken as input for the XBeach model can therefore not be taken too close to the shore, as the grid cell covers the whole bay of Matanzas and the surrounding area. Additionally, a less refined grid results in less detailed hydrodynamic modelling results.

It is chosen not to set the tide as a boundary condition in the Delft3D model. This decision is made because on the east side of the grid there is a very large sea domain and the tidal conditions will not be constant over the corresponding curved open boundary. The tide is variable both in time and space around these boundaries. The influence of the tide in the project area is very limited and consequently the influence of this varying water level is small on the hydrodynamic processes. Super positioning the tide on the modelled water levels is therefore acceptable.

For the grid used in Delft3D bathymetry data is used that covers the whole area. However, near Cuba there are a lot more bathymetry points available. This leads to large interpolation at the areas of the grid where not a lot of points are available, such as near Puerto Rico and the Dominican Republic. As the hurricanes propagate through these areas the resulting computations may be influenced by this lack of detailed bathymetry.

The closed boundaries that area generated within the Delft3D grid originate from two methods. One type of closed boundary is created by the use of land boundaries for Cuba and the other type is created by the use of the bathymetry. The use of land boundaries is more detailed, since it exactly resembles the position of land. However, also with the land boundaries there is a discrepancy, since the grid that is used is not very refined, creating a rough connection between the land boundary and the grid. Through the bathymetry the grid cells that did not have bathymetry points are transformed into land, but through the use of grid cell averaging the small island were seen as water. As there are less islands in the model than there are in reality, the process that is modelled in Delft3D is not the same.

In the Holland formula the radius of the hurricane depends on the maximum velocity, the central pressure within the hurricane and the latitude at which it is located. However, in the Delft3D input file for the Spiderweb grid only one radius can be used as input. Therefore, the radius is averaged over its track leading to some more inaccurate wind and pressure fields. Moreover, the Spiderweb grid is taken to be the same size in longitude and latitude, which gives a small distortion as in UTM zone 17N, 1 latitude is not the same as 1 longitude if converted into kilometers.

The Spiderweb grid is created as such that the peak with high wind velocities is captured well, however in the Delft3D model the wind velocity in each grid cell is the average of the wind velocities from the Spiderweb grid. This still dilutes the wind velocities a bit, but it is better than not having the extreme wind speeds as input at all as this might greatly underestimate the influence of the wind on wave and flow generation.

For the validation of the Delft3D model there are not a lot of observation stations available. Three observation stations are found that have information about the wind speeds, wave heights and water levels. However, the observation stations are located far away from the CTE. Next to this, the observation points in Delft3D can only be positioned in the middle of a grid cell and therefore are not located at the exact coordinates as in reality.

The wind speed validation cannot be executed very accurately, since the best track that is used for Irma in the Delft3D model differs from the real Irma track. Therefore, the measured wind speeds at the observation station is not equal to the observation point that is used in Delft3D, because the station might be located in the eye of the storm whereas the observation point is located in the outskirts of the hurricane.

For the validation of the wave heights the stations that were first used seemed to be inaccurate due to hurricane José that came into the picture shortly after hurricane Irma passed the station, thus resulting in wave heights generated by hurricane José that were not present in the Delft3D model. The only other option to validate the model on wave height is to look at observations that were done at the North coast of Cuba, however these observations can have an unknown inaccuracy.

The fit that is used to remove the tidal signal from the observed water levels in the observation stations consists of two simplified components that differ from reality, therefore the resulting graph without a tide is not completely true to reality creating a comparison with the Delft3D model that is slightly off.

9.1.6 Results synthetic hurricanes

In order to compare the results for Delft3D an observation point was placed as close as possible to the CTE. However, as said before, the grid that is used is not very refined resulting in gathered data that is approximately 30-40 km from the coast. Since the results are all extracted from the same observation points it is possible to compare them, however the results of Delft3D do not resemble the results near the CTE.

The new grid that is used to cover synthetic hurricanes that follow track 3 is less refined at the area of interest than the original grid and also the new grid is not validated. Therefore, the results for synthetic hurricanes that follow track 3 are less accurate than hurricanes that follow track 1 and 2 and are thus modelled on the original grid.

In the first part of synthetic hurricanes the wind speeds were not as desired. From the Delft3D runs with these faulty synthetic hurricanes it is chosen to look at combination 14 and 18 in more detail, since they created the highest waves. Due to the errors in the wind speeds it is not confirmed that these combinations were the normative ones.

It was initially predicted that hurricanes moving with the group celerity generate the highest waves, however from the results from the model it seems that the slower travelling hurricanes generate higher waves. This can be due to the fact that no iterative process was performed and therefore the hurricanes do not actually move with the group celerity. Another reasoning is that the hurricanes moves to a new location every hour and therefore it does not follow the generated waves accurately and the amplification that this phenomenon should provide is not imitated by the model.

As the wind speeds were not modelled well, there is a discrepancy between pressure and wind. It is unclear to what extend the pressure distribution in the hurricane was altered. The surge and pressure are closely related, thus there is a large uncertainty in the water levels that the model calculates.

To be able to generate the correct wind and pressure fields in part 2 of the synthetic hurricanes a few simplifications were made. The Holland formula coefficients that were calibrated for hurricane Irma did not give good representations of the wind speed for the synthetic hurricanes. Therefore, these coefficients are changed as such that the maximum velocity for each time step is close to the value given in the best track.

To compare the results for XBeach, a closest shore coordinate is used to get results from the model. This point is located as close to the shore as possible, but it might be possible that not all near-shore processes are included in the final result.

For combinations 1, 13 (low) and 13 (high) a different XBeach grid is used. It can be seen from results that this new XBeach grid results in water levels that are not correct. Due to time limitations (XBeach run takes 30 hours) no new grid is made to compute the correct water level values for these combinations. It is assumed that the wave generation is hardly influenced by these faulty water levels, which might lead to some inaccuracies.

Synthetic hurricanes are run with a constant forward speed, whereas real hurricanes have translational velocities that differ over their track. This could create smaller and/or larger waves than expected, since hurricanes when for example travelling slower during a short period of time create higher waves during that period. If this period were to be close to the area of interest, this assumption might lead to an underestimation of the wave heights and storm surge.

The results from Delft3D and XBeach with respect to the generated wave heights and storm surge differ. This is due to the underlying processes that are modelled in these programs. Delft3D gives input to XBeach and XBeach uses this information without any knowledge about the generating forces in Delft3D. Hence, the resulting output from XBeach might be slightly underestimating the storm surge, since there is no knowledge about the wind and pressure field that creates part of this storm surge.

The XBeach model gives H_{rms} values as output. The significant wave height is equal to about 1.4 times the $H_{rms.}$ In the case for this report this would lead to extremely high wave heights and consequently a very overdesigned sea defense. Therefore, a close examination of the XBeach results is performed. It is seen that

the relation between the increase in storm surge and the expected decrease in significant wave height does not hold. Hence, the radiation stress and wave set-up formulas are used to create a force balance within the XBeach domain with reasonable values of depth and incoming wave heights. This analysis may lead to a different significant wave height than would occur in real life. However, also the output of XBeach is not equal to reality, meaning that outcomes very close to the shore may have the same uncertainty as when done analytically.

9.1.7 Current design check and variants

The cross-shore profile of the coast at the CTE is schematized by a foreshore and a vertical cliff. Firstly, it is not known whether this cross-shore profile is the right one at all locations at the CTE, but it is assumed to be so. Secondly, the schematization that has been applied to this profile does not correspond completely to the reality, but it is close and gives the possibility for overtopping calculations.

The influence of H_{m0} is very large on the outcome of the probabilistic method, as can be seen by the large α factor. Since the significant wave height differs quite a lot during the hours of the storm, it is important to take into account how these deviations might induce errors and uncertainties in the overtopping discharges. However, since the significant wave height is the main contributor to the overtopping mechanism, it is logical that it has a very large influence on the uncertainty of the overtopping values.

The berm correction factor γ_b is taken to be smaller than the recommended value of 0.6 for sections B and C. This recommendation has not been following because of the fact that the berm for these sections is very large and this must lead to a decrease in the overtopping discharges. For these cases, the schematization that has been used in the calculations is less accurate and therefore this value for the berm correction factor can be justified.

For variant 1 a pile screen is implemented. The influence of such a pile screen on the transmission of waves is approached by a simple formula, however it is not known exactly what the influence of the height of the piles has on this transmission. It is assumed that the piles would need to be 2 meters above HWL, but it is uncertain how much this would influence the transmission. Furthermore, it is unknown how deep the piles need to be drilled into the foreshore and if this is feasible at all, since the soil structure is rocky, but also largely unknown.

Variant 2 proposes a drainage system with a pumping station, drainage channel in combination with a drainage wall. For the computations within this variant the storm discharge consists out of cooling water, overtopping water and overland flow.

The calculated amount of overtopping per segment is assumed to be summed up and enter at the beginning of each segment. This means that this situation is the most normative one as in reality the overtopped water enters the drainage channel right behind the sea wall.

The amount of overland flow depends on the rainfall intensity and the runoff coefficient of the catchment area west of the CTE. The catchment area is assumed to have a rocky soil with macro pores and a very low infiltration capacity. Hence, the value of the runoff coefficient is taken to be quite large. This might lead to inaccuracies in the estimation of the overland flow.

For variant 3 the only way to reduce overtopping is by adjusting the current sea wall. It is assumed that adjusting only the bullnose of the sea wall does not lead to a sufficient reduction, since the exact geometry of the wall is not known. Additionally, it is assumed that it is possible to add concrete elements to the current sea wall. Also, for such adjustments it is assumed that the allowable overtopping discharge can be increased to 100 l/s/m.

The variants proposed for the inlet channel assume that it is possible to make adjustments to the current inlet channel and that it is possible to construct new elements within this channel.

In the Multi Criteria Analysis several weight factors are thought of, all of which have different weights that have been come up with and are based on the current situation in Cuba and what it is thought are the most

important aspects of a good design. Hence, the weighted average of each of the variants for each section is only a qualitative indication of the performance of the variant.

9.1.8 Final solution

In the final design all calculations have been done with reinforcement steel. In the original design carbon fibre was used as reinforcement. Since the information about this material is lacking, calculations would not have been as reliable if this was used in the design. It is assumed that reinforcement steel is available as a construction material, otherwise the design needs to be adjusted to suit the carbon fibre. The downside of reinforcement steel is mainly that it can be corroded by the sea water, this is taken into account when choosing the concrete cover.

The spacing of the struts is every two meters. In the design checks a 1D calculation has been done where the wall is treated as a beam. For a small spacing of the struts this is a justified simplification. When the distance between the struts becomes larger a 2D calculation is required and the wall needs to be treated as a slab. It is assumed that for two meters the 1D simplification holds and that with simple transverse reinforcement any bending in this direction is taken care of. For an optimal design the transverse reinforcement should be designed and an optimization step can be made with the strut spacing and transverse reinforcement.

Only general stability checks have been done for this design regarding global and internal stability. The detailing of the connection between bottom of the wall and the original design has not been worked out. The same holds for the connection between the strut and the structure. At the bullnose also detailing is required and in an optimal design a strut and tie model needs to be made.

The initial estimation of the dimensions has been checked in this design. These were taken such that they satisfy the unity checks with some margin. In an optimal design several iteration steps need to be done in order to get a more economical design.

In front of the inlet channel the berm is removed, for this reason the waves will have more energy and there will be more overtopping. Since the berm reduction factor in area A-1 was 0.6, it is assumed that there will be 40% more overtopping at all times. The Minikin method for the impulsive wave force does not include a factor for the berm so these factors will be unchanged. It could be reasoned that a method could be used which yields higher forces since Minikin is a lower bound method which was justified by the presence of a berm. The increased overtopping over the wall is not seen as a complication because of the large discharge capacity of the channel to return the overtopped water back to sea.

Lastly only section A-1 and A-2 have been treated fully in the final design. Naturally when the design would be executed also detailed calculation for section B are needed.

Bibliography

Allsop, N. W., van der Meer, J. W., Bruce, T., De Rouck, J., Kortenhaus, A., Pullen, T., . . . Zanuttigh, B. (2018). EurOtop. Manual on wave overtopping of sea defences and related structures.

Allsop, van der Meer, Bruce, De Rouck, Kortenhaus, Pullen, & Schuttrumpf. (2018). EurOtop - Manual on wave overtopping of sea defences and related structures.

Baldock, H. B. (1998). Cross-shore hydrodynamics within an unsaturated surf zone. *Coastal Engineering 34*, 173-193.

BBA Pumps. (2019). *High Capacity Flood Control Pumps - BA700G D810.* Opgehaald van BBA Pumps: www.bbapumps.com/en/products

Borkowf, C. (2002). Computing the nonnull asymptotic variance and the asymptotic relative efficiency of Spearman's rank correlation. *Computational Statistical Data Analysis*, 271-286.

Bretschneider, C. (1957). *Hurricane design wave practices.*

Cordova. (2019, 12). Instructions about the multidisciplinairy project.

de Boer, G., Poelhekke, L., Schlepers, M., & Vrolijk, E. (2014). Improving Oasis Beach. *Creating a sustainable and attractive beach around hotel Oasis in Varadero, Cuba.*

Deltares. (2019). *Delft3D - QUICKIN user manual.* Deltares.

Emanuel, K. (sd). *Tropical Cyclones.* Massachusetts : Massachusetts Institute of Technology.

Embrechts, P., Klüppelberg, C., & Mikosch, T. (1997). *Modelling Extremal Events for Insurance and Finance.* New York: Springer.

EurOtop. (2018). *Manual on wave overtopping of sea defences and related structures.*

Federal Research Division. (2002). *Cuba: a country study.*

Genest, C., & Favre, A.-C. (2007). Everything You Always Wanted to Know About Copula Modeling but Were Afraid to Ask . *Journal of Hydrologic Engineering*, 347-368.

Holland, G. J., Belanger, J. I., & Fritz, A. (2010). A Revised Model for Radial Profiles of Hurricane Winds. *Monthly Weather Review*, 4393-4401.

Homewood, P. (2019). *Tropcal Hurricanes in the age of global warming.* The Global Warming Policy Foundation.

Instituto de Meteorlogia Cuba. (2013). *Informe final para rehabilitacion del malecon tradicional.*

Jesús, V. d. (2019, 10 04). *Mantenimiento en la Antonio Guiteras: Parada para ganar potencia*. Opgehaald van Granma: www.granma.cu/cuba/2019-10-04/mantenimiento-en-la-antonio-guiteras-parada-para-ganar-potencia-04-10-2019-00-10-13

Jones, W. D. (2008, 04 23). *How much water does it take to make electricity*. Opgehaald van IEEE SPECTRUM ENERGY: https://spectrum.ieee.org/energy/environment/how-much-water-does-it-take-to-make-electricity

Kotz, S., & Nadarajah, S. (2000). *Extreme Value Distributions.* London: Imperial College Press.

Montgomery, M., & Smith, R. (sd). Tropical Cyclone Formation: Theory and Idealized Modeling.

National Hurricane Center. (1975). *Structure of a Small, Intense Hurricane - Inez 1966.*

National Hurricane Center. (1996). *Preliminary Report Hurricane Lili.*

National Hurricane Center. (1999). *Preliminary report Hurricane Irene.*

National Hurricane Center. (2002). *Tropical Cyclone Report Hurricane Michelle.*

National Hurricane Center. (2006). *Tropical Cyclone Report Hurricane Rita.*

National Hurricane Center. (2009). *Tropical Cyclone Report Gustav* .

National Hurricane Center. (2009). *Tropical Cyclone report Hurricane Ike.*

National Hurricane Center. (2009). *Tropical Cyclone Report Tropical Storm Fay.*

National Hurricane Center. (2014). *Preliminary Report Hurricane Georges.*

National Hurricane Center. (2014). *Tropical Cyclone Report Hurricane Dennis.*

National Hurricane Center. (2018, 6). *Tropical Cyclone Report - Hurricane Irma.*

National Oceanic and Atmospheric Administration. (2019). *National Oceanic and Atmospheric Administration*. Opgehaald van National Oceanic and Atmospheric Administration: http://www.prh.noaa.gov/cphc/summaries/

NOAA. (2017, September 8). *NASA TV*. Opgehaald van NASA: www.nasa.gov/image-feature/geocolor-image-of-hurricane-irma

Ochi, M. K. (1993). On hurricane generated seas. *International convention of waves* . American society of civil engineers .

P., C. J., & al., A. S. (2018). *National hurricane center tropical cyclone report.* National Hurricane Center.

Pearson, J., Kortenhaus, A., Bruce, T., & Allsop, N. (2003). Influence of parapets and recurves on wave overtopping and wave loading of complex vertical walls. *Coastal Structures 2003*, 369–381.

Pumpscout. (2019). *Pump Types Guide - Find the right pump for the job*. Opgehaald van Pumpscout: www.pumpscout.com/articles-scout-guide

Rahmstorf, S. (2010). A new view on sea level rise. *Nature Reports Climate Change, 4,* 44–45.

Roelvink, J. (1993). Dissipation in random wave groups incident on a beach. *Coastal engineering 19,* 127-150.

Rubio Sauvalle, M., Hernández Valdés, K., Olivera Ascanio, W., Cervera Castro, D., Aponte Trimiño, N., & Batista Faz, L. M. (2018). *Estudio de riesgos naturales inversiones.*

Sainsbury, B., & McCarthy, C. (2017). *Lonely Planet of Cuba.* Lonely Planet Global Limited.

Schauer, J. (sd). *Tropical Cyclone Rainfall.* Miami, FL: National Hurricane Center - Tropical Analyis and Forecast Branch Lead Forecaster.

Science Kennesaw. (sd). Opgehaald van http://science.kennesaw.edu/~jdirnber/oceanography/LecturesOceanogr/LecTides/116.jp

Scott, D., Simpson, M. C., & Sim, R. (2012). The vulnerability of Caribbean coastal tourism to scenarios of climate change related sea level rise. *Journal of Sustainable Tourism*, 883-898.

Senn, H., & Hiser, H. (1959). *On the origin of hurricane spiral rain bands.* Miami: University of Miami.

The Netherlands Standardization Institute. (2011). *NEN-1990-1*.

TU Delft. (2019). *Manual Hydraulic Structures.* TU Delft.

Unesco-IHE institute for Water Education, Deltares, Delft University of Technology. (2010). *Xbeach Model Description and Manual* . Delft.

United Nations. (2018). *World Statistics Pocket Book 2018 Edition.* New York: United Nations Publication.

Unknown Author. (2017). *Evaluación del riesgo por oleaje extremo en el tramo frente a la termoeléctrica Antonio Guiteras en la costa Norte de la bahía Matanzas.* Havana.

van Oldenborgh, G., van der Wiel, K., Sebastian, A., Singh, R., Arrighi, J., Otto, F., . . . Cullen, H. (2017, 08). Attribution of extreme rainfall from Hurricane Harvey.

Vatvani, D., Zweers, N. C., & al., e. (2012). *Storm surge and wave simulations in the Gulf of Mexico using a consistent drag relation for atmospheric and storm surge models.* Nat. Hazards Earth Syst. Sci.

Video footage of Hurricane Irma (2017). [Film].

Video footage of Irma razing over the power plant (2017). [Film].

Voorendt, M., & Molenaar, W. (2019). Manual Hydraulic Structures. Delft, the Netherlands.

Young, I. (1988). Parametric Hurricane Wave Prediction Model. *Journal of Waterway Port Coastal and Ocean Engineering*.

Appendix

A. Current sea defense

This appendix contains information about the sea wall currently being constructed.

Overview current sea defense

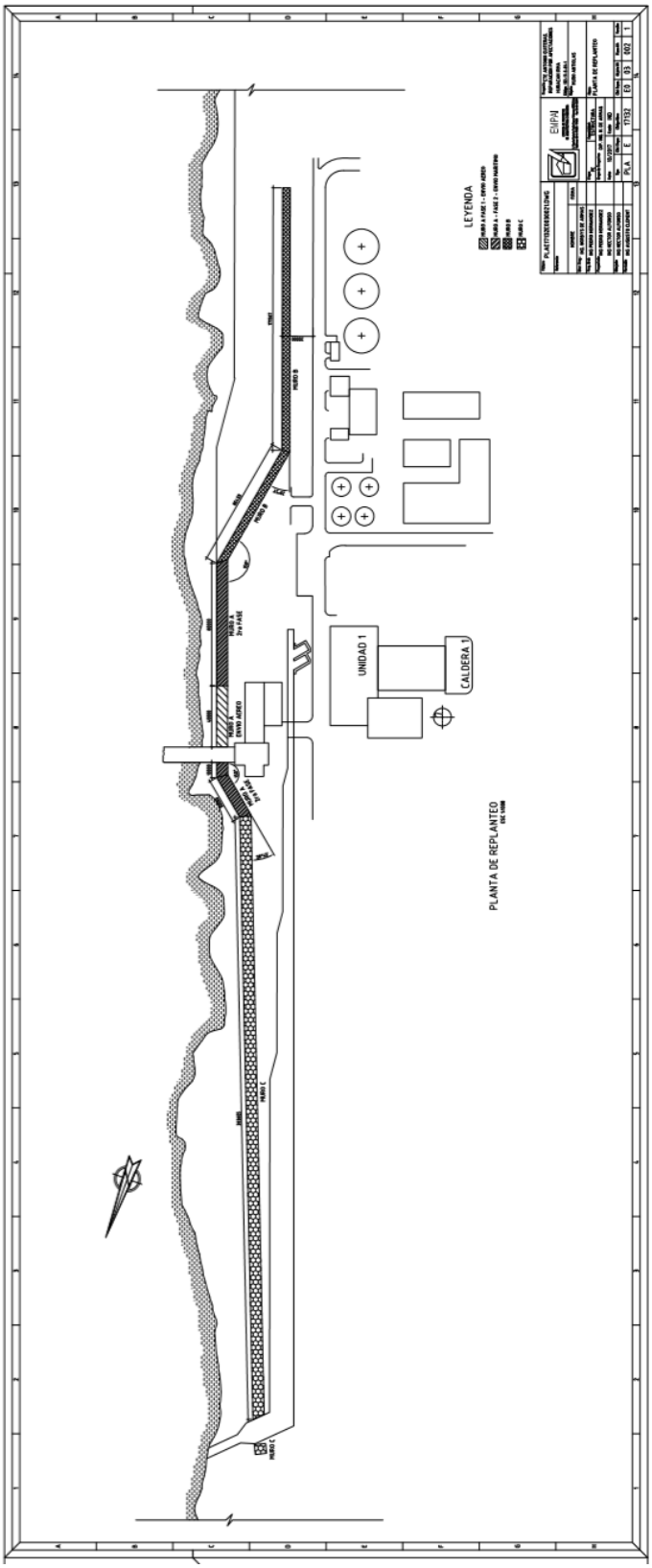

Figure 181 – Technical drawing of the lay out of the current defense wall

Technical drawings of the sea wall sections

Figure 182 – Technical drawing of the current defense wall detail

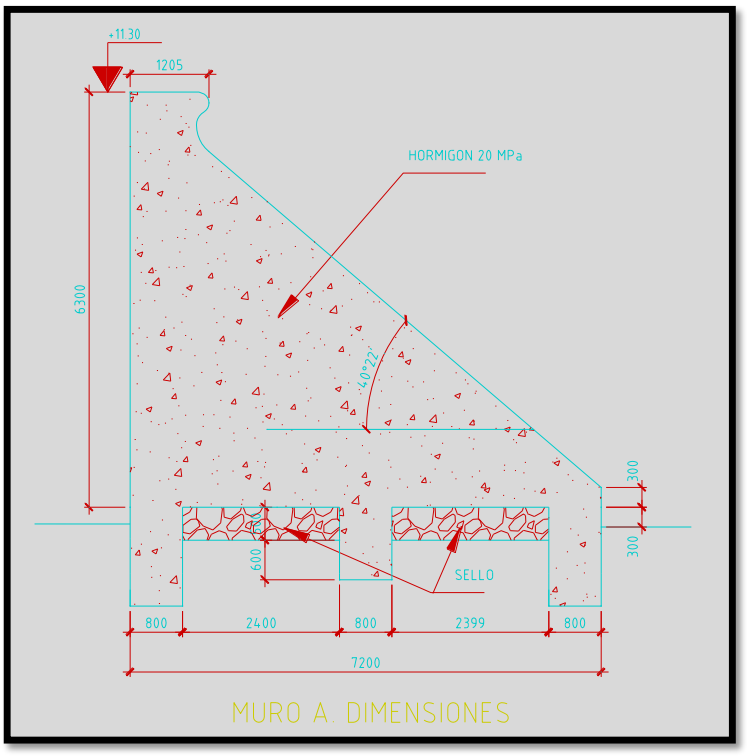

Figure 183 – Technical drawing of the current defense wall part A

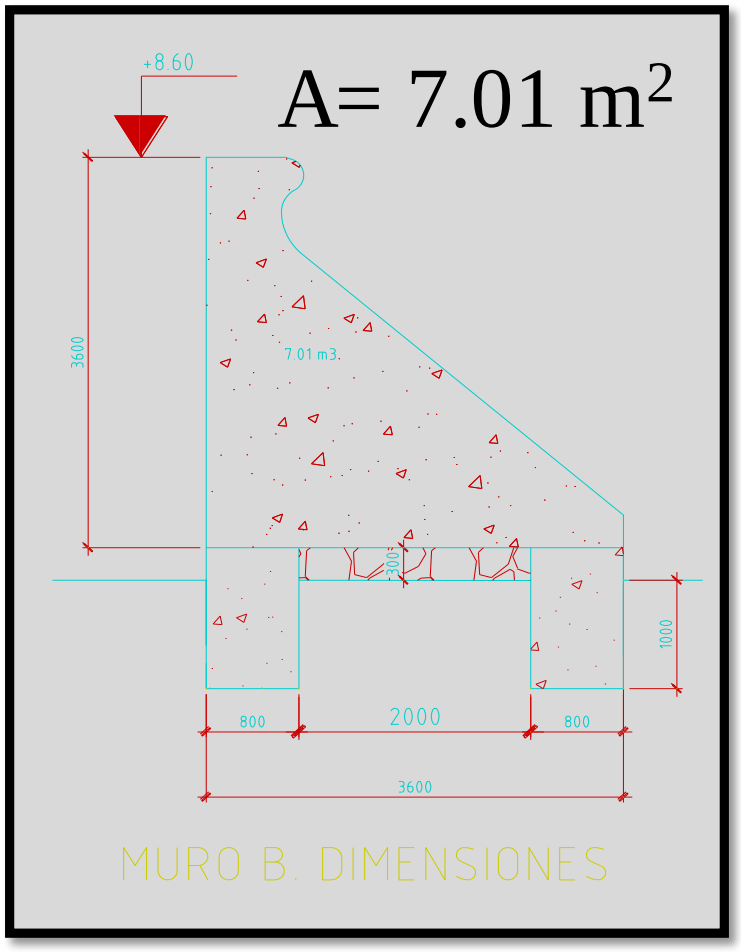

Figure 184 – Technical drawing of the current defense wall part B

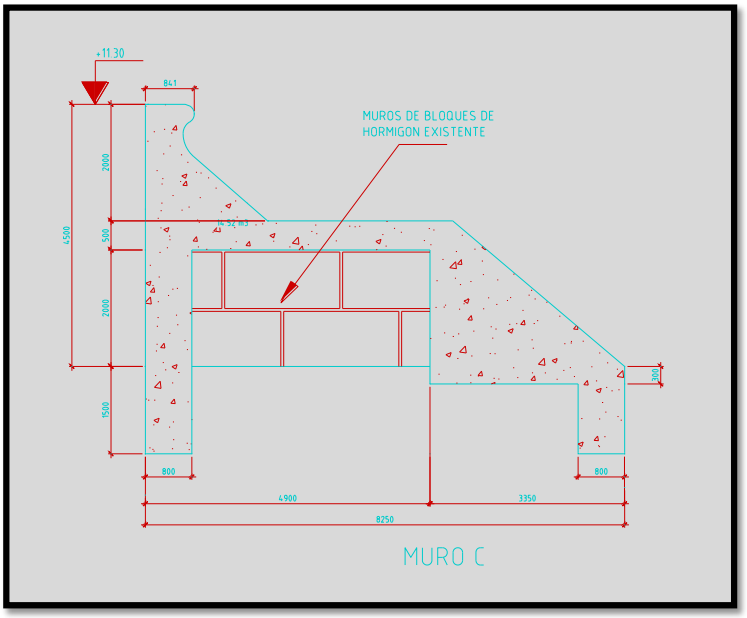

Figure 185 – Technical drawing of the current defense wall part C

B. Fault tree

The fault tree is cut into two pieces to make it readable.

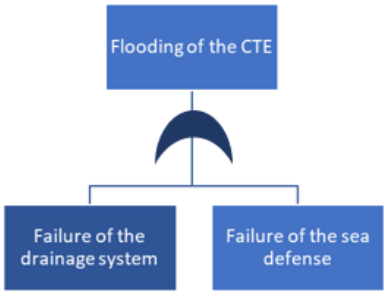

Failure of the drainage system

The left side of the failure tree is focused on failure of the drainage system.

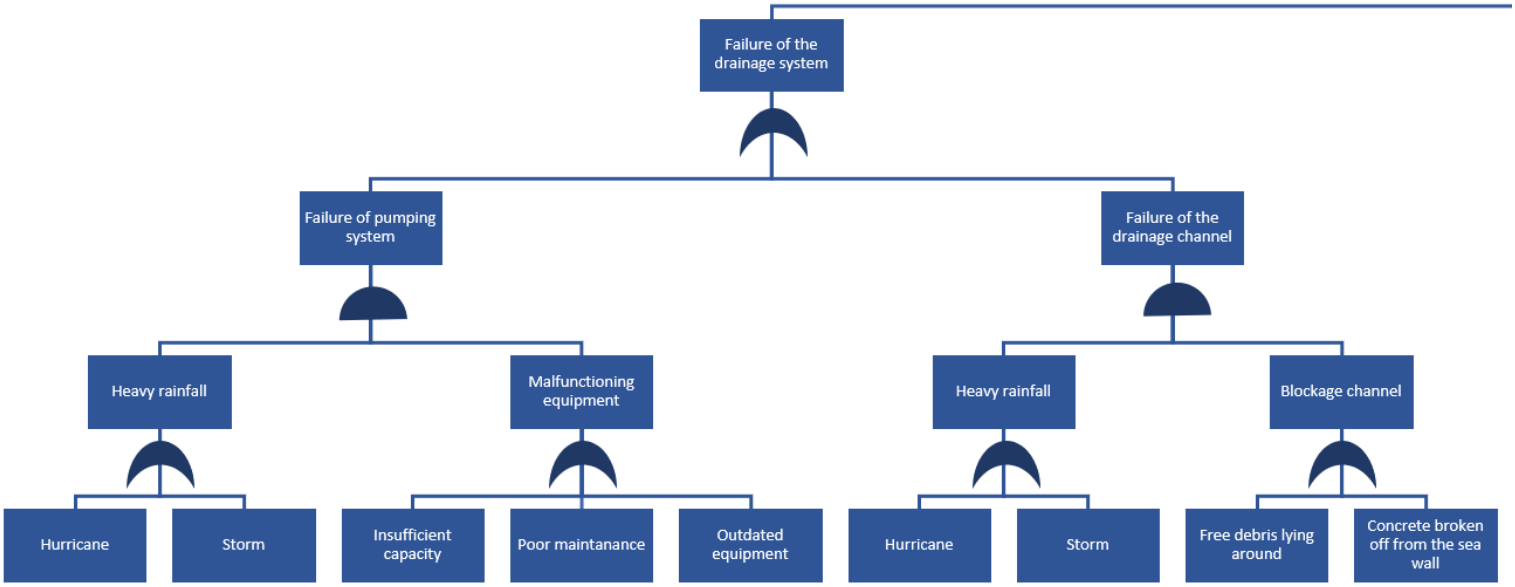

Figure 186 – Failure of the drainage system

Failure of the sea defense

The right side of the fault tree is focused on the failure of the sea defense.

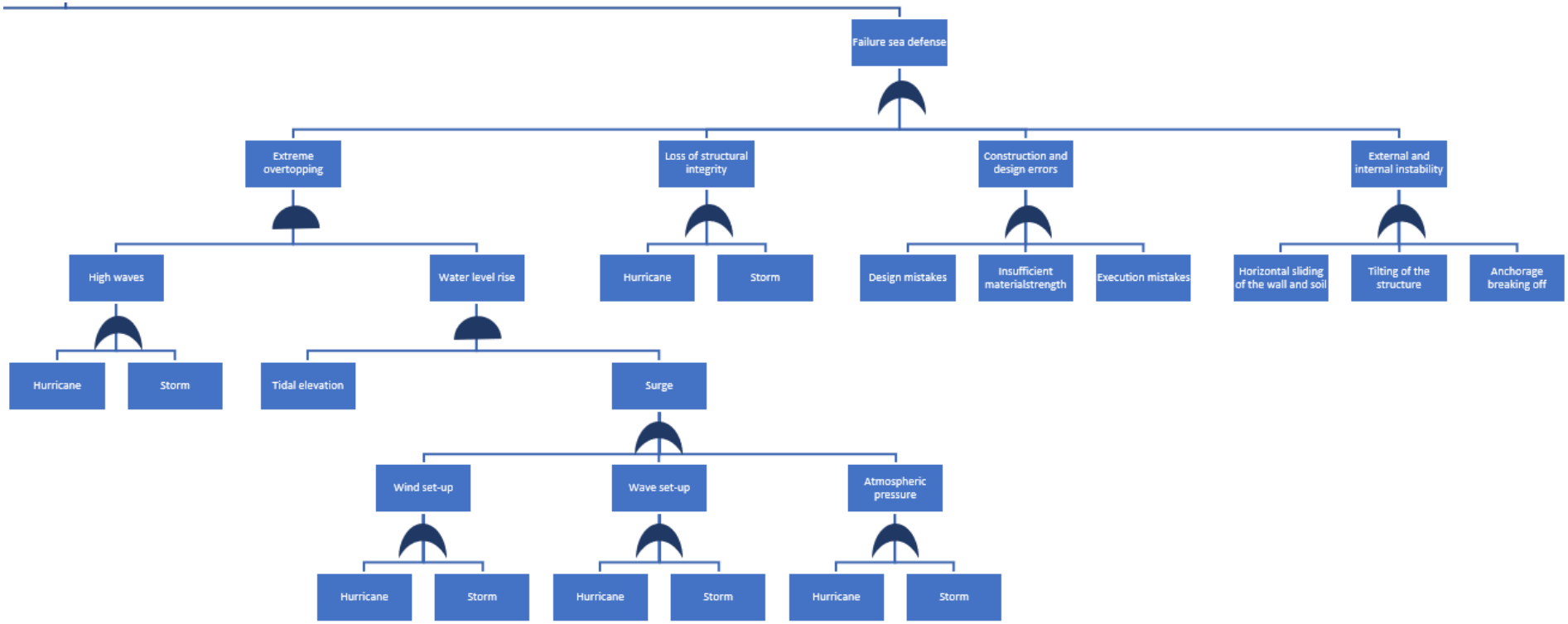

Figure 187 – Failure of the sea defense

C. Deterministic approach of synthetic hurricanes

This appendix gives additional figures about the correlation between variables. Furthermore, it includes a Matlab script used to find and count past hurricanes with track 1, 2 and 3. In the last part of the appendix a table of the original combinations of synthetic hurricanes is added together with their probabilities of occurrence calculations.

Correlations between variables

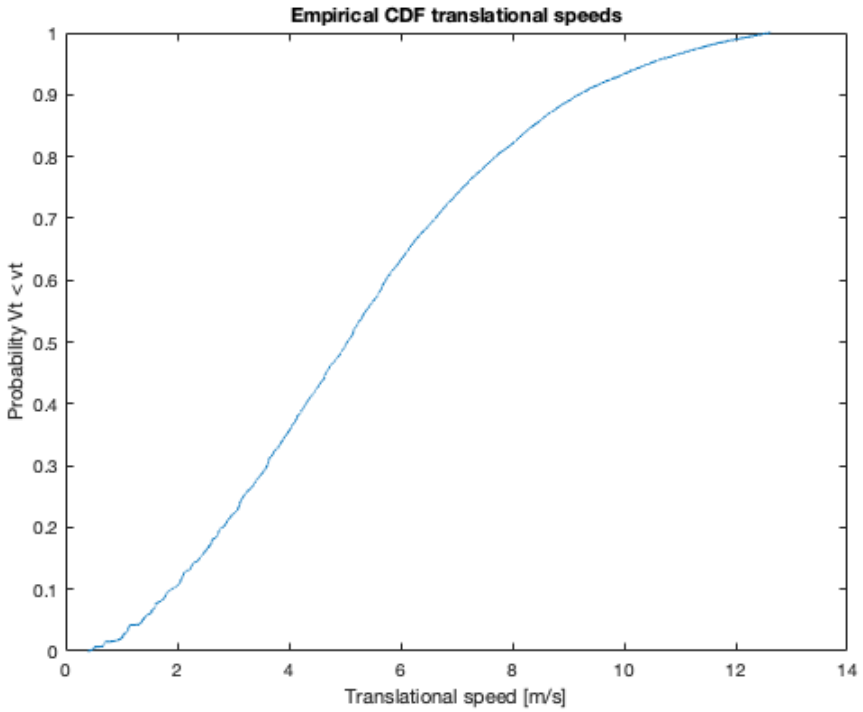

Figure 188 – CDF translational velocity

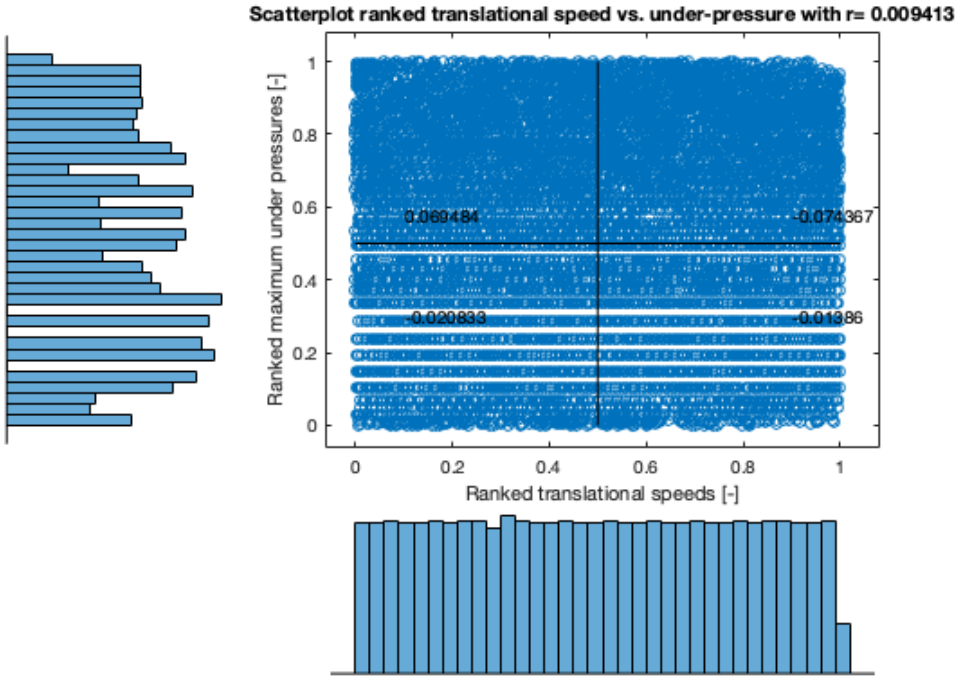

Figure 189 – Scatterplot ranked translational speed vs under-pressure

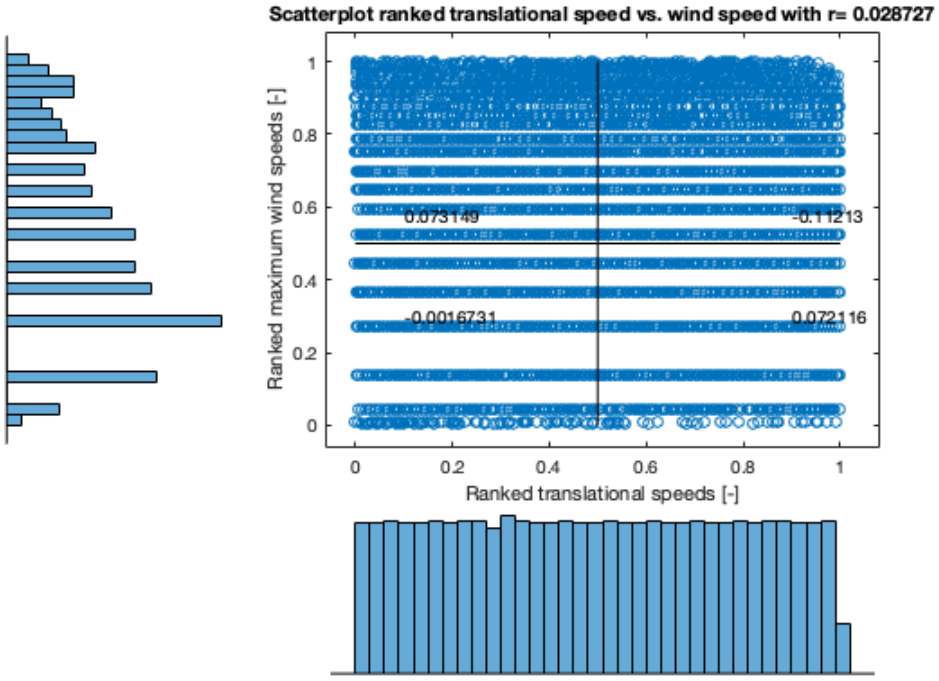

Figure 190 – Scatterplot ranked translational speed vs wind speed

Matlab script to find and count hurricanes with tracks 1, 2 and 3

By looking at the database of past hurricanes, the number of hurricanes which comply with the three established tracks are filtered. For each track two or three lines are placed. The hurricanes passing these lines are counted and showed in a graphs. On the next three pages, the Matlab script can be found which is written to detect and count the number of hurricanes with tracks 1, 2 and 3.

```
clear all
load('Lon.mat');
load('Lat.mat');
track1=0;
track2=0;
track3=0;
x_track1=NaN(max(size(Lon,1)),size(Lon,2));
y_track1=NaN(max(size(Lat,1)),size(Lat,2));
x_track2=NaN(max(size(Lon,1)),size(Lon,2));
y_track2=NaN(max(size(Lat,1)),size(Lat,2));
x_track3=NaN(max(size(Lon,1)),size(Lon,2));
y_track3=NaN(max(size(Lat,1)),size(Lat,2));
for i=1:size(Lon,2)
    %% Track 1 (crossing Cuba)
    xn = Lon(:,i);
    yn = Lat(:,i);
    x = xn(isnan(xn)==0 & isnan(yn)==0);
    y = yn(isnan(xn)==0 & isnan(yn)==0);
    xmin=-83;
    xmax=-80;
    ymin=22;
    ymax=23;

    dy_up=y-ymax;
    dy_do=ymin-y;
    if min(dy_up(dy_up>0))>0 & min(dy_do(dy_do>0))>0
        check=1;
        I_up=y(dy_up==min(dy_up(dy_up>0)));
        I_do=y(dy_do==min(dy_do(dy_do>0)));
        x_up=x(y==I_up(1));
        x_do=x(y==I_do(1));
    else
        check=0;
        x_up=NaN;
        x_do=NaN;
    end
    if x_up>xmin & x_up<xmax & x_do>xmin & x_do<xmax & check==1
        track1=track1+1;
        x_track1(1:length(x),i)=x;
        y_track1(1:length(y),i)=y;
    end
    n3=track1;
    T3=167/n3;

    %% Track 2 (close to shore)
    x1=-82;
    x2=-81;
    x3=-80;
    ymin1=23;
    ymax1=24.3;
    ymin2=22.8;
    ymax2=24.1;
    ymin3=22.5;
    ymax3=23.8;

    dx_right=x-x2;
    dx_left=x1-x;
    if min(dx_right(dx_right>0))>0 & min(dx_left(dx_left>0))>0
        check=1;
        I_right=y(dx_right==min(dx_right(dx_right>0)));
        I_left=y(dx_left==min(dx_left(dx_left>0)));
        y_r=y(y==I_right(1));
        y_l=y(y==I_left(1));
    else
        check=0;
        y_r=NaN;
        y_l=NaN;
    end
    if y_r>ymin2 & y_r<ymax2 & y_l>ymin1 & y_l<ymax1 & check==1
        track2=track2+1;
        x_track2(1:length(x),i)=x;
        y_track2(1:length(y),i)=y;
    end

    dx_right=x-x3;
    dx_left=x2-x;
    if min(dx_right(dx_right>0))>0 & min(dx_left(dx_left>0))>0
        check=1;
        I_right=y(dx_right==min(dx_right(dx_right>0)));
        I_left=y(dx_left==min(dx_left(dx_left>0)));
        y_r=y(y==I_right(1));
        y_l=y(y==I_left(1));
    else
        check=0;
        y_r=NaN;
        y_l=NaN;
    end
    if y_r>ymin3 & y_r<ymax3 & y_l>ymin2 & y_l<ymax2 & check==1
        track2=track2+1;
        x_track2(1:length(x),i)=x;
        y_track2(1:length(y),i)=y;
    end
    n1=track2;
    T1=167/n1;
```

```
%% Track 3 (far away from shore)
x1=-82;
x2=-81;
x3=-80;
ymin1=24.3;
ymax1=25.3;
ymin2=24.1;
ymax2=25.1;
ymin3=23.8;
ymax3=24.8;

dx_right=x-x2;
dx_left=x1-x;
if min(dx_right(dx_right>0))>0 & min(dx_left(dx_left>0))>0
    check=1;
    I_right=y(dx_right==min(dx_right(dx_right>0)));
    I_left=y(dx_left==min(dx_left(dx_left>0)));
    y_r=y(y==I_right(1));
    y_l=y(y==I_left(1));
else
    check=0;
    y_r=NaN;
    y_l=NaN;
end
if y_r>ymin2 & y_r<ymax2 & y_l>ymin1 & y_l<ymax1 & check==1
    track3=track3+1;
    x_track3(1:length(x),i)=x;
    y_track3(1:length(y),i)=y;
end
    dx_right=x-x3;
    dx_left=x2-x;
    if min(dx_right(dx_right>0))>0 & min(dx_left(dx_left>0))>0
        check=1;
        I_right=y(dx_right==min(dx_right(dx_right>0)));
        I_left=y(dx_left==min(dx_left(dx_left>0)));
        y_r=y(y==I_right(1));
        y_l=y(y==I_left(1));
    else
        check=0;
        y_r=NaN;
        y_l=NaN;
    end
    if y_r>ymin3 & y_r<ymax3 & y_l>ymin2 & y_l<ymax2 & check==1
        track3=track3+1;
        x_track3(1:length(x),i)=x;
        y_track3(1:length(y),i)=y;
    end
    n2=track3;
    T2=167/n2;

end
%%
figure(1);
xmin=-83;
xmax=-80;
ymin=22;
ymax=23;
worldmap([14 32],[-90 -50])
load coastlines
plotm(coastlat,coastlon)
hold on
tracks=plotm(y_track1,x_track1,'k');
passage=plotm([ymin, ymin],[xmin,xmax],'b');
plotm([ymax, ymax],[xmin,xmax],'b')
hold off
title(['Track 3: Hurricanes passing over Cuba from 1851-2018, T=',num2str(T3),' years']);
xlabel('Longitude');
ylabel('Latitude');
legend([tracks(1,1), passage],'Hurricane tracks','Passage','location','southeast');

%%
figure(2);
x1=-82;
x2=-81;
x3=-80;
ymin1=23;
ymax1=24.3;
ymin2=22.8;
ymax2=24.1;
ymin3=22.5;
ymax3=23.8;
worldmap([14 32],[-90 -50])
load coastlines
plotm(coastlat,coastlon)
hold on
tracks=plotm(y_track2,x_track2,'k');
irma=plotm(Lat(:,1849),Lon(:,1849),'r');
passage=plotm([ymin1,ymax1],[x1,x1],'b');
plotm([ymin2,ymax2],[x2,x2],'b')
plotm([ymin3,ymax3],[x3,x3],'b')
hold off
title(['Track 1: Hurricanes passing close to Cuba from 1851-2018, T=',num2str(T1),' years']);
xlabel('Longitude');
ylabel('Latitude');
```

```
legend([tracks(1,1), passage, irma],'Hurricane tracks','Passage','Irma track','location','southeast');

figure(3);
x1=-82;
x2=-81;
x3=-80;
ymin1=24.3;
ymax1=25.3;
ymin2=24.1;
ymax2=25.1;
ymin3=23.8;
ymax3=24.8;
worldmap([14 32],[-90 -50])
load coastlines
plotm(coastlat,coastlon)
hold on
tracks=plotm(y_track3,x_track3,'k');
passage=plotm([ymin1,ymax1],[x1,x1],'b');
plotm([ymin2,ymax2],[x2,x2],'b')
plotm([ymin3,ymax3],[x3,x3],'b')
hold off
title(['Track 2: Hurricanes passing far away from Cuba from 1851-2018, T=',num2str(T2),' years']);
xlabel('Longitude');
ylabel('Latitude');
legend([tracks(1,1), passage],'Hurricane tracks','Passage','location','southeast');


figure(4);
worldmap([14 32],[-90 -50])
load coastlines
plotm(coastlat,coastlon)
hold on
track3=plotm(y_track1,x_track1,'k');
track1=plotm(y_track2,x_track2,'b');
track2=plotm(y_track3,x_track3,'r');
hold off
title('All hurricanes close to Cuba from 1851-2018');
xlabel('Longitude');
ylabel('Latitude');
legend([track1(1,1), track2(1,1),track3(1,1)],'Track 1','Track 2','Track 3','location','southeast');
```

Original combinations of synthetic hurricanes

Table 51 shows the original combinations of synthetic hurricanes, including the track 2 hurricanes. In the final simulations these combinations are left out, creating a new table of only 12 combinations.

Combination	Wind speed	Forward speed [m/s]	Track	Initial sea conditions
1	High	13.3	1	Rough
2	High	3	1	Rough
3	High	13.3	2	Rough
4	High	3	2	Rough
5	High	13.3	3	Rough
6	High	3	3	Rough
7	Medium	10.2	1	Rough
8	Medium	3	1	Rough
9	Medium	10.2	2	Rough
10	Medium	3	2	Rough
11	Medium	10.2	3	Rough
12	Medium	3	3	Rough
13	Low	7.8	1	Rough
14	Low	3	1	Rough
15	Low	7.8	2	Rough
16	Low	3	2	Rough
17	Low	7.8	3	Rough
18	Low	3	3	Rough

Table 51 – Combinations synthetic hurricanes

Matlab script to generate the synthetic hurricanes

On the next pages, the script used to generate the best tracks of the synthetic hurricanes. The file generates the wind velocities, the pressure values and the locations of the spiderweb grid, which is the input for the Delft3D model.

```
clear all
load('Irma_96hours.mat');

x=Irma96hours(:,6);
y=Irma96hours(:,7);
vmax=Irma96hours(:,11);
pc=Irma96hours(:,10);

%% OPTIONS %%
vhigh=1;
vmed=1.5;
vlow=2;
T1=0; %no vertical translation
T2=1.5; %shift 1.5 latitude up
T3=-1.5; %shift 1.5 latitude down

%% INPUT PARAMETERS %%
vfac = 1/###; %select which type of maximum wind speed
v1_ms = ###; %in m/s given for option 1
T = ###; %choose the track
name = 'Irma#.txt';
%%
v1 = km2deg(v1_ms/1000); %in deg/s for option 1
t0 = Irma96hours(1,5); %start time
te = Irma96hours(end,5); %end time
n = (te-t0) + 1; %number of hourly points
nn = (te-t0)*12 + 1; %number of 5-minutely points
v1 = v1*3600;
t = linspace(t0,te,n); %hourly time
tn = linspace(t0,te,nn); %time per 5 minutes

xn = interp1(t,x,tn,'line');
yn = interp1(t,y,tn,'line');
vmaxn = interp1(t,vmax,tn,'line');
pcn = interp1(t,pc,tn,'line');

for i=1:nn-1
    d(i) = sqrt((xn(i+1)-xn(i)).^2 + (yn(i+1)-yn(i)).^2);
    v(i) = d(i);
    dydd(i) = (yn(i+1)-yn(i))/d(i);
    dxdd(i) = (xn(i+1)-xn(i))/d(i);
end
vms = deg2km(v)*1000/(5*60);

j=1;
x1(j)=xn(j);
y1(j)=yn(j);
vmax1(j)=vmaxn(j);
pc1(j)=pcn(j);
slopex = dxdd(j);
slopey = dydd(j);
dxdd = [dxdd,0];
dydd = [dydd,0];
vmsn = [vms,0];
v = [v,0];
vnew = v(j);
stop=0;

while stop==0
    v(j)=v1;
    vnew = v(j);
    j=j+1;
    x1(j)=x1(j-1)+slopex*vnew;
    y1(j)=y1(j-1)+slopey*vnew;
    dx=xn-x1(j);
    dy=yn-y1(j);
    d=sqrt(dx.^2+dy.^2);
    I = d==min(d);
    X1=xn(I);
    Y1=yn(I);
    Vmax1=vmaxn(I);
    Vx1=vmsn(I);
    Vy1=vmsn(I);
    Pc1=pcn(I);
    x1(j)=X1(1);
    y1(j)=Y1(1);
    pc1(j)=Pc1(1);
    vmax1(j)=Vmax1(1);
    slopex = dxdd(I);
    slopex = slopex(1);
    slopey = dydd(I);
    slopey = slopey(1);
    vx(j)=slopex*Vx1(1);
    vy(j)=slopey*Vy1(1);
    vnew = v(I);
    vnew = vnew(1);
    if x1(j)==xn(end) && y1(j)==yn(end)
        stop=1;
    end
    if j==1000
        stop = 1;
    end
end
Irma=fopen(name,'wt');
```

```
data_format = [];
for i=1:11
    if i<6
        data_format = [data_format,"%3.0f"];
    else
        data_format = [data_format,"%3.4f"];
    end
end
data_format = [data_format, '\r\n'];
data_format = join(data_format,' ');

for k=1:j
    if k==1
        for i=1:48
            if i==1
                hold1(1,3)=Irma96hours(1,3)-48/24;
                hold1(1,4)=Irma96hours(1,4);
                hold1(1,5)=1;
            else
                hold1(i,3)=hold1(i-1,3);
                hold1(i,4)=hold1(i-1,4)+100;
                hold1(i,5)=hold1(i-1,5)+1;
            end
            if hold1(i,4)==2400
               hold1(i,4)=0;
               hold1(i,3)=hold1(i-1,3)+1;
            end
            hold1(i,6)=x1(1);
            hold1(i,7)=y1(1) + T;
            hold1(i,8)=0;
            hold1(i,9)=0;
            hold1(i,10)=10;
            hold1(i,11)=1013.2-5;
            hold1(i,1)=Irma96hours(1,1);
            hold1(i,2)=Irma96hours(1,2);
            fprintf(Irma,data_format,hold1(i,:));
        end
        Irma1(1,3)=Irma96hours(1,3);
        Irma1(1,4)=Irma96hours(1,4);
        Irma1(1,5)=hold1(end,5);
    else
        Irma1(k,3)=Irma1(k-1,3);
        Irma1(k,4)=Irma1(k-1,4)+100;
        Irma1(k,5)=Irma1(k-1,5)+1;
    end
    if Irma1(k,4)==2400
        Irma1(k,4)=0;
        Irma1(k,3)=Irma1(k-1,3)+1;
    end
    Irma1(k,6)=x1(k);
    Irma1(k,7)=y1(k) + T;
    Irma1(k,8)=vx(k);
    Irma1(k,9)=vy(k);
    Irma1(k,10)=vmax1(k)*vfac;
    Irma1(k,11)=1000-(1000-pc1(k))*vfac;
    Irma1(k,1)=Irma96hours(1,1);
    Irma1(k,2)=Irma96hours(1,2);
    fprintf(Irma,data_format,Irma1(k,:));
end
fclose(Irma);


%% Create figures
figure(1);
plot(x1,y1,'-r*');
hold on
plot(x,y,'k.');
hold off
legend({'Track1','Irma hourly'},'location','best');
title(['Hurricane along Irma track with v = ',num2str(v1_ms),' m/s with duration of ',num2str(j),' hours']);
xlabel('Longitude');
ylabel('Latitude');


ts = timeseries(vms);
ts.Name = 'Translational speed';
ts.TimeInfo.Units = 'minutes';
ts.TimeInfo.Increment = 5;
ts.TimeInfo.StartDate = '07-Sep-2017 20:00:00';
ts.TimeInfo.Format = 'dd-mm-yy';

figure(2);
subplot(311);
plot(xn,yn);
title('Original Irma path with translational velocities')
ylabel('Latitude');
xlabel('Longitude');
subplot(312);
plot(xn,[vms,vms(end)]);
xlabel('Longitude');
ylabel('Trans. velocity [m/s]');
subplot(313)
plot(ts)
```

```
ylabel('Trans. velocity [m/s]');

figure(3);
plot(Irma1(:,6),Irma1(:,7),'-r*');
hold on
plot(x,y,'k.');
hold off
legend({'Synthetic track','Irma hourly'},'location','best');
title(['Synthetic hurricane track with v = ',num2str(v1_ms),' m/s with duration of ',num2str(j),' hours']);
xlabel('Longitude');
ylabel('Latitude');
```

Matlab script to calculate the probability of occurrence of the combinations

The probability of occurrence theory is explained in Chapter 4. The Matlab script used to implement these equations can be found on the next two pages.

```
clear all

load('Vmax_max.mat');
load('vtras_mean.mat');
load('I_track1.mat');
load('I_track2.mat');
load('I_track3.mat');


I_vh = Vmax_max>80;
I_vm = Vmax_max>53;
I_vl = Vmax_max>40;

vh = sum(I_vh);
vm = sum(I_vm);
vl = sum(I_vl);

I_vtras_h = (vtras_mean<14.8 & vtras_mean>11.8);
I_vtras_l = (vtras_mean<4.5 & vtras_mean>1.5);
I_vtras_78 = (vtras_mean<9.3 & vtras_mean>6.3);
I_vtras_102 = (vtras_mean<11.7 & vtras_mean>8.7);

vtras_h_vh1 = sum(vtras_mean(I_vh)<14.8 & vtras_mean(I_vh)>11.8);
vtras_h_vh2 = sum(vtras_mean(I_vh)>13.3);

vtras_l_vh1 = sum(vtras_mean(I_vh)<4.5 & vtras_mean(I_vh)>1.5);
vtras_l_vh2 = sum(vtras_mean(I_vh)<3);

vtras_h_vm1 = sum(vtras_mean(I_vm)<14.8 & vtras_mean(I_vm)>11.8);
vtras_h_vm2 = sum(vtras_mean(I_vm)>13.3);

vtras_l_vm1 = sum(vtras_mean(I_vm)<4.5 & vtras_mean(I_vm)>1.5);
vtras_l_vm2 = sum(vtras_mean(I_vm)<3);

vtras_h_vl1 = sum(vtras_mean(I_vl)<14.8 & vtras_mean(I_vl)>11.8);
vtras_h_vl2 = sum(vtras_mean(I_vl)>13.3);

vtras_l_vl1 = sum(vtras_mean(I_vl)<4.5 & vtras_mean(I_vl)>1.5);
vtras_l_vl2 = sum(vtras_mean(I_vl)<3);

vtras_78_vh = sum(vtras_mean(I_vh)<9.3 & vtras_mean(I_vh)>6.3);

vtras_78_vm = sum(vtras_mean(I_vm)<9.3 & vtras_mean(I_vm)>6.3);

vtras_78_vl = sum(vtras_mean(I_vl)<9.3 & vtras_mean(I_vl)>6.3);

vtras_102_vh = sum(vtras_mean(I_vh)<11.7 & vtras_mean(I_vh)>8.7);

vtras_102_vm = sum(vtras_mean(I_vm)<11.7 & vtras_mean(I_vm)>8.7);

vtras_102_vl = sum(vtras_mean(I_vl)<11.7 & vtras_mean(I_vl)>8.7);


%%%
I_vh_vtras_h = I_vh'.*I_vtras_h;
I_vm_vtras_h = I_vm'.*I_vtras_h;
I_vl_vtras_h = I_vl'.*I_vtras_h;

I_vh_vtras_l = I_vh'.*I_vtras_l;
I_vm_vtras_l = I_vm'.*I_vtras_l;
I_vl_vtras_l = I_vl'.*I_vtras_l;

I_vh_vtras_78 = I_vh'.*I_vtras_78;
I_vm_vtras_78 = I_vm'.*I_vtras_78;
I_vl_vtras_78 = I_vl'.*I_vtras_78;

I_vh_vtras_102 = I_vh'.*I_vtras_102;
I_vm_vtras_102 = I_vm'.*I_vtras_102;
I_vl_vtras_102 = I_vl'.*I_vtras_102;


vh_vtras_h = sum(I_vh'.*I_vtras_h);
vm_vtras_h = sum(I_vm'.*I_vtras_h);
vl_vtras_h = sum(I_vl'.*I_vtras_h);

vh_vtras_l = sum(I_vh'.*I_vtras_l);
vm_vtras_l = sum(I_vm'.*I_vtras_l);
vl_vtras_l = sum(I_vl'.*I_vtras_l);

vh_vtras_78 = sum(I_vh'.*I_vtras_78);
vm_vtras_78 = sum(I_vm'.*I_vtras_78);
vl_vtras_78 = sum(I_vl'.*I_vtras_78);

vh_vtras_102 = sum(I_vh'.*I_vtras_102);
vm_vtras_102 = sum(I_vm'.*I_vtras_102);
vl_vtras_102 = sum(I_vl'.*I_vtras_102);

A1 = sum(I_track1.*I_vh_vtras_h);
A2 = sum(I_track1.*I_vh_vtras_l);
A3 = sum(I_track3.*I_vh_vtras_h);
A4 = sum(I_track3.*I_vh_vtras_l);
A5 = sum(I_track1.*I_vm_vtras_102);
A6 = sum(I_track1.*I_vm_vtras_l);
A7 = sum(I_track3.*I_vm_vtras_102);
```

```
A8 = sum(I_track3.*I_vm_vtras_l);
A9 = sum(I_track1.*I_vl_vtras_78);
A10 = sum(I_track1.*I_vl_vtras_l);
A11 = sum(I_track3.*I_vl_vtras_78);
A12 = sum(I_track3.*I_vl_vtras_l);


%% New calculation
clear all
load('Vmax_max.mat');
load('vtras_mean.mat');
vtras_mean(Vmax_max>80)
[f,x]=ecdf(vtras_mean);
ecdfhist(f,x);
```

D. Evaluation of past hurricanes

Ten past hurricanes that have caused significant damage to the province of Matanzas are Inez (1996), Lili (1996), Georges (1998), Irene (1999), Michelle (2001), Dennis (2005), Rita (2005), TC Fay (2008), Gustav (2008) and Ike (2008). These are analyzed in the following chapter.

Hurricane Inez (1966)

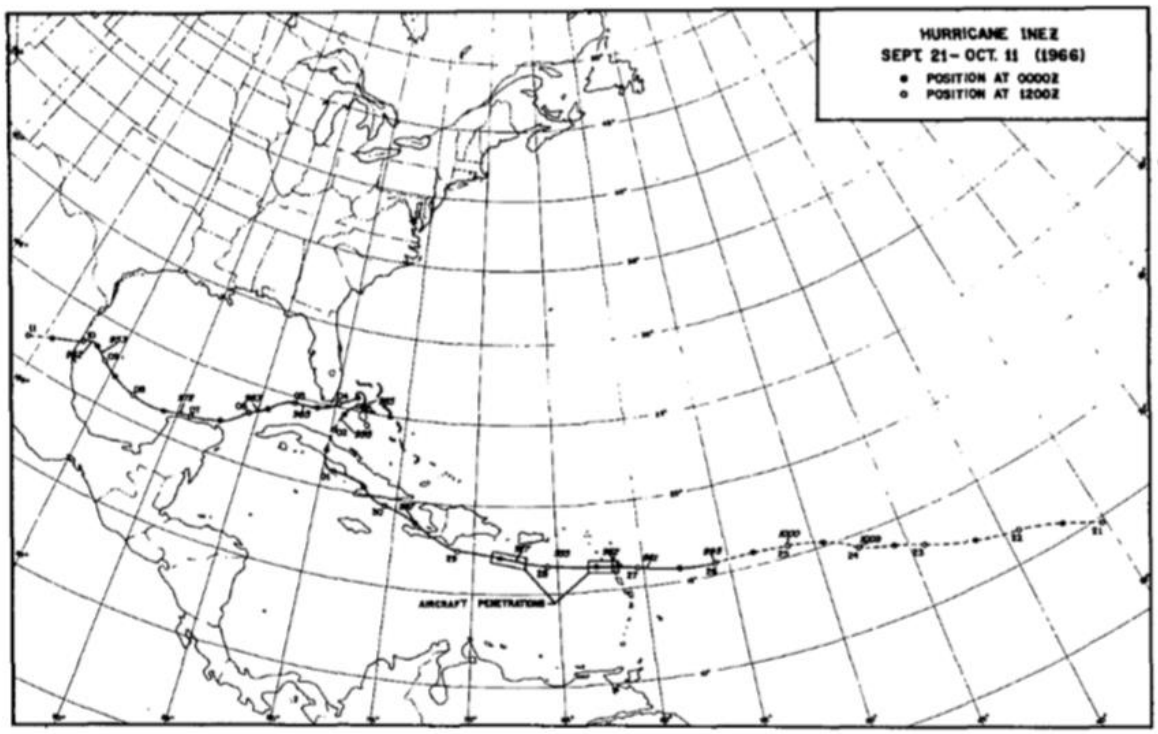

Figure 191 – Best track positions for hurricane Inez, 21 September - 11 October 1966

Date	26 September – 11 October
Duration	16 days
Category	4
Position to shore	Over land, close to Matanzas
Forward speed	7 m/s
Maximum windspeed	65 m/s (130 kt)
Initial sea-state	Unknown
Recorded rainfall	Unknown

Table 52 – Overview hurricane Inez

Inez was a small but intense hurricane. It passed through the North of the Caribbean with medium forward speed and made landfall at the southside of Cuba. After the landfall the hurricane continued over sea, where the waves had to start growing again.

Inez will be classified as a hurricane with high windspeeds, high forward speed, and as an hurricane over land and close to the shore of Matanzas. The initial sea-state is unknow. (National Hurricane Center, 1975)

Hurricane Lili (1996)

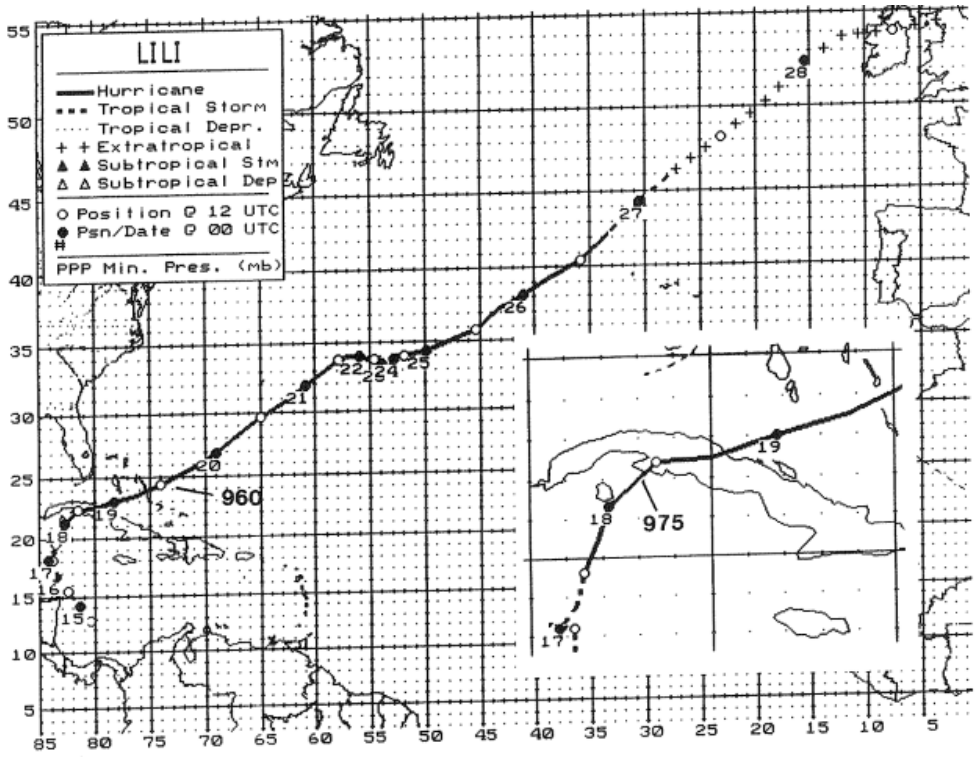

Figure 192 – Best track positions for Hurricane Lili, 14 - 27 October 1996

Date	17 October – 26 October
Duration	9 days
Category	3
Position to shore	Over land, close to Matanzas
Forward speed	12 m/s
Maximum windspeed	50 m/s (100 kt)
Initial sea-state	Unknown
Recorded rainfall	26 inches 10 – 30 inches

Table 53 – Overview hurricane Lili

Lili originated in Africa and moved through the Caribbean, mostly damaging Cuba and the Bahamas. The eye of the hurricane passed over Ìsla de Juventud and made landfall at the south coast of Cuba in the Matanzas Province. It crossed straight over central Cuba and did not diminish in strength. Lili reached its peak strength when it passed the Bahamas.

This hurricane will be classified as one with medium windspeeds, a high forward speed, and as a hurricane over land and close to the shore of Matanzas. The initial sea-state is unknown. (National Hurricane Center, 1996)

Hurricane Georges (1998)

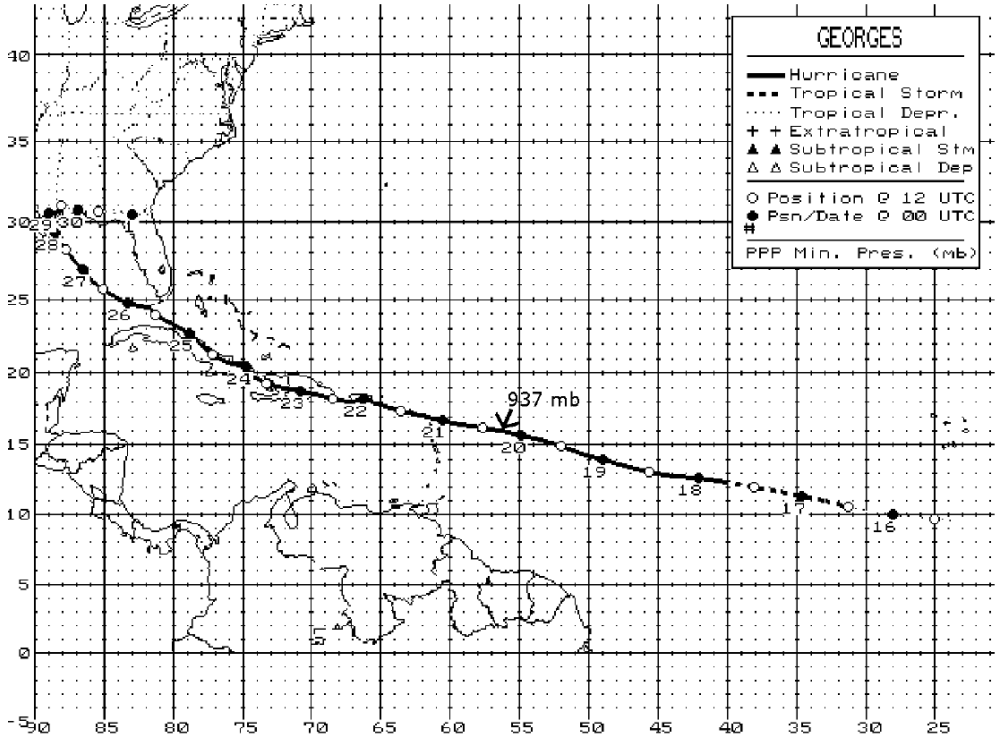

Figure 193- Best track positions for Hurricane Georges, 15 September – 1 October

Date	17 September – 28 September
Duration	12 days
Category	4
Position to shore	Close to the shore of Matanzas
Forward Speed	6 m/s
Maximum Wind speed	66 m/s (135 kt)
Initial sea state	Unknown
Recorded Rainfall	24.21 inch

Table 54 - Overview Hurricane Georges

Georges was a long lasting hurricane, causing many fatalities along its track. Georges made 7 landfalls. Georges produced a lot of rainfall with the recorded maximum in Cuba being 24.21 inch (National Hurricane Center, 2014).

Georges travelled a long distance over sea and along the northern coast of Cuba, close to Matanzas, wind speed is classified as high with a low forward speed..

Hurricane Irene (1999)

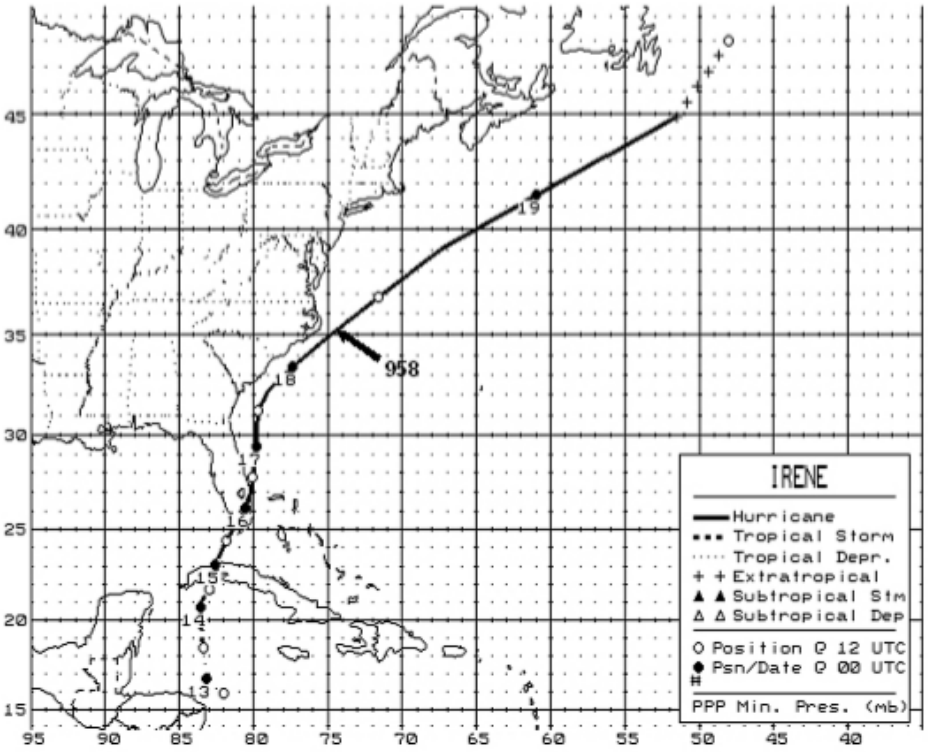

Figure 194 – Best track positions for Hurricane Irene, 13-19 October 1999

Date	15 October – 18 October
Duration	4 days
Category	2
Position to shore	Close to shore
Forward speed	12.2 m/s
Maximum windspeed	49 m/s (95 kt)
Initial sea-state	Rough
Recorded rainfall	10 – 20 inches

Table 55 – Overview hurricane Irene

Irene started off as an area of low pressure in the southwest part of the Caribbean, accompanied by disorganized clouds and thunderstorms. Therefore, it did not look like a tropical cyclone in the beginning which normally starts off with a tropical depression. Only when a tropical wave reached the western Caribbean Sea on the 11th of October it showed the signs of a developing tropical cyclone.

Irene reached its hurricane status just before making landfall over the Isla de Juventud, but new analysis of the data indicate that it was probably a tropical storm while crossing Cuba. It then 'again' reached a hurricane status near Florida. The recorded rainfall in Playa Giron was 11.9 inches and in Havana 4.8 inches were reported.

This hurricane will be classified with low windspeeds, a high forward speed and as a hurricane over land and close to the shore of Matanzas. Because thunderstorms preceded the hurricane, a rough initial sea-state will be assumed. (National Hurricane Center, 1999)

Hurricane Michelle (2001)

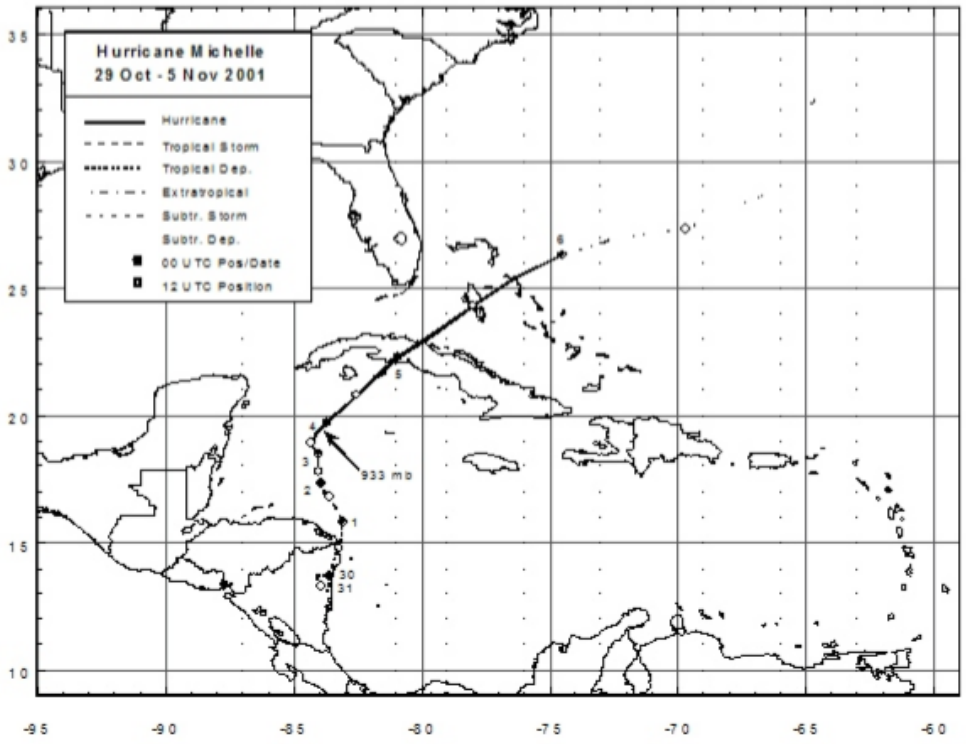

Figure 195 – Best track of Hurricane Michelle, 29 October - 5 November 2001

Date	2 November – 5 November
Duration	4 days
Category	4
Position to shore	Over land, close to Matanzas
Forward speed	3 m/s
Maximum windspeed	60 m/s (120 kt)
Initial sea-state	Rough
Recorded rainfall	29.69 inch

Table 56 – Overview hurricane Michelle

Michelle was a late-season hurricane which caused the most damage in Cuba and the Bahamas. It started as a tropical wave at the coast of Africa and went over the Caribbean waters. It made landfall at the south coast of Cuba and crossed the land close to Havana and the bay of Matanzas.

The hurricane is categorized with high windspeeds, a low forward speed and as a hurricane over land and close to the shore of Matanzas. According to the tropical cyclone report of the National Hurricane Center, high surge occurred caused by a prolonged period of strong onshore winds and above normal tides. The report also states that Michelle started as a slow moving hurricane. Therefore the initial sea-state is assumed to be rough. (National Hurricane Center, 2002)

Hurricane Dennis (2005)

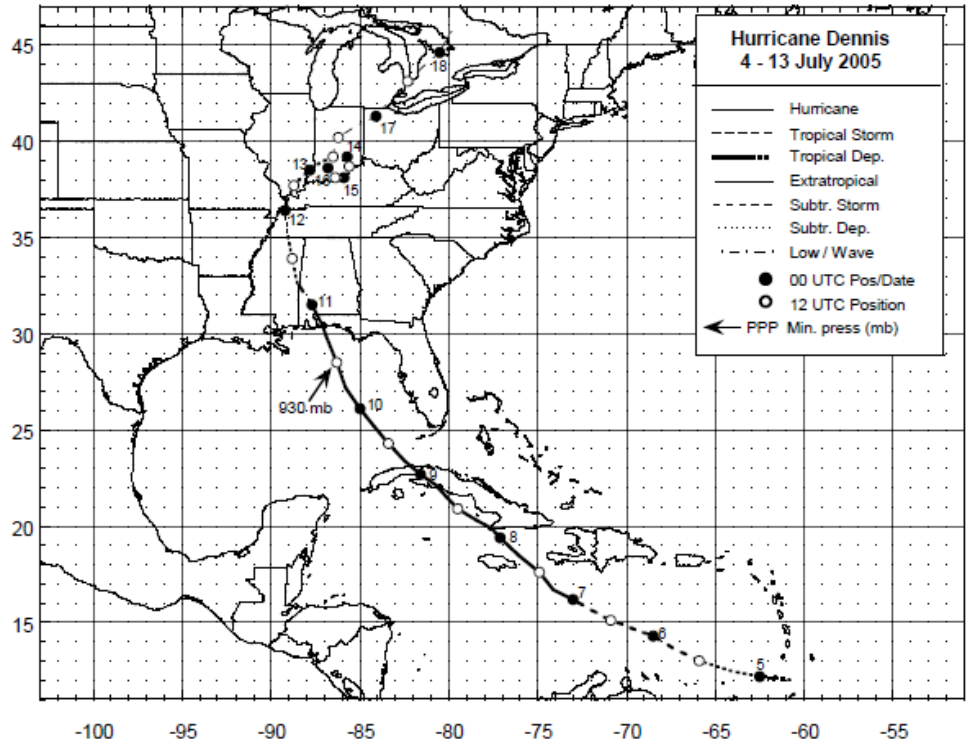

Figure 196 - Best track of Hurricane Dennis, 4 - 13 July 2005

Date	7 July – 10 July
Duration	4 days
Category	4
Position to shore	Over land, close to Matanzas
Forward speed	7 m/s
Maximum windspeed	65 m/s (130 kt)
Initial sea-state	Unknown
Recorded rainfall	27.67 inch

Dennis formed westward from the coast of Africa and developed into a tropical depression, Dennis reached hurricane strength on July 7 and intensified rapidly to a category 4 hurricane. Dennis made Landfall near Punta de Ingles in south-eastern Cuba. Dennis weakened travelling over Cuba but intensified again over the Gulf of Mexico. Dennis produced heavy rainfall in Cuba with reports of 27.67 inch in 24 hours. (National Hurricane Center, 2014)

The wind speed of Dennis is classified as high, with a high forward speed, with a track over land close to Matanzas.

Hurricane Rita (2005)

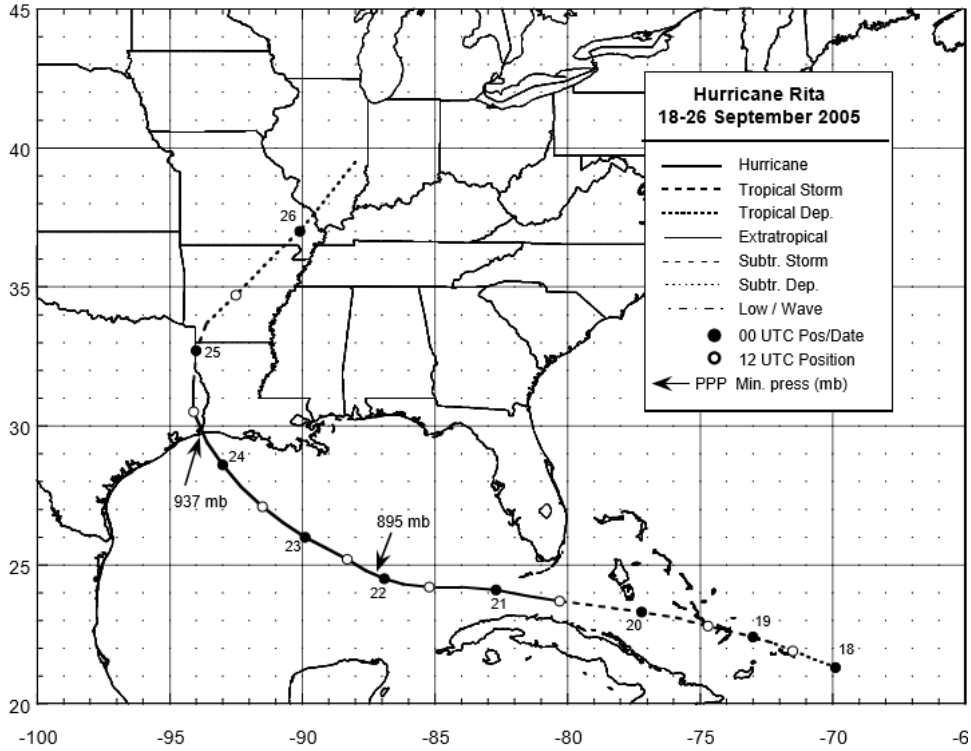

Figure 197 – Best track positions for Hurricane Rita, 18-26 September 2005

Date	20 November – 24 November
Duration	5 days
Category	5
Position to shore	Medium
Forward speed	4 m/s
Maximum windspeed	80 m/s (= 155 kt)
Initial sea-state	Rough
Recorded rainfall	5 – 10 inches

Table 57 – Overview hurricane Rita

Rita was an intense hurricane of category 5. When it passed Cuba, it was still strengthening and on the 22th of November it reached its peak. It weakened before making landfall in the US till a category 3 hurricane. The hurricane was mainly over sea and only touched the coast of Yucatan.

The hurricane is categorized with high windspeeds and a low forward speed. Rita passed around 200 km from the coast of Matanzas and therefore categorized of medium distance to shore. The tropical cyclone report of the National Hurricane Center states that the cold frond preceding and causing Rita, produced a large and disorganized area of disturbed weather. Therefore, the initial sea-state is assumed to be rough. (National Hurricane Center, 2006)

Tropical Storm Fay (2008)

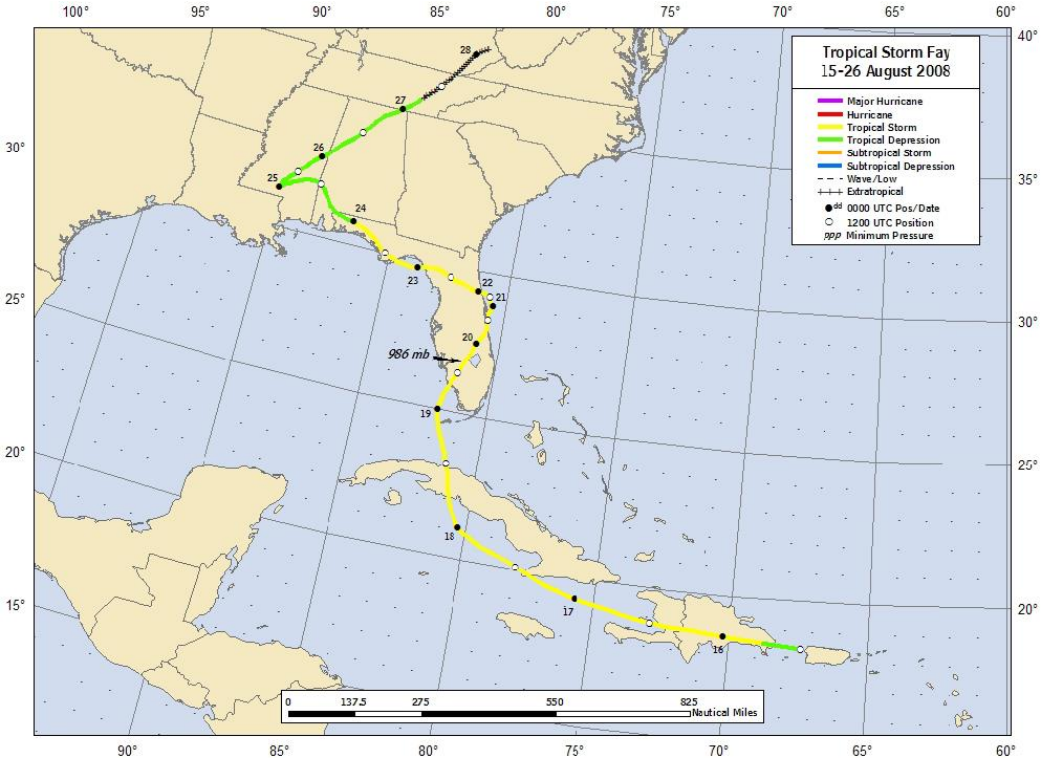

Figure 198- Best track positions for Tropical Storm Fay, 15-26 August

Date	N.A.
Duration	N.A.
Category	N.A
Position to shore	Over land, close to Matanzas
Forward Speed	3.5 m/s
Maximum windspeed	29 m/s (60 kt)
Initial sea-state	Unknown
Recorded rainfall	18.23 inch

Table 58 - Overview Tropical Storm Fay

Fay was a long-lasting tropical storm that made eight landfalls. Fay did not reach hurricane status but nevertheless caused extensive flooding in Cuba. It made landfall along the south-central coast of Cuba. Heavy rainfall was the most notable hazard caused by Fay. (National Hurricane Center, 2009)

Fay is not classified as a hurricane because of its low windspeeds, therefore the wind speed is qualified as ‘very low’. The forward speed is classified as ‘low’. The track position is classified as over land and close to the shore of Matanzas. There is not enough information about the initial sea state.

Hurricane Gustav (2008)

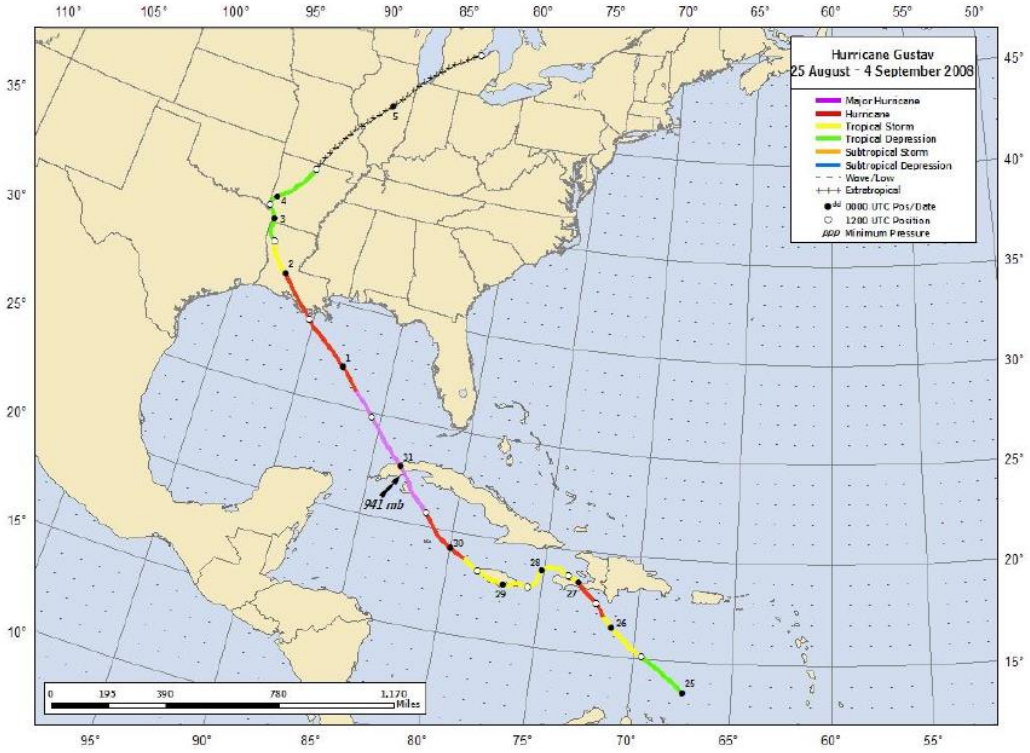

Figure 199 - Best track positions for Hurricane Gustav, 25 August - 4 September

Date	26, 29 August - 1 September
Duration	1 day and 4 days
Category	3
Position to shore	Over land, close to Matanzas
Forward Speed	'Fast'
Maximum Wind speed	61 m/s (125 knts)
Initial sea state	Rough
Recorded Rainfall	Total max. 11.70

Table 59 - Overview Hurricane Gustav

Gustav caused a considerable damage in Cuba and Matanzas. Gustav rapidly intensified from a tropical storm to a hurricane and made landfall in Haiti. Moving along the southern coast of Cuba at a large distance it made landfall in Cuba first at Isla de Juventud. The hurricane weakened over Cuba and emerged close to Havana. (National Hurricane Center, 2009)

The wind speed is classified as strong, with a fast forward speed and an approach to close to Matanzas over land. Since Gustav was preceded by Tropical Storm Fay it can be assumed that the sea state was rough.

Hurricane Ike (2008)

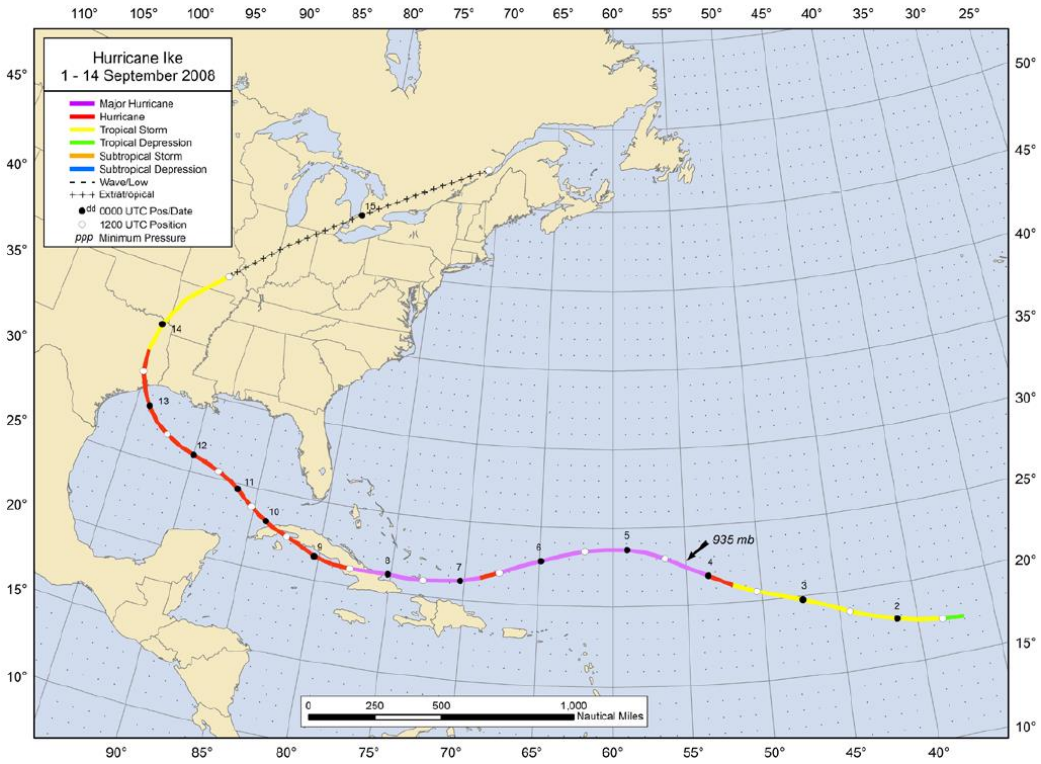

Figure 200 - Best track position Hurricane Ike, 1 – 14 September

Date	3 September – 13 September
Duration	11 days
Category	3 - 4
Position to shore	Over land, along southern shore
Forward Speed	12 m/s
Maximum Wind speed	62 m/s (125 kt)
Initial sea state	Rough
Recorded Rainfall	13.77 inch

Table 60 - Overview Hurricane Ike

Ike was a long lived hurricane that caused extensive damage, it reached peak intensity 4 over the open waters of the Atlantic. Ike made landfall in Cuba at this intensity, near Cabo Lucrecia, Ike lost some of its strength over Cuba. Waves as high as 50 feet have (unofficialy) been reported in the city of Baracoa in Cuba where Ike first made landfall. (National Hurricane Center, 2009)

The wind speed and the forward speed are ranked as ‘high’. The initial sea state is assumed to be rough because of the rapid succession of Hurricane Ike after Tropical storm Fay and Hurricane Gustav.

E. Delft3D model

The main part of this appendix consist of Python files to create the spiderweb grid. At the end a Least-squares model is added, which is used to capture the tidal behavior of the area and remove it from the signal in order to capture only the influence of Irma on the water level.

Spiderweb grid creator

The next figure shows the Python script used to create a spiderweb grid.

```
"""
Created on Wed Nov 27 15:35:25 2019

@author: Matthijs
"""
import matplotlib.pyplot as plt
import numpy as np
import pylab
#%%
ht=np.loadtxt('Irma_v1.txt') #Load the trajectory of the hurricane
xh=ht[:,6]
yh=ht[:,5]
#%%
#SET YOUR SPIDERGRID PARAMETERS
rmax=6 #Longitude dimensions thus in degrees
col_step=360 #Spider grid dimensions. In how many parts would you like
row_step=400 #How many circles do you want to draw around your middle p
#%%
dangle=(360./col_step)/180.*np.pi
dr=rmax/row_step
length=(col_step*row_step)
gtot=np.full((length,2*len(xh)),np.nan) #Make an empty grid
#%%
for h in range(len(xh)):
    xga=np.full(length,np.nan) #Make empty temporary arrays
    yga=np.full(length,np.nan) #Make empty temporary arrays
    xga[0]=xh[h] #Fill in the middle point of the web
    yga[0]=yh[h] #Fill in the middle point of the web
    for col in range(col_step): #iterate through web
        for row in range(row_step): #iterate through web
            x=(row+1)*dr*np.sin(dangle*col)+xh[h]
            y=(row+1)*dr*np.cos(dangle*col)+yh[h]
            xga[col+row*col_step]=x
            yga[col+row*col_step]=y
    gtot[:,h*2]=xga
    gtot[:,h*2+1]=yga
#%%
a=plt.figure(figsize=(10,8))
plt.plot(gtot[:,-2],gtot[:,-1],'.')
plt.title('Initial grid nodes combined with spider web grid nodes')
plt.xlabel('degrees')
plt.ylabel('degrees')
pylab.xlim([xga-1.1*rmax,xga+1.1*rmax])
pylab.ylim([yga-1.1*rmax,yga+1.1*rmax])
plt.savefig('test1.png')
#plt.close(a)
#%%
np.savetxt('simple_spider.txt',gtot,fmt='%.4e') #save the grid file
```

Figure 201 – Python script of the spiderweb grid

Spiderweb grid input file for Delft3D

The next figure shows the text file which is the input file for the Delft3D model.

```
FileVersion = 1.03
filetype = meteo_on_spiderweb_grid
NODATA_value = -999.000
n_cols =    3
n_rows =    5
grid_unit = m
spw_radius = 100597.9
spw_rad_unit = m
n_quantity =    3
quantity1 = wind_speed
quantity2 = wind_from_direction
quantity3 = p_drop
unit1 = m s-1
unit2 = degree
unit3 = Pa
TIME =  0.0 hours since 2017-09-05 20:00:00 +00:00
x_spw_eye = 1558173.3
y_spw_eye = 2336904.2
p_drop_spw_eye =    500.0
4.5418 3.9441 3.9441
11.0308 10.8143 10.8143
11.3406 11.4137 11.4137
10.5344 10.7050 10.7050
9.6559 9.8570 9.8570
85.7696 206.0071 325.9483
81.5392 201.9828 321.9240
65.0000 184.9816 305.0184
65.0000 184.9936 305.0064
65.0000 185.0007 304.9993
488.8720 490.6313 490.6313
429.8409 436.4646 436.4646
366.0295 374.4198 374.4198
314.4684 323.3037 323.3037
274.3340 282.9819 282.9819
```

Figure 202 – Spiderweb .txt input file

This file is created with a Python script. This script can be found on the next four pages.

```
%%%%%% Note: - atmospheric pressure assumed 1 atm
%%%%%%       - n_rows & n_cols input manually
%%%%%%       - radius, date and total time steps input manually
%%%%%%       - change start hours, min, etc. manually in ~line 351

%% Clear the workspace
clear
clc
disp('Start script')
%% Load the hurricane path, velocities and pressures
disp('Load files')
load 'Irma_v8.txt';
load 'Irma_v8_UTM.txt';
filename='d3d_Irma_v8.txt';
b=Irma_v8;
c=Irma_v8_UTM;
%% Select amount of hours to simulate
ts = size(b,1);
%% Create different data sets from loaded files
hx_utm=c(:,6);
hy_utm=c(:,7);
time=b(1:ts,5);
n=length(time);
aa=b(1:ts,1);
mm=b(1:ts,2);
dd=b(1:ts,3);
hh=b(1:ts,4);
hx=b(1:ts,6);
hy=b(1:ts,7);
vhx=b(1:ts,8);
vhy=b(1:ts,9);
Pc=b(1:ts,11);
vrmax=b(1:ts,10);
%% Load spider grid and manually input n_cols, n_rows and spw_radius
disp('Load spider grid')
load simple_spider.txt
a=simple_spider;
n_cols = 360; %divide 360 degrees in n_cols parts
n_rows = 200; % divde spw_radius in n_rows parts

year = 2017;
month = 9;
day = 5;
hours = size(a,2)/2;
xn=a(:,1:2:2*hours);
yn=a(:,2:2:2*hours);

%% Calculate mean radius of the hurricane in meters
radius=zeros(ts-48,1);
for j=1:ts-48
    r=distance(hy(j),hx(j),mean(yn(:,j)),max(xn(:,j)),'degrees');
    radius(j)= deg2km(r)*1000;
    r=distance(hy(j),hx(j),max(yn(:,j)),mean(xn(:,j)),'degrees');
    radius(j)= (radius(j)+deg2km(r)*1000)/2;
end
spw_radius = mean(radius); %m

%% Some data to be saved in computation
Vvx = zeros(size(xn,1),ts);
Vvy = zeros(size(yn,1),ts);
pressure = zeros(size(yn,1),ts);
dir = zeros(size(yn,1),ts);
%% Create the fixed part of the Delft3D input file
disp('Create Delft3D input file');
d3d=fopen(filename,'wt');
intro = 'FileVersion = %4.2f \n';
fprintf(d3d,intro,1.03);
intro = 'filetype = meteo_on_spiderweb_grid \n';
fprintf(d3d,intro);
intro = 'NODATA_value = %4.3f \n';
fprintf(d3d,intro,-999.000);
intro = 'n_cols = %4.0f \n';
fprintf(d3d,intro,n_cols);
intro = 'n_rows = %4.0f \n';
fprintf(d3d,intro,n_rows);
intro = 'grid_unit = m \n';
fprintf(d3d,intro);
intro = 'spw_radius = %4.1f \n';
fprintf(d3d,intro,spw_radius);
intro = 'spw_rad_unit = m \n';
fprintf(d3d,intro);
intro = 'n_quantity = %4.0f \n';
fprintf(d3d,intro,3);
intro = 'quantity1 = wind_speed \n';
fprintf(d3d,intro);
intro = 'quantity2 = wind_from_direction \n';
fprintf(d3d,intro);
intro = 'quantity3 = p_drop \n';
fprintf(d3d,intro);
intro = 'unit1 = m s-1 \n';
fprintf(d3d,intro);
intro = 'unit2 = degree \n';
fprintf(d3d,intro);
intro = 'unit3 = Pa \n';
```

```
fprintf(d3d,intro);

%% Create format to fit size of matrix with velocities, directions and pressures
data_format = [];
for i=1:n_cols
    data_format = [data_format,"%3.4f"];
end
data_format = [data_format, '\r\n'];
data_format = join(data_format,' ');

%% Start to loop through all the hours
disp('Start to loop through hours')
for mainloop=1:n
  i=mainloop;
%% Calculate the velocity 10 m from the water surface
%%%%%% The speed of the track of the hurricane is subtracted from the
%%%%%% maximum speed
vmax10m(i)= vrmax(i)-(vhx(i)^2+vhy(i)^2)^0.5;

%% Calculate the velocity including the planetary boundary layer
vmaxapbl(i)=vmax10m(i)/0.7;

%% Calculate the radius with the maximum velocity rmax1 in km
rmax1=(46.29*exp(-0.0153*vmaxapbl(i)+0.0166*hy(i)));


%% Calculate the pressure difference in eye (Pn-Pc) (mbar)
dp1=(1013.2-Pc(i));
%% Create a time and date variable
temp=int2str(hh(i));
%% Create wind and pressure field for each node

%% Calculate distance for each node to the eye of the hurricane
%%%%% calculate x-distance for of each grid point to the center of hurricane
distx=abs(xn(:,i)-hx(i));
%%%%% change latitude longitude to km
distx=deg2km(distx);
%%%%% calculate y-distance for of each grid point to the center of hurricane
disty=abs(yn(:,i)-hy(i));
%%%%% change latitude longitude to km
disty=deg2km(disty);
%%% now calculate distance using distance function with arclength and
%%% azimuth
%%%% for spidergrid the grid changes for each time step!!!
[r,AZ]=distance(hy(i),hx(i),yn(:,i),xn(:,i),'degrees');
distm= deg2km(r);

 %% Calculate the Coriolis force
%%%%% calculate Coriolis force, only influenced by latitude
fc1=2*(7.29212)*(10.^(-5))*sin(hy(i)*pi/180);

%% Calculate factor B for each time step, dependend on vmax, rmax and hy
B=1.0036+0.0173*vmaxapbl(i)-0.0313*log(rmax1)+0.0087*hy(i);
if B<1.67
B=1.67;
elseif B>2.14
B=2.14;
end

%% Calculate the hurricane path velocity
Vtras(i)=sqrt(vhx(i).^2+vhy(i).^2);

%% Calculate velocity gradient using Holland formula
roaire=1.15; %kg/m3
xxx=0.5+(((distm-rmax1)/(500-rmax1))*0.15);
gamma=1;
H1=(B*(dp1)*100)/roaire;
H2=((rmax1./distm).^B);
H3= (exp(-((rmax1./distm).^B)));
%%%%% if r larger than rmax1 then coriolis effect plays role in velocity
H4=gamma*((distm.*fc1)/2).^2;
H5=gamma*((distm.*fc1)/2);

%% Calculate rotational velocity for each node
vgrholland=zeros(size(distm));
vgrholland(distm==0)=0;
vgrholland(distm<=rmax1)=(H1*H2(distm<=rmax1).*H3(distm<=rmax1)).^xxx(distm<=rmax1);
vgrholland(distm>rmax1)=(H1*H2(distm>rmax1).*H3(distm>rmax1)+H4(distm>rmax1)).^xxx(distm>rmax1)-(H5(distm>rmax1)) ;

 %% Calculate the angel fo the velocity vector with the Isobaric Line (normal vector)

%%%%% due to the low pressure in the middle of the hurricane, the air far
%%%%% from the center is pointed towards the middle. This means that the
%%%%% velocity vectors are not pointed perpendicular to the center.
TE = zeros(size(distm));
TE(distm>0 & distm<=rmax1)=10*(distm(distm>0 & distm<=rmax1)/rmax1);
TE(rmax1<distm & distm<=1.2*rmax1)=10+75*((distm(rmax1<distm & distm<=1.2*rmax1)/rmax1)-1);
TE(TE==0)=25;

%% Calculate the x and y components of the wind velocity
%%%% The loop and if statements replaced by the following:
fii=zeros(size(distm));
```

```
alpha1=zeros(size(distm));
alphahirad=zeros(size(distm));
% first quadrant
fii(AZ>0 & AZ<90)=atand(disty(AZ>0 & AZ<90)./distx(AZ>0 & AZ<90));
alphah1(AZ>0 & AZ<90)=90+fii(AZ>0 & AZ<90)+TE(AZ>0 & AZ<90);
alphahirad(AZ>0 & AZ<90)=alphah1(AZ>0 & AZ<90)*pi/180;
% second quadrant
fii(AZ>270 & AZ<360)=atand(distx(AZ>270 & AZ<360)./disty(AZ>270 & AZ<360));
alphah1(AZ>270 & AZ<360)=180+fii(AZ>270 & AZ<360)+TE(AZ>270 & AZ<360);
alphahirad(AZ>270 & AZ<360)=alphah1(AZ>270 & AZ<360)*pi/180;
% third quadrant
fii(AZ>180 & AZ<270)=atand(disty(AZ>180 & AZ<270)./distx(AZ>180 & AZ<270));
alphah1(AZ>180 & AZ<270)=270+fii(AZ>180 & AZ<270)+TE(AZ>180 & AZ<270);
alphahirad(AZ>180 & AZ<270)=alphah1(AZ>180 & AZ<270)*pi/180;
% fourth quadrant
fii(AZ>90 & AZ<180)=atand(distx(AZ>90 & AZ<180)./disty(AZ>90 & AZ<180));
alphah1(AZ>90 & AZ<180)= fii(AZ>90 & AZ<180)+TE(AZ>90 & AZ<180);
alphahirad(AZ>90 & AZ<180)=alphah1(AZ>90 & AZ<180)*pi/180;
% AZ==0
alphah1(AZ==0)=180+TE(AZ==0);
alphahirad(AZ==0)=alphah1(AZ==0)*pi/180;
% AZ==180
alphah1(AZ==180)=0+TE(AZ==180);
alphahirad(AZ==180)=alphah1(AZ==180)*pi/180;
% AZ==90
alphah1(AZ==90)=90+TE(AZ==90);
alphahirad(AZ==90)=alphah1(AZ==90)*pi/180;
% AZ==270
alphah1(AZ==270)=270+TE(AZ==270);
alphahirad(AZ==270)=alphah1(AZ==270)*pi/180;


   %% Calculate the x and y velocity without translation
 % viento  del huracan
 %%%% wind velocity without translation
 Vvhx=vgrholland.*cos(alphahirad);
 Vvhy=vgrholland.*sin(alphahirad);
 Vvr=sqrt((Vvhx).^2+(Vvhy).^2);

%% Adjust the velocity for the translation
 %%%%% calculate translation velocity of each grid point. Calculated
 %%%%% relatively to the maximum velocity
 vhxa=vhx(i)*(vgrholland/vmaxapbl(i));
 vhya=vhy(i)*(vgrholland/vmaxapbl(i));
 Vtr=sqrt(vhx(i).^2+vhy(i).^2);
%% Calculate the total x,y and total velocities
%%%%% wind velocity with translation
 Vvx(:,i)=(Vvhx+vhxa)*0.7;
 Vvy(:,i)=(Vvhy+vhya)*0.7;
 VvR=sqrt(Vvx(:,i).^2+Vvy(:,i).^2);
 max(VvR)
 %%%% first block input of Delft3D

%% calculate the directions
%%%% second block input of Delft3D
%%% Q1 %%%
dir(Vvx>0 & Vvy>0)=270-atand(abs(Vvy(Vvx>0 & Vvy>0))./abs(Vvx(Vvx>0 & Vvy>0)));
%%% Q2 %%%
dir(Vvx>0 & Vvy<0)=270+atand(abs(Vvy(Vvx>0 & Vvy<0))./abs(Vvx(Vvx>0 & Vvy<0)));
%%% Q3 %%%
dir(Vvx<0 & Vvy<0)=90-atand(abs(Vvy(Vvx<0 & Vvy<0))./abs(Vvx(Vvx<0 & Vvy<0)));
%%% Q4 %%%
dir(Vvx<0 & Vvy>0)=90+atand(abs(Vvy(Vvx<0 & Vvy>0))./abs(Vvx(Vvx<0 & Vvy>0)));
%%% 180 degrees %%%
dir(Vvx==0 & Vvy>0)=180;
%%% 0 degrees %%%
dir(Vvx==0 & Vvy<0)=0;
%%% 270 degrees %%%
dir(Vvx>0 & Vvy==0)=270;
%%% 90 degrees %%%
dir(Vvx<0 & Vvy==0)=90;



 %% Calculate the pressure for each node in Pa

%%% Holland method 2010
%%%%% pressure exponentially increasing from middle to the side (in Pa)
pressure(:,i) = 100000-((((Pc(i)+dp1*exp(-(rmax1./distm)).^B))*0.009869232667)*10000);

%% write delft3d_spider.txt and add data for each hour
time = 'TIME = %4.1f hours since %4.0f-09-05 20:00:00 +00:00 \n';
fprintf(d3d,time,[i-1,year]);
x_spw_eye = 'x_spw_eye = %8.1f \n';
fprintf(d3d,x_spw_eye,hx_utm(i));
y_spw_eye = 'y_spw_eye = %8.1f \n';
fprintf(d3d,y_spw_eye,hy_utm(i));
p_drop_spw_eye = 'p_drop_spw_eye = %8.1f \n';
fprintf(d3d,p_drop_spw_eye,(dp1)*100);
wind_speed = reshape(VvR,[n_rows,n_cols]);
fprintf(d3d,data_format,wind_speed);
direction = reshape(dir(:,i),[n_rows,n_cols]);
fprintf(d3d,data_format,direction);
atm_pres = reshape(pressure(:,i),[n_rows,n_cols]);
```

```
fprintf(d3d,data_format,atm_pres);
if i==floor(n/4)
    disp('25% of timesteps created')
elseif i==floor(n/2)
    disp('50% of timesteps created')
elseif i==floor(3*n/4)
    disp('75% of timesteps created')
end
end
disp('Close Delft3D input file');
fclose(d3d);
disp('Computation done');
```

Least-squares model

The datasets for the buoys 8723970 and 8724580 include the tidal signal at that location. Since the Delft3D model does not take a tidal signal as an input, this signal needs to be subtracted from the dataset. To do so, a daily and twice-daily tide are subtracted from the water level data. Also, in order to bring the water level data reference point to the same value as the Delft3D model, a constant water level is subtracted from the water level data.

This is all done by using a least-squares model is used that takes this constant water level and these tidal components into account.

First the system of equations is set up to make a least-squares model with a constant, a daily tide and a twice-daily tide. The system of equations looks as such:

Equation 70: System of equations

$$b + a_1 \sin(\omega_0 t + \theta_0) + a_2 \sin(\omega_1 t + \theta_1) = y$$

Equation 71: Modified system of equations

$$b + A_1 \sin(\omega_0 t) + B_1 \cos(\omega_0 t) + A_2 \sin(\omega_1 t) + B_2 \cos(\omega_1 t) = y$$

Equation 72: Matrix multiplication

$$A * \vec{v} = y$$

Equation 73: Matrix 'A'

$$A = \begin{matrix} 1 & \sin(\omega_0 t) & \cos(\omega_0 t) & \sin(\omega_1 t) & \cos(\omega_1 t) \\ \vdots & \vdots & \vdots & \vdots & \vdots \\ 1 & \sin(\omega_0 t) & \cos(\omega_0 t) & \sin(\omega_1 t) & \cos(\omega_1 t) \end{matrix}$$

Equation 74: Vector 'v'

$$\vec{v} = \begin{matrix} b \\ A_1 \\ B_1 \\ A_2 \\ B_2 \end{matrix}$$

Here the radial frequencies of the sinusoidal tidal components are known and the water levels time series is given for (t, y), meaning this system of equations can be solved with a least-squares method. The following equation shows how the least square values of the parameters are determined. In Equation 75 the system of equations is solved using a least-squares method.

Equation 75: Solving least squares

$$\hat{v} = (A' * A)^{-1} * A' * y$$

The ‘A’ and ‘B’ parameters are however a combination of the amplitudes and phases of the sine and cosine functions with the same radial frequency. They can be combined using Equation 76:

Equation 76: Combination of amplitudes

$$a_i = \sqrt{A_i^2 + B_i^2}$$

The phase shift θ of the signal can be calculated as follows:

$$\theta_i = \tan^{-1}(B_i)$$

This leads to the following set-up of the tidal signal ‘i’:

Equation 77: Tidal signal 'i'

$$h_i(t) = A_i \sin(\omega_i t) + B_i \cos(\omega_i t) = \sqrt{A_i^2 + B_i^2} * \sin\left(\omega_i t + \tan^{-1}(B_i)\right)$$

This means that the signal ‘i’ is translated θ_i back in time.

Hence, using the least-squares method the ‘best’ fit for the tidal cycle at the stations 8723970 and 8724850 are obtained and can be subtracted from the water level timeseries.

F. PROB2B calculations for the final design

Failure probability current design

The following PROP2B files are created to calculated the failure probability of the different sections of the current design for the qmax = 34 l/s/m. The most likely overtopping i.e. the 50% failure probability overtopping was also established using these calculation.

```
Number of calculations (FORM)  : 261

PARAMETERS:
Variable             qmax        1.540E-01

Beta  :  5.016E-01
P_f   :  3.080E-01

           Model        Parameter            alfa               X
 1      Variable                C       -4.983E-01       1.550E-03
 2      Variable              Hm0       -8.316E-01       6.874E000
 3      Variable        Sealevel        -7.399E-03       4.602E-01
 4      Variable            Surge       -2.624E-02       1.602E000
 5      Variable             Tide       -8.048E-03       3.002E-01
 6      Variable               Tp       -1.017E-01       1.265E001
 7      Variable               Ts        0.000E00        1.130E001
 8      Variable                g        0.000E00        9.810E000
 9      Variable               gb       -1.279E-01       6.038E-01
 10     Variable               go        0.000E00        7.200E-01
 11     Variable               gp       -1.279E-01       1.178E000
 12     Variable               kb       -1.279E-01       7.347E-01

          z-value
 1       3.560E-02
 261     1.258E-05

SUMMARY OF PARAMETRIC CALCULATIONS :
     qmax            beta             P_f
 3.400E-02         -1.276        8.990E-01
 4.400E-02         -1.011        8.440E-01
 5.400E-02         -0.789        7.848E-01
 6.400E-02         -0.597        7.246E-01
 7.400E-02         -0.427        6.653E-01
 8.400E-02         -0.275        6.084E-01
 9.400E-02         -0.137        5.546E-01
 1.040E-01         -0.011        5.044E-01
 1.140E-01          0.106        4.579E-01
 1.240E-01          0.214        4.151E-01
 1.340E-01          0.316        3.760E-01
 1.440E-01          0.411        3.404E-01
 1.540E-01          0.502        3.080E-01
```

Figure 203 - FORM analysis section A-1

Number of calculations (FORM) : 261

PARAMETERS:
Variable qmax 1.440E-01

Beta : 3.571E-01
P_f : 3.605E-01

	Model	Parameter	alfa	X
1	Variable	C	-5.026E-01	1.508E-03
2	Variable	Hm0	-8.302E-01	6.763E000
3	Variable	Sealevel	-7.254E-03	4.601E-01
4	Variable	Surge	-2.572E-02	1.601E000
5	Variable	Tide	-7.891E-03	3.001E-01
6	Variable	Tp	-9.992E-02	1.264E001
7	Variable	Ts	0.000E00	1.130E001
8	Variable	g	0.000E00	9.810E000
9	Variable	gb	-1.257E-01	6.027E-01
10	Variable	go	0.000E00	7.500E-01
11	Variable	gp	-1.257E-01	1.175E000
12	Variable	kb	-1.257E-01	7.333E-01

	z-value
1	2.067E-02
261	9.172E-06

SUMMARY OF PARAMETRIC CALCULATIONS :

qmax	beta	P_f
3.400E-02	-1.316	9.060E-01
4.400E-02	-1.054	8.541E-01
5.400E-02	-0.834	7.978E-01
6.400E-02	-0.643	7.400E-01
7.400E-02	-0.475	6.827E-01
8.400E-02	-0.324	6.272E-01
9.400E-02	-0.188	5.744E-01
1.040E-01	-0.062	5.248E-01
1.140E-01	0.054	4.786E-01
1.240E-01	0.161	4.359E-01
1.340E-01	0.262	3.966E-01
1.440E-01	0.357	3.605E-01

Figure 204 - FORM analysis section A-2

Number of calculations (FORM) : 261

PARAMETERS:
Variable qmax 2.040E-01

Beta : 7.016E-01
P_f : 2.415E-01

	Model	Parameter	alfa	X
1	Variable	C	-5.678E-01	1.279E-02
2	Variable	Hm0	-7.643E-01	6.983E000
3	Variable	Sealevel	-7.738E-03	4.602E-01
4	Variable	Surge	-2.735E-02	1.603E000
5	Variable	Tide	-8.416E-03	3.003E-01
6	Variable	Tp	-1.271E-01	1.269E001
7	Variable	Ts	0.000E00	8.600E000
8	Variable	g	0.000E00	9.810E000
9	Variable	gb	-1.596E-01	3.034E-01
10	Variable	go	0.000E00	7.200E-01
11	Variable	gp	-1.596E-01	1.183E000
12	Variable	kb	-1.596E-01	7.382E-01

	z-value
1	5.813E-02
261	6.831E-06

SUMMARY OF PARAMETRIC CALCULATIONS :

qmax	beta	P_f
3.400E-02	-1.621	9.475E-01
4.400E-02	-1.363	9.136E-01
5.400E-02	-1.139	8.726E-01
6.400E-02	-0.941	8.266E-01
7.400E-02	-0.763	7.773E-01
8.400E-02	-0.602	7.263E-01
9.400E-02	-0.453	6.749E-01
1.040E-01	-0.316	6.240E-01
1.140E-01	-0.188	5.746E-01
1.240E-01	-0.068	5.271E-01
1.340E-01	0.045	4.819E-01
1.440E-01	0.153	4.393E-01
1.540E-01	0.255	3.995E-01
1.640E-01	0.352	3.625E-01
1.740E-01	0.445	3.283E-01
1.840E-01	0.534	2.968E-01
1.940E-01	0.619	2.679E-01
2.040E-01	0.702	2.415E-01

Figure 205 - FORM analysis section B

```
Number of calculations (FORM)  : 248

PARAMETERS:
Variable             qmax        1.540E-01

Beta   :  1.655E000
P_f    :  4.901E-02

          Model        Parameter            alfa               X
 1      Variable                C       -4.731E-01       1.870E-03
 2      Variable              Hm0       -8.365E-01       7.763E000
 3      Variable        Sealevel       -8.530E-03       4.606E-01
 4      Variable            Surge       -3.024E-02       1.608E000
 5      Variable             Tide       -9.278E-03       3.008E-01
 6      Variable               Tp       -1.152E-01       1.279E001
 7      Variable               Ts        0.000E00        1.130E001
 8      Variable                g        0.000E00        9.810E000
 9      Variable               gb       -1.439E-01       2.764E-01
 10     Variable               go        0.000E00        7.200E-01
 11     Variable               gp       -1.439E-01       1.198E000
 12     Variable               kb       -1.439E-01       7.474E-01

         z-value
 1      1.007E-01
 248    2.642E-05

SUMMARY OF PARAMETRIC CALCULATIONS :
     qmax            beta             P_f
 3.400E-02         -0.402        6.563E-01
 4.400E-02         -0.088        5.352E-01
 5.400E-02          0.172        4.318E-01
 6.400E-02          0.395        3.465E-01
 7.400E-02          0.591        2.774E-01
 8.400E-02          0.766        2.219E-01
 9.400E-02          0.924        1.777E-01
 1.040E-01          1.069        1.426E-01
 1.140E-01          1.203        1.146E-01
 1.240E-01          1.327        9.230E-02
 1.340E-01          1.443        7.454E-02
 1.440E-01          1.552        6.036E-02
 1.540E-01          1.655        4.901E-02
```

Figure 206 - FORM analysis section C

Parametric study variants

In this section the failure probability of the different sections are calculated while varying a parameter of interest.

Wave height reduction

The failure probability for the different sections are calculated for different wave heights.

Beta : -1.565E000
P_f : 9.412E-01

	Model	Parameter	alfa	X
1	Variable	C	-9.883E-01	4.718E-04
2	Variable	Sealevel	-4.485E-03	4.597E-01
3	Variable	Surge	-1.591E-02	1.596E000
4	Variable	Tide	-4.878E-03	2.996E-01
5	Variable	Tp	-6.289E-02	1.250E001
6	Variable	Ts	0.000E00	1.130E001
7	Variable	g	0.000E00	9.810E000
8	Variable	gb	-7.963E-02	5.925E-01
9	Variable	go	0.000E00	7.200E-01
10	Variable	gp	-7.963E-02	1.155E000
11	Variable	kb	-7.963E-02	7.209E-01
12	Variable	qmax	0.000E00	3.400E-02

	z-value
1	-8.522E-02
261	7.854E-07

SUMMARY OF PARAMETRIC CALCULATIONS :

Hm0	beta	P_f
3.500E000	5.442	2.648E-08
3.600E000	4.898	4.837E-07
3.700E000	4.389	5.698E-06
3.800E000	3.911	4.597E-05
3.900E000	3.463	2.674E-04
4.000E000	3.042	1.174E-03
4.100E000	2.648	4.043E-03
4.200E000	2.280	1.131E-02
4.300E000	1.935	2.651E-02
4.400E000	1.613	5.342E-02
4.500E000	1.312	9.474E-02
4.600E000	1.032	1.510E-01
4.700E000	0.772	2.200E-01
4.800E000	0.531	2.977E-01
4.900E000	0.308	3.791E-01
5.000E000	0.102	4.595E-01
5.100E000	-0.088	5.352E-01
5.200E000	-0.263	6.039E-01
5.300E000	-0.424	6.643E-01
5.400E000	-0.572	7.162E-01
5.500E000	-0.707	7.602E-01
5.600E000	-0.831	7.969E-01
5.700E000	-0.944	8.274E-01
5.800E000	-1.048	8.526E-01
5.900E000	-1.142	8.734E-01
6.000E000	-1.229	8.905E-01
6.100E000	-1.309	9.047E-01
6.200E000	-1.381	9.164E-01
6.300E000	-1.448	9.262E-01
6.400E000	-1.509	9.344E-01
6.500E000	-1.565	9.412E-01

Figure 207 - FORM analysis section A-1, wave height reduction, qmax = 34 l/s/m

```
Beta  : -1.596E000
P_f   :  9.448E-01

          Model        Parameter            alfa               X
 1      Variable                C       -9.892E-01       4.525E-04
 2      Variable        Sealevel        -4.309E-03       4.597E-01
 3      Variable            Surge       -1.528E-02       1.596E000
 4      Variable             Tide       -4.687E-03       2.996E-01
 5      Variable               Tp       -6.040E-02       1.250E001
 6      Variable               Ts        0.000E00        1.130E001
 7      Variable                g        0.000E00        9.810E000
 8      Variable               gb       -7.647E-02       5.927E-01
 9      Variable               go        0.000E00        7.500E-01
 10     Variable               gp       -7.647E-02       1.156E000
 11     Variable               kb       -7.647E-02       7.211E-01
 12     Variable             qmax        0.000E00        3.400E-02

         z-value
 1      -9.019E-02
 261     8.709E-07

SUMMARY OF PARAMETRIC CALCULATIONS :
      Hm0             beta              P_f
 3.500E000           5.265         7.042E-08
 3.600E000           4.728         1.137E-06
 3.700E000           4.224         1.199E-05
 3.800E000           3.753         8.756E-05
 3.900E000           3.310         4.662E-04
 4.000E000           2.896         1.891E-03
 4.100E000           2.508         6.074E-03
 4.200E000           2.145         1.598E-02
 4.300E000           1.806         3.547E-02
 4.400E000           1.490         6.817E-02
 4.500E000           1.195         1.161E-01
 4.600E000           0.921         1.785E-01
 4.700E000           0.667         2.525E-01
 4.800E000           0.431         3.331E-01
 4.900E000           0.214         4.154E-01
 5.000E000           0.013         4.948E-01
 5.100E000          -0.172         5.681E-01
 5.200E000          -0.341         6.336E-01
 5.300E000          -0.497         6.904E-01
 5.400E000          -0.640         7.388E-01
 5.500E000          -0.770         7.794E-01
 5.600E000          -0.890         8.132E-01
 5.700E000          -0.999         8.411E-01
 5.800E000          -1.099         8.641E-01
 5.900E000          -1.190         8.830E-01
 6.000E000          -1.273         8.986E-01
 6.100E000          -1.350         9.115E-01
 6.200E000          -1.420         9.222E-01
 6.300E000          -1.484         9.311E-01
 6.400E000          -1.542         9.385E-01
 6.500E000          -1.596         9.448E-01
```

Figure 208 - FORM analysis section A-2 reduced wave height, qmax = 34 l/s/m

PARAMETERS:
Variable Hm0 6.500E000

Beta : -1.794E000
P_f : 9.636E-01

	Model	Parameter	alfa	X
1	Variable	C	-9.915E-01	2.994E-03
2	Variable	Sealevel	-3.909E-03	4.597E-01
3	Variable	Surge	-1.379E-02	1.596E000
4	Variable	Tide	-4.251E-03	2.996E-01
5	Variable	Tp	-5.359E-02	1.250E001
6	Variable	Ts	0.000E00	8.600E000
7	Variable	g	0.000E00	9.810E000
8	Variable	gb	-6.786E-02	2.963E-01
9	Variable	go	0.000E00	7.200E-01
10	Variable	gp	-6.786E-02	1.156E000
11	Variable	kb	-6.786E-02	7.211E-01
12	Variable	qmax	0.000E00	3.400E-02

	z-value
1	-1.127E-01
261	1.444E-06

SUMMARY OF PARAMETRIC CALCULATIONS :

Hm0	beta	P_f
4.000E000	1.889	2.946E-02
4.100E000	1.519	6.444E-02
4.200E000	1.180	1.190E-01
4.300E000	0.871	1.920E-01
4.400E000	0.589	2.779E-01
4.500E000	0.333	3.696E-01
4.600E000	0.100	4.601E-01
4.700E000	-0.110	5.439E-01
4.800E000	-0.301	6.183E-01
4.900E000	-0.473	6.820E-01
5.000E000	-0.629	7.354E-01
5.100E000	-0.770	7.793E-01
5.200E000	-0.897	8.151E-01
5.300E000	-1.012	8.442E-01
5.400E000	-1.116	8.678E-01
5.500E000	-1.210	8.869E-01
5.600E000	-1.296	9.024E-01
5.700E000	-1.373	9.151E-01
5.800E000	-1.444	9.256E-01
5.900E000	-1.508	9.342E-01
6.000E000	-1.567	9.414E-01
6.100E000	-1.620	9.474E-01
6.200E000	-1.669	9.525E-01
6.300E000	-1.715	9.568E-01
6.400E000	-1.756	9.605E-01
6.500E000	-1.794	9.636E-01

Figure 209 - FORM analysis section B reduced waveheight, qmax = 34 l/s/m

Number of calculations (FORM) : 261

PARAMETERS:
Variable Hm0 6.500E000

Beta : -6.314E-01
P_f : 7.361E-01

	Model	Parameter	alfa	X
1	Variable	C	-9.477E-01	1.041E-03
2	Variable	Sealevel	-9.410E-03	4.597E-01
3	Variable	Surge	-3.337E-02	1.597E000
4	Variable	Tide	-1.024E-02	2.997E-01
5	Variable	Tp	-1.316E-01	1.252E001
6	Variable	Ts	0.000E00	1.130E001
7	Variable	g	0.000E00	9.810E000
8	Variable	gb	-1.665E-01	2.672E-01
9	Variable	go	0.000E00	7.200E-01
10	Variable	gp	-1.665E-01	1.158E000
11	Variable	kb	-1.665E-01	7.223E-01
12	Variable	qmax	0.000E00	3.400E-02

	z-value
1	-1.965E-02
261	9.084E-09

SUMMARY OF PARAMETRIC CALCULATIONS :

Hm0	beta	P_f
4.500E000	4.059	2.464E-05
4.600E000	3.674	1.194E-04
4.700E000	3.309	4.681E-04
4.800E000	2.963	1.522E-03
4.900E000	2.636	4.195E-03
5.000E000	2.326	1.001E-02
5.100E000	2.033	2.102E-02
5.200E000	1.756	3.951E-02
5.300E000	1.495	6.744E-02
5.400E000	1.249	1.059E-01
5.500E000	1.017	1.546E-01
5.600E000	0.799	2.122E-01
5.700E000	0.594	2.763E-01
5.800E000	0.402	3.439E-01
5.900E000	0.222	4.122E-01
6.000E000	0.054	4.785E-01
6.100E000	-0.103	5.411E-01
6.200E000	-0.250	5.986E-01
6.300E000	-0.386	6.504E-01
6.400E000	-0.513	6.961E-01
6.500E000	-0.631	7.361E-01

Figure 210 - FORM analysis section C, Hm0 reduction qmax = 34 l/s/m

Top of structure increase

The failure probability of the sections is calculated for different top of structure heights.

```
PARAMETERS:
Variable                Ts        1.750E001

Beta   :  5.967E-01
P_f    :  2.754E-01

           Model         Parameter            alfa               X
 1      Variable                 C       -4.959E-01       1.578E-03
 2      Variable               Hm0       -8.327E-01       6.947E000
 3      Variable         Sealevel        7.813E-04       4.600E-01
 4      Variable             Surge        2.356E-03       1.600E000
 5      Variable              Tide        8.452E-04       3.000E-01
 6      Variable                Tp       -1.029E-01       1.266E001
 7      Variable                 g        0.000E00        9.810E000
 8      Variable                gb       -1.293E-01       6.046E-01
 9      Variable                go        0.000E00        7.200E-01
 10     Variable                gp       -1.293E-01       1.179E000
 11     Variable                kb       -1.293E-01       7.356E-01
 12     Variable              qmax        0.000E00        3.400E-02

          z-value
 1       9.623E-03
 261     3.114E-06

SUMMARY OF PARAMETRIC CALCULATIONS :
       Ts             beta              P_f
 1.500E001          -0.110        5.438E-01
 1.510E001          -0.081        5.321E-01
 1.520E001          -0.051        5.204E-01
 1.530E001          -0.022        5.087E-01
 1.540E001           0.007        4.971E-01
 1.550E001           0.036        4.855E-01
 1.560E001           0.065        4.740E-01
 1.570E001           0.094        4.625E-01
 1.580E001           0.123        4.511E-01
 1.590E001           0.151        4.398E-01
 1.600E001           0.180        4.286E-01
 1.610E001           0.208        4.174E-01
 1.620E001           0.237        4.064E-01
 1.630E001           0.265        3.955E-01
 1.640E001           0.293        3.847E-01
 1.650E001           0.321        3.740E-01
 1.660E001           0.349        3.635E-01
 1.670E001           0.377        3.531E-01
 1.680E001           0.405        3.428E-01
 1.690E001           0.433        3.327E-01
 1.700E001           0.460        3.227E-01
 1.710E001           0.488        3.129E-01
 1.720E001           0.515        3.033E-01
 1.730E001           0.542        2.938E-01
 1.740E001           0.570        2.845E-01
 1.750E001           0.597        2.754E-01
```

Figure 211 - FORM analysis section A-1, Top of structure increase, qmax = 34 l/s/m

```
Number of calculations (FORM)  : 261

PARAMETERS:
Variable               Ts        1.800E001

Beta  :  6.745E-01
P_f   :  2.500E-01

          Model        Parameter            alfa               X
 1      Variable                C       -4.938E-01       1.600E-03
 2      Variable              Hm0       -8.332E-01       7.007E000
 3      Variable        Sealevel        1.174E-03       4.600E-01
 4      Variable            Surge        3.720E-03       1.600E000
 5      Variable             Tide        1.272E-03       3.000E-01
 6      Variable               Tp       -1.039E-01       1.267E001
 7      Variable                g        0.000E00        9.810E000
 8      Variable               gb       -1.305E-01       6.053E-01
 9      Variable               go        0.000E00        7.500E-01
 10     Variable               gp       -1.305E-01       1.180E000
 11     Variable               kb       -1.305E-01       7.364E-01
 12     Variable             qmax        0.000E00        3.400E-02

          z-value
 1       1.097E-02
 261     3.351E-06

SUMMARY OF PARAMETRIC CALCULATIONS :
       Ts            beta              P_f
 1.500E001         -0.161        5.638E-01
 1.520E001         -0.102        5.407E-01
 1.540E001         -0.044        5.176E-01
 1.560E001          0.013        4.947E-01
 1.580E001          0.071        4.719E-01
 1.600E001          0.127        4.493E-01
 1.620E001          0.184        4.271E-01
 1.640E001          0.240        4.053E-01
 1.660E001          0.295        3.839E-01
 1.680E001          0.351        3.630E-01
 1.700E001          0.405        3.426E-01
 1.720E001          0.460        3.228E-01
 1.740E001          0.514        3.036E-01
 1.760E001          0.568        2.850E-01
 1.780E001          0.621        2.672E-01
 1.800E001          0.675        2.500E-01
```

Figure 212 - FORM analysis section A-2, Top of structure increase, qmax = 34 l/s/m

PARAMETERS:
Variable Ts 1.500E001

Beta : 5.276E-01
P_f : 2.989E-01

	Model	Parameter	alfa	X
1	Variable	C	-4.959E-01	1.557E-03
2	Variable	Hm0	-8.289E-01	6.892E000
3	Variable	Sealevel	-1.556E-03	4.600E-01
4	Variable	Surge	-5.791E-03	1.600E000
5	Variable	Tide	-1.695E-03	3.000E-01
6	Variable	Tp	-1.017E-01	1.265E001
7	Variable	g	0.000E00	9.810E000
8	Variable	gb	-1.901E-01	3.045E-01
9	Variable	go	0.000E00	7.200E-01
10	Variable	gp	-1.278E-01	1.168E000
11	Variable	kb	-6.421E-02	9.015E-01
12	Variable	qmax	0.000E00	3.400E-02

	z-value
1	8.398E-03
261	2.854E-06

SUMMARY OF PARAMETRIC CALCULATIONS :

Ts	beta	P_f
1.100E001	-0.866	8.067E-01
1.120E001	-0.790	7.854E-01
1.140E001	-0.716	7.629E-01
1.160E001	-0.641	7.394E-01
1.180E001	-0.568	7.150E-01
1.200E001	-0.495	6.897E-01
1.220E001	-0.423	6.637E-01
1.240E001	-0.351	6.372E-01
1.260E001	-0.280	6.102E-01
1.280E001	-0.209	5.830E-01
1.300E001	-0.140	5.555E-01
1.320E001	-0.070	5.281E-01
1.340E001	-0.002	5.007E-01
1.360E001	0.066	4.736E-01
1.380E001	0.134	4.468E-01
1.400E001	0.201	4.204E-01
1.420E001	0.267	3.946E-01
1.440E001	0.333	3.695E-01
1.460E001	0.398	3.451E-01
1.480E001	0.463	3.216E-01
1.500E001	0.528	2.989E-01

Figure 213 - FORM analysis section B, Top of Structure increase, qmax = 34 l/s/m

Number of calculations (FORM) : 235

PARAMETERS:
Variable Ts 1.400E001

Beta : 3.416E000
P_f : 3.174E-04

	Model	Parameter	alfa	X
1	Variable	C	-4.504E-01	2.323E-03
2	Variable	Hm0	-8.351E-01	9.115E000
3	Variable	Sealevel	-3.818E-03	4.606E-01
4	Variable	Surge	-1.382E-02	1.608E000
5	Variable	Tide	-4.156E-03	3.007E-01
6	Variable	Tp	-1.335E-01	1.306E001
7	Variable	g	0.000E00	9.810E000
8	Variable	gb	-1.650E-01	2.852E-01
9	Variable	go	0.000E00	7.200E-01
10	Variable	gp	-1.650E-01	1.236E000
11	Variable	kb	-1.650E-01	7.712E-01
12	Variable	qmax	0.000E00	2.000E-01

	z-value
1	1.759E-01
235	2.770E-05

SUMMARY OF PARAMETRIC CALCULATIONS :

Ts	beta	P_f
1.200E001	2.435	7.453E-03
1.220E001	2.538	5.582E-03
1.240E001	2.639	4.153E-03
1.260E001	2.740	3.072E-03
1.280E001	2.840	2.258E-03
1.300E001	2.938	1.651E-03
1.320E001	3.036	1.200E-03
1.340E001	3.132	8.672E-04
1.360E001	3.228	6.235E-04
1.380E001	3.323	4.460E-04
1.400E001	3.416	3.174E-04

Figure 214 - FORM analysis section C, Top of structure increase, qmax = 34 l/s/m

Parametric study top of structure and bullnose correction factor

In this section two parameters of interest are varied; the top of structure height and the bullnose correction factor. The failure probability for each combination of top of structure height and bullnose correction factor is determined both for q_{max} = 34 l/s/m and q_{max} = 100 l/s/m

```
PARAMETERS:
Variable                kb         1.000E00
Variable                Ts         1.330E001

Beta  : -9.817E-01
P_f   :  8.369E-01

          Model         Parameter            alfa                X
 1      Variable                 C       -5.780E-01        1.060E-03
 2      Variable               Hm0       -7.985E-01        5.769E000
 3      Variable         Sealevel        -2.965E-03        4.599E-01
 4      Variable             Surge       -1.064E-02        1.598E000
 5      Variable              Tide       -3.226E-03        2.998E-01
 6      Variable                Tp       -8.178E-02        1.252E001
 7      Variable                 g        0.000E00         9.810E000
 8      Variable                gb       -1.034E-01        5.939E-01
 9      Variable                go        0.000E00         7.200E-01
 10     Variable                gp       -1.034E-01        1.158E000
 11     Variable              qmax        0.000E00         3.400E-02

         z-value
 1      -5.451E-02
 265    -4.592E-06

SUMMARY OF PARAMETRIC CALCULATIONS :
       kb              Ts              beta             P_f
 3.000E-01       1.130E001         -0.296        6.163E-01
 3.000E-01       1.150E001         -0.214        5.849E-01
 3.000E-01       1.170E001         -0.134        5.532E-01
 3.000E-01       1.190E001         -0.054        5.215E-01
 3.000E-01       1.210E001          0.025        4.900E-01
 3.000E-01       1.230E001          0.103        4.588E-01
 3.000E-01       1.250E001          0.181        4.281E-01
 3.000E-01       1.270E001          0.258        3.982E-01
 3.000E-01       1.290E001          0.334        3.690E-01
 3.000E-01       1.310E001          0.410        3.409E-01
 3.000E-01       1.330E001          0.485        3.138E-01
 4.000E-01       1.130E001         -0.636        7.377E-01
 4.000E-01       1.150E001         -0.559        7.121E-01
 4.000E-01       1.170E001         -0.483        6.855E-01
 4.000E-01       1.190E001         -0.408        6.583E-01
 4.000E-01       1.210E001         -0.333        6.304E-01
 4.000E-01       1.230E001         -0.259        6.020E-01
 4.000E-01       1.250E001         -0.185        5.734E-01
 4.000E-01       1.270E001         -0.112        5.446E-01
 4.000E-01       1.290E001         -0.040        5.158E-01
 4.000E-01       1.310E001          0.032        4.872E-01
 4.000E-01       1.330E001          0.103        4.589E-01
 5.000E-01       1.130E001         -0.887        8.124E-01
 5.000E-01       1.150E001         -0.813        7.920E-01
 5.000E-01       1.170E001         -0.741        7.706E-01
 5.000E-01       1.190E001         -0.669        7.481E-01
 5.000E-01       1.210E001         -0.597        7.248E-01
 5.000E-01       1.230E001         -0.526        7.006E-01
 5.000E-01       1.250E001         -0.456        6.757E-01
 5.000E-01       1.270E001         -0.386        6.501E-01
```

Figure 215 - FORM analysis section A-1, Top of structure and bullnose correction factor parametric analysis, qmax = 34 l/s/m

PARAMETERS:

Variable	kb	5.000E-01
Variable	Ts	1.450E001

Beta : 1.660E-01
P_f : 4.341E-01

	Model	Parameter	alfa	X
1	Variable	C	-5.129E-01	1.451E-03
2	Variable	Hm0	-8.346E-01	6.617E000
3	Variable	Sealevel	-2.056E-03	4.600E-01
4	Variable	Surge	-7.526E-03	1.600E000
5	Variable	Tide	-2.239E-03	3.000E-01
6	Variable	Tp	-9.830E-02	1.262E001
7	Variable	g	0.000E00	9.810E000
8	Variable	gb	-1.238E-01	6.012E-01
9	Variable	go	0.000E00	7.500E-01
10	Variable	gp	-1.238E-01	1.172E000
11	Variable	qmax	0.000E00	3.400E-02

	z-value
1	2.655E-04
253	8.782E-07

SUMMARY OF PARAMETRIC CALCULATIONS :

kb	Ts	beta	P_f
3.000E-01	1.130E001	-0.345	6.350E-01
3.000E-01	1.150E001	-0.265	6.043E-01
3.000E-01	1.170E001	-0.185	5.732E-01
3.000E-01	1.190E001	-0.105	5.420E-01
3.000E-01	1.210E001	-0.027	5.107E-01
3.000E-01	1.230E001	0.051	4.797E-01
3.000E-01	1.250E001	0.128	4.491E-01
3.000E-01	1.270E001	0.204	4.190E-01
3.000E-01	1.290E001	0.280	3.897E-01
3.000E-01	1.310E001	0.355	3.612E-01
3.000E-01	1.330E001	0.430	3.337E-01
3.000E-01	1.350E001	0.503	3.073E-01
3.000E-01	1.370E001	0.577	2.821E-01
3.000E-01	1.390E001	0.649	2.581E-01
3.000E-01	1.410E001	0.721	2.354E-01
3.000E-01	1.430E001	0.793	2.140E-01
3.000E-01	1.450E001	0.863	1.939E-01
4.000E-01	1.130E001	-0.683	7.527E-01
4.000E-01	1.150E001	-0.607	7.280E-01
4.000E-01	1.170E001	-0.531	7.024E-01
4.000E-01	1.190E001	-0.456	6.759E-01
4.000E-01	1.210E001	-0.382	6.488E-01
4.000E-01	1.230E001	-0.308	6.211E-01
4.000E-01	1.250E001	-0.235	5.930E-01
4.000E-01	1.270E001	-0.163	5.647E-01
4.000E-01	1.290E001	-0.091	5.363E-01
4.000E-01	1.310E001	-0.020	5.079E-01
4.000E-01	1.330E001	0.051	4.798E-01
4.000E-01	1.350E001	0.121	4.519E-01

Figure 216 - FORM analysis section A-2, Top of structure and bullnose correction factor parametric analysis, qmax = 34 l/s/m

Beta : 9.741E-02
P_f : 4.612E-01

	Model	Parameter	alfa	X
1	Variable	C	-5.240E-01	1.123E-02
2	Variable	Hm0	-8.244E-01	6.564E000
3	Variable	Sealevel	-7.464E-03	4.600E-01
4	Variable	Surge	-2.633E-02	1.600E000
5	Variable	Tide	-8.117E-03	3.000E-01
6	Variable	Tp	-1.037E-01	1.261E001
7	Variable	g	0.000E00	9.810E000
8	Variable	gb	-1.306E-01	3.004E-01
9	Variable	go	0.000E00	7.200E-01
10	Variable	gp	-1.306E-01	1.171E000
11	Variable	qmax	0.000E00	3.400E-02

	z-value
1	-1.503E-03
241	4.431E-07

SUMMARY OF PARAMETRIC CALCULATIONS :

kb	Ts	beta	P_f
2.500E-01	8.600E000	-0.383	6.492E-01
2.500E-01	9.000E000	-0.190	5.752E-01
2.500E-01	9.400E000	0.003	4.988E-01
2.500E-01	9.800E000	0.195	4.228E-01
2.500E-01	1.020E001	0.385	3.501E-01
2.500E-01	1.060E001	0.574	2.831E-01
2.600E-01	8.600E000	-0.437	6.688E-01
2.600E-01	9.000E000	-0.244	5.964E-01
2.600E-01	9.400E000	-0.052	5.208E-01
2.600E-01	9.800E000	0.139	4.449E-01
2.600E-01	1.020E001	0.328	3.714E-01
2.600E-01	1.060E001	0.516	3.029E-01
2.700E-01	8.600E000	-0.488	6.871E-01
2.700E-01	9.000E000	-0.296	6.164E-01
2.700E-01	9.400E000	-0.105	5.418E-01
2.700E-01	9.800E000	0.085	4.661E-01
2.700E-01	1.020E001	0.274	3.921E-01
2.700E-01	1.060E001	0.461	3.223E-01
2.800E-01	8.600E000	-0.536	7.040E-01
2.800E-01	9.000E000	-0.345	6.351E-01
2.800E-01	9.400E000	-0.155	5.617E-01
2.800E-01	9.800E000	0.034	4.864E-01
2.800E-01	1.020E001	0.222	4.121E-01
2.800E-01	1.060E001	0.409	3.414E-01
2.900E-01	8.600E000	-0.582	7.198E-01
2.900E-01	9.000E000	-0.393	6.527E-01
2.900E-01	9.400E000	-0.203	5.805E-01
2.900E-01	9.800E000	-0.015	5.059E-01
2.900E-01	1.020E001	0.173	4.315E-01
2.900E-01	1.060E001	0.359	3.600E-01
3.000E-01	8.600E000	-0.627	7.346E-01
3.000E-01	9.000E000	-0.438	6.693E-01

Figure 217 - FORM analysis section B Top of structure and bullnose correction factor parametric analysis, qmax = 34 l/s/m

```
Number of calculations (FORM)  : 274

PARAMETERS:
Variable               kb        2.000E-01

Beta  :  2.172E-01
P_f   :  4.140E-01

          Model        Parameter           alfa              X
 1      Variable                C       -5.110E-01       1.467E-03
 2      Variable              Hm0       -8.351E-01       6.657E000
 3      Variable        Sealevel        -7.170E-03       4.601E-01
 4      Variable            Surge       -2.543E-02       1.601E000
 5      Variable             Tide       -7.799E-03       3.001E-01
 6      Variable               Tp       -9.894E-02       1.262E001
 7      Variable               Ts        0.000E00        1.130E001
 8      Variable                g        0.000E00        9.810E000
 9      Variable               gb       -1.245E-01       6.016E-01
 10     Variable               go        0.000E00        7.200E-01
 11     Variable               gp       -1.245E-01       1.173E000
 12     Variable             qmax        0.000E00        3.400E-02

          z-value
 1       1.562E-03
 274     1.115E-06

SUMMARY OF PARAMETRIC CALCULATIONS :
       kb             beta             P_f
 5.000E-02          2.273        1.150E-02
 6.000E-02          1.975        2.414E-02
 7.000E-02          1.730        4.185E-02
 8.000E-02          1.522        6.401E-02
 9.000E-02          1.343        8.971E-02
 1.000E-01          1.185        1.180E-01
 1.100E-01          1.045        1.480E-01
 1.200E-01          0.919        1.790E-01
 1.300E-01          0.805        2.104E-01
 1.400E-01          0.701        2.417E-01
 1.500E-01          0.605        2.727E-01
 1.600E-01          0.516        3.029E-01
 1.700E-01          0.434        3.322E-01
 1.800E-01          0.357        3.606E-01
 1.900E-01          0.285        3.879E-01
 2.000E-01          0.217        4.140E-01
```

Figure 218 - FORM analysis section A-1, bullnose correction factor reduction, qmax = 34 l/s/m

Number of calculations (FORM) : 274

PARAMETERS:
Variable kb 3.000E-01

Beta : -3.452E-01
P_f : 6.350E-01

	Model	Parameter	alfa	X
1	Variable	C	-5.339E-01	1.289E-03
2	Variable	Hm0	-8.243E-01	6.228E000
3	Variable	Sealevel	-6.574E-03	4.599E-01
4	Variable	Surge	-2.331E-02	1.599E000
5	Variable	Tide	-7.151E-03	2.999E-01
6	Variable	Tp	-9.133E-02	1.257E001
7	Variable	Ts	0.000E00	1.130E001
8	Variable	g	0.000E00	9.810E000
9	Variable	gb	-1.152E-01	5.976E-01
10	Variable	go	0.000E00	7.500E-01
11	Variable	gp	-1.152E-01	1.165E000
12	Variable	qmax	0.000E00	3.400E-02

	z-value
1	-1.668E-02
274	-2.398E-06

SUMMARY OF PARAMETRIC CALCULATIONS :

kb	beta	P_f
5.000E-02	2.206	1.370E-02
1.000E-01	1.125	1.303E-01
1.500E-01	0.549	2.916E-01
2.000E-01	0.164	4.349E-01
2.500E-01	-0.121	5.482E-01
3.000E-01	-0.345	6.350E-01

Figure 219 - FORM analysis section A-2, bullnose correction factor reduction, qmax = 34 l/s/m

PARAMETERS:
Variable kb 1.500E-01

Beta : 3.702E-01
P_f : 3.556E-01

	Model	Parameter	alfa	X
1	Variable	C	-5.814E-01	1.197E-02
2	Variable	Hm0	-7.738E-01	6.754E000
3	Variable	Sealevel	-8.166E-03	4.601E-01
4	Variable	Surge	-2.883E-02	1.602E000
5	Variable	Tide	-8.881E-03	3.002E-01
6	Variable	Tp	-1.223E-01	1.265E001
7	Variable	Ts	0.000E00	8.600E000
8	Variable	g	0.000E00	9.810E000
9	Variable	gb	-1.537E-01	3.017E-01
10	Variable	go	0.000E00	7.200E-01
11	Variable	gp	-1.537E-01	1.177E000
12	Variable	qmax	0.000E00	3.400E-02

	z-value
1	4.027E-03
261	7.942E-07

SUMMARY OF PARAMETRIC CALCULATIONS :

kb	beta	P_f
5.000E-02	2.394	8.343E-03
6.000E-02	2.016	2.191E-02
7.000E-02	1.710	4.361E-02
8.000E-02	1.455	7.280E-02
9.000E-02	1.238	1.079E-01
1.000E-01	1.049	1.471E-01
1.100E-01	0.883	1.887E-01
1.200E-01	0.734	2.313E-01
1.300E-01	0.601	2.738E-01
1.400E-01	0.480	3.155E-01
1.500E-01	0.370	3.556E-01

Figure 220 - FORM analysis section B, bullnose correction factor reduction, qmax = 34 l/s/m

PARAMETERS:
Variable Ts 1.130E001

Beta : 1.144E000
P_f : 1.264E-01

	Model	Parameter	alfa	X
1	Variable	C	-4.827E-01	1.731E-03
2	Variable	Hm0	-8.353E-01	7.369E000
3	Variable	Sealevel	-8.032E-03	4.604E-01
4	Variable	Surge	-2.848E-02	1.605E000
5	Variable	Tide	-8.737E-03	3.005E-01
6	Variable	Tp	-1.094E-01	1.273E001
7	Variable	g	0.000E00	9.810E000
8	Variable	gb	-1.370E-01	6.094E-01
9	Variable	go	0.000E00	7.200E-01
10	Variable	gp	-1.370E-01	1.188E000
11	Variable	kb	-1.370E-01	3.047E-01
12	Variable	qmax	0.000E00	1.000E-01

	z-value
1	5.134E-02
248	1.624E-05

SUMMARY OF PARAMETRIC CALCULATIONS :

Ts	beta	P_f
9.300E000	0.104	4.587E-01
9.400E000	0.159	4.369E-01
9.500E000	0.214	4.154E-01
9.600E000	0.268	3.943E-01
9.700E000	0.322	3.736E-01
9.800E000	0.376	3.534E-01
9.900E000	0.429	3.338E-01
1.000E001	0.483	3.147E-01
1.010E001	0.535	2.962E-01
1.020E001	0.588	2.784E-01
1.030E001	0.640	2.612E-01
1.040E001	0.692	2.446E-01
1.050E001	0.743	2.287E-01
1.060E001	0.794	2.136E-01
1.070E001	0.845	1.991E-01
1.080E001	0.895	1.853E-01
1.090E001	0.946	1.722E-01
1.100E001	0.996	1.597E-01
1.110E001	1.045	1.480E-01
1.120E001	1.095	1.368E-01
1.130E001	1.144	1.264E-01

Figure 221- FORM analysis section A-1, parametric top of structure with bullnose factor 0.3, qmax = 100 l/s/m

Number of calculations (FORM) : 248

PARAMETERS:
Variable Ts 1.130E001

Beta : 1.084E000
P_f : 1.391E-01

	Model	Parameter	alfa	X
1	Variable	C	-4.839E-01	1.715E-03
2	Variable	Hm0	-8.351E-01	7.323E000
3	Variable	Sealevel	-7.974E-03	4.604E-01
4	Variable	Surge	-2.827E-02	1.605E000
5	Variable	Tide	-8.674E-03	3.005E-01
6	Variable	Tp	-1.087E-01	1.272E001
7	Variable	g	0.000E00	9.810E000
8	Variable	gb	-1.362E-01	6.089E-01
9	Variable	go	0.000E00	7.500E-01
10	Variable	gp	-1.362E-01	1.187E000
11	Variable	kb	-1.362E-01	3.044E-01
12	Variable	qmax	0.000E00	1.000E-01

	z-value
1	4.932E-02
248	1.598E-05

SUMMARY OF PARAMETRIC CALCULATIONS :

Ts	beta	P_f
9.300E000	0.052	4.794E-01
9.400E000	0.106	4.576E-01
9.500E000	0.161	4.361E-01
9.600E000	0.215	4.149E-01
9.700E000	0.269	3.941E-01
9.800E000	0.322	3.737E-01
9.900E000	0.375	3.538E-01
1.000E001	0.428	3.344E-01
1.010E001	0.480	3.156E-01
1.020E001	0.532	2.973E-01
1.030E001	0.584	2.796E-01
1.040E001	0.635	2.626E-01
1.050E001	0.686	2.462E-01
1.060E001	0.737	2.305E-01
1.070E001	0.788	2.154E-01
1.080E001	0.838	2.011E-01
1.090E001	0.888	1.873E-01
1.100E001	0.937	1.743E-01
1.110E001	0.987	1.619E-01
1.120E001	1.036	1.502E-01
1.130E001	1.084	1.391E-01

Figure 222 - FORM analysis section A-2, parametric top of structure with bullnose factor 0.3, qmax = 100 l/s/m

Number of calculations (FORM) : 248

PARAMETERS:
Variable Ts 8.600E000

Beta : 9.990E-01
P_f : 1.589E-01

	Model	Parameter	alfa	X
1	Variable	C	-5.624E-01	1.353E-02
2	Variable	Hm0	-7.631E-01	7.191E000
3	Variable	Sealevel	-7.407E-03	4.603E-01
4	Variable	Surge	-2.621E-02	1.604E000
5	Variable	Tide	-8.056E-03	3.004E-01
6	Variable	Tp	-1.327E-01	1.273E001
7	Variable	g	0.000E00	9.810E000
8	Variable	gb	-1.662E-01	3.050E-01
9	Variable	go	0.000E00	7.200E-01
10	Variable	gp	-1.662E-01	1.189E000
11	Variable	kb	-1.662E-01	3.050E-01
12	Variable	qmax	0.000E00	1.000E-01

	z-value
1	4.005E-02
248	4.980E-06

SUMMARY OF PARAMETRIC CALCULATIONS :

Ts	beta	P_f
6.600E000	-0.082	5.325E-01
6.700E000	-0.027	5.107E-01
6.800E000	0.028	4.888E-01
6.900E000	0.083	4.670E-01
7.000E000	0.137	4.454E-01
7.100E000	0.192	4.239E-01
7.200E000	0.247	4.026E-01
7.300E000	0.301	3.817E-01
7.400E000	0.355	3.611E-01
7.500E000	0.410	3.410E-01
7.600E000	0.464	3.214E-01
7.700E000	0.518	3.022E-01
7.800E000	0.572	2.837E-01
7.900E000	0.626	2.657E-01
8.000E000	0.679	2.484E-01
8.100E000	0.733	2.318E-01
8.200E000	0.787	2.158E-01
8.300E000	0.840	2.005E-01
8.400E000	0.893	1.859E-01
8.500E000	0.946	1.721E-01
8.600E000	0.999	1.589E-01

Figure 223 - FORM analysis section B, parametric top of structure with bullnose factor 0.3, qmax = 100 l/s/m

The design

For the calculation of the pipes the most likely overtopping needs to be calculated. This is done by doing a parametric study of qmax for the configuration of the final design. The most likely overtopping is the 50% failure probability value.

```
Number of calculations (FORM)  : 261

PARAMETERS:
Variable             qmax        1.000E-01

Beta  :  4.801E-01
P_f   :  3.156E-01

           Model        Parameter            alfa               X
 1      Variable                C       -4.987E-01       1.544E-03
 2      Variable              Hm0       -8.310E-01       6.857E000
 3      Variable         Sealevel       -1.047E-02       4.602E-01
 4      Variable            Surge       -3.700E-02       1.603E000
 5      Variable             Tide       -1.138E-02       3.003E-01
 6      Variable               Tp       -1.014E-01       1.265E001
 7      Variable               Ts        0.000E00        1.010E001
 8      Variable                g        0.000E00        9.810E000
 9      Variable               gb       -1.275E-01       6.037E-01
 10     Variable               go        0.000E00        7.500E-01
 11     Variable               gp       -1.275E-01       1.177E000
 12     Variable               kb       -1.275E-01       3.018E-01

          z-value
 1       2.190E-02
 261     7.923E-06

SUMMARY OF PARAMETRIC CALCULATIONS :
     qmax            beta             P_f
 5.000E-02         -0.398        6.548E-01
 6.000E-02         -0.178        5.706E-01
 7.000E-02          0.014        4.942E-01
 8.000E-02          0.185        4.265E-01
 9.000E-02          0.340        3.671E-01
 1.000E-01          0.480        3.156E-01
```

Figure 224 - FORM analysis Section A2, parametric qmax, Ts = 10.1 m, bullnose factor = 0.3

G. Matrixframe output final design

Using Matrixframe the internal forces and moments are calculated for the final design for all load cases.

Shear force all load cases

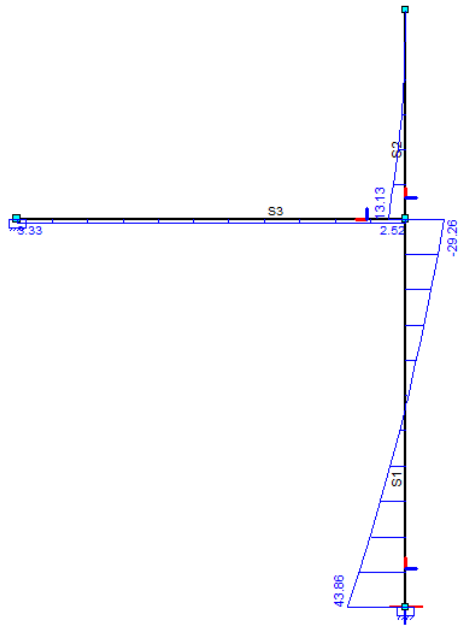

Figure 225 - shear force full basin no wave

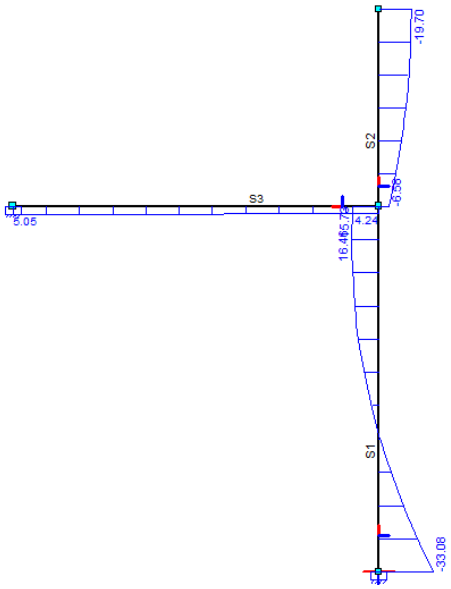

Figure 226 - Shear force all forces

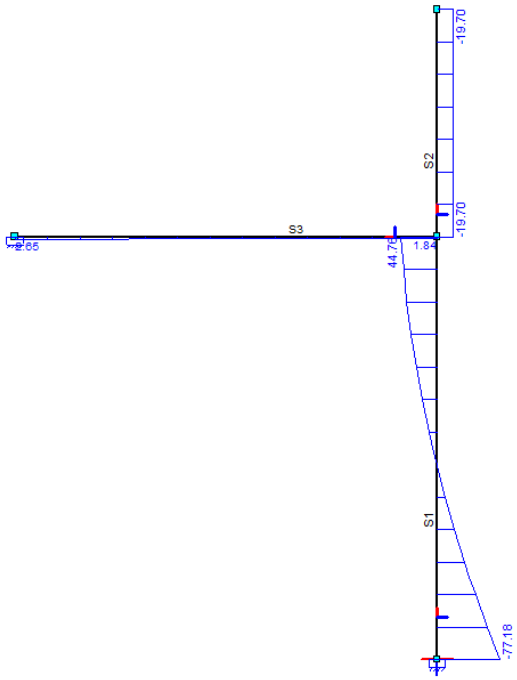

Figure 227 - empty basin with wave impact

Moment distribution all load cases

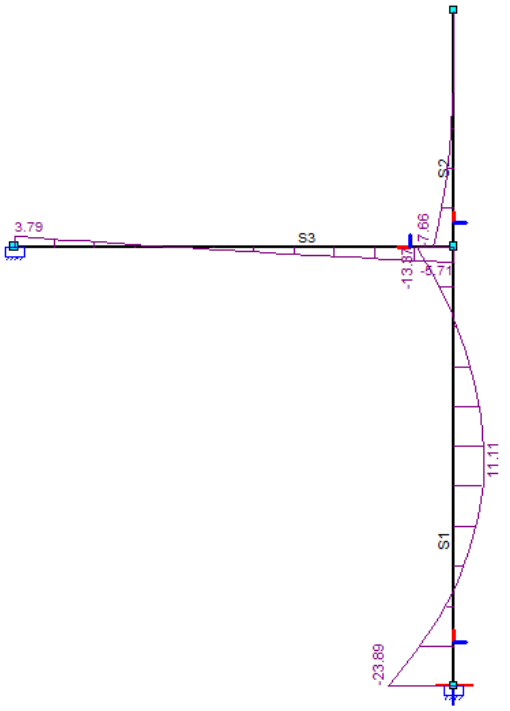

Figure 228 - Moment distribution full basin no wave impact

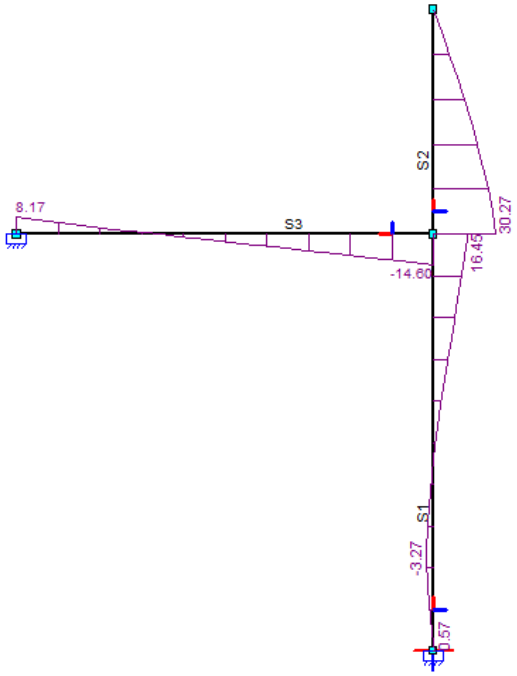

Figure 229- moment distribution all loads

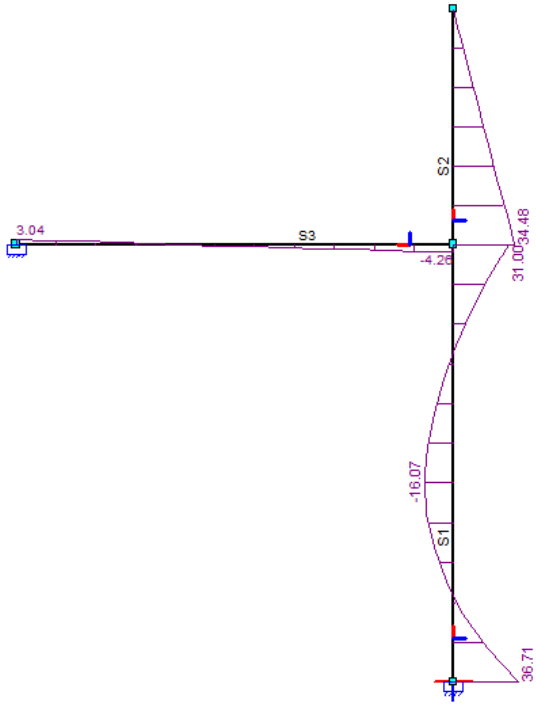

Figure 230 - Moment distribution empty tank, full wave impact

Normal force all load cases

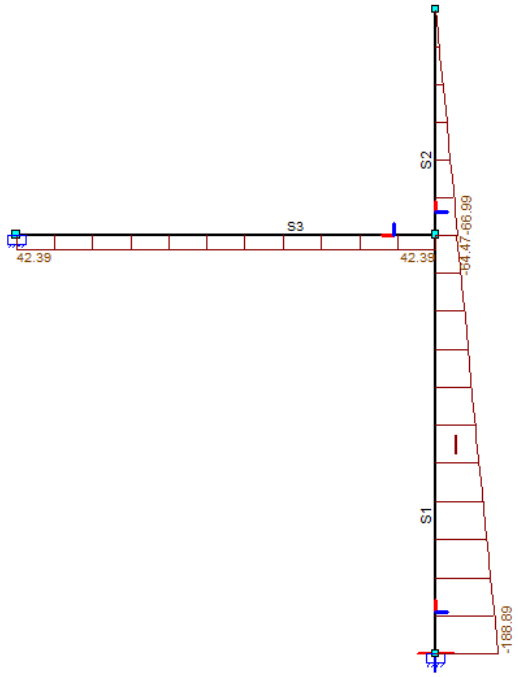

Figure 231 - Normal force full basin no wave

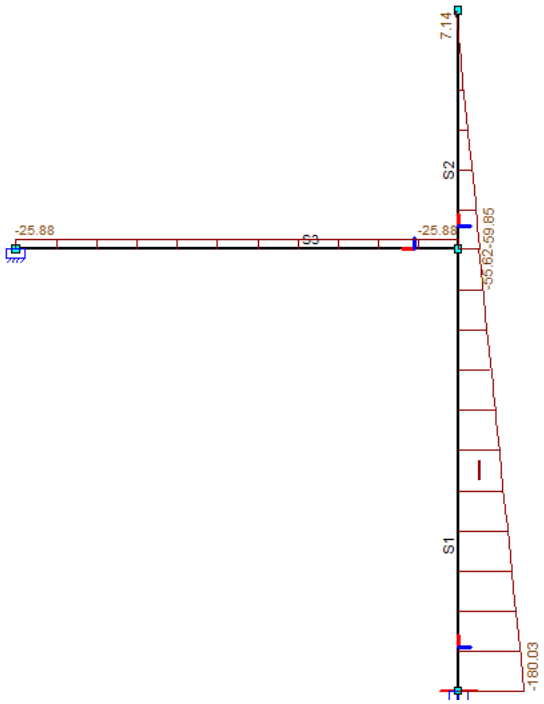

Figure 232- Normal force all loads

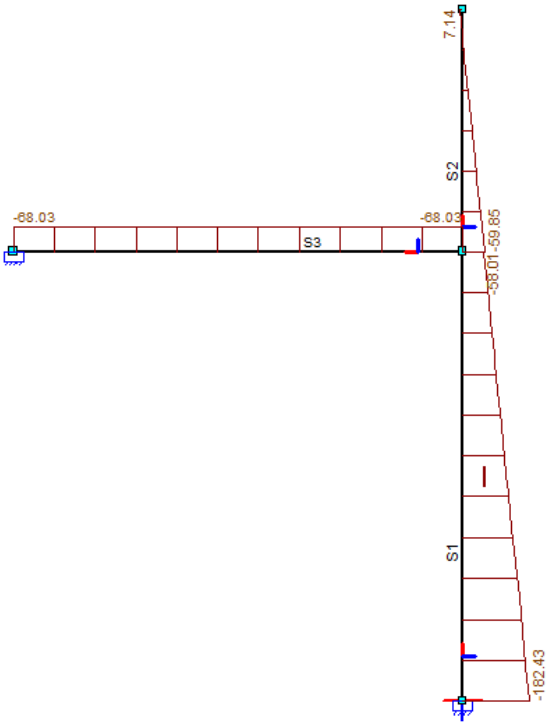

Figure 233 - Normal force, empty basin full wave impact

Lowering of water level basin to h = 4 m

To get an idea of the influence of the water on the side of the basin on the internal forces of the structure the water level was lowered. This information is used in designing the discharge capacity of the pipes. This was done for the load case when full wave impact is also present.

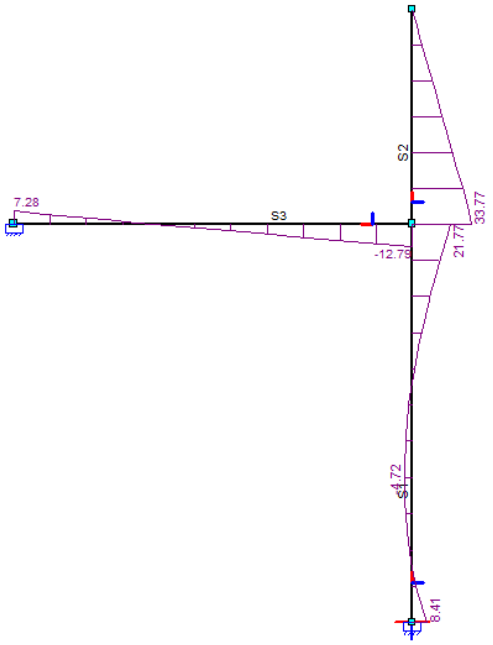

Figure 234 - moment distribution h = 4 m

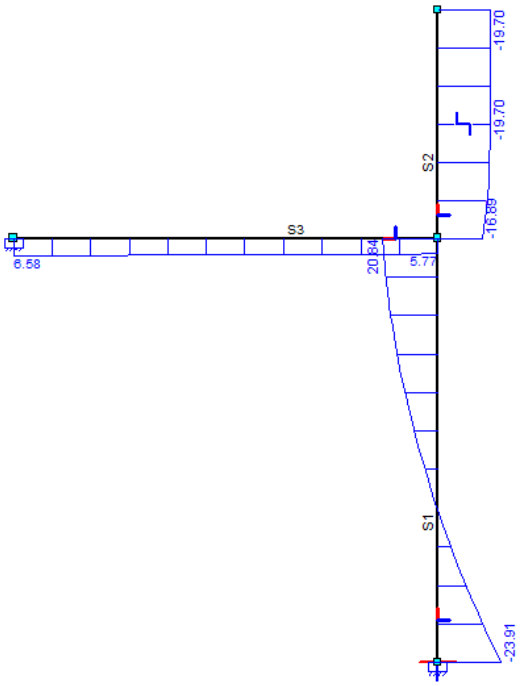

Figure 235 - Shear force diagram h = 4 m

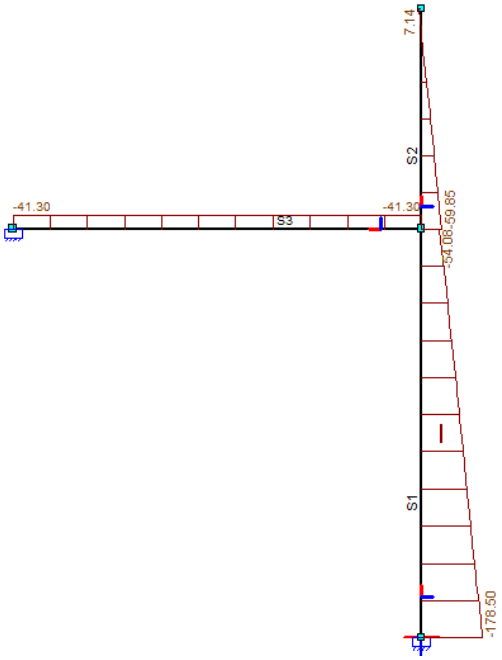

Figure 236 - Normal force diagram h = 4 m

Lowering of water level basin to h = 3 m

To get an idea of the influence of the water on the side of the basin on the internal forces of the structure the water level was lowered. This information is used in designing the discharge capacity of the pipes. This was done for h = 3 m for both the load case with and without wave impact.

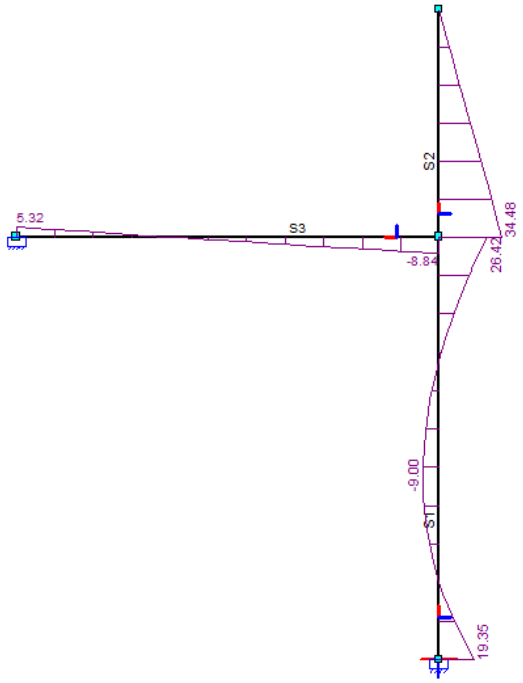

Figure 237 - Moment distribution, h = 3 m, wave impact

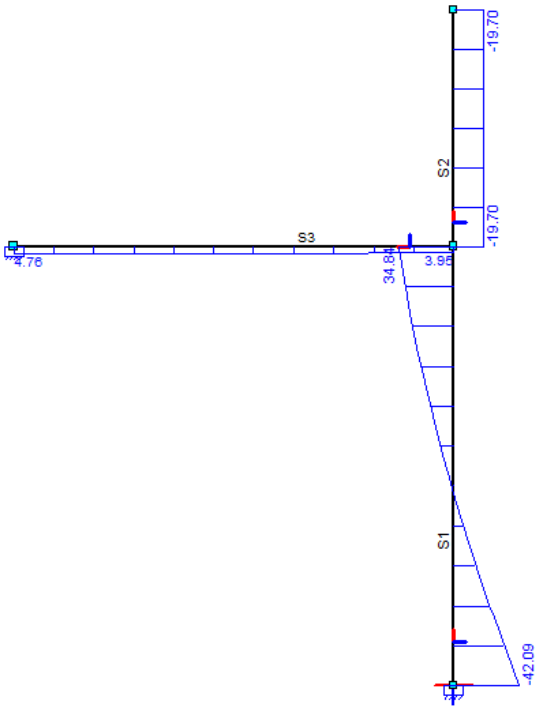

Figure 238 - Shear force diagram, h = 3 m, wave impact

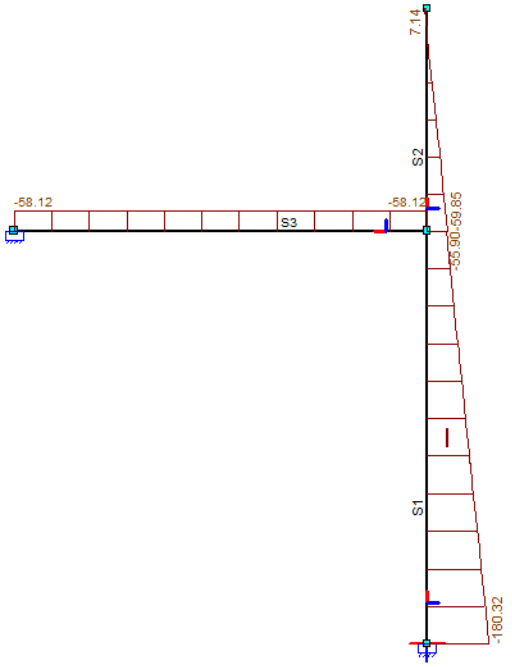

Figure 239 - Normal force diagram, h = 3 m, wave impact

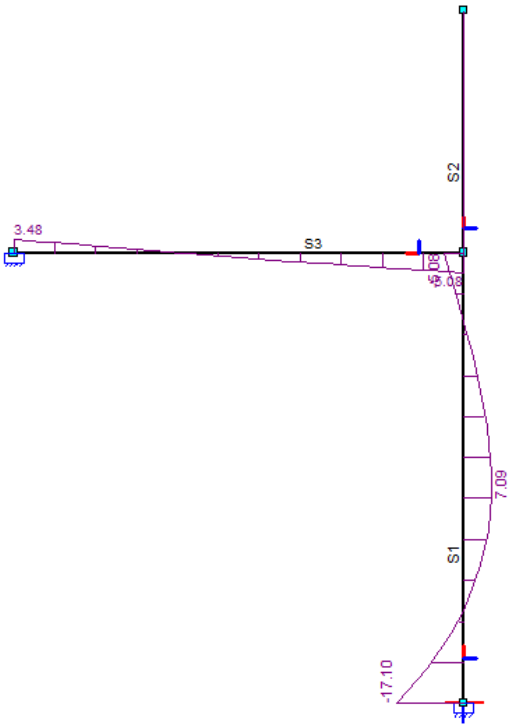

Figure 240 - Moment distribution, h = 3 m, no wave

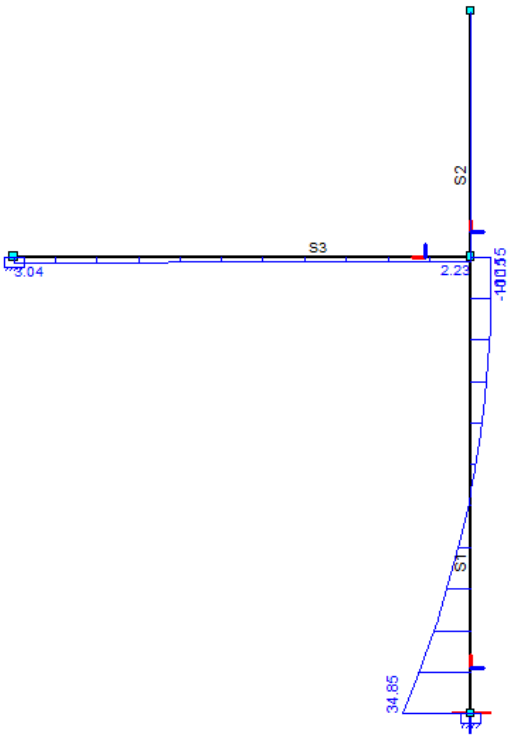

Figure 241 - Shear force, h = 3, no wave

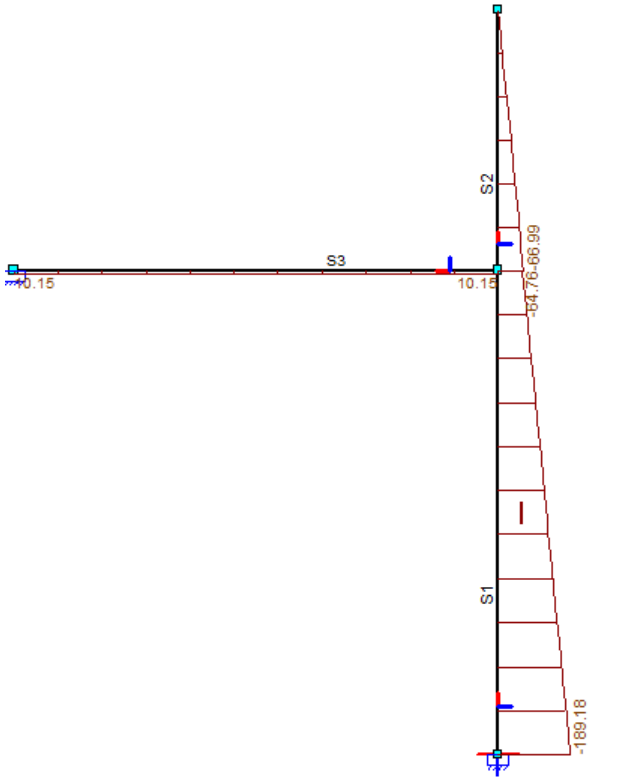

Figure 242 - Normal force diagram, h = 3 m, no wave

Inlet channel

For the new configuration of the wall above the inlet channel the moments, and shear and normal force are also modelled in Matrixframe.

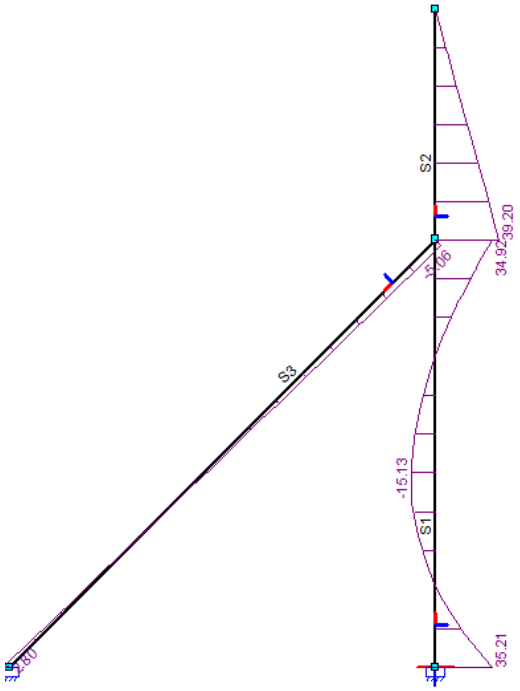

Figure 243 - Moment distribution wall inlet channel, only wave impact

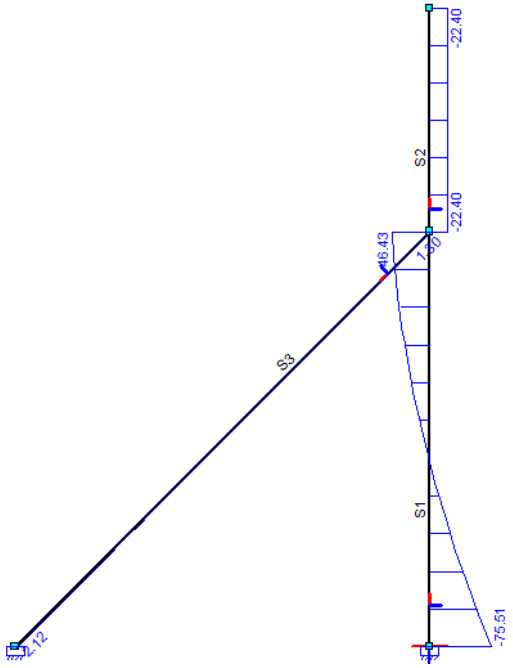

Figure 244 - Shear force diagram wall inlet channel, only wave impact

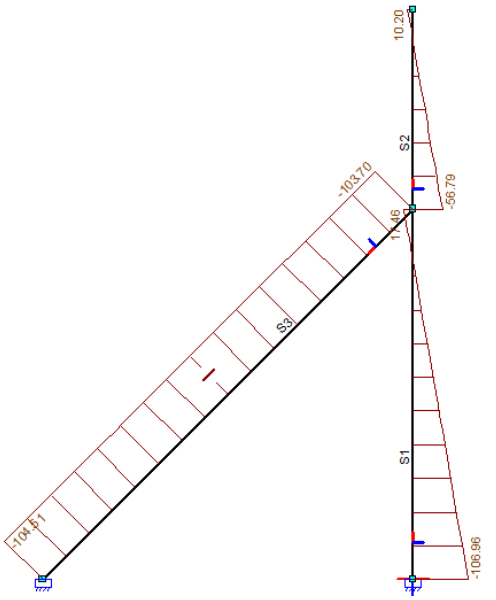

Figure 245 - Normal force diagram wall inlet channel, only wave impact